



**Maria João
Valente Quental**

**Sistemas aquosos bifásicos para a purificação e
preservação de compostos com atividade biológica**

**Aqueous biphasic systems for the purification and
preservation of biologically active compounds**



**Maria João
Valente Quental**

Sistemas aquosos bifásicos para a purificação e preservação de compostos com atividade biológica

Aqueous biphasic systems for the purification and preservation of biologically active compounds

Tese apresentada à Universidade de Aveiro para cumprimento dos requisitos necessários à obtenção do grau de Doutor em Bioquímica, realizada sob a orientação científica do Doutora Mara Guadalupe Freire Martins, Investigadora Coordenadora do Departamento de Química, CICECO, da Universidade de Aveiro, e coorientação do Professor Doutor João Manuel da Costa e Araújo Pereira Coutinho, Professor Catedrático do Departamento de Química, CICECO, da Universidade de Aveiro.

Apoio financeiro do POCTI no âmbito do III Quadro Comunitário de Apoio.

O doutoramento agradece o apoio financeiro da FCT e do FSE no âmbito do III Quadro Comunitário de Apoio (SFRH/BD/109765/2015).

Parte da investigação que conduziu aos resultados aqui apresentados foi financiada pelo Conselho Europeu de Investigação ao abrigo do Sétimo ProgramaQuadro da União Europeia (FP7/2007-2013)/ERC no. 337753



Dedico este trabalho aos dois homens da minha vida....

o júri

Presidente

Professor Doutor António José Arsénia Nogueira
Professor Catedrático da Universidade de Aveiro

Doutora Maria Raquel Murias Dos Santos Aires Barros
Professora Catedrática da Universidade de Lisboa

Doutor José António Couto Teixeira
Professor Catedrático da Universidade do Minho

Doutora Fani Pereira De Sousa
Professora Auxiliar da Universidade da Beira Interior

Doutora Ana Maria Conceição Ferreira
Investigadora da Universidade de Aveiro

Doutora Mara Guadalupe Freire Martins
Investigadora Coordenadora em regime laboral da Universidade de Aveiro

Agradecimentos

Quantas vezes dei por mim a imaginar o que eu escreveria nos agradecimentos da minha tese de doutoramento, e agora que chegou a altura, parece-me quase impossível agradecer a todas as pessoas que fizeram parte desta jornada numa única página.

Trilhar este caminho só foi possível com o apoio, energia e força de várias pessoas, a quem dedico especialmente esta tese.

À Doutora Mara Freire, orientadora desta tese, agradeço todo apoio e partilha de saberes que ocorreu ao longo de todo este trabalho. Ao Professor João Coutinho, coorientador, agradeço a oportunidade de fazer parte do seu grupo de investigação, bem como as valiosas contribuições feitas a este trabalho.

A todos os membros do Path, por me fazerem sentir muito querida, pela prontidão ajudar nas mais diversas situações, e por todos os momentos de partilha que tivemos ao longo destes últimos 4 anos. Obrigada à família que tive oportunidade de construir dentro do laboratório, que vou levar para toda a minha vida comigo. Ritinha, Márcia, Ana Paula, Manu, obrigada pela paciência, palavras doces e pelos “ralhetes” muito necessários quando o drama teimava em instalar-se. Obrigada Joana e Cláudia porque apesar de já distantes fisicamente, estiveram sempre comigo. Diana e Mafalda, vocês tornaram esta jornada inesquecível, obrigada pela cumplicidade companheirismo, compreensão, juntas somos realmente mais fortes. Obrigada Aninha, primeiro por eu ser a única pessoa que te posso chamar assim sem te arrepiar os cabelos, e por todo o apoio incondicional, paciência extrema e carinho durante todos estes anos, na realidade nunca vou ter forma de te agradecer, és uma amiga muito especial.

Por fim e nunca menos importante, agradeço à minha família, obrigada filhote por toda a paciência e compreensão, mesmo quando na verdade não percebias o porque de muitas situações. Obrigada ao amor da minha vida por tanta coisa que é impossível descrever em palavras, mas sem ti nada disto teria sido possível.

palavras-chave

Biomoléculas, atividade biológica, antioxidantes, aminoácidos, proteínas, ácidos nucleicos, líquidos iônicos, sistemas aquosos bifásicos, extração, purificação, preservação.

Resumo

As biomoléculas com atividade biológica apresentam um papel central em diversos processos e funções biológicas. Dada a sua importância, o desenvolvimento de técnicas de separação/purificação que não comprometam a sua estabilidade e atividade biológica é de extrema relevância.

Neste trabalho, foram estudados sistemas aquosos bifásicos constituídos por líquidos iônicos (LI-SABs), para a extração, purificação e preservação de compostos bioativos. Os biocompostos estudados compreendem antioxidantes, aminoácidos, proteínas (incluindo anticorpos) e ácidos nucleicos. Inicialmente foram estudados SABs constituídos por LIs com catiões da família do tetrabutílfosfônio e tetrabutilamônio, e hidratos de carbono ou aminoácidos como agentes de *salting-out*. Estes novos sistemas demonstraram ser plataformas de extração muito competitivas quando comparados com os SABs convencionais na extração de antioxidantes e de misturas de aminoácidos alifáticos-aromáticos, permitindo ainda a recuperação dos compostos alvo através de uma etapa de extração em fase sólida e a reciclagem do LI. Nos trabalhos seguintes, foram desenvolvidos novos SABs para a extração e purificação de proteínas. Foram sintetizados LIs com capacidade tampão e aplicados na formação de SABs para a extração da albumina do soro de bovino. Posteriormente, SABs constituídos por um polímero e por LIs compreendendo o catião colínio e aniões derivados de ácidos naturais foram desenvolvidos para a extração de anticorpos, nomeadamente imunoglobulina G (IgG). Com estes sistemas foi possível, numa única etapa, a extração completa de ambas as proteínas para a fase rica em LI, sem comprometer a sua estabilidade. O último conjunto de trabalhos desenvolvido foca-se na aplicação de soluções aquosas de LIs para a estabilização e preservação de ácidos nucleicos, nomeadamente o ácido ribonucleico (RNA). Nestes trabalhos provou-se ser possível manter a integridade e estabilidade do RNA em soluções aquosas de LIs, e que a maioria dos LIs a 20% não apresentam citotoxicidade para linhas celulares humanas. Finalmente, avaliaram-se SABs como estratégias integradas de preservação-extração. O RNA foi extraído na totalidade e num único passo para a fase rica em LI, que pode atuar como meio de preservação. Em ambos os trabalhos, o RNA foi recuperado e o LI reciclado.

Embora ainda sejam necessários alguns estudos adicionais, nesta tese demonstrou-se a versatilidade de SABs constituídos por LIs como técnica alternativa de extração e preservação, destacando-se também o seu potencial de aplicação em diversos processos biotecnológicos.

keywords

Biocompounds, biological activity, antioxidants, amino acids, proteins, nucleic acids, ionic liquids, aqueous biphasic systems, extraction, purification, preservation.

Abstract

Events involving biomolecules with biological activity have a central role in biological processes and functions. Based on their relevance, the development of techniques for their separation/purification without compromising their stability and biological activity is of utmost importance.

In this work, aqueous biphasic systems composed of ionic liquids (IL-based ABS) were investigated as alternative techniques for the extraction, purification and preservation of bioactive compounds. The biocompounds investigated comprise antioxidants, amino acids, proteins (including antibodies), and nucleic acids. It is first demonstrated the development of new ABS comprising tetraalkylphosphonium- and tetraalkylammonium-based ILs and carbohydrates or amino acids as salting-out agents. These systems proved to be competitive extraction platforms for antioxidants and aromatic-aliphatic amino acid mixtures when compared to more conventional ABS. Furthermore, it was demonstrated that it is possible to recover the target compounds by a solid-phase extraction step, allowing the IL recycling. In the following set of works, novel ABS for the separation of proteins were considered. Self-buffering ILs of a biological-derived nature were synthesized and used to form ABS to extract bovine serum albumin. In the same line, cholinium-based ILs combined with anions derived from natural acids were combined with a polymer to form ABS to extract antibodies, namely immunoglobulin G (IgG). In both works, the complete extraction of the proteins to the IL-rich phase was achieved in a single step, without compromising the proteins integrity. The last set of works is related with the use of ILs aqueous solutions and IL-based ABS to preserve and extract nucleic acids. It was demonstrated that the RNA integrity and stability are maintained in aqueous solutions of appropriate ILs, and that most ILs at 20 wt% display no cytotoxicity towards human cell lines. Finally, ABS were investigated as integrated extraction-preservation strategies. RNA completely partitions to the IL-rich phase in one-step, which could act as the preservation medium. In both works, RNA was successfully recovered and the IL recycled.

Although additional research is still required, the high versatility of IL-based ABS as alternative extraction and preservation media was demonstrated in this thesis, while highlighting their potential to be used in a variety of biotechnological processes.

Contents

List of tables	IX
List of figures.....	X
List of symbols.....	XIV
List of abbreviations.....	XV
List of acronyms	XVI
1. Introduction	1
1.1. Scopes and objectives	3
1.2. Ionic liquids (ILs)	6
1.2.1. IL as preservation media	8
1.2.2. IL-based aqueous biphasic systems (IL-based ABS) as separation processes	9
1.3. Extraction and purification of biocompounds using IL-based ABS	13
1.3.1. Antioxidants and amino acids	13
1.3.2. Proteins	20
1.3.3. Nucleic acids	25
1.4. References	27
2. Extraction of antioxidants and separation of amino acids using IL-based ABS	33
2.1. Extraction of antioxidants using aqueous biphasic systems formed by carbohydrates and tetralkylphosphonium- or tetralkylammonium-based ionic liquids	35
2.2. Separation of aromatic and aliphatic amino acids mixtures using ionic-liquid-based aqueous biphasic systems	52
3. Extraction and purification of proteins using IL-based ABS	65
3.1. Purification of BSA using aqueous biphasic systems formed by self-buffering ionic liquids	67
3.2. Extraction and purification of immunoglobulin G using aqueous biphasic systems formed by bio-based ionic liquids	93
4. Preservation and separation of nucleic acids using IL aqueous solutions and ABS	113
4.1. Aqueous solutions of cholinium-based Good's buffers as preservation media for recombinant small RNAs.....	115
4.2. Integrated extraction-preservation strategies for RNA using aqueous biphasic systems formed by ionic liquids	136
5. Final remarks & future work.....	153
List of publications.....	157
List of publications in the thesis.....	159

Other publications	159
Appendix A.....	161
A1.	163
A2.	170
Appendix B.....	177
B1.	179
B2.	187
Appendix C.....	201
C1.	203
C2.	207

List of tables

Table 1.1 Physical and chemical properties of amino acids found in proteins ¹⁰⁰	17
Table 1.2 Phase-forming components of IL-based ABS and interactions occurring in the extraction of amino acids.....	20
Table 1.3 Summary of IL-based ABS used for the extraction of proteins and results obtained.	23
Table 2.1.1 Octanol-water partition coefficients ($\log K_{ow}$) of the studied carbohydrates ²⁶	44
Table 2.1.2 Dissociation constants of the studied phenolic acids ²⁶	46
Table 3.1.1 Protonation constants of GB/GB-ILs in water at 25 °C and $I = 0.1$ M of NaNO_3	78
Table 3.1.2 EC_{50} values after 30 min of exposure time with the 95% confidence limits (within brackets) for $[\text{P}_{4444}][\text{GB}]$ and $[\text{P}_{4444}]\text{Cl}$	80
Table 3.1.3 Extraction efficiencies of serum bovine albumin, EE_{BSA} (%), in the ABS composed of $[\text{P}_{4444}][\text{GB}] + \text{K}_3\text{C}_6\text{H}_5\text{O}_7$ at 25 °C, and at the described mixture compositions.	83
Table 3.1.4 Secondary structure analysis (infrared spectra) of BSA in conventional $[\text{P}_{4444}][\text{GBs}]/[\text{P}_{4444}]\text{Cl}$ at pH 7.4.....	84
Table 3.1.5 Interaction energies of $[\text{P}_{4444}][\text{GB}]/[\text{P}_{4444}]\text{Cl}$ at 25 °C	87
Table 3.1.6 Recovery efficiencies of serum bovine albumin from serum sample, EE_{BSA} (%), BSA Purity, Purity_{BSA} (%), and BSA yield, Yield_{BSA} (%), in the ABS composed of $[\text{P}_{4444}][\text{GB}] + \text{C}_6\text{H}_5\text{K}_3\text{O}_7$ at 25 °C.	90
Table 3.2.1 Physicochemical properties of the synthesized bio-based ionic liquids.....	101
Table 3.2.2 Logarithm of octanol-water partition coefficients ($\text{Log}K_{ow}$) of the acids used to synthesize bio-based ILs ⁴³	103
Table 3.2.3 Extraction efficiencies of IgG (EE_{IgG} %) and IgG recovery yield (Y_{IgG} %) in ABS formed by an aqueous solution containing IgG at $1 \text{ mg}\cdot\text{mL}^{-1}$	104
Table 4.2.1 Melting temperature of RNA in 0.05 % DEPC-treated water and in AA-ILs (20 wt%) aqueous solutions after 1 h and 15 days of incubation at 25 °C.....	145

List of figures

Figure 1.1 Layout of the current thesis.....	5
Figure 1.2 Most common applications of ionic liquids.	7
Figure 1.3 Evolution of the ionic liquid's applications according to their chemical structures....	8
Figure 1.4 Scheme of the different phase-forming components used to create IL-based ABS, mechanisms involved, and advantages and disadvantages of these systems.....	11
Figure 1.5 Chemical structures of hydroxybenzoic acid derivatives: I) vanillic acid; II) syringic acid, III) protocatechuic acid; IV) gallic acid; V) ferulic acid; VI) p-coumaric; VII) caffeic acid; VIII) sinapic acids.....	14
Figure 1.6 Chemical structures, names and abbreviations of all amino acids extracted and separated with IL-based ABS.....	18
Figure 2.1.1 Chemical structures of the studied carbohydrates (CHs) and ionic liquids (ILs) able to form ABS.....	38
Figure 2.1.2 A- Phase diagrams of ABS composed of IL + D-(-)-fructose + H ₂ O at 25 °C: [P ₄₄₄₄]Br (◆); [P ₄₄₄ (OC ₂)]Br (▲); [P ₄₄₄₄][Oct] (★); [P ₄₄₄₄][Hex] (⊕); [P ₄₄₄₄][But] (■); [P ₄₄₄₁][MeSO ₄] (—); [N ₄₄₄₄]Br (◇); [N ₄₄₄ (OC ₂)]Br (Δ). B- Phase diagrams of ABS composed of [P ₄₄₄₄]Br + carbohydrate + H ₂ O at 25 °C: sucrose (■); D-(-)- fructose (◆); D-sorbitol (●); xylitol (▲); maltitol (✱)..	43
Figure 2.1.3 Extraction efficiencies (EE%) of the studied systems for phenolic acids at 25 °C. ■■■ correspond to gallic acid (GA), syringic acid (SA), and vanillic acid (VA), respectively. Chemical structures and log(K _{ow}) values of the studied antioxidants are also presented ²⁷	45
Figure 2.1.4 Extraction efficiencies (EE%) of the studied systems for phenolic acids in the ABS formed by [P ₄₄₄₄]Br + CH + H ₂ O at 25°C, at different pH values. ■■■ correspond to gallic acid (GA), syringic acid (SA) and vanillic acid (VA), respectively.....	47
Figure 2.1.5 Extraction efficiencies (EE%) of the studied systems for phenolic acids in the ABS formed by [P ₄₄₄₄]Br + D-(-)-fructose + H ₂ O at different temperatures. ■■■ correspond to gallic acid (GA), syringic acid (SA) and vanillic acid (VA), respectively.	48
Figure 2.1.6 Scheme of the phenolic acids and ILs recovery, together with the IL recycling process.	49
Figure 2.1.7 Extraction efficiencies (EE%) of the gallic acid in the ABS formed by [P ₄₄₄₄]Br + D-(-)-fructose + H ₂ O in 3 cycles of extraction, where the last two correspond to the recycled IL.....	49
Figure 2.2.1 Chemical structures of the investigated amino acids and schematic view of the proposed process for the selective separation of aliphatic and aromatic amino acids mixtures.....	55
Figure 2.2.2 Chemical structure of the studied ILs.	56

Figure 2.2.3 Phase diagrams of ABS composed of ILs + amino acids + H ₂ O at 25 °C: [P ₄₄₄ (14)]Cl + L-Lys·HCl (▲); [P ₄₄₄₄]Br + L-Lys·HCl (●); [N ₄₄₄₄]Br + L-Lys·HCl (■); [P ₄₄₄₄]Br + L-Pro (◆); [P ₄₄₄ (14)]Cl + L-Pro (—); [P ₄₄₄₁][MeSO ₄] + L-Pro (+); [P ₄₄₄ (14)]Cl + L-Lys (—); [P ₄₄₄₄]Br + L-Lys (*); [P ₄₄₄₁][MeSO ₄] + L-Lys (×).....	59
Figure 2.2.4 Extraction efficiencies of amino acids (<i>EE_{aa}</i> %) in the studied systems at 25 °C. ■ represents the <i>EE_{aa}</i> % of aliphatic amino acids to the IL-rich opposite phase.....	60
Figure 2.2.5 Extraction efficiency (<i>EE_{aa}</i> %) of L-Trp in the system formed by [P ₄₄₄₄]Br + L-Lys + H ₂ O (TLL ≈80), at different pH values (7, 10 and 12).....	62
Figure 3.1.1 Chemical structure of the studied [P ₄₄₄₄]Cl/[P ₄₄₄₄][GB] ILs.....	70
Figure 3.1.2 A Plots of pH vs. mL of 0.1 mol·dm ⁻³ of NaOH/HCl added to 10.0 mL of 0.05 mol·dm ⁻³ of GB-IL ([P ₄₄₄₄][MES] (blue line), [P ₄₄₄₄][TES] (green line), [P ₄₄₄₄][HEPES] (red line), [P ₄₄₄₄][CHES] (magenta line), and [P ₄₄₄₄][TRICINE] (black line)) in water at (25.0 ± 0.1) °C; the reverse titration region is for mL of 0.1 mol·dm ⁻³ of HCl added to 10.0 mL of 0.05 mol·dm ⁻³ of GB-IL. B Buffer capacity as a function of pH for 0.05 M of GB-IL titrated with 0.1 mol·dm ⁻³ of HCl/NaOH at (25.0 ± 0.1) °C.	77
Figure 3.1.3 Protonation equilibria of MES and [P ₄₄₄₄][MES].	77
Figure 3.1.4 A pH titration curves of 1·10 ⁻³ M of MES and [P ₄₄₄₄][MES] at 25 °C and <i>I</i> = 0.1 M of NaNO ₃ . The dashed lines are the calculated pH from the refinement operations. B Species-distribution diagrams of 1·10 ⁻³ M of MES and [P ₄₄₄₄][MES] at 25 °C and <i>I</i> = 0.1 M of NaNO ₃	78
Figure 3.1.5 Plots of pH vs. mL of 0.1 mol·dm ⁻³ of NaOH/HCl added to a mixture of 10.0 mL of 0.05 mol·dm ⁻³ [P ₄₄₄₄][MES]+[P ₄₄₄₄][HEPES]+[P ₄₄₄₄][CHES] at (25.0 ± 0.1) °C.....	79
Figure 3.1.6 A Ternary phase diagrams for the systems composed of IL + K ₃ C ₆ H ₅ O ₇ + water at 25 °C and atmospheric pressure in wt% B and in mol.kg ⁻¹ (right): (●) [P ₄₄₄₄][TRICINE], (●) [P ₄₄₄₄][MES], (●) [P ₄₄₄₄][HEPES], (●) [P ₄₄₄₄][TES], (●) [P ₄₄₄₄][CHES], and (●) [P ₄₄₄₄]Cl.....	81
Figure 3.1.7 Gaussian curve-fitting analysis of amide I spectra of BSA in 0.05 M of [P ₄₄₄₄]Cl (a) and in 0.05 M of [P ₄₄₄₄][TES] at pH 7.4.	84
Figure 3.1.8 The intensity distribution graph of BSA in (0.05 and 0.5) M of [P ₄₄₄₄]Cl/[P ₄₄₄₄][TES]/[P ₄₄₄₄][TRICINE]/[P ₄₄₄₄][HEPES], at pH 7.4 and 25 °C.	85
Figure 3.1.9 σ-profiles of [P ₄₄₄₄]Cl (black line), [P ₄₄₄₄][HEPES] (red line), [P ₄₄₄₄][TES] (blue line), [P ₄₄₄₄][TRICINE] (olive line), [P ₄₄₄₄][CHES] (purple line), and [P ₄₄₄₄][MES] (green line).	86
Figure 3.1.10 Molecular docking of BSA with A [MES] ⁻ , B [CHES] ⁻ , and C [P ₄₄₄₄] ⁺	88
Figure 3.1.11 Size exclusion chromatograms of a BSA solution in PBS (0.5 g L ⁻¹) (—), Bovine serum solution (—), top phase of [P ₄₄₄₄][TRICINE] + K ₃ C ₆ H ₅ O ₇ (—), top phase of [P ₄₄₄₄][TES] + K ₃ C ₆ H ₅ O ₇ (—), top phase of [P ₄₄₄₄][HEPES] + K ₃ C ₆ H ₅ O ₇ (—), top phase of [P ₄₄₄₄][MES] + K ₃ C ₆ H ₅ O ₇ (—), top phase of [P ₄₄₄₄][CHES] + K ₃ C ₆ H ₅ O ₇ (—)..	89
Figure 3.2.1 Chemical structures of the synthesized bio-based ILs.....	100

Figure 3.2.2 Phase diagrams for ABS composed of PPG 400 + bio-based ILs + H ₂ O in wt% (left) and in molality units (right) at 25 °C and under atmospheric pressure. [Ch][Gly] (✕); [Ch][Qui] (◆); [Ch][Gal] (—); [Ch][Pyr] (■), [Ch][Asc] (▲); [Ch][IA] (●). Lines correspond to the fitting of the experimental data using Equation 1.....	102
Figure 3.2.3 Size-exclusion chromatograms of pure IgG and IgG obtained in the bottom phases (IL-rich phases) after extraction and purification by ABS. IgG peak is characterized by a retention time around 15.6 min.....	106
Figure 3.2.4 Extraction efficiencies of IgG (EE_{IgG} %), IgG recovery yield (Y_{IgG} %) and IgG percentage purity (%) from rabbit serum in ABS composed of PPG 400 (30 wt%) + bio-based IL (25 wt%) + 45 wt% of rabbit serum (diluted at 1:10 (v/v); pH ≈ 7).	107
Figure 3.2.5 FTIR spectra of IgG in presence of A 10 mM PBS (pH 7.4), B 25 wt% [Ch][IA] + 30 wt% PPG 400 + H ₂ O, C 25 wt% [Ch][Gly] + 30 wt% PPG 400 + H ₂ O, D 25 wt% [Ch][Asc] + 30 wt% PPG 400 + H ₂ O and E 25 wt% [Ch][Pyr] + 30 wt% PPG 400 + H ₂ O. F SDS-PAGE of IgG at a 200 µg/mL concentration <i>per</i> lane in: PBS buffer 10 mM, pH 7.4 (1), [Ch][IA] (2), [Ch][Gly] (3), [Ch][Pyr] (4), [Ch][Asc] (5), [Ch][Qui] (6) and [Ch][Gal] with 25 wt% of each IL.	109
Figure 4.1.1 Polyacrylamide gel electrophoresis of sRNA in the presence of aqueous solutions of 20 and 50 wt% of the following ILs: [Ch][DHP], [Ch][MES], [Ch][HEPES], [Ch][TES], and [Ch][TRICINE]. RNA control samples without ILs are also included.....	123
Figure 4.1.2 CD spectra (200 – 320 nm) of sRNA in the absence and presence of ILs: (A) 20 and 50 wt% of [Ch][MES]; (B) 20 and 50 wt% of [Ch][DHP]. For each set, the dark green line represents RNA, the red line corresponds to RNA in 20 wt% IL, the brown line to 20 wt% IL, the light green line to RNA in 50 wt% IL, and the blue line to 50 wt% IL. sRNA was incubated for 1 h at 4 °C.	124
Figure 4.1.3 CD melting curves (265 nm) of a sRNA fraction from <i>E. coli</i> DH5α. sRNA was incubated for 1 h at 4 °C with (A) 20 wt% IL, and (B) 50 wt% IL: absence of IL (red); [Ch][MES], blue; [Ch][TES], green; [Ch][HEPES], yellow; [Ch][TRICINE], purple; [Ch][DHP], grey; and Buff[Ch][DHP], pink.	126
Figure 4.1.4 Average zeta potential (mV) of sRNA, ILs in aqueous solution, and ILs with the sRNA fraction from <i>E. coli</i> , at distinct IL concentrations: (A) 20 wt%, and (B) 50 wt%.	127
Figure 4.1.5 Snapshot of a 20-residue long linear sRNA chain in [Ch][MES] and [Ch][DHP] (left and right, respectively). The RNA chain is depicted as purple cartoon and the IL components as teal, yellow and orange spheres for [Ch] ⁺ , [MES] ⁻ and [DHP] ⁻ , respectively. Only ions at a distance up to 4 Å from the chain surface are shown.	129
Figure 4.1.6 CD melting curves (265 nm) of a sRNA fraction from <i>E. coli</i> DH5α at different incubation periods and distinct temperatures. (A) sRNA incubated with 20 wt% of ILs for 15 days	

at room temperature (25 ± 1 °C); (B) for 15 days at 4 °C; (C) for 30 days at room temperature (25 ± 1 °C); and (D) for 30 days at 4 °C: absence of IL (red); [Ch][MES], blue; [Ch][TES], purple; [Ch][HEPES], green; [Ch][TRICINE], yellow; and Buff[Ch][DHP], grey.	130
Figure 4.1.7 Viability of two human cell lines in presence of sRNA-IL aqueous solutions: (A) Fibroblasts, and (B) HeLa cells. Cell viability was measured using the MTS assay, and is shown as percentage of control (%).	132
Figure 4.1.8 Scheme describing the recovery of recombinant <i>E. coli</i> sRNAs from aqueous solutions of GB-ILs and the IL recycling. 3 cycles were successfully carried out with [Ch][MES] and [Ch][HEPES] for mixtures incubated during 1 h.	133
Figure 4.2.1 Chemical structures of the studied [Ch][AA] ILs.....	140
Figure 4.2.2 Electrophoretic analysis of the integrity of RNA in 0.05 % DEPC-treated water and RNA in presence of aqueous solutions of 20 wt% of the studied ILs.	144
Figure 4.2.3 Average zeta potential (mV) of RNA dissolved in 0.05 % DEPC-treated water and in 20 wt% AA-ILs aqueous solutions.	146
Figure 4.2.4 Cytotoxic effect of AA-ILs in two different human cell lines: Fibroblasts (left) and HeLa (right).....	147
Figure 4.2.5 Agarose gel electrophoresis of the ABS coexisting phases at the mixture point: 20 wt% of PPG 400 + 20 wt% of AA-IL + 60 wt% of RNA in DEPC-treated water ($400 \mu\text{g}\cdot\text{L}^{-1}$). RNA in 0.05 % DEPC-treated water was used as control sample and a marker is also included.....	149
Figure 4.2.6 Agarose gel electrophoresis of the ABS coexisting phases at the mixture point: 20 wt% of PPG 400 + 20 wt% of AA-IL + 60 wt% of RNA in DEPC-treated water ($400 \mu\text{g}\cdot\text{L}^{-1}$). RNA in 0.05 % DEPC-treated water was used as control sample and a marker is also included.....	150
Figure 4.2.7 Schematic diagram of the proposed integrated extraction-preservation process of RNA, where all steps occur at <i>ca.</i> 25 °C, while foreseeing its use as biotherapeutic.	151

List of symbols

a_H –	acid concentration	R^2 –	correlation coefficient
a_{eff} –	effective contact area	R_x –	recovery efficiency of compound x
b_H –	base concentration	w_i^j –	weight of component j in the phase i
C_a –	number of moles of strong acid	wt% –	weight percentage
C_b –	number of moles of strong base	v_0 –	initial volume
C_{hb} –	hydrogen-bonding strength coefficient	v_x –	volume of compound x added
CD –	circular dichroism	$Y_x(\%)$ –	yield of compound x
CD^{max} –	highest ellipticity	S –	selectivity
CD^{min} –	lowest ellipticity	sl –	electrode potential slope
E –	potential of the glass electrode	T –	temperature
E° –	standard electrode potential	T_m –	melting temperature
E_{HB} –	hydrogen-bonding energy	T_H –	hydrogen ion concentration
E_i –	total mean interaction energy	τ_{vdW} –	element-specific parameter for dispersion parameters
$E_{i,vdW}$ –	van der Waals interaction energy	x_i –	mole fraction of component i
$E_{i,misfit}$ –	electrostatic interaction energy	$[x]$ –	concentration of component x
E_{vdW} –	van der Waals energy	$[x]_i$ –	concentration of component x in the phase i
$EE_x(\%)$ –	extraction efficiency percentage of component x	α' –	general constant
EC_{50} –	effective concentration yielding 50% of inhibition of the bacteria luminescence	α –	ratio between the weight of the salting-out specie rich phase and the total weight of the mixture
K_{ow} –	octanol-water partition coefficient	σ_{hb} –	polarization charge density for hydrogen bond
K_x –	partition coefficient of component x	γ_i^∞ –	activity coefficient at infinite dilution
mV –	electrode potential	γ –	correction factor for the base concentration.
$peakArea_x^{IL}$ –	HPLC peak area of compound x in the IL rich phase	λ –	wavelength
pK_a	acid dissociation constant		
$P_x(\%)$ –	percentage purity of compound x		
R_H	hydrodynamic radius		

List of abbreviations

AA –	amino acid	L-Cys –	L-cysteine
ABS –	aqueous biphasic system	L-Ile –	L-isoleucine
Ala –	alanine	L-Lys·HCl	L-lysine hydrochloride
A ₂₆₀ –	absorbance values at 260 nm	L-Tyr –	L-tyrosine
A ₂₈₀ –	absorbance values at 280 nm	L-Trp –	L-tryptophan
Azo –	azocaseine	L-Phe –	L-phenylalanine
ATR –	attenuated total reflectance	L-Pro –	L-proline
BSA –	bovine serum albumin	L-Val –	L-valine
GBs –	Good's Buffers	MES –	2-(N-morpholino) ethanesulfonic acid
BHb –	bovine hemoglobin	Myo –	myoglobin
CD –	circular dichroism	Ova –	ovalbumin
CH –	carbohydrate	PBS –	phosphate buffered saline
CHES –	2-(cyclohexylamino)ethanesulfonic acid	PEG –	polyethylene glycol
COSMO –	continuum solvation model	pI –	isoelectric point
Cyt-c –	cytochrome c	PPG –	polypropylene glycol
DL-Asp –	DL -aspartic Acid	RNA –	ribonucleic acid
DESS –	deep eutectic solvents	RNAi –	ribonucleic acid interference
DNA –	deoxyribonucleic acid	TRICINE –	N-[tris(hydroxymethyl)]methyl]glycine
DEPC –	(diethyl pyrocarbonate)-treated water	TL –	tie line
dsRNAs –	exogenous doublestranded RNA	TLL –	tie line length
FBS –	fetal bovine serum	Try –	trypsin
FTIR –	fourier transform infrared spectroscopy	SDS-PAGE–	sodium dodecyl sulfate polyacrylamide gel electrophoresis
HSA –	human serum albumin	SOD –	superoxide dismutase
Gly –	glycine	SEC –	size-exclusion chromatography
Hb –	hemoglobin	SPE –	solid phase extraction
HEPES –	2-[4-(2-hydroxyethyl)piperazin-1-yl]ethanesulfonic acid	UV-Vis –	ultraviolet–Visible
HPLC –	high-performance liquid chromatography		
HRP –	horseradish peroxidase		
Ig –	immunoglobulin		
IL –	ionic liquid		
Leu –	leucine		
Lys –	lysine		
L-Ala –	L-alanine		
Lyz –	Lysozyme		
L-Arg –	L-arginine		
L-Asn –	L-asparagine		

List of acronyms

Ionic liquid cations

[Ch]⁺– cholinium
[C₄mim]⁺– 1-butyl-3-methylimidazolium
[C₂mim]⁺– 1-ethyl-3-methylimidazolium
[N_{011(2OH)}]⁺– N,N-dimethylethanolamine propionate
[N₄₄₄₄]⁺– tetrabutylammonium
[N₃₃₃₃]⁺– tetrapropylammonium
[N₄₄₄(OC₂)]⁺– tri(n-butyl)[2-ethoxy-2-oxoethyl]ammonium
[P₄₄₄₁]⁺– tributylmethylphosphonium
[P₄₄₄₄]⁺– tetrabutylphosphonium
[P₄₄₄₂]⁺– ethyl(tributyl)phosphonium
[P_{i(444)1}]⁺– tri(isobutyl)methylphosphonium
[P₄₄₄₍₁₄₎]⁺– tri(isobutyl)methylphosphonium
[P₄₄₄(OC₂)]⁺– tri(n-butyl)[2-ethoxy-2-oxoethyl]phosphonium

Ionic liquid anions

[Abt][–]– abietate
[Ac][–]– acetate
[Arg][–]– arginate
[Asc][–]– L-ascorbate
[Asp][–]– asparaginate
Br[–]– bromide
Cl[–]– chloride
[CF₃SO₃][–]– trifluoromethanesulfonate
[DHP][–]– dihydrogenphosphate
[Et₂PO₄][–]– diethylphosphate
[Gal][–]– galactouronate
[Gen][–]– genistisinate
[Gly][–]– glycolate
[Glu][–]– glutamate
[IB][–]– indole-3-butyrate
[Lac][–]– lactate
[Lys][–]– lysinate
[MeSO₄][–]– methylsulphate
[DCA][–]– dicyanamide
[TOS][–]– tosylate
[Pyr][–]– pyruvate
[Pro][–]– propionate
[Qui][–]– quinate

1. Introduction

1.1. Scopes and objectives

Significant attention is given today on the development of integrated and sustainable technologies to extract and purify bioactive compounds, such as antioxidants, amino acids, proteins and nucleic acids, which should be able to preserve or improve their biological activities¹. However, separation techniques are complex in nature due to the multi-step approaches required and difficulties in isolating the target compounds at high yields, with high purity levels and preserved biological activities. Separation techniques such as distillation, centrifugation, dialysis, induced precipitation and solid-phase extraction, including chromatographic techniques, are commonly applied². Some of these processes may present several drawbacks when dealing with biologically active compounds, which in addition to low recovery yields and poor selectivity, may also compromise their stability and biological activity. Accordingly, over the years, separation techniques have been optimized with the goal of being cost-effective, integrated and sustainable, while allowing the preservation of the stability and biological activity of the target compounds³⁻⁵.

The main objective of this PhD work consists on the development of cost-effective separation techniques for bioactive compounds, namely antioxidants, amino acids, proteins and nucleic acids, by the use of aqueous biphasic systems (ABS) formed by ionic liquids (ILs). Not only the extraction and purification steps have been considered, but also the development of integrated strategies in which one of the ABS phases could act as the preservation media. ABS were chosen due to their high-water content, whereas ILs were considered as phase-forming components due to their tailoring abilities by their chemical structure design. Despite the efforts carried out by different authors on the use of IL-based ABS for the extraction of biocompounds⁶, the ILs preferentially chosen display moderate toxicity and low biodegradability. Most studies based on IL-based ABS comprise ILs formed by imidazolium cations and fluorinated anions. In this work, other ILs families of a more biocompatible nature have been investigated. There are also significant concerns associated to inorganic salts when dealing with biologically active compounds, and alternative phase-forming components to create IL-based ABS were investigated, such as polymers, amino acids and carbohydrates.

This PhD thesis starts with an overview of the literature (Chapter 1) on the use of ionic liquids as preservation media of the target biocompounds of this thesis, namely antioxidants, amino acids, proteins and nucleic acids, and on the use of aqueous biphasic systems formed by ILs for the extraction and purification of biomolecules. Chapter 1 is presented according to the biocompounds classes, namely: (i) antioxidants and amino acids as representatives of small molecules; (ii) proteins and antibodies; and (iii) nucleic acids. Chapter 2 comprises the works

developed with ABS formed by more biocompatible ILs and compounds derived from biological sources, as carbohydrates and amino acids, to extract and separate small biomolecules (antioxidants and amino acids). Chapter 2.1 reports on the development of a novel type of IL-based ABS, where non-aromatic and non-fluorinated (tetraalkylphosphonium and tetraalkylammonium-based) ILs were combined with carbohydrates to form ABS. In addition to the ternary phase diagrams characterization, their potential as extractive platforms for antioxidants (gallic, vanillic and syring acids) was evaluated, revealing that these systems are competitive in terms of extraction performance. Chapter 2.2 comprises the use of ABS formed by phosphonium- and ammonium-based ILs and aliphatic amino acids, namely L-Proline, L-Lysine and L-Lysine-HCl. Their application in the extraction of aromatic amino acids (L-phenylalanine and L-tryptophan) was ascertained, allowing to propose an integrated platform to simultaneously separate mixtures of aliphatic and aromatic amino acids from fermentation media or from protein hydrolysates. In summary, the described works comprise ABS formed by more biocompatible ILs and salting-out agents, envisioning the development of efficient and sustainable extraction/purification platforms.

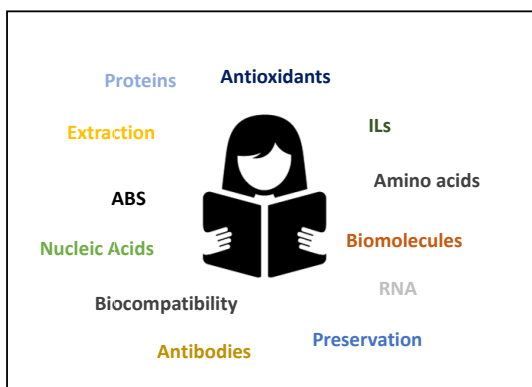
In Chapter 3.1, biological buffers (Good's buffers) commonly used in biochemical and biological studies were used as anions of tetrabutylphosphonium-based ILs, allowing to create ABS with the organic salt potassium citrate. These ILs were synthesized and characterized, and the respective ternary phase diagrams determined. Their separation performance was evaluated towards bovine serum albumin (BSA), both from model solutions and from real bovine serum samples. Chapter 3 ends with the application of IL-based ABS as alternative methods to improve the downstream processing of antibodies. In Chapter 3.2, biocompatible ILs, comprising the cholinium cation and anions derived from natural acids, were combined with polypropylene glycol with a molecular weight of 400 g·mol⁻¹ (PPG 400) to form ABS to purify IgG from rabbit serum. The stability of IgG before and after the extraction step was investigated. The two works demonstrate the high performance of IL-based ABS to recover proteins from real samples, such as bovine and rabbit sera, without compromising the proteins stability.

RNA isolation and their medium/long-term stability are still major challenges given their high susceptibility to ribonucleases degradation. Thus, novel techniques which could afford both the purification and preservation of nucleic acids are in crucial demand. Chapter 4 comprises a series of works in which these challenges were considered for RNA. Chapter 4.1 describes the potential of aqueous solutions of cholinium-based ILs combined with anions derived from Good's buffers as preservation media of recombinant small RNAs from *Escherichia coli*. The appraisal of these solutions as potential stabilizing and preservation media of RNA was carried out based on the integrity and structural stability of RNA and cytotoxicity of the aqueous solutions. RNA was

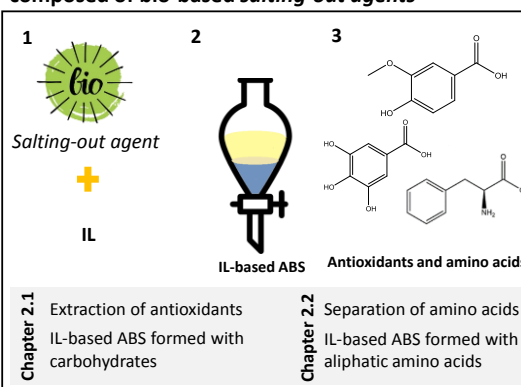
recovered from the ILs aqueous solutions and the IL was recycled. Chapter 4.2 is focused on the development of integrated extraction-preservation processes using IL-based ABS. Based on the fact that amino acids have been used as affinity ligands in chromatographic strategies to separate RNA, ILs formed by the cholinium cation and different amino acids as anions were studied. ABS formed by ILs and PPG 400 were appraised to extract RNA from a lysate sample, after which the IL-rich phase was successfully used as the preservation medium. RNA was recovered from the IL-rich phase and the IL was recycled.

The current thesis comprises a set of works with a common goal: creation of more sustainable and efficient IL-based ABS to extract, purify and preserve high-value biomolecules. New types of IL-based ABS formed by new combinations of phase-forming components are herein presented. Most of the works carried out address not only the target compound recovery and biological activity, but also the ILs and additional solvents recycling. To a better understanding of this thesis organization, a schematic representation of its layout is given in Figure 1.1.

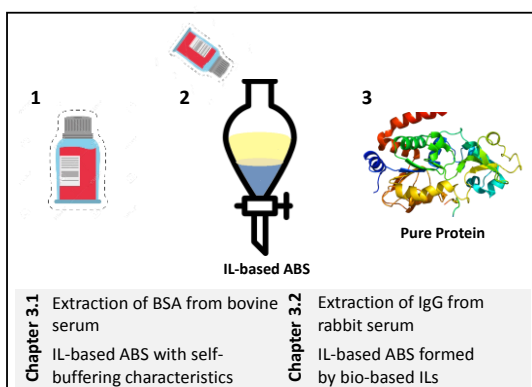
1. Introduction



2. Extraction of biocompounds with ABS composed of bio-based salting-out agents



3. Proteins extraction/purification using IL-based ABS



4. Integrated extraction-preservation strategies for RNA

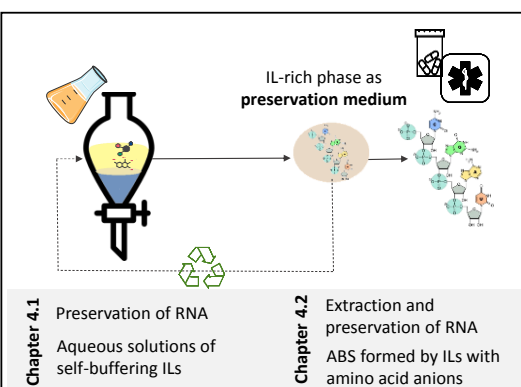


Figure 1.1 Layout of the current thesis.

1.2. Ionic liquids (ILs)

The introduction of the “Green Chemistry” concept⁷ triggered the research on more benign solvents and processes; the introduction of the twelve principles of Green Chemistry and the increased importance of sustainable development changed the path by which biotechnological processes are being created. The increasing research on novel materials and solvents that have a minor impact on the environment and health has become a priority. Among neoteric solvents investigated within the Green Chemistry field, ionic liquids (ILs) have been one of the most investigated classes. Undoubtedly, water is the greenest solvent overall, and as such, aqueous solutions of ILs should be considered as more environmentally friendly alternative solvents of lower cost.

ILs are salts typically composed of a large and asymmetric organic cation and an organic or inorganic anion⁸. Due to the large size of their ions, ILs tend to be liquid at temperatures close to room temperature. They have fascinating properties, such as high chemical, thermal and electrochemical stability, non-flammability, negligible volatility at atmospheric conditions (displayed by aprotic ILs), excellent solvation capacity for organic and inorganic species, and are able to act as improved stabilizing media for valued-added biocompounds, such as proteins and nucleic acids^{9, 10}.

ILs have been used as solvents¹¹, co-solvents¹², reagents in biocatalysis¹³, proteins¹⁴ and nucleic acids preservation¹⁵, and as extraction solvents of a wide range of biomolecules⁶. Over the last two decades, ILs have evolved from potential solvents for the solubilisation and preservation of biomass^{16, 17} and bioactive compounds¹¹, to selective solvents for the extraction and purification of a large number of biomolecules^{6, 18, 19}, as schematically represented in Figure 1.2. Several authors demonstrated that ILs and their aqueous solutions can enhance the stability of proteins, enzymes and DNA²⁰. Different studies have linked these ILs features to their cation and anion chemical structures, and since it is possible to create the most suitable IL to a target application, they are also known as “designer solvents”⁶. This tunable designer character thus allows the development of more effective biotechnological platforms¹⁸.

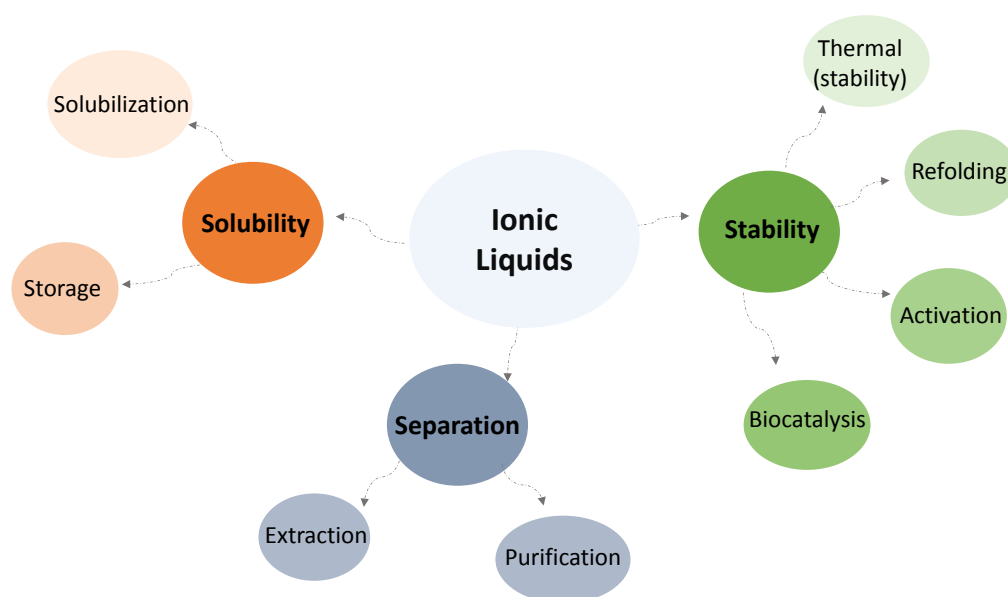


Figure 1.2 Most common applications of ionic liquids.

Besides all the benefits of ILs as solvents in biotechnological applications, their biocompatibility is still the main challenge. To this end, ILs should be biocompatible and of low toxicity. However, several studies have shown that ILs may display relevant eco- and cytotoxicity²¹. It has been shown that their toxic features are highly dependent on their chemical structure, being widely accepted that the head group of the cation has a deciding role in the toxicity and longer alkyl side chains (higher hydrophobic character) have a more severe effect²¹. However, the toxicity of the IL anion, although usually with a lower impact, cannot be neglected²¹. Among the several chemical characteristics of ILs, the ILs toxicity is usually higher when aromatic rings and fluorinated anions are present²².

The most commonly studied IL cations are pyrrolidinium, imidazolium, piperidinium and pyridinium, usually combined with halogens (chloride, bromide) or fluorinated anions (hexafluorophosphate, tetrafluoroborate and bis(trifluoromethylsulfonyl)imide). Their use in a wide number of applications related with biomolecules (activity, stability, kinetic, stability and separation) has been published²³, although some disadvantages such as high cost, high toxicity and low biodegradability may be associated to most of these ILs²¹. More recently, new IL classes have been proposed, based on the combination of anions derived from carbohydrates, amino acids, organic acids, alkylsulfates, or alkylphosphates, most of the times combined with the cholinium cation²¹. Figure 1.3 summarizes some chemical structures of ILs and how they evolved along time.

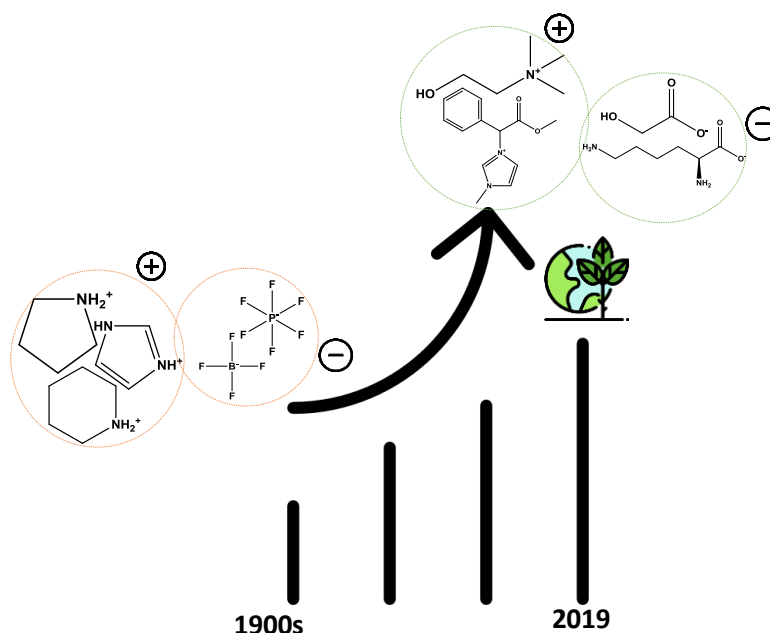


Figure 1.3 Evolution of the ionic liquid's applications according to their chemical structures.

1.2.1. IL as preservation media

It has been reported that the stability and activity of biomolecules, such as proteins and nucleic acids, can be significantly enhanced by ILs²⁴. For instance, ILs and their aqueous solutions have shown to keep or improve the enzymatic activity of several enzymes, such as Lipases (*Candida Antarctica* lipase B^{25, 26}, *Pseudomonas Cepacia* lipase²⁷ and *Candida Rugosa* lipase²⁸), penicillin G acylase²⁹, α -chymotrypsin³⁰, cellulase³¹ and laccases^{32,33}, which are important results when foreseeing their application in biocatalysis²⁴. Moreover, ILs are also effective solvents for the storage and preservation of proteins and nucleic acids with pharmaceutical potential²⁴. Heller et al.²³ proved that the solubilisation of proteins in ILs can be a solution to avoid aggregation and to improve their stability²³. Fujita and Ohno³⁴ investigated the effectiveness of dihydrogen phosphate ([Ch][DHP]) as a novel solvent for metalloproteins. [Ch][DHP] effectively dissolves these proteins, while preserving their native and secondary structure³⁴. Despite these good results, recent studies proved that ILs aqueous mixtures are preferred, because of the higher solubilities and/or increased stabilities afforded, as well as the reduced associated costs³⁵. Baker and Heller³⁶ demonstrated that aqueous mixtures of 1-butyl-3-methyl imidazolium chloride ([C₄mim]Cl) influence the structure of cytochrome c (cyt-c) and human serum albumin (HSA) in a concentration dependent way. Depending on the protein used, [C₄mim]Cl has a different impact in the oligomerization state³⁶. Attri et al.³⁷ found a relation between the ILs hydrophobicity and their stabilizing effects³⁷. The authors³⁷ demonstrated that less hydrophobic ILs such as tetraethylammonium acetate ([N₂₂₂₂][Ac]) and

tetraethylammonium phosphate $[N_{2222}][PO_4]$ are able to stabilize α -chymotrypsin, while more hydrophobic ILs do not favour the protein stability³⁷, being in agreement with other works in the literature with the proteins lysozyme³⁸ and BSA³⁹.

In addition to proteins and enzymes, nucleic acids are also macromolecules that easily lose their stability and integrity⁴¹. Motivated by this challenge, Vijayaraghavan et al.⁴² investigated the stability of DNA in a series of hydrated cholinium-based ILs⁴². The authors found⁴² that the chemical and structural stability of DNA is preserved up to one year using ILs. Despite the good results achieved, it is known that factors like pH, temperature, and ionic strength can affect the DNA helical structure⁴¹. Therefore, these are parameters that need to be carefully considered when “building” bioprocesses for these macromolecules. The stability of siRNA in ILs aqueous solutions has also been investigated, showing that aqueous solutions of [Ch][DHP] improve the biological stability of siRNA in the presence of RNase A, prolonging the macromolecule shelf life for up to three months⁴³. The authors⁴³ suggested that with a properly-designed IL it is possible to eliminate the need for lyophilization or refrigeration for siRNA storage, while facilitating the siRNA transportation and handling.

In summary, using adequate ILs as solvents allows to prevent protein denaturation and/or aggregation, enhance enzymatic activity, and the preservation of the DNA and RNA native structure. However, given the plethora of ILs chemical structures and value-added biomolecules with relevant biological characteristics, further studies are still essential while carefully controlling factors such as the ILs hydrophobicity, polarity, viscosity and ionic strength that may influence the solubilisation and stabilization of different biomolecules.

1.2.2. IL-based aqueous biphasic systems (IL-based ABS) as separation processes

Most biologically relevant compounds are produced or are present in complex media, thus requiring extraction and purification steps. The recovery and purification steps of bioactive compounds are however the main responsible for the current high cost of most of these products⁴⁴. Therefore, there is a crucial demand on the development of cost-effective and sustainable processes. Among these, aqueous biphasic systems (ABS) have been investigated for the recovery and purification of a wide diversity of biocompounds⁴⁵.

ABS were first presented to the scientific community in 1896, when Beijerinck discovered that agar and gelatin formed two aqueous phases when mixed at certain concentrations in aqueous media⁴⁶. However, only in the 1950s, ABS were recognized as an extractive/separation technique by Albertson⁴⁷. ABS are liquid-liquid systems that can act as liquid-liquid extraction approaches, consisting in two immiscible aqueous-rich phases that can be created by mixing two polymers, a polymer with a salt or two salts in aqueous media¹⁸. Due to their water-rich content,

and thus biocompatible nature that can be achieved by the proper selection of the phase-forming components and compositions, ABS have been applied in the purification of different biological entities, such as cells, virus, organelles, nucleic acids, lipids, amino acids, proteins, enzymes and antibodies⁴⁸⁻⁵⁰. This technique comprises a large number of interesting characteristics; it is relatively simple and inexpensive, easily operated and scaled-up, has a high-resolution capacity and allows the clarification, purification and concentration steps to be integrated^{48, 49}.

Traditional polymer-based ABS have been investigated for decades⁵¹; however, they usually present a high viscosity and lack of tailoring ability due to the constraints associated to the polymers chemical structures and salts employed. For instance, polymer-polymer systems display two immiscible phases with high hydrophobic character that lead to minimal polarities differences between the phases, whereas salt-polymer systems have a highly hydrophobic phase and a highly hydrophilic and high ionic strength phase¹⁸. In 2003, Rogers and co-workers⁵² proposed novel ABS by mixing ILs with salts, which have proved later to overcome the major drawbacks associated to traditional polymer-based ABS⁵³.

The main advantage of using ILs in ABS relies on their tailored solvation/extraction ability, which arises from the proper manipulation of their cation/anion chemical structures^{6, 54}. With the replacement of the polymer- or salt-rich phases by an IL-rich phase, it is possible to tailor the phases' polarities⁶. Moreover, IL-based ABS are substantially less viscous than polymer-based ABS, displaying faster phases separation rates^{55, 56}. Further advantages can be associated to the ILs application in ABS when used as substitutes of inorganic salt. For instance, the ABS corrosive character is decreased, and the salts precipitation is also avoided (a result of the ILs lower melting temperatures and higher water solubility)⁵⁷.

Due to the plethora of available water miscible ILs, it is possible to combine them with a vast range of compounds. It has been shown that IL-based ABS can be created with salts, polymers, amino acids and carbohydrates^{18, 58}. Figure 1.4 summarizes the phase-forming components that can be used to create IL-based ABS and their advantages and disadvantages. Regarding the underlying mechanisms for ABS formation, it has been demonstrated that salts, amino acids and carbohydrates induce the salting-out of the IL⁵⁹, whereas the phenomenon related to IL-polymer mixtures is more complex, where polymer-IL interactions play an important role⁶⁰. These mechanisms are also summarized in Figure 1.4. It should be however remarked that contrarily to salts, there is a reduced number of ILs able to undergo liquid-liquid demixing in aqueous media when combined with amino acids, carbohydrates or Good's buffers due to their weak salting-out ability⁶.

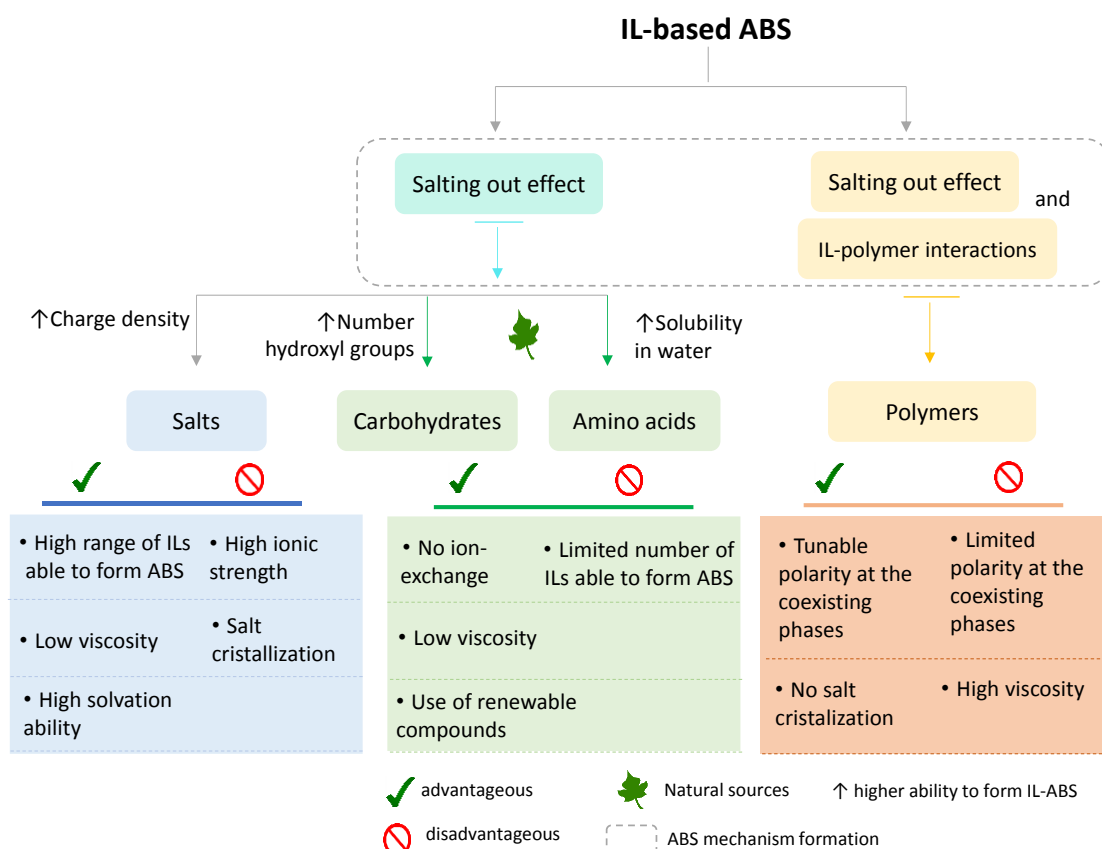


Figure 1.4 Scheme of the different phase-forming components used to create IL-based ABS, mechanisms involved, and advantages and disadvantages of these systems.

When the goal is to create effective extraction/purification systems for a given biomolecule using IL-based ABS, it has to be taken into account that different parameters related to the system properties influence the partition behaviour of a target product through the ABS coexisting phases^{61, 62}. Thus, it is necessary to have into account factors such as the ionic strength, pH, temperature, and type and concentration of the phase-forming components⁶². In addition to these, the partitioning of solutes in IL-based ABS is also ruled by solute–solvent and specific solute–IL interactions⁶³. Salting-out effects, water content in the phases, and hydrophobic, hydrogen-bonding and Coulombic interactions between the target compound and the IL have been described as the main factors affecting the solutes partitioning in IL-based ABS¹⁸. Regarding the target compound to be extracted, properties like size and polarity also need to be considered⁶⁴.

Different studies on biomolecules partitioning in IL-based ABS demonstrated that in the presence of a salt with a strong salting-out character, *e.g.* tripotassium phosphate (K_3PO_4) or sodium carbonate (Na_2CO_3), biomolecules preferentially partition to the IL-rich phase due to the

exerted salting-out effect⁶⁵⁻⁶⁷. Further studies demonstrated that the migration pattern of solutes in IL + salt and in IL + polymer ABS may be ruled by hydrophobic interactions⁶⁸⁻⁷⁰ and electrostatic interactions^{70, 71}. Accordingly, the separation of target solutes can be improved by changing the phase-forming components nature and by changing the hydrophobic properties of a given phase by varying parameters such as tie-line length (TLL) or water content⁶. When considering electrostatic interactions and solutes that may suffer speciation according to the pH, the pH of the system may be also manipulated in order to promote enhanced separations⁷². It has been shown that the biomolecules extraction in IL-based ABS is an endothermic process, with an increase in the extraction efficiency as temperature increases⁷³. Still, it is always necessary to be aware of the target compound temperature limitations in what concerns its stability⁷⁰. Overall, the selection of the ABS conditions (phase-forming components, composition, temperature, pH) must be carried out based on the physicochemical properties of the target compound and contaminants in order to achieve improved separations, without compromising their structure and stability.

Based on the exposed, it is necessary to consider a balance between the properties of the ABS phase-forming components, nature of the target compounds and process conditions in order to achieve high extraction efficiencies, recovery yields and purity levels. An overview of the biomolecule's properties considered in this PhD thesis and the application of IL-based ABS for their extraction and purification is provided below.

1.3. Extraction and purification of biocompounds using IL-based ABS

1.3.1. Antioxidants and amino acids

Diminished levels of antioxidants and the increased production of reactive species lead to oxidative stress, which is responsible for the acceleration of aging and an underlying factor in the pathogenesis of wide range of diseases, such as cancer, cardiovascular diseases, neural disorders, among others⁷⁵. In 1995, antioxidants were defined as “any substance that when present at low concentrations compared with that of an oxidizable substrate significantly delays or inhibits the oxidation of that substrate”⁷⁶. Through the years, this definition underwent some updates, and an antioxidant is a substance that delays the oxidation of proteins, carbohydrates, lipids and DNA⁷⁷.

The antioxidant activity occurs by different paths: as inhibitors of free radical oxidation reactions by inhibiting formation of free lipid radicals; by interrupting the propagation of the autoxidation chain reaction (chain breaking antioxidants); as singlet oxygen quenchers; through synergism with other antioxidants; as reducing agents which convert hydroperoxides into stable compounds; as metal chelators that convert metal pro-oxidants (iron and copper derivatives) into stable products; and as inhibitors of pro-oxidative enzymes (lipooxygenases)⁷⁸.

Antioxidants are categorized into two major groups: enzymatic and non-enzymatic oxidants⁷⁹. The major classes of compounds with antioxidant activity are non-enzymatic ones, such as vitamins (vitamin C and vitamin E), carotenoids (carotenes and xanthophylls) and polyphenols (flavonoids, phenolic acids, lignans and stilbenes)⁸⁰. For human beings these three groups of antioxidants are exogenously obtained as part of a diet or as dietary supplements, being phenolic acids, secondary plant metabolites, the most important for dietary applications⁸⁰. Moreover, polyphenolic extracts are attractive ingredients for cosmetics and pharmacy due to their beneficial biological properties⁸¹. Phenolic acids work as chelators and free radical scavengers with impact over hydroxyl and peroxy radicals, superoxide anions, and peroxynitrites⁸². Depending on the number and location of hydroxyl groups on the aromatic ring, phenolic acids can be divided into two categories: derivatives of benzoic acid and derivatives of cinnamic acid⁸³. These compounds are formed by a benzene ring bonded to a carboxylic group (benzoic acids) or to a propenoic acid (cinnamic acids). Hydroxycinnamic acid derivatives include ferulic, caffeic, p-coumaric and sinapic acids, while hydroxybenzoic acid derivatives comprise vanillic, syringic, gallic and protocatechuic acids⁸⁴. Their chemical structures are provided in Figure 1.5.

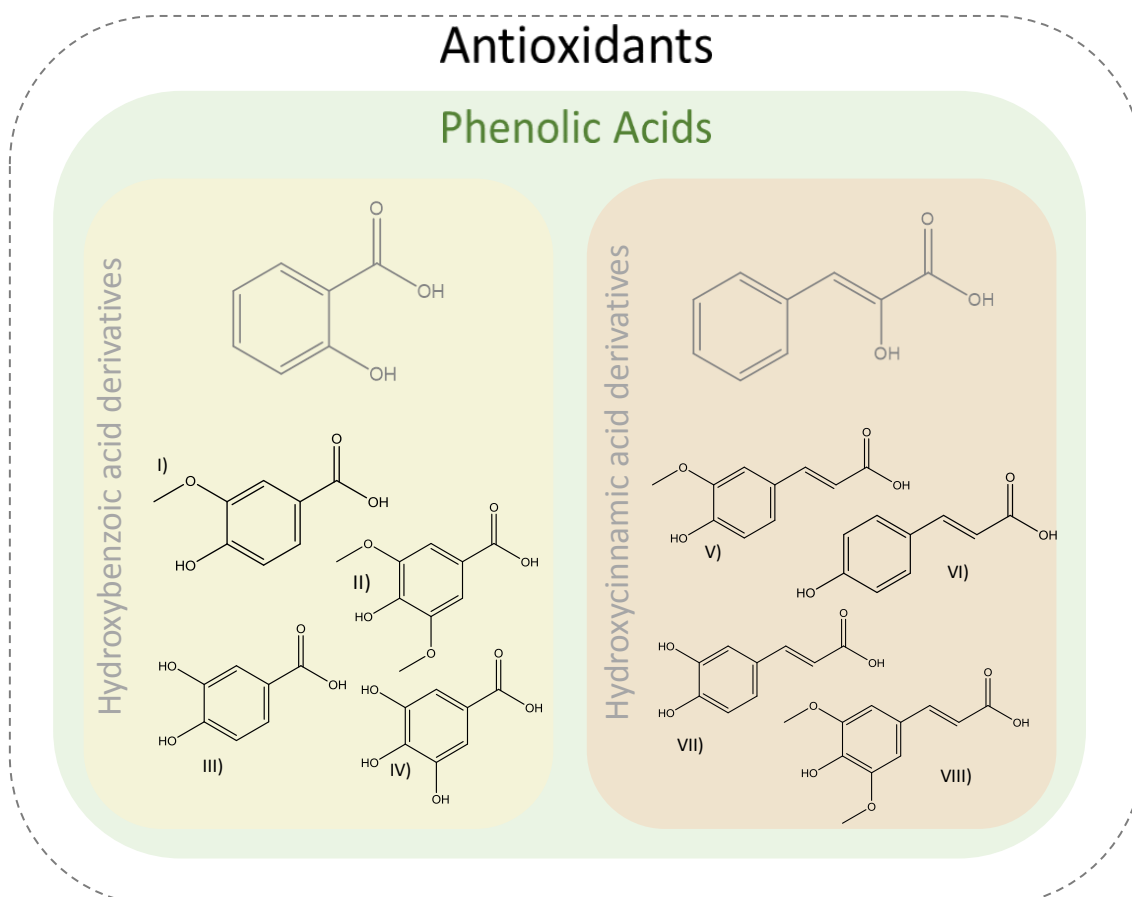


Figure 1.5 Chemical structures of hydroxybenzoic and hydroxycinnamic acid derivatives: I) vanillic acid; II) syringic acid, III) protocatechuic acid; IV) gallic acid; V) ferulic acid; VI) p-coumaric; VII) caffeic acid; and VIII) sinapic acid.

Cinnamic and benzoic acid derivatives exist in virtually all plant foods (*e.g.* fruits, vegetables, and grains) and are physically dispersed throughout the plant in seeds, leaves, roots, and stems⁸⁵. Phenolic acids are generally esterified or in a glycosylated form in plants, and only a minor fraction exists as “free acids”. These different forms of phenolic acids show variable suitability for different extraction conditions and vary in their susceptibility to degradation⁸⁶. The majority are linked through ester, ether, or acetal bonds, either to structural components of the plant or to other natural products (*e.g.* flavonoids, glucose, terpenes)^{87, 88}.

The relevance of phenolic acids has led to the development of effective techniques for their extraction and purification. Liquid-liquid and solid-phase extraction (SPE) are commonly used techniques⁸⁹, while using solvents such as methanol, ethanol, acetone, diethyl ether, and ethyl acetate⁹⁰. Soxhlet extraction is commonly applied to extract phenolic acids from biomass samples. More recent extraction methods including ultrasound-assisted extraction, microwave-assisted extraction, ultrasound-microwave-assisted extraction, and supercritical fluid extraction. Although these methods allow to achieve short extraction times and decrease the consumption

and release of volatile organic solvents, they require a higher initial investment⁹¹. Following the extraction step, purification may be also required, in which solid-phase extraction is one of the most used techniques to purify phenolic acids⁹².

With the goal of Identifying novel and effective purification platforms for antioxidants, IL-based ABS have been largely investigated for the separation of vanillin, gallic acid, vanillic acid, and syringic acid⁵⁵. In two pioneering works^{55, 93}, imidazolium-based ILs were combined with K_3PO_4 for vanillin extraction and with dipotassium phosphate (K_2HPO_4), monopotassium phosphate (KH_2PO_4) and sodium sulfate (Na_2SO_4) for the separation of gallic acid.

Both works showed that the extraction capacity of these systems is strongly affected by the pH, which is due to the low pK_a values of vanillin and gallic acid^{55, 93}. Cláudio et al⁹³ shown that vanillin preferentially migrates to the IL-rich phase, while at low pH values the neutral form of gallic acid favourably migrates to the IL-rich phase and at high pH values its anionic form concentrates in the salt-rich phase. This pH-driven phenomenon was later demonstrated to be of high relevance in the fractionation of mixtures of phenolic compounds and to proceed with back extraction studies and solvent reuse⁹⁴. Remarkably, in each extraction cycle, the IL recovery efficiency was between 94 and 95%, without losses in the extractive performance of the corresponding ABS⁹⁴.

In 2015, the isolation of high purity secoisolariciresinol diglucoside, a multi-functional pharmaceutical, from flaxseed, was improved with an ultrasonic-assisted extraction followed by IL-ABS formation by the addition of Na_2SO_4 ⁹⁵. Similarly, it was possible to fractionate and recover bioactive hydroxycinnamic compounds from stressed carrot by using IL-ABS formed by $[C_2mim][Ac]$ /potassium based buffers⁹⁶, where recovery yields up to 85.4% were achieved. Santos et al.⁹⁷ used an IL-based ABS (composed of PEG and sodium polyacrylate and ILs as electrolytes) as an integrated approach for the fractionation of phenolic compounds from a complex matrix⁹⁷. Again, a pH-driven phenomenon was observed, being the electrostatic interactions between the anionic form of the phenolic acids and the ILs identified as the driving forces in separation. After the successful fractionation of phenolic compounds, their isolation and recycling of the phase-forming components were demonstrated⁹⁷. In all these studies imidazolium-based ILs were used to create ABS, thus reinforcing the work carried out in this PhD thesis on the finding of more biocompatible alternatives.

Amino acids are found in living organisms in both their free forms and bound by amide linkages in peptides and proteins⁹⁸. Known as the “building blocks” of proteins, enzymes, and other compounds present in the human body, amino acids play an important role in several physiological phenomena (metabolism, gene expression, signal transduction). Amino acids play a vital role in energy production, energy transfer, and muscle activity⁹⁹. Therefore, amino acids

are critical compounds in animal and human nutrition, being also employed in clinical, cosmetic, and food industries⁹⁹.

Amino acids are amphoteric molecules, which depending on the pH of the surrounding medium. Amino acids have a characteristic isoelectric point (pI), which largely depends on the nature of their side chain. Mono amino monocarboxylic amino acids (with non-ionizable R groups) are diprotic acids at low pH and exist in several ionic forms as the pH is increased. Amino acids with ionizable R groups have additional ionic species, depending on the pH of the medium and pK_a of the R group¹⁰⁰. Amino acids are classified as neutral, acidic and basic¹⁰¹. The neutral amino acid group is the largest one, comprising phenylalanine (Phe), tyrosine (Tyr), proline (Pro), tryptophan (Trp), histidine (His), serine (Ser), threonine (Thr), glycine (Gly), leucine (Leu), isoleucine (Ile), alanine (Ala), valine (Val), cysteine (Cys) and methionine (Met)¹⁰¹. The acidic amino acid group comprises aspartic acid (Asp) and glutamic acid (Glu), while the basic amino acid group comprises arginine (Arg), lysine (Lys) and histidine (His)¹⁰⁰.

The amino acids solubility in water is directly related to their structure. Hydrophobic amino acids are formed by nonpolar side chains, such as alkyl groups or aromatic groups. On the other hand, hydrophilic neutral amino acids contain functional groups able to form hydrogen bonds with water, such as hydroxyl (-OH) and sulfhydryl (-SH) groups. The hydrophilic acidic amino acids have a second carboxyl group attached to their R group (Asp and Glu), while hydrophilic-basic amino acids have R groups formed either by a second primary amino group (Lys), a guanidino group (Arg) or an imidazole group (His). The solubility character of each amino acid is reflected in their hydropathic index, a scale used to measure the tendency of an amino acid to partition to an aqueous environment (negative values) or a hydrophobic environment (positive values)¹⁰⁰. Table 1.1 summarizes the physical and chemical properties of amino acids found in proteins¹⁰⁰.

Table 1.1 Physical and chemical properties of amino acids found in proteins¹⁰⁰.

Amino acid	Mw (g/mol)	pK _{a1}	pK _{a2}	pK _r	pI	Hydrophathic index
Nonpolar						
Aliphatic R groups						
Gly	75	2.34	9.60		5.97	-0.4
Ala	89	2.34	9.69		6.01	1.8
Val	117	2.32	9.62		5.97	4.2
Leu	131	2.36	9.60		5.98	3.8
Ile	131	2.36	9.68		6.02	4.6
Met	149	2.28	9.20		5.74	1.9
Pro	115	1.99	10.96		6.48	1.6
Aromatic R groups						
Phe	165	1.83	9.13		5.48	2.8
Tyr	181	2.20	9.11	10.07	5.66	-1.3
Trp	204	2.38	9.39		5.89	-0.9
Polar						
Uncharged R groups						
Ser	105	2.21	9.15		5.68	-0.8
Thr	119	2.11	9.62		5.87	-0.7
Cys	121	1.96	10.28	8.18	5.07	2.5
Asn	132	2.02	5.41		5.41	-3.5
Gln	146	2.17	9.13		5.65	-3.5
Positively charged R groups						
Glu	147	2.19	9.67	4.2	3.22	-3.5
Asp	133	1.88	9.60	3.6	2.77	-3.5
Negatively charged R groups						
Lys	146	2.18	8.95	10.53	9.74	-3.9
His	155	1.82	9.17	6.00	7.59	-3.2
Arg	174	2.17	9.04	12.48	10.76	-45

The amino acids separation field is quite complete when considering their derivatization and use of chromatographic techniques¹⁰²; however, less attention has been paid to the downstream processing of natural-derived amino acids, which usually comprises several stages: solvent extraction, centrifugation and/or filtration¹⁰³, and/or concentration/crystallisation^{104, 105} steps. Usually, during these sequential methods are employed aggressive solvents like perchloric acid or hydrochloric acid, formic acid, methanol, among others¹⁰⁶⁻¹⁰⁸. If a chromatographic step is

further needed, there is an increase in the process cost and extraction time¹⁰⁹. Wastes will also be larger¹⁰⁷.

Aiming at identifying alternative separation processes for amino acids, in 2009, IL-based ABS were for the first time used in the extraction of the essential amino acid L-Trp, where two similar works^{110, 111} were published. In the two works, L-Trp presented a preferential migration to the IL-rich phase, and compared to the cation effect, the IL anion influence on the amino acids partitioning revealed to be less relevant. These works demonstrated that IL-based ABS allow extractions substantially more extensive than those obtained with conventional PEG-based ABS, reinforcing the suitability of IL-based ABS to recover L-Trp and perhaps other amino acids. After these works, different amino acids were successfully extracted by this technique (their names and chemical structures are given in Figure 1.6). The most relevant works and results are discussed below. The partitioning behaviour of L-Trp, Gly, Ala, Val and Leu in ABS formed by imidazolium-based ILs paired with acetate or bromide anions was investigated^{112, 113}, where it was found that more hydrophobic IL cations lead to best extraction results^{112, 113}. Nevertheless, this trend was not obtained with different IL families. The ILs' type/family directly influences the occurrence of different interactions between ILs and amino acids¹¹⁴.

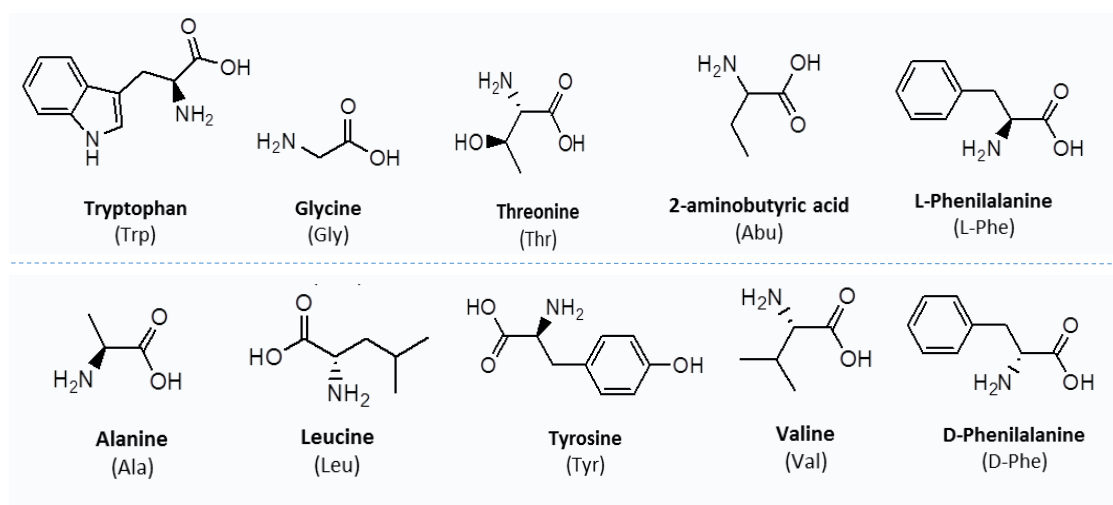


Figure 1.6 Chemical structures, names and abbreviations of all amino acids extracted and separated with IL-based ABS.

After a first series of works on the use of imidazolium-based ILs, the concern on the true sustainability of IL-based ABS started to emerge, and researchers moved to more biocompatible and biodegradable ILs. In this line, ABS formed by ILs comprising the cholinium cation and long chain carboxylate anions were used to extract amino acids¹¹⁵. With the same goal, Zafarani-Moattar and Hamzehzadeh⁶⁸ introduced an organic salt to avoid the use of inorganic ones in IL-

based ABS for the extraction of L-Trp, L-Phe, L-Tyr, L-Leu and L-Val. Hydrophobic interactions were described as the driving force ruling the amino acids separation; however, other parameters, including amino acid size, accessible surface area and polarizability also revealed to be important. This study was later extended, and the same organic salt was conjugated with imidazolium-, pyrrolidinium-, phosphonium- and ammonium-based ILs for L-Trp extraction¹¹⁶. The authors demonstrated that when the IL-rich phase exhibits a pH between the pK_{a1} and pK_{a2} (2.38 and 9.39, respectively) of L-Trp, good extraction are achieved (between 72% and 99% in a single-step). The authors¹¹⁶ also observed that the IL anion has a stronger effect on the partition coefficients of L-Trp when in acidic environment, which is a direct consequence of the speciation of L-Trp¹¹⁶.

Still on the demand to develop more environmentally benign and biocompatible ABS, Zafarani-Moattar and Hamzehzadeh¹¹⁷ proceed with amino acids extraction using ABS formed by a non-toxic, biodegradable and thermo-sensitive polymer, namely PPG 400, and hydrophilic ILs. In polymer-IL-based ABS, L-Tyr displayed a preferential partition towards the polymer-rich phase while L-Trp kept the preference to the IL-rich phase. This difference was attributed to the lack of one pyrrole ring in L-Tyr when compared to L-Trp¹¹⁷. The salt replacement by a polymer resulted in significantly lower partition coefficient values. This result highlights the need to strike a balance between the phase-forming components properties, the target compounds nature and the processing conditions to achieve the highest separation efficiency. Even so, the opposite partition of the two amino acids may be seen as a promising trend when envisaging the development of fractionation platforms of amino acids from complex and raw mixtures. With the same perspective, Freire et al.⁵⁸ replaced the typically used inorganic/organic salts by mono- and disaccharides to form ABS with ILs. Despite the advantages associated to carbohydrates, the extraction efficiencies obtained in this work were significantly lower (~50%) than those previously observed with typical ABS formed by ILs and salts⁵⁸.

Concerning the use of more biocompatible and less toxic IL-based ABS but still trying to have efficient extraction results, more recently, organic biological buffers, namely Good's Buffers (GBs), were used together with ILs to form ABS¹¹⁸. Single-step extraction efficiencies of L-Trp and L-Phe to the GB-rich phase, ranging between 22.4% and 100.0%, were obtained. Contrarily to the IL-salt ABS behavior, in most of the GB-based ABS studied the amino acid preferentially migrated to the more hydrophilic (GB-rich) phase, which was justified by the role of H-bonding and dispersive forces promoted by the predominant zwitterionic form of both amino acids at the system's pH. In two of the studied ABS, L-Phe completely partitioned to the GB-rich phase, while L-Trp showed a preferential affinity to the opposite phase¹¹⁸. These result are a good indicator of systems able to separate amino acids mixtures, such as from a fermentation broth

or from hydrolysed peptide mixtures. Table 1.2 summarizes the IL-based ABS studied and the main interactions discussed as ruling the amino acids partitioning.

Table 1.2 Phase-forming components of IL-based ABS and interactions occurring in the extraction of amino acids.

ILs	2 nd ABS component	Main interactions
[C _n C ₁ im][Ac](<i>n</i> = 4, 6, 8), [C _n C ₁ im]Br (<i>n</i> =4, 6, 8)	K ₂ PO ₄	hydrophobic interactions ¹¹⁹
[P ₁₁ (444)1][Tos], [P ₄₄₄₁][MeSO ₄], [P ₄₄₄₄]Br	K ₃ PO ₄	hydrogen bonding, $\pi\cdots\pi$, dispersive, electrostatic interactions ¹¹⁴
[C ₄ mim]Br	C ₆ H ₅ K ₃ O ₇	hydrophobic interactions ⁶⁸
[Ch][C ₃ H ₇ COO], [Ch][C ₅ H ₁₁ COO], [Ch][C ₇ H ₁₅ COO], [Ch][C ₁₁ H ₂₃ COO]	K ₃ PO ₄	hydrogen bonding, IL self- aggregation phenomenon ¹¹⁵
[C ₄ mim][CF ₃ SO ₃], [C ₄ mim][SCN], [C ₄ mim]Cl, [C ₄ mpip]Cl, [C ₄ mpyr]Cl, [C ₄ mim][DCA], [P ₄₄₄₄]Cl, [N ₄₄₄₄]Cl	C ₆ H ₅ K ₃ O ₇	electrostatic interactions ¹¹⁶
[C ₂ C ₁ im]Br	PPG 400	$\pi\cdots\pi$ and H-bonding ¹¹⁷
[C ₄ C ₁ im][CF ₃ SO ₃]	D-sorbitol, xylitol, D-maltitol, D-(+)-glucose, sucrose, D-(+)- galactose, D-(+)-xylose, L(+)- arabinose, D-(-)- arabinose, D-(+)-maltose, D-(-)-fructose	$\pi\cdots\pi$ and H-bonding ⁵⁸
[C ₄ mim][CF ₃ SO ₃], [C ₄ mim][BF ₄]	TRICINE, HEPES, TES	hydrogen bonding, dispersive forces ¹¹⁸

Despite the focus on the development of sustainable and economically viable purification processes, in all the described works the isolation and recovery of amino acids from the ABS phases in which they are enriched was however neglected.

1.3.2. Proteins

Proteins are essential components of living organisms, being responsible for critical physiological functions, including gene expression, signal transduction, metabolism, and immunity¹⁰⁰. They comprise several physiologically relevant groups, amongst which are

enzymes, hormones and antibodies¹⁰⁰. Proteins may also have diagnostic and prognostic significance in a large set of diseases^{120, 121}. An abnormal increase or decrease of proteins levels in serum and/or urine, for example, can be used as a disease biomarker. These biomarkers not only improve the early stage diagnosis of several pathologies, but also allow to evaluate the response to therapy and to predict possible relapses^{122, 123}. As a result of their diverse functions in organisms, and variety of potential applications, proteins have a major impact in several industries, such as cosmetic¹²⁴, food¹²⁵ and pharmaceutical¹²⁶. This has justified the growing demand for new and better strategies to proceed to their recovery/purification and/or production.

When produced or present in complex media, proteins purification processes can be divided into three steps: capture, intermediate purification and polishing step. The main goal of the first step (capture) is to achieve a fast isolation, stabilization and concentration of the target protein¹²⁷. During the intermediate purification step, most of the bulk contaminants are removed. Finally, the polishing step further improves the target protein purification, allowing to eliminate the most difficult impurities such as aggregates of the target protein¹²⁷. To successfully carry out these steps, it is mandatory to have knowledge on some specific properties of the target proteins, *e.g.* molecular weight, charge, hydrophobicity, pI, and solubility.

Proteins with different molecular weight can be separated by sodium dodecyl sulfate polyacrylamide gel electrophoresis (SDS-PAGE) and size-exclusion chromatography (SEC)¹²⁸. The protein pI is also valuable to design effective separation processes and to select the optimum extraction/purification conditions (pH and ionic strength)¹²⁷. Protein solubility is also a key parameter in the proteins extraction/purification field¹²⁹, in which the induced precipitation of target proteins can be carried out. Proteins have unique tertiary structures, kept together by van der Waals forces, ionic and hydrophobic interactions, and hydrogen bonding. Conditions capable of destabilizing these forces, like temperature, pH, ionic strength and additives should be carefully considered^{128, 130}.

The common applied extraction/purification techniques are based on the proteins specific features¹²⁸. Techniques like precipitation, dialysis, gel electrophoresis, isoelectric focusing, two dimensional electrophoresis and different chromatographic techniques (*e.g.* ion exchange, affinity, high-pressure liquid chromatography (HPLC)) are among the most applied techniques to separate and purify proteins^{131, 132}. However, most of these proteins extraction and separation methods need to be combined and are thus multi-step and laborious¹³³, and costly¹³⁴, reinforcing the need of developing novel platforms to extract and purify proteins.

For the development of new protein extraction/purification strategies it is important to take in account their labile nature¹²⁷. Proteins remain in their native (folded) state under physiological

conditions, while their denatured (unfolded) state may be induced by thermal or chemical unfolding¹⁰⁰. These changes normally result in the impairment of their biological activity. Based on the proteins delicate character, and also on the problems that arise from the conventional extraction/purification techniques, IL-based ABS have been investigated¹⁸.

The pioneering work on the use of IL-based ABS for the extraction of proteins was reported by Du et al.¹³⁵, where the goal was to quantify proteins acting as biomarkers in human urine. Upon phase separation, proteins were mainly concentrated in the IL-rich phase, while most contaminant proteins remained in the salt-rich layer. By increasing the amount of inorganic salt, the authors¹³⁵ additionally observed an increase in the extraction efficiency (from 90% to 100%) of bovine serum albumin (BSA) (structural homologue of HSA) to the IL-rich phase, as well as a maximum enrichment factor of 20 (attained by a second phase separation)¹³⁵. Moreover, by spectroscopic techniques (Ultraviolet–Visible (UV/Vis) and Fourier Transform Infrared spectroscopy (FTIR spectra)) the authors¹³⁵ studied the proteins structural integrity and biological properties after the separation process, demonstrating that no alterations in the BSA structure were induced. The significant achievements of this work encourage other researchers to use IL-based ABS to extract proteins. Different types of proteins from distinct sources (extracts, human and animal fluids, etc.) were investigated. Among them are different enzymes, such as lysozyme (lyz)¹³⁶⁻¹³⁸, trypsin (try)^{70, 136}, lipase¹³⁹, cyt-c⁷⁰, azocasein (Azo)¹⁴⁰, pepsin¹³⁷, horseradish peroxidase (HRP)¹⁴¹, superoxide dismutase (SOD)¹⁴²; antibodies, namely immunoglobulin Y¹⁴³ and G¹⁴⁴ (IgY and IgG, respectively); and hemoproteins like myoglobin (myo)¹³⁷, hemoglobin (Hb)¹³⁶ and BSA^{70, 135, 145-147}. Table 1.3 summarizes the investigated IL-based ABS and results obtained with proteins.

In addition to the investigation on the IL-based ABS separation performance, several works focused on addressing the protein partitioning driving forces, where properties such as pH, temperature, IL and salt concentration were studied^{70, 137, 148}. Hydrophobic interactions were stated as the driving force in the protein partition in IL-based ABS^{70, 137}, whereas Shu et al.³⁹ demonstrated that the extraction of BSA into ILs is an entropically driven phenomenon, resulting from both hydrophobic and electrostatic interactions. These latter results were further supported by other researchers^{136, 149}. When dealing with proteins, the pH seems to be one of the most important parameters to be considered. In fact, some studies showed that the closer the pH of the system is to the pI of each protein, more significant are the hydrophobic interactions and easier it is the manipulation of the proteins migration between the phases^{113, 148}. Studies at variable pH values showed that the extraction efficiency of cyt-c decreases as the pH increases, indicating that electrostatic interactions can influence the partitioning¹⁴⁸. In addition to the pH, the amount of water in each phase was suggested to influence the proteins

partition¹³⁷. All these findings correspond to relevant knowledge when the goal is to develop effective separation platforms for proteins.

Table 1.3 Summary of IL-based ABS used for the extraction of proteins and results obtained.

Protein	ABS constituents	Extraction Efficiency (%)	Protein stability
BSA	Imidazolium-based ILs + Phosphate-based salts	$> 90^{135}$; $> 95^{137}$; $> 85^{70}$	Proved ^{70, 136} Increased ¹³⁷
Try		93^{136} ; $> 95^{70}$	Proved ^{70, 136}
Myo		$\approx 60^{137}$	NV
Lys		$> 85^{137, 138}$; $> 94^{136}$	NV
Hb		95^{136}	NV
Cyt-c		$> 90^{70}$	NV
γ -globulin		$> 80^{70}$	NV
Papain		98^{150}	Proved ¹⁵⁰
HRP		80^{141}	Proved ¹⁴¹
SOD		84^{142}	Proved ¹⁴²
Lipase	Imidazolium-based ILs + K_2CO_3	$> 80^{139}$	Proved ¹³⁹
BSA	Ammonium-based ILs + Phosphate-based salts	99^{151}	Proved ¹⁵¹
Ova		68^{151}	NV
Hb		59^{151}	NV
BSA	Good-buffer-based ILs + Phosphate-based salts	100^{152}	Proved ¹⁵²
BSA	Cholinium-based ILs + Phosphate-based salts	100^{153}	Proved ¹⁵³
Ova		97^{153}	NV
Lys		95^{153}	NV
Try		103^{153}	NV
BSA	Cholinium-Good-buffer-based ILs + Polymer	85^{154} ; $100^{146, 147}$; $\approx 90^{145}$	Proved ^{146, 147}
Papain		$> 90^{154}$	NV
Lys		$> 95^{154}$	NV
Try		$> 90^{154}$; $\approx 90^{145}$	NV
IgY		$79-94^{143}$	Proved ¹⁴³
IgG		100^{144}	NV
Cyt-c	Protic-based ILs + Polymer	100^{140}	Proved ¹⁴⁰
Azo		100^{140}	Proved ¹⁴⁰

In addition to the largely investigated imidazolium-based ILs, other families were also studied, such as ammonium-based ILs^{155, 145, 146}. Under the optimum conditions, ABS formed by N,N-dimethylethanolamine propionate ($[N_{011(20H)}][Pro]$) allowed to reach 99.5% of extraction efficiency of BSA¹⁵¹. However, Bisht et al.¹⁵⁶ demonstrated that thermal stability of lysozyme gradually decreases with the increasing of the ammonium-based ILs concentration. The stability

of lysozyme in ILs was monitored using circular dichroism spectroscopy (CD)¹⁵⁷. These results highlight that the type of IL used (cation and anion chemical structures) has a strong influence not only in the proteins partition but also in their stability.

On the search for alternative and more biocompatible ILs, naturally-derived ILs (from cholinium, carboxylic acids, amino acids and Good's buffers) were increasingly adopted for the extraction and separation of proteins. Wu et al.¹⁵⁸ used a new class of biocompatible amino-acid-based ILs combined with K_2HPO_4 to separate cyt-c, where the preferential partition of the protein towards the IL-rich phase was found (with partition coefficients ranging from 2.83 to 20.7). Cholinium chloride and derivatives were considered in the design of ABS to extract and purify several proteins (BSA, try, papain and lysozyme)^{154,153}. With systems formed by KH_2PO_4 , BSA was extracted in a large extent towards the IL-rich phase (99.8 %)¹⁵³. In the same line of research, ILs formed by cholinium and anions derived from carboxylic acids were combined with the polymer PPG 400 to form ABS and to extract proteins¹⁵⁴. The partition coefficients of lysozyme were found to be lower in ABS comprising higher amounts of phase-forming components and lower water content. The authors claimed that a more structured IL-rich phase resulting from adding IL entails the energy needed to destroy the IL-water network, thus hindering the protein migration to the IL-rich phase¹⁵⁴. Furthermore, ABS formed by cholinium-based ILs + PPG 400 not only allowed an efficient extraction performance (86-100%) but also proved to act as stabilizers and promoters of the enzymes activity^{4, 154, 159}. In order to address biocompatibility and to maintain the pH,s while avoiding the use of additional buffers solutions, alternative ILs with buffering characteristics were later introduced¹⁵². Such ILs, namely Good's buffer ILs (GB-IL), were firstly proposed in 2014¹⁵², being formed by anions derived from biological buffers¹⁵². The authors¹⁵² demonstrated the self-buffering characteristics of these new ILs and their ability to form ABS and to extract BSA. Remarkably, an extraction efficiency of 100% in a single step to the GB-IL-rich phase was obtained in most systems¹⁵². The authors also performed a series of studies based on FTIR to ascertain the impact of GB-ILs on the protein's stability. In general, it was found that these GB-ILs display a higher stabilizing effect over the studied protein when compared to conventional ILs¹⁵².

Although a significant number of works can be found in the literature using IL-based ABS to extract proteins, few addressed the proteins recovery and recyclability of the phase-forming components. Freire and co-workers¹⁶⁰ studied the recyclability and reusability of phosphonium- and ammonium-based ILs after the extraction of BSA to the IL-rich phase. The extraction efficiencies were maintained at 100% in three-step sequential extractions comprising both the BSA recovery and the IL reusability¹⁶⁰. An important achievement was obtained during this work with the protein recovery by a simple dialysis¹⁶⁰. Li et al.¹⁵⁴ used the PPG 400 thermosensitive

polymer in the formulation of ABS, allowing an easy recovery of the polymer by increasing temperature.

Most studies reported and discussed up to now were carried out with pure proteins and only the extraction efficiency of IL-based ABS was addressed. However, value-added proteins with biological, clinical, pharmaceutical and industrial relevance are usually present in complex media. Therefore, further investigations envisaging the purification of proteins from complex sources using IL-based ABS are strongly recommended, while evaluating simultaneously the extraction efficiency, recovery yield and purification factor. In this field, Taha et al.¹⁴³ prepared novel ABS formed by cholinium-GB-based ILs and PPG 400 for the extraction of immunoglobulin Y from egg yolk. The combination of GB-ILs with PPG 400 in ABS allowed the preferential partitioning of IgY to the IL-rich phase¹⁴³. Despite the good extraction efficiencies obtained (ranging between 79.0 and 94.0 %), the greatest challenge was to completely purify IgY since the total separation of IgY from the major contaminant proteins was not achieved¹⁴³. IL-based ABS were used to separate IgG from rabbit serum, where extraction efficiencies of 100% and recovery yields > 80% were obtained. By the end of the process the authors obtained IgG with a purity level of 49% in a single-step¹⁴⁴. An ultracentrifugation step was then performed allowing the IgG recovery from the IL-rich phase, and an increase in the IgG purity up to 66%¹⁴⁴.

The results attained with IL-based ABS in the extraction of different proteins encourages the replacement of conventional methods by this technique. Accordingly, in the current work, alternative ABS composed of more biocompatible ILs families combined with salts or polymers were investigated as alternative extraction/purification platforms for proteins.

1.3.3. Nucleic acids

Nucleic acids, *viz.* deoxyribonucleic acid (DNA) and ribonucleic acid (RNA), are biopolymers of nucleotides that play important roles in many chemical reactions and gene expression¹⁰⁰. Both DNA and RNA are formed by successive nucleotides covalently linked through phosphate-group “bridges”, resulting in the most polar biopolymers, being therefore soluble in most polar solvents and insoluble in non-polar solvents¹⁰⁰. DNA is more stable at a slightly alkaline pH and dissolves better in buffer aqueous solutions than in water. RNA, on the other hand, can tolerate a slightly acidic pH and dissolves readily in water¹⁰⁰. Working with RNA provides different challenges from working with DNA¹⁶¹. At ambient and physiological conditions, the stability of the DNA structure, β -helical, is restricted to fairly low and its lifetime is limited (up to about 1 month) due to the hydrolytic attack causing deamination and depurination of its base pairs¹⁶². To work with RNA, the demands on the processes and source material are much higher, not only

due to the RNA poorer stability (short half-life)¹⁶³, but also due to the ubiquitous presence of ribonucleases (RNases), which are present in blood, tissues, and in most bacteria and fungi¹⁶⁴.

Human gene therapy is undoubtedly the “gold application” of nucleic acids, and by definition is “the introduction of new genetic material into the cells of an individual with the intention of producing a therapeutic benefit”¹⁶⁵. It started in 1997, when Paterson et al.¹⁶⁶ used a single stranded DNA to inhibit the translation of a complementary RNA in a cell-free system. Since then, nucleic acids studies became one of the most important strategies to the understanding of fundamental basis of human life, and also for the development of effective therapeutics¹⁶⁷. Regarding DNA-based drugs, one of the strongest advantages over the currently available pharmaceuticals, is their selective capacity to recognize molecular targets and pathways, which imparts a tremendous action specificity¹⁶⁸. On the other hand, the discovery of RNA interference (RNAi) strengthened and allowed the expansion of the contemporary knowledge on gene regulation^{169, 170}. Nowadays, DNA- and RNA-based drugs are promising candidates for drug therapy of a wide range of diseases, including cancer, neurological disorders such as Parkinson's disease and Alzheimer's disease, and cardiovascular disorders. However, and apart from the type of application, the nucleic acids purity and integrity are essential parameters. Efficient purification approaches can be developed if some criteria are fulfilled, namely: (1) effective disruption of cells or tissue; (2) inactivation of nucleases to avoid the nucleic acids degradation; and (3) recovery of nucleic acids free of contaminants and with high integrity².

Based on the exposed, the extraction/purification of nucleic acids is still a challenge. The choice of method depends on the type of nucleic acid, starting material (prokaryotic hosts, tissue samples, whole organisms, cell cultures, body fluids), intended downstream application, and requirements in yield, quality, purity, and scale-up. Up to date, two methods prevail, a chemical extraction based and a solid-phase extraction method^{171, 172}. The chemical method falls on the use of a solution composed of phenol and chloroform (and guanidinium thiocyanate in the case of RNA extraction), followed by ethanol precipitation¹⁷¹. This organic-based extraction can be also carried out using commercial available reagents, as TRIzol® (Ambion), TRI (Sigma-Aldrich), NZYMidiprep (NZYTech) (specific for DNA) and Ribozol™ (AMRESCO's) (specific for RNA). However, besides being a time-consuming and laborious protocol, due to the use of denaturing agents and organic solvents^{171, 173} this chemical extraction is extremely toxic and compromises the operator's health^{140, 142}. On the other hand, SPE consists of a method based on the adsorption capacity of nucleic acids to specific materials/surfaces¹⁷³. With the significantly decrease of samples preparation time and creation of simpler and safer technologies, the use of the latter method is nowadays preferred. Still, additional purification protocols need to be used to remove process-associated impurities, since apart from the type of application, the nucleic

acids purity and integrity are always essential. Nowadays, affinity chromatography¹⁷⁴, RNA affinity tags¹⁷⁵ and amino acid based chromatography¹⁷⁶ are often used¹⁷⁷. Particular attention has been given to the amino acid-based chromatography since it exploits the biological interactions that are established within the cell (hydrophobic interactions and hydrogen bonds) by using immobilized amino acids (*e.g.* L-lysine, L-arginine or histidine) as specific ligands^{176, 178}. The recognition of the nucleic acids achieved with these supports allows its selective recovery from complex mixtures with high efficiency and high purity^{176, 178}. Still, these techniques are time-consuming, expensive and of low yield. Furthermore, it is of high relevance to develop purifying protocols for nucleic acids while ensuring their stability and biological activity at the final stage of process.

Inspired by the “designer solvent” status of ILs^{18,179} and their stabilizing properties when used as solvents⁴², the IL-related academia has been successful at developing pioneering extractive technologies comprising nucleic acids¹⁸⁰⁻¹⁸². Most of these works were however carried out with hydrophobic ILs and DNA. The lack of work regarding RNA is probably due to its poorer stability and more complex manipulation. In 2012, Dejuam and Dechao¹⁸³, used ABS formed by 1-butyl-3-methylimidazolium tetrafluoroborate ($[\text{C}_4\text{C}_1\text{im}][\text{BF}_4]$) and KH_2PO_4 to extract DNA¹⁸³. The authors¹⁸³ observed that with the IL addition to the salt solution (KH_2PO_4) there was a decrease in the 260 nm absorbance values (A_{260}) of the initial substrate, meaning that the nucleic acid is extracted to the IL-rich phase. The ratio A_{260}/A_{280} was 1.701, thus close to 1.8 (the ratio accepted as a good-quality and “pure” DNA indicator)¹⁸³. Recently, novel ABS composed of ILs and deep eutectic solvents (DESs) were developed and used to efficiently extract DNA. Systems involving IL-based DES and betaine-based ILs lead to a high extraction efficiency of 95.9% when compared to other two ABS categories tested¹⁸⁴. The authors claimed that the formation of IL-DNA aggregates played an important role in the process of DNA extraction. These systems were successfully applied in the selective separation of DNA from cyt-c and DNA from bovine hemoglobin (BHb), where the DNA mainly partitioned to IL-rich bottom phase¹⁸⁴.

Despite the lack in the literature in what concerns the use of IL-based ABS to extract nucleic acids, these systems seem to be a good extraction/purification alternative. Moreover, the already reported results regarding the improvement on the DNA and RNA stability by using ILs as solvents encourages the use of IL-based ABS as integrated strategies for the purification and stabilization of nucleic acids^{15, 43, 185-189}.

1.4. References

1. R. W. Kates, W. C. Clark, R. Corell, J. M. Hall, C. C. Jaeger, I. Lowe, J. J. McCarthy, H. J. Schellnhuber, B. Bolin, N. M. Dickson, S. Faucheux, G. C. Gallopin, A. Grübler, B. Huntley, J. Jäger, N. S. Jodha, R. E.

- Kasperson, A. Mabogunje, P. Matson, H. Mooney, B. Moore, T. O'Riordan and U. Svedin, *Science*, 2001, 292, 641-642.
2. S. C. Tan and B. C. Yip, *J. Biomed. Biotechnol.*, 2009, 2009.
 3. G. J. G. Chávez, J. A. Villa, J. F. A. Zavala, J. B. Heredia, D. Sepulveda, E. M. Yahia and G. A. G. Aguilar, *Compr Rev. Food Sci. Food Saf.*, 2013, 12, 5-23.
 4. M. V. Quental, M. Caban, M. M. Pereira, P. Stepnowski, J. A. P. Coutinho and M. G. Freire, *Biotechnol. J.*, 2015, 10, 1457-1466.
 5. L. Wang, C. L. Weller, V. L. Schlegel, T. P. Carr and S. L. Cuppett, *Bioresour. Technol.* 2008, 99, 1373-1382.
 6. L. McQueen and D. Lai, *Front. Chem.*, 2019, 7, 1-10.
 7. P. T. Anastas and J. C. Warner, *Green Chemistry: Theory and Practice*, Oxford University Press, 2000.
 8. K. R. Seddon, *J. Chem. Technol. Biotechnol.*, 1997, 68, 351-356.
 9. M. Naushad, Z. A. Alothman, A. B. Khan and M. Ali, *Int. J. Biol. Macromol.*, 2012, 51, 555-560.
 10. R. Vijayaraghavan, A. Izgorodin, V. Ganesh, M. Surianarayanan and D. R. MacFarlane, *Angew. Chem. Int. Ed.*, 2010, 49, 1631-1633.
 11. A. P. S. Brogan and J. P. Hallett, *J. Am. Chem. Soc.*, 2016, 138, 4494-4501.
 12. K. De Winter, K. Verlinden, V. Kren, L. Weignerova, W. Soetaert and T. Desmet, *Green Chem.*, 2013, 15, 1949-1955.
 13. C. E. Paul and V. G. Fernández, *Ionic Liquids in Lipid Processing and Analysis*, AOCS Press, 2016.
 14. H. Zhao, *J. Chem. Technol. Biotechnol.*, 2016, 91, 25-50.
 15. I. Mamajanov, A. E. Engelhart, H. D. Bean and N. V. Hud, *Angew. Chem. Int. Ed.*, 2010, 49, 6310-6314.
 16. R. P. Swatloski, S. K. Spear, J. D. Holbrey and R. D. Rogers, *J. Am. Chem. Soc.*, 2002, 124, 4974-4975.
 17. D. A. Fort, R. C. Remsing, R. P. Swatloski, P. Moyna, G. Moyna and R. D. Rogers, *Green Chem.*, 2007, 9, 63-69.
 18. M. G. Freire, A. F. Claudio, J. M. Araujo, J. A. Coutinho, I. M. Marrucho, J. N. C. Lopes and L. P. Rebelo, *Chem. Soc. Rev.*, 2012, 41, 4966-4995.
 19. H. Passos, M. G. Freire and J. A. P. Coutinho, *Green Chem.*, 2014, 16, 4786-4815.
 20. A. F. M. Claudio, M. C. Neves, K. Shimizu, J. N. Canongia Lopes, M. G. Freire and J. A. P. Coutinho, *Green Chem.*, 2015, 17, 3948-3963.
 21. A. Jordan and N. Gathergood, *Chem. Soc. Rev.*, 2015, 44, 8200-8237.
 22. R. F. Frade and C. A. Afonso, *Hum. Exp. Toxicol.*, 2010, 29, 1038-1054.
 23. W. T. Heller, H. M. O'Neill, Q. Zhang and G. A. Baker, *J. Phys. Chem. B*, 2010, 114, 13866-13871.
 24. R. Patel, M. Kumari and A. B. Khan, *Appl. Biochem. Biotechnol.*, 2014, 172, 3701-3720.
 25. R. M. Lau, F. V. Rantwijk, K. R. Seddon and R. A. Sheldon, *Organic Lett.*, 2000, 2, 4189-4191.
 26. A. P. De Los Ríos, F. J. H. Fernández, F. A. Martínez, M. Rubio and G. Villora, *Biocatal. Biotransfor.*, 2007, 25, 151-156.
 27. P. Vidya and A. Chadha, *J. Mol. Catal. B Enzym.*, 2009, 57, 145-148.
 28. S. J. Nara, J. R. Harjani and M. M. Salunkhe, *Tetrahedron Lett.*, 2002, 43, 2979-2982.
 29. A. P. Ríos, F. J. H. Fernández, M. Rubio, D. Gómez and G. Villora, *J. Chem. Technol. Biotechnol.*, 2007, 82, 190-195.
 30. P. Lozano, T. de Diego, J. P. Guegan, M. Vaultier and J. L. Iborra, *Biotechnol. Bioeng.*, 2001, 75, 563-569.
 31. Y. Wang, M. Radosevich, D. Hayes and N. Labbé, *Biotechnol. Bioeng.*, 2011, 108, 1042-1048.
 32. S. Galai, A. P. Ríos, F. J. H. Fernández, S. H. Kacem and F. T. Alonso, *RSC Advances*, 2015, 5, 16173-16189.
 33. A. P. Tavares, O. Rodriguez and E. A. Macedo, *Biotechnol. Bioeng.*, 2008, 101, 201-207.
 34. K. Fujita and H. Ohno, *Biopolymers*, 2010, 93, 1093-1099.
 35. C. Schröder, *Top. Curr. Chem.*, 2017, 375, 25.
 36. G. A. Baker and W. T. Heller, *Chem. Eng. J.*, 2009, 147, 6-12.
 37. P. Attri, P. Venkatesu and A. Kumar, *Phys. Chem. Chem. Phys.*, 2011, 13, 2788-2796.
 38. S. Yamaguchi, E. Yamamoto, S. Tsukiji and T. Nagamune, *Biotechnol. Prog.*, 2008, 24, 402-408.
 39. Y. Shu, M. Liu, S. Chen, X. Chen and J. Wang, *J. Phys. Chem. B*, 2011, 115, 12306-12314.
 40. Z. Yang, *J. Biotechnol.*, 2009, 144, 12-22.
 41. M. Sivapragasam, M. Moniruzzaman and M. Goto, *Biotechnol. J.*, 2016, 11, 1000-1013.
 42. R. Vijayaraghavan, A. Izgorodin, V. Ganesh, M. Surianarayanan and D. R. MacFarlane, *Angew. Chem. Int. Ed.*, 2010, 49, 1631-1633.
 43. R. R. Mazid, U. Divisekera, W. Yang, V. Ranganathan, D. R. MacFarlane, C. Cortez-Jugo and W. Cheng, *Chem. Comm.*, 2014, 50, 13457-13460.
 44. H. Itoh, M. Thien, T. Hatton and D. Wang, *Biotechnol. Bioeng.*, 1990, 35, 853-860.
 45. S. Y. Lee, I. Khoiroh, C. W. Ooi, T. C. Ling and P. L. Show, *Sep. Purif. Rev.*, 2017, 46, 291-304.
 46. M. W. Beijerinck, *Centr.-Bl. f. Bakter. u. Parasitenk.*, 1896, 2, 698-699.
 47. P. Å. Albertsson, *Nature*, 1958, 182, 709-711.
 48. I. F. Ferreira, A. M. Azevedo, P. A. J. Rosa and M. A. Barros, *J. Chromatogr.*, 2008, 1195, 94-100.

49. A. M. Azevedo, A. G. Gomes, P. A. J. Rosa, I. F. Ferreira, A. M. M. O. Pisco and M. A. Barros, *Sep. Purif. Technol.*, 2009, 65, 14-21.
50. M. J. R. Angel, V. Pino, S. C. and A. Berthod, *J. Chromatogr.*, 2007, 1151, 65-73.
51. M. Iqbal, Y. Tao, S. Xie, Y. Zhu, D. Chen, X. Wang, L. Huang, D. Peng, A. Sattar, M. A. B. Shabbir, H. I. Hussain, S. Ahmed and Z. Yuan, *Biol. Proced. Online*, 2016, 18, 18-18.
52. K. E. Gutowski, A. Grant, H. D. Willauer, J. G. Huddleston, R. P. Swatloski, J. D. Holbrey and R. D. Rogers, *J. Am. Chem. Soc.*, 2003, 125, 6632-6633.
53. R. D. Rogers and M. A. Eiteman, *Aqueous Biphasic Separations: Biomolecules to Metal Ions*, Springer, 2012.
54. M. Freemantle, *Chem. Eng. News*, 1998, 76, 32-37.
55. A. F. M. Cláudio, M. G. Freire, C. S. R. Freire, A. J. D. Silvestre and J. A. P. Coutinho, *Sep. Purif. Technol.*, 2010, 75, 39-47.
56. M. V. Quental, H. Passos, K. A. Kurnia, J. A. Coutinho and M. G. Freire, *J. Chem. Eng. Data*, 2015, 60, 1674-1682.
57. M. G. Freire, J. F. Pereira, M. Francisco, H. Rodriguez, L. P. Rebelo, R. D. Rogers and J. A. Coutinho, *Chemistry*, 2012, 18, 1831-1839.
58. M. G. Freire, C. L. S. Louros, L. P. N. Rebelo and J. A. P. Coutinho, *Green Chem.*, 2011, 13, 1536-1545.
59. M. Domínguez-Pérez, L. I. N. Tomé, M. G. Freire, I. M. Marrucho, O. Cabeza and J. A. P. Coutinho, *Sep. Sci. Technol.*, 2010, 72, 85-91.
60. C. M. S. S. Neves, S. Shahriari, J. Lemus, J. F. B. Pereira, M. G. Freire and J. A. P. Coutinho, *Phys. Chem. Chem. Phys.*, 2016, 18, 20571-20582.
61. P. Rosa, I. Ferreira, A. Azevedo and M. A. Barros, *J. Chrom. A*, 2010, 1217, 2296-2305.
62. A. Azevedo, P. Rosa, I. F., A. Pisco, J. Vries, R. Korpelaar, T. Visser and M. A. Barros, *Sep. Purif. Technol.*, 2009, 65, 31-39.
63. H. Passos, T. B. V. Dinis, E. V. Capela, M. V. Quental, J. Gomes, J. Resende, P. P. Madeira, M. G. Freire and J. A. P. Coutinho, *Phys. Chem. Chem. Phys.*, 2018.
64. S. P. M. Ventura, F. A. e Silva, M. V. Quental, D. Mondal, M. G. Freire and J. A. P. Coutinho, *Chem. Reviews*, 2017, 117, 6984-7052.
65. M. G. Freire, C. M. S. S. Neves, I. M. Marrucho, J. N. Canongia Lopes, L. P. N. Rebelo and J. A. P. Coutinho, *Green Chem.*, 2010, 12, 1715-1718.
66. C. F. Marques, T. Mourao, C. M. Neves, A. S. Lima, I. B. Palheiros, J. A. Coutinho and M. G. Freire, *Biotechnol. Prog.*, 2013, 29, 645-654.
67. M. Larriba, S. Omar, P. Navarro, J. Garcia, F. Rodriguez and M. G. Miquel, *RSC Advances*, 2016, 6, 18751-18762.
68. M. T. Z. Moattar and S. Hamzehzadeh, *Biotechnol. Prog.*, 2011, 27, 986-997.
69. J. Wang, Y. Pei, Y. Zhao and Z. Hu, *Green Chem.*, 2005, 7, 196-202.
70. Y. Pei, J. Wang, K. Wu, X. Xuan and X. Lu, *Sep. Purif. Technol.*, 2009, 64, 288-295.
71. Y. Lu, W. Lu, W. Wang, Q. Guo and Y. Yang, *Talanta*, 2011, 85, 1621-1626.
72. J. A. Asenjo and B. A. Andrews, *J. Chromatogr. A*, 2011, 1218, 8826-8835.
73. R. L. Souza, R. A. Lima, J. A. P. Coutinho, C. M. F. Soares and Á. S. Lima, *Sep. Purif. Technol.*, 2015, 155, 118-126.
74. B. A. Andrews, A. S. Schmidt and J. A. Asenjo, *Biotechnol. Bioeng.*, 2005, 90, 380-390.
75. E. Birben, U. M. Sahiner, C. Sackesen, S. Erzurum and O. Kalayci, *World Allergy Organ J.*, 2012, 5, 9-19.
76. B. Halliwell, *Free Radic. Res. Commun.*, 1990, 9, 1-32.
77. U. Satyanarayana, *Biochemistry*, Elsevier Health Sciences, 2014.
78. M. Carrocho and I. C. F. R. Ferreira, *Food Chem. Toxicol.*, 2013, 51, 15-25.
79. M. N. Alam, N. J. Bristi and M. Rafiqzaman, *Saudi Pharm. J.*, 2013, 21, 143-152.
80. P. G. Anantharaju, P. C. Gowda, M. G. Vimalambike and S. V. Madhunapantula, *Nutr. J.*, 2016, 15, 99.
81. O. V. Zillich, U. Schweiggert-Weisz, P. Eisner and M. Kersch, *Int. J. Cosmet. Sci.*, 2015, 37, 455-464.
82. M. d. S. Lima, I. d. S. V. Silani, I. M. Toaldo, L. C. Corrêa, A. C. T. Biasoto, G. E. Pereira, M. T. B. Luiz and J. L. Ninow, *Food Chem.*, 2014, 161, 94-103.
83. A. Khoddami, M. A. Wilkes and T. H. Roberts, *Molecules*, 2013, 18, 2328-2375.
84. M. Sova, *Mini Rev. Med. Chem.*, 2012, 12, 749-767.
85. R. J. Robbins, *J. Agric. Food Chem.*, 2003, 51, 2866-2887.
86. K. A. Ross, T. Beta and S. D. Arntfield, *Food Chem.*, 2009, 113, 336-344.
87. M. Winter and K. Herrmann, *J. Agric. Food Chem.*, 1986, 34, 616-620.
88. S. Klick and K. Herrmann, *Phytochemistry*, 1988, 27, 2177-2180.
89. M. Tasioula-Margari and E. Tsabolatidou, *Antioxidants*, 2015, 4, 548-562.
90. P. G. Salas, A. M. Soto, A. S. Carretero and A. F. Gutierrez, *Molecules*, 2010, 15, 8813-8826.
91. L. Wang and C. L. Weller, *Trends Food Sci. Technol.*, 2006, 17, 300-312.
92. A. M. G. Caravaca, A. C. Pancorbo, B. C. Diaz, A. S. Carretero and A. F. Gutierrez, *Electrophoresis*, 2005, 26, 3538-3551.

93. A. F. M. Cláudio, A. M. Ferreira, C. S. R. Freire, A. J. D. Silvestre, M. G. Freire and J. A. P. Coutinho, *Sep. Purif. Technol.*, 2012, 97, 142-149.
94. A. F. M. Cláudio, C. F. C. Marques, I. B. Palheiros, M. G. Freire and J. A. P. Coutinho, *Green Chem.*, 2014, 16, 259-268.
95. Z. J. Tan, C. Y. Wang, Z. Z. Yang, Y. J. Yi, H. Y. Wang, W. L. Zhou and F. F. Li, *Molecules*, 2015, 20, 17929-17943.
96. J. C. S. Rangel, D. A. J. Velázquez, L. C. Zevallos and J. Benavides, *J. Chem. Technol. Biotechnol.*, 2016, 91, 144-154.
97. J. H. P. M. Santos, M. Martins, A. J. D. Silvestre, J. A. P. Coutinho and S. P. M. Ventura, *Green Chem.*, 2016, 18, 5569-5579.
98. V. J. Hruby, *J. Pharm. Sci.*, 75, 323.
99. G. Zhu, X. Zhu, Z. Xiao, R. Zhou, N. Feng and Y. Niu, *Biomass. Conver. Bior.*, 2015, 5, 309-320.
100. D. L. Nelson, A. L. Lehninger and M. M. Cox, *Lehninger Principles of Biochemistry*, W. H. Freeman, 2008.
101. J. A. Marinsky and Y. Marcus, *Ion Exchange and Solvent Extraction: A Series of Advances*, Taylor & Francis, 1995.
102. P. G. Rigas, *Meas. Sci. Technol.*, 2012, 40, 161-193.
103. M. Li, Z.-Q. Zhu and A. E. Rodrigues, *Ind. Eng. Chem. Res.*, 2002, 41, 251-256.
104. K. Soda, K. Yonaha, H. Misono and M. Osugi, *FEBS Lett.*, 1974, 46, 359-363.
105. K. Drauz, I. Grayson, A. Kleemann, H.-P. Krimmer, W. Leuchtenberger and C. Weckbecker, *Ullmann's Encyclopedia of Industrial Chemistry*, Wiley-VCH Verlag GmbH & Co. KGaA, 2000.
106. T. Perez-Palacios, J. Ruiz, J. M. Barat, M. C. Aristoy and T. Antequera, *Meat sci.*, 2010, 85, 121-126.
107. T. Palacios, M. A. Barroso, J. Ruiz and T. Antequera, *Int. J. Anal. Chem.*, 2015, 2015, 8.
108. A. Mustafa, P. Åman, R. Andersson and A. Kamal-Eldin, *Food Chem.*, 2007, 105, 317-324.
109. J. Csapó, C. Albert, K. Lóki and Z. Csapó-Kiss, *Acta Univ. Sapientiae, Aliment.*, 2008, 1, 5-29.
110. C. M. Neves, S. P. Ventura, M. G. Freire, I. M. Marrucho and J. A. Coutinho, *J. Phys. Chem. B*, 2009, 113, 5194-5199.
111. S. P. M. Ventura, C. M. S. S. Neves, M. G. Freire, I. M. Marrucho, J. Oliveira and J. A. P. Coutinho, *J. Phys. Chem. B*, 2009, 113, 9304-9310.
112. Z. Li, Y. Pei, L. Liu and J. Wang, *J. Chem. Thermodyn.*, 2010, 42, 932-937.
113. Y. Kohno and H. Ohno, *Phys. Chem. Chem. Phys.*, 2012, 14, 5063-5070.
114. C. L. S. Louros, A. F. M. Cláudio, C. M. S. S. Neves, M. G. Freire, I. M. Marrucho, J. Pauly and J. A. P. Coutinho, *Int. J. Mol. Sci.*, 2010, 11, 1777-1791.
115. Y. Xie, H. Xing, Q. Yang, Z. Bao, B. Su and Q. Ren, *ACS Sustai. Chem. Eng.*, 2015, 3, 3365-3372.
116. H. Passos, A. R. Ferreira, A. F. M. Cláudio, J. A. P. Coutinho and M. G. Freire, *Biochem. Eng. J.*, 2012, 67, 68-76.
117. M. T. Zafarani-Moattar, S. Hamzehzadeh and S. Nasiri, *Biotechnol. Prog.*, 2012, 28, 146-156.
118. A. Luís, T. B. V. Dinis, H. Passos, M. Taha and M. G. Freire, *Biochem. Eng. J.*, 2015, 101, 142-149.
119. Y. Pei, Z. Li, L. Liu and J. Wang, *J. Chromatogr. A*, 2012, 1231, 2-7.
120. D. R. Ciocca and S. K. Calderwood, *Cell Stress & Chaperones*, 2005, 10, 86-103.
121. C. Giaginis, S. Vgenopoulou, P. Vielh and S. Theocharis, *Histol. Histopathol.*, 2010, 25, 351-370.
122. N. A. Brunzel, *Fundamentals of Urine and Body Fluid Analysis*, Elsevier Health Sciences, 2013.
123. R. Hoffmann, *Advances in Health care Technology Care Shaping the Future of Medical*, Springer, 2006.
124. G. Secchi, *Clin. Dermatol.*, 2008, 26, 321-325.
125. P. W. Goodenough, *Mol. Biotechnol.*, 1995, 4, 151-166.
126. U. Leurs, U. H. Mistarz and K. D. Rand, *Eur. J. Pharm. Biopharm.*, 2015, 93, 95-109.
127. G. Healthcare, Strategies for Protein Purification <http://www.gelifesciences.com/webapp/wcs/stores/servlet/catalog/en/GELifeSciences-pt/service-and-support/handbooks/>, (accessed 22-05-2017, 2017).
128. B. A. Lodish, S. L. Zipursky, *Molecular Cell Biology*, W. H. Freeman, 2000.
129. D. Martínez-Maqueda, B. Hernández-Ledesma, L. Amigo, B. Miralles and J. Á. G. Ruiz, *Proteomics in Foods: Principles and Applications*, Springer, 2013.
130. L. J. Cseke, P. B. Kaufman, G. K. Podila and C. J. Tsai, *Handbook of Molecular and Cellular Methods in Biology and Medicine*, CRC Press, 2003.
131. S. M. B. L. Zhao, A. E. Ghaly, M. S. Brooks, D. Dave, *J. Food. Process. Technol.*, 2011, 2.
132. T. J. Berg J. M., Stryer L., *Biochemistry*, W H Freeman, 2002.
133. M. A. Livshits, E. Khomyakova, E. G. Evtushenko, V. N. Lazarev, N. A. Kulemin, S. E. Semina, E. V. Generozov and V. M. Govorun, *Scientific reports*, 2015, 5, 17319.
134. M. Tang, J. Vejjayan and H. Ibrahim, *J. Venom. Anim. Toxins Incl. Trop. Dis.*, 2011, 17, 442-450.
135. Z. Du, Y. L. Yu and J. H. Wang, *Chemistry*, 2007, 13, 2130-2137.
136. X. Lin, Y. Wang, Q. Zeng, X. Ding and J. Chen, *Analyst*, 2013, 138, 6445-6453.
137. S. Dreyer, P. Salim and U. Kragl, *Biochem. Eng. J.*, 2009, 46, 176-185.

138. Y. Pei, L. Li, Z. Li, C. Wu and J. Wang, *Sep. Sci. Technol.*, 2012, 47, 277-283.
139. F. J. Deive, A. Rodríguez, A. B. Pereiro, J. M. M. Araújo, M. A. Longo, M. A. Z. Coelho, J. N. C. Lopes, J. M. S. S. Esperança, L. P. N. Rebelo and I. M. Marrucho, *Green Chem.*, 2011, 13, 390-396.
140. H. Passos, A. Luís, J. A. P. Coutinho and M. G. Freire, *Sci. Rep.*, 2016, 6, 20276.
141. Q. Cao, L. Quan, C. He, N. Li, K. Li and F. Liu, *Talanta*, 2008, 77, 160-165.
142. J. S. Martinez, M. R. Palomares and J. Benavides, *Biotechnol. Prog.*, 2014, 30, 1326-1334.
143. M. Taha, M. R. Almeida, F. A. Silva, P. Domingues, S. P. Ventura, J. A. Coutinho and M. G. Freire, *Chemistry*, 2015, 21, 4781-4788.
144. C. C. Ramalho, C. M. Neves, M. V. Quental, J. A. Coutinho and M. G. Freire, *J. Chem. Technol. Biotechnol.*, 2018, 93, 1931-1939.
145. C. P. Song, R. N. Ramanan, R. Vijayaraghavan, D. R. MacFarlane, E. S. Chan and C. W. Ooi, *ACS Sustai. Chem. Eng.*, 2015, 3, 3291-3298.
146. M. V. Quental, M. Caban, M. M. Pereira, P. Stepnowski, J. A. Coutinho and M. G. Freire, *Biotechnol. J.*, 2015, 10, 1457-1466.
147. M. Taha, M. V. Quental, I. Correia, M. G. Freire and J. A. Coutinho, *Process Biochem.*, 2015, 50, 1158-1166.
148. T. L. Greaves and C. J. Drummond, *Chem. Rev.*, 2008, 108, 206-237.
149. H. Yan, J. Wu, G. Dai, A. Zhong, H. Chen, J. Yang and D. Han, *J. Lumin.*, 2012, 132, 622-628.
150. Z. Bai, Y. Chao, M. Zhang, C. Han, W. Zhu, Y. Chang, H. Li and Y. Sun, *J. Chem.*, 2013, 2013, 6.
151. J. Chen, Y. Wang, Q. Zeng, X. Ding and Y. Huang, *Anal. Methods*, 2014, 6, 4067-4076.
152. M. Taha, F. A. Silva, M. V. Quental, S. P. M. Ventura, M. G. Freire and J. A. P. Coutinho, *Green Chem.*, 2014, 16, 3149-3159.
153. S. Huang, Y. Wang, Y. Zhou, L. Li, Q. Zeng and X. Ding, *Anal. Methods*, 2013, 5, 3395-3402.
154. Z. Li, X. Liu, Y. Pei, J. Wang and M. He, *Green Chem.*, 2012, 14, 2941-2950.
155. S. Dreyer and U. Kragl, *Biotechnol. Bioeng.*, 2008, 99, 1416-1424.
156. M. Bisht, A. Kumar and P. Venkatesu, *Int. J. Biol. Macromol.*, 2015, 81, 1074-1081.
157. J. C. Ioannou, A. M. Donald and R. H. Tromp, *Food Hydrocolloids*, 2015, 46, 216-225.
158. C. Wu, J. Wang, Z. Li, J. Jing and H. Wang, *J. Chromatogr. A*, 2013, 1305, 1-6.
159. M. Taha, M. V. Quental, I. Correia, M. G. Freire and J. A. P. Coutinho, *Process Biochem.*, 2015, 50, 1158-1166.
160. M. M. Pereira, S. N. Pedro, M. V. Quental, Á. S. Lima, J. A. P. Coutinho and M. G. Freire, *J. Biotechnol.*, 2015, 206, 17-25.
161. G. H. L. Sciences, *Nucleic Acid Sample Preparation for Downstream Analyses: Principles and Methods*, <http://www.gelifesciences.com/webapp/wcs/stores/servlet/catalog/en/GELifeSciences-pt/service-and-support/handbooks>, (accessed 23- 05, 2017).
162. A. Benedetto and P. Ballone, *ACS Sustai. Chem. Eng.*, 2016, 4, 392-412.
163. G. Brooks, *Biotechnology in Healthcare: An Introduction to Biopharmaceuticals*, Pharmaceutical Press, 1998.
164. L. Buckingham, *Molecular Diagnostics: Fundamentals, Methods and Clinical Applications*, F.A. Davis Company, 2012.
165. W. F. Anderson, *Science*, 1992, 256, 808-813.
166. B. M. Paterson, B. E. Roberts and E. L. Kuff, *Proc. Natl. Acad. Sci. U.S.A.*, 1977, 74, 4370-4374.
167. M. L. Stephenson and P. C. Zamecnik, *Proc. Natl. Acad. Sci. U.S.A.*, 1978, 75, 285-288.
168. S. T. Crooke, *Nucleic Acid Ther.*, 1998, 8, 115-122.
169. A. Fire, S. Xu, M. K. Montgomery, S. A. Kostas, S. E. Driver and C. C. Mello, *Nature*, 1998, 391, 806-811.
170. C. Y. Chu and T. M. Rana, *J. Cell. Physiol.*, 2007, 213, 412-419.
171. P. Chomczynski and N. Sacchi, *Nature protocols*, 2006, 1, 581-585.
172. I. O. Agbagwa, S. Datta, P. G. Patil, P. Singh and N. Nadarajan, *Genet. Mol. Res.*, 2012, 11, 4632-4639.
173. I. Vomelova, Z. Vanickova and A. Sedo, *Folia biologica*, 2009, 55, 243-251.
174. A. K. Shakya, A. Srivastava and A. Kumar, *Curr. Protoc. Nucleic Acid. Chem.*, 2015, 63, 10.16.11-10.
175. S. C. Walker, F. H. Scott, C. Srisawat and D. R. Engelke, *Methods Mol. Biol.*, 2008, 488, 23-40.
176. P. Pereira, A. Sousa, J. Queiroz, I. Correia, A. Figueiras and F. Sousa, *Chromatogr. B Analyt. Technol. Biomed. Life Sci.*, 2014, 951-952, 16-23.
177. P. Pereira, J. A. Queiroz, A. Figueiras and F. Sousa, *J. Chromatogr. B*, 2016, 1021, 45-56.
178. F. Sousa, S. Freitas, A. R. Azzoni, D. M. Prazeres and J. Queiroz, *Appl. Biochem. Biotechnol.*, 2006, 45, 131-140.
179. H. Zhao, *J. Chem. Technol. Biotechnol.*, 2015, 90, 19-25.
180. T. Li, M. D. Joshi, D. R. Ronning and J. L. Anderson, *J. Chromatogr. A*, 2013, 1272, 8-14.
181. K. D. Clark, O. Nacham, H. Yu, T. Li, M. M. Yamsek, D. R. Ronning and J. L. Anderson, *Anal. Chem.*, 2015, 87, 1552-1559.

182. E. Gonzalez Garcia, A. K. Ressmann, P. Gaertner, R. Zirbs, R. L. Mach, R. Krska, K. Bica and K. Brunner, *Anal. Bioanal. Chem.*, 2014, 406, 7773-7784.
183. D. J. Huang and D. C. Huang, *Adv. Mat. Res.*, 2012, 455-456, 477-482.
184. P. Xu, Y. Wang, J. Chen, X. Wei, W. Xu, R. Ni, J. Meng and Y. Zhou, *Talanta*, 2018, 189, 467-479.
185. H. Tateishi-Karimata and N. Sugimoto, *Nucleic Acids Res.*, 2014, 42, 8831-8844.
186. H. Tateishi-Karimata and N. Sugimoto, *Angew. Chem. Int. Ed.*, 2012, 51, 1416-1419.
187. A. Haque, I. Khan, S. I. Hassan and M. S. Khan, *J. Mol. Liq.*, 2017, 237, 201-207.
188. M. Marušič, H. Tateishi-Karimata, N. Sugimoto and J. Plavec, *Biochimie*, 2015, 108, 169-177.
189. K. Jumbri, M. B. Abdul Rahman, E. Abdulmalek, H. Ahmad and N. M. Micaelo, *Phys. Chem. Chem. Phys.*, 2014, 16, 14036-14046.

2. Extraction of antioxidants and separation of amino acids using IL-based ABS

2.1. Extraction of antioxidants using aqueous biphasic systems formed by carbohydrates and tetralkylphosphonium- or tetralkylammonium-based ionic liquids

Based on the published communication:¹ Maria V. Quental, Matheus M. Pereira, Ana M. Ferreira, Sónia N. Pedro, Shahla Shahriari, Aminou Mohamadou, João A. P. Coutinho and Mara G. Freire. *Green Chem.*, 2018, 20, 2978-2983.

Abstract

Aiming at establishing more effective and sustainable separation processes, herein we propose the use of carbohydrates combined with tetralkylphosphonium- and tetralkylammonium-based ionic liquids (ILs) to form aqueous biphasic systems (ABS). It was observed that the ability of carbohydrates to create ABS with ILs closely follows the carbohydrates octanol-water partition coefficients. These novel systems are competitive extraction platforms when compared against more conventional ABS formed by ILs and salts or fluorinated ILs and carbohydrates. It seems that an increase in the hydrophobicity of ILs improves the extraction performance for antioxidants, and no relation between the carbohydrate nature and the systems extraction efficiency was found. Parameters such pH and temperature prove to not have significant effect on the extrative performance of the proposed systems. Finally, it is shown that these systems can be efficiently recovered and reused.

Introduction

During the past decade there was a significant effort on the study of ionic-liquid-based aqueous biphasic systems (IL-based ABS) as alternative separation platforms¹. ABS are water-rich systems. This is an important feature when dealing with biologically active compounds with interest to the food and pharmaceutical industries², as well as when considering some environmental and health hazards of volatile organic solvents. Although ABS composed of polymers and/or salts are known since the 50's³, the use of ILs in ABS has led to a wide range of new liquid-liquid systems with remarkable extraction efficiencies and enhanced selectivity, as a result of the ILs tunable features⁴. A large number of works describing the application of these

¹**Contributions:** M.G.F. and J.A.P.C. conceived and directed this work. M.V.Q., A.M.F., S.S., S.N.P. and M.M.P. acquired the experimental data. M.V.Q., M.G.F. and J.A.P.C. interpreted the obtained experimental data. The manuscript was mainly written by M.V.Q. and M.G.F. with contributions from the remaining authors.

systems in the separation of amino acids⁵, proteins^{6, 7}, pharmaceuticals^{8, 9}, persistent pollutants¹⁰, among others, from model solutions to real complex media, is currently available.

Albeit ABS have been described as benign and biocompatible alternative separation systems, most of the studied IL-based ABS are formed by pairing imidazolium ILs and inorganic salts¹, which may rise some biodegradability and toxicity concerns. This fact triggered the research on ILs derived from natural sources and/or by combining ILs with polymers, carbohydrates or amino acids, aiming at developing more bio- and environmentally-friendly ABS¹¹⁻¹⁶. In particular, ABS composed of ILs and carbohydrates have been previously reported¹⁶⁻¹⁸. These studies were focused on offering a greener character to ABS using carbohydrates, non-toxic and renewable compounds, instead of high charge density inorganic salts. While promising advances towards more sustainable separation techniques have been achieved, all these studies employed ILs comprising aromatic cations and fluorinated anions. These fluoride-based ILs are more expensive, some are non-water-stable¹⁹, and in general they are environmentally persistent²⁰. The use of ILs with fluorinated anions, usually paired with imidazolium- and pyridinium-based cations, is however required to have more hydrophobic ILs able to undergo liquid-liquid demixing in presence of weak salting-out species, such as carbohydrates. In this context, there is still the need to find new ILs that could replace the commonly used ILs by others of a more sustainable nature. To the best of our knowledge, there are no reports in the literature regarding the use of ILs with higher biodegradability, lower toxicity and lower cost²¹, such as tetralkylphosphonium- and tetralkylammonium-based paired with non-fluorinated anions, to form ABS with carbohydrates. Focused on addressing this challenge, novel ABS composed of carbohydrates and tetralkylphosphonium- and tetralkylammonium-based ILs are herein studied. The carbohydrates investigated comprise: (i) monosaccharides, such as D-(-)-fructose, D-(+)-glucose, xylose, and D-(+)-mannose; (ii) disaccharides, such as D-(+)-maltose, and sucrose; and (iii) polyols, such as maltitol, xylitol, and D-sorbitol. The description and chemical structures of the carbohydrates and ILs investigated are displayed in Figure 2.1.1. These novel systems were then investigated as alternative separation platforms for phenolic acids with antioxidant character, namely gallic acid, syringic acid and vanillic acid.

Experimental procedure

Materials - The carbohydrates used were D-(-)-fructose (purity > 98.0 wt% from Panreac), D-(+)-glucose (purity > 99.5 wt% from Scharlau), D-(+)-mannose (purity > 99.0 wt% from Aldrich), D-(+)-maltose (> 98.0 wt% from Sigma), sucrose (purity > 99.5 wt% from Himedia), maltitol (purity > 95.0 wt% from Acros Organics), xylitol (purity > 99.0 wt% from Sigma), D-(+)-xylose (purity \geq 99.0 wt%, from Carlo Erba) and D-sorbitol (purity > 99.0 wt% Fluka). Gallic acid (purity > 99.5 wt%), syringic acid (purity > 98 wt%) and vanillic acid (purity > 97 wt%) were acquired from Merck and Sigma-Aldrich and Alfa Aesar, respectively. Tetra-n-butylphosphonium hydroxide ($[P_{4444}][OH]$, 40 wt % in water from Aldrich). Phosphonium-based ILs, namely tributylmethylphosphonium methylsulphate, ($[P_{4441}][MeSO_4]$, purity > 99 wt%), tetrabutylphosphonium bromide, ($[P_{4444}][Br]$, purity > 96 wt%), and tetrabutylphosphonium chloride, ($[P_{4444}][Cl]$, purity > 96 wt%), were kindly provided by Cytec Industries, Inc. The tetrabutylammonium bromide, ($[N_{4444}][Br]$, purity > 98 wt%) was acquired from Fluka. The ILs tri(n-butyl)[2-ethoxy-2-oxoethyl]phosphonium bromide ($[P_{444}(OC_2)][Br]$) and tri(n-butyl)[2-ethoxy-2-oxoethyl]ammonium bromide ($[N_{444}(OC_2)][Br]$) were synthesized and characterized according to protocol described in the literature²². Tetrabutylphosphonium butanoate ($[P_{4444}][But]$), tetrabutylphosphonium hexanoate ($[P_{4444}][Hex]$) and tetrabutylphosphonium octanoate ($[P_{4444}][Oct]$) were synthesized according to the literature². Briefly, an aqueous solution of each carboxylic acid was added drop-wise to $[P_{4444}][OH]$ solution with a slight equimolar excess. The solution was stirred at room temperature during 12 h; then, the reaction mixture obtained was evaporated at 60 °C under vacuum. A mixture of acetonitrile and methanol (1:1) was added to the viscous liquid previously obtained, stirred vigorously at room temperature until the precipitation of the unreacted buffer, which was posteriorly removed by filtration. The solvent (acetonitrile + methanol) was evaporated and the ILs were dried under vacuum for 4 days at room temperature (25 °C)².

The materials used in these ILs synthesis were 2-bromoacetic acid ethyl ester, ethyl acetate, tri(n-butyl)phosphine and tri(n-butyl)amine, purchased from Sigma-Aldrich. Butyric acid (> 99.9 wt%, from Riedel de Haen), hexanoic acid (> 99.0 wt%, from Aldrich) and octanoic acid (> 98.0 wt%, from Sigma-Aldrich) were used. The organic salt potassium citrate tribasic monohydrate ($C_6H_5K_3O_7 \cdot H_2O \geq 99$ wt% pure) was acquired from Sigma-Aldrich.

The ABS studied at higher pH values were established by using aqueous solutions of sodium hydroxide (NaOH, ≥ 99.5 wt% pure), purchased from José Manuel Gomes dos Santos. The water employed was double distilled, passed across a reverse osmosis system and further treated with a Milli-Q plus 185 water purification apparatus.

The SPE cartridge used in the solid-phase extractions to recover phenolic acids was Oasis HLB (200 mg) from Waters. Methanol used was of HPLC grade, acquired from Sigma-Aldrich.

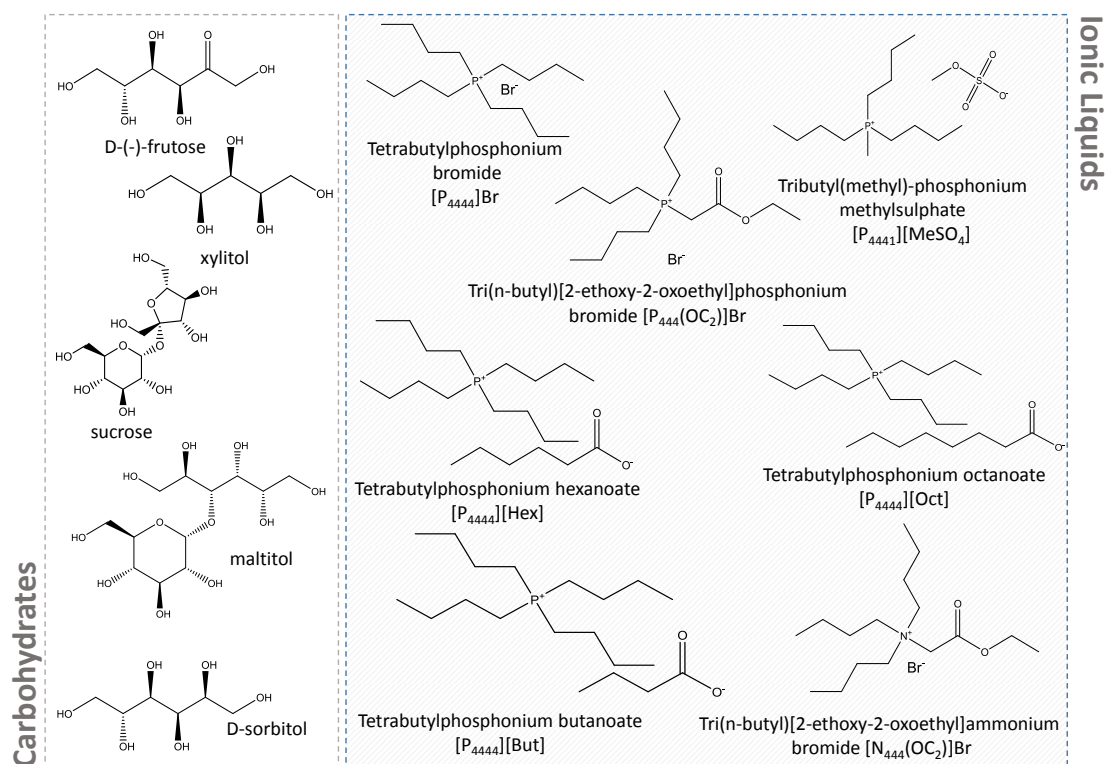


Figure 2.1.1 Chemical structures of the studied carbohydrates (CHs) and ionic liquids (ILs) able to form ABS.

Phase diagrams and tie-lines (TLs) - Two methods were used to evaluate the possibility of creating ABS by combining ILs and carbohydrates in aqueous media: cloud point titration and turbidimetric titration at 15, 25, 35 and 45 (± 1) °C and atmospheric pressure. The cloud point titration method was used to determine the ternary phase diagrams with the ILs $[P_{4441}][MeSO_4]$, $[P_{444(OC_2)}][Br]$ and $[P_{4444}][Br]$ combined with D-(-)-fructose. Aqueous solutions of D-(-)-fructose at ≈ 75 wt% and aqueous solutions of the different ILs at ≈ 90 wt% were gravimetrically prepared and used for the determination of the binodal curves. The dropwise addition of the aqueous IL solution to each carbohydrate aqueous solution was carried out until the detection of a cloudy (biphasic) solution, followed by the dropwise addition of water until the formation of a clear and limpid solution. Dropwise additions were carried out under constant stirring and atmospheric pressure. The ternary systems compositions were determined by weight quantification of all components ($\pm 10^{-4}$ g), using an analytical balance, Mettler Toledo Excellence XS205 DualRange. The turbidimetric titration method was used to determine the ternary phase diagrams with the IL $[P_{4444}][Br]$ combined with sucrose, maltitol, and xylitol at 25 °C, and for $[P_{444(OC_2)}][Br]$ with D-(-)-

fructose at 25 (± 1 °C). This method was also used for the determination of the binodal curves of the ABS formed by [P₄₄₄₄]Br + D-(-)-fructose at 15, 35 and 45 (± 1) °C. Various mixtures of carbohydrate, IL and water were gravimetrically prepared within the biphasic region, in glass tubes up to 1 g and thoroughly mixed. Water was added until a clear solution was identified. With the knowledge of the initial mixture composition and of the added water amount, the system composition was determined and a new point on the binodal curve identified. The mixture compositions were gravimetrically determined ($\pm 10^{-4}$ g) at 15, 25, 35 and 45 (± 1) °C.

Tie-lines (TLs), which correspond to the composition of each phase for a given mixture composition, were determined by a gravimetric method originally proposed by Merchuk et al.²³. Each mixture composition was determined by the weight quantification of all components added within $\pm 10^{-4}$ g (Mettler Toledo Excellence XS205 Dual Range). The tie-lines (TLs), which give the composition of each phase for a given mixture composition, were determined gravimetrically at 25 °C according to the original method reported by Merchuk et al.²³ The experimental binodal curves were fitted by Equation 1:

$$[IL] = A \exp[(B[CH]^{0.5}) - (C[CH]^3)] \quad (\text{Equation 1})$$

where [IL] and [CH] are the IL and carbohydrates weight fraction percentages, respectively, and the coefficients A, B, and C are fitting parameters. The parameters were determined using the Sigma Plot 11.0 software. TLs and tie-line lengths (TLLs) were determined by the lever-arm rule through the relationship between the top phase composition and the overall system composition, according to the following equations (Equations 2-5):

$$[IL]_{IL} = A \exp[(B[CH]_{IL}^{0.5}) - (C[CH]_{IL}^3)] \quad (\text{Equation 2})$$

$$[IL]_{CH} = A \exp[(B[CH]_{CH}^{0.5}) - (C[CH]_{CH}^3)] \quad (\text{Equation 3})$$

$$[IL]_{IL} = \left(\frac{[IL]_M}{\alpha} \right) - \left(\frac{(1-\alpha)}{\alpha} \right) [IL]_{CH} \quad (\text{Equation 4})$$

$$[CH]_{IL} = \left(\frac{[CH]_M}{\alpha} \right) - \left(\frac{(1-\alpha)}{\alpha} \right) [CH]_{CH} \quad (\text{Equation 5})$$

where, subscripts IL, CH, and M correspond to the top (IL-rich), bottom (carbohydrate-rich) and mixture phases, respectively. The parameter α is the ratio between the mass of the IL-rich phase and the total mass of the two phases. The system solution results in the composition wt% of the

IL and carbohydrate in the top and bottom phases. For the calculation of each tie-line length (TLL), Equation 6 was used:

$$TLL = \sqrt{([CH]_{IL} - [CH]_{CH})^2 + ([IL]_{IL} - [IL]_{CH})^2} \quad (\text{Equation 6})$$

For the determination of each TL, a ternary mixture at the biphasic region was prepared by weight, vigorously stirred, and further submitted to centrifugation for 30 min at 25 (\pm 1) °C. Each phase was carefully separated and weighted, and each TL determined by the application of the lever-arm rule.

Phenolic acids extraction and pH studies - Aqueous solutions of each studied antioxidant were prepared (0.006 mol.dm³ for gallic acid, and 0.030 mol.dm³ for vanillic and syringic acids) and used as the aqueous solution required to form the biphasic systems in the separation studies. Two different mixture compositions were used: 35 wt% of carbohydrate + 40 wt% of [P₄₄₄₄]Br, and 50 wt% of D-(-)-fructose + 25 wt% IL (IL = [P₄₄₄₄]Br, [P₄₄₄₁][MeSO₄], [P₄₄₄(OC₂)]Br, [N₄₄₄₄]]Br, and [N₄₄₄(OC₂)]Br). Moreover, for comparison purposes, the systems formed by 50 wt% of D-(-)-sorbitol or sucrose + 25 wt% [C₄mim][CF₃SO₃], and 25 wt% of [P₄₄₄₄]Br + 38 wt% of C₆H₅K₃O₇, were also investigated. Each mixture was vigorously stirred and centrifuged for 30 min at 15, 25 and 45 °C. After a careful separation of both phases, the quantification of the antioxidants in each phase was carried by UV-spectroscopy, using a UV-spectrophotometry (SYNERGY|HT microplate reader, BioTek), at a wavelength of 272 nm for gallic acid, 280 nm for vanillic acid and 272 nm for syringic acid. At least three individual experiments were performed in order to determine the average in the partition coefficients and extraction efficiencies, as well as the respective standard deviations. Blank control samples without adding antioxidants were always used. The extraction studies at different pH values were attained using aqueous solutions of NaOH at different concentrations to prepare the IL solutions used in the partitioning studies. The pH of each aqueous phase was determined at 25 (\pm 1) °C using an HI 9321 Microprocessor pH meter (HANNA instruments).

Recovery of the phenolic acids and recyclability of the ABS components - The recovery of the studied phenolic acids from the IL-rich phase was performed by solid-phase extraction, with Oasis HLB cartridges previously washed with methanol (1 mL). Each IL-rich phase containing phenolic acids was passed through the column (SPE1), in which phenolic acids are adsorbed, followed by 1 mL of acidic water (pH *ca.* 2) (SPE2) and 1 mL of methanol (SPE3). All these

fractions were collected since they contain the IL present in the original IL-rich phase. The phenolic fraction was finally desorbed by the addition of 1 mL of methanol (SPE4). All fractions were collected, and the phenolic acids quantified by UV-Vis spectroscopy using calibration curves previously established. The IL recovery and absence in the phenolic acids fraction was confirmed through ^1H NMR spectroscopy (Bruker AMX 300) operating at 300 MHz, and the respective losses determined gravimetrically ($\pm 10^{-4}$ g).

After the phenolic acid's separation through SPE, the fractions containing IL were submitted to evaporation under vacuum at room temperature, up to constant weight since only the IL and carbohydrate are the non-volatile species. The recovered IL + carbohydrate was then reused in the creation of a novel ternary system, and their extraction performance for gallic acid accessed by HPLC-DAD (Shimadzu, model PROMINENCE). HPLC analyses were performed with an analytical C18 reversed-phase column (250×4.60 mm), kinetex 5 μm C18 100 A, from Phenomenex. The mobile phase used was a gradient system of 0.1% TFA-ultra-pure water with of TFA (phase A) and 0.1% TFA-acetonitrile (phase B), previously degassed by ultrasonication. The separation was conducted using the following gradient mode: 0 min 25% of B, 42 min 42% of B, 45 min of B, and then returned to initial conditions during 20 min to ensure the column stabilization. The flow rate used was $0.8 \text{ mL} \cdot \text{min}^{-1}$ and using an injection volume of 30 μL . DAD was set at 272 nm. Each sample was analysed at least in duplicate. The column oven and the autosampler operated at a controlled temperature of 25 $^{\circ}\text{C}$. Under these conditions, gallic acid displays a retention time of 3.4 min.

Results and Discussion

ABS phase diagrams - To identify the ILs and carbohydrates compositions able to form ABS, and to employ these systems in separation and purification processes, the respective phase diagrams, tie-lines, and tie-line lengths were determined at 25 $^{\circ}\text{C}$. To address the effect of temperature in their liquid-liquid demixing ability, phase diagrams of the ABS formed by $[\text{P}_{4444}]\text{Br}$ + D-(-)-fructose + water were also determined at 15, 35 and 45 $^{\circ}\text{C}$. The ILs and carbohydrates pairs able to form ABS are represented in Figure 2.1.2, together with the respective ternary phase diagrams and fitted solubility curves (*cf.* the Appendix A1 with detailed information). Mixtures above the solubility curves form a two-phase system, while mixture compositions below the curve are monophasic.

From Figure 2.1.2 it is clear that there is a set of non-aromatic and non-fluorinated ILs able to form ABS with carbohydrates, including more benign ILs, namely analogues to glycine-betaine ($[\text{N}_{444}(\text{OC}_2)]\text{Br}$), a naturally occurring and low cost amino acid. Glycine-betaine can be found in

sugar beet molasses (up to 27 wt%), after the extraction of sucrose, and is still an underexploited by-product of the sugar industry²⁴. Therefore, the identified ABS formed by the glycine-betaine IL analogue and carbohydrates can also be envisioned as possible separation strategies in this type of industry, while allowing the use of glycine-betaine and their derivatives as food supplements²⁴, and in cosmetic lotions and formulations²⁵.

In aqueous media, the competition between the IL ions and carbohydrates for water solvation is dominated by the carbohydrates that will thus act as salting-out species, further leading to the exclusion of the IL to a second aqueous phase. This mechanism is supported by the trend obtained, in which the more hydrophilic carbohydrates (*e.g.* those with more –OH groups and with higher ability for hydrogen-bonding with water) combined with more hydrophobic ILs are more prone to form ABS. Taking into account the solubility curves obtained with fructose (Figure 2.1.2 A), the following ILs rank to create ABS with fructose was found: $P_{4444}Br > [P_{444}(OC_2)]Br > [P_{4444}][Oct] \sim [P_{4444}][Hex] > [P_{4444}][But] \sim [P_{4441}][MeSO_4] \sim [N_{4444}][Br] > [N_{444}(OC_2)]Br$. $[P_{4444}]Br$ is the most effective IL to create ABS. In fact, this IL can form ABS with monosaccharides, disaccharides and polyols. Compared to $[P_{4444}]Br$, $[P_{4444}]Cl$ has an anion of higher hydrogen-bond basicity, and thus with more affinity for water, being less prone to be salted-out. Therefore, this IL does not form ABS with any of the studied carbohydrates. Furthermore, an increase in the alkyl chain of the ILs comprising carboxylate anions leads to an increase in the ABS formation capacity, as expected given their increased hydrophobicity as the alkyl side chains length increases. In the same line, $[P_{4441}][MeSO_4]$, comprising a shorter alkyl chain and an anion of higher hydrogen-bond basicity than Br^- , is less susceptible to be salted-out by carbohydrates and to form ABS. Comparing the pairs $[N_{444}(OC_2)]Br$ vs. $[N_{4444}]Br$ and $[P_{444}(OC_2)]Br$ vs. $[P_{4444}]Br$, it is observed a decrease on the efficiency to form ABS when additional ester groups are present (with a higher aptitude to hydrogen-bond with water). In summary, the lower the IL hydrophilic nature or affinity for water, the higher it is its ability to form ABS with carbohydrates - following the trend observed in IL-salt ABS, in which salts also act as salting-out species¹.

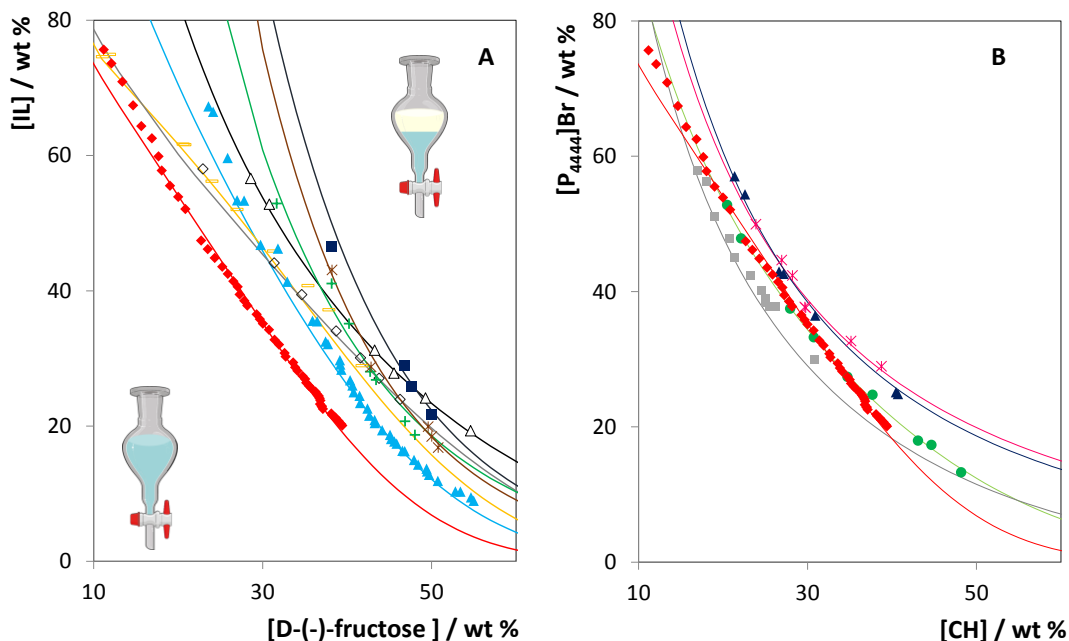


Figure 2.1.2 A- Phase diagrams of ABS composed of IL + D-(-)-fructose + H₂O at 25 °C: [P₄₄₄₄]Br (◆); [P₄₄₄(OC₂)]Br (▲); [P₄₄₄₄][Oct] (★); [P₄₄₄₄][Hex] (+); [P₄₄₄₄][But] (■); [P₄₄₄₁][MeSO₄] (—); [N₄₄₄₄]Br (◇); [N₄₄₄(OC₂)]Br (Δ). B- Phase diagrams of ABS composed of [P₄₄₄₄]Br + carbohydrate + H₂O at 25 °C: sucrose (■); D-(-)- fructose (◆); D-sorbitol (●); xylitol (▲); maltitol (✱).

The phase diagrams of the ABS formed by [P₄₄₄₄]Br + D-(-)-fructose were determined at different temperatures (from 15 to 45 °C), with an almost negligible decrease on the liquid-liquid demixing ability as temperature increases. The corresponding data are shown in the Appendix A1 at Table A.1.6. This trend could be seen as a major advantage when designing these systems for scaled-up strategies in terms of energetic inputs.

Previous works focused on ABS composed of a wide variety of carbohydrates and ILs constituted by fluorinated anions and imidazolium¹⁷ or pyridinium¹⁸ cations. Although these ILs are highly distinct from those investigated in this work, a similar trend for the carbohydrates salting-out ability was identified. The comparison of the phase diagrams obtained in this work with those previously reported with other ILs is shown in the Appendix A1, Figure A.1.1. In general, disaccharides are better salting-out agents than polyols, and the former are better salting-out agents than monosaccharides (this trend is more clear in molality units as shown in Figure A.1.1 in Appendix A1 since discrepancies arising from the different carbohydrates molecular weights are avoided). As previously identified¹⁷, two features of the carbohydrates seem to rule their salting-out ability: the number of –OH groups and their relative positions at C(2) and C(4). It has been shown that the carbohydrates hydrogen-bonding ability with water depends on the spacing and orientation of their polar groups, in which the C(4) axial/equatorial

ratio has a significant impact. In this work, we have additionally observed that the ability of carbohydrates to create ABS with ILs closely follows the carbohydrates octanol-water partition coefficients, which are given in the Table 2.1.1²⁶.

Table 2.1.1 Octanol-water partition coefficients ($\log K_{ow}$) of the studied carbohydrates²⁶.

Carbohydrates	$\log K_{ow}$
D-(-)-fructose	-3.27
D-(+)-glucose	-2.93
D-(+)-maltose	-4.70
Sucrose	-4.53
Maltitol	-5.50
Xylitol	-3.10
D-sorbitol	-3.73

In summary, a set of non-aromatic and non-fluorinated ILs prone to form ABS with carbohydrates was identified, contributing towards the development of more sustainable IL-based ABS.

Extraction of phenolic acids using ABS - Taking advantage of their more attractive features, the possible application of the proposed ABS in separation processes of interest to the food, nutraceutical and pharmaceutical industries was ascertained. These systems were evaluated in terms of their extraction performance for antioxidants, namely vanillic (VA), gallic (GA) and syringic (SA) acids. All extractions experiments were carried out at two mixture compositions in the biphasic regime: 35 wt% of carbohydrate + 40 wt% of [P₄₄₄₄]Br and 50 wt% of carbohydrate + 25 wt% of [P₄₄₄₄]Br, [P₄₄₄₁][MeSO₄] or [P₄₄₄(OC₂)]Br, allowing us to address the effects of both the mixture composition and IL nature. In all the investigated ABS, the sugar-rich aqueous phase corresponds to the bottom phase (as confirmed by us by conductivity), while the upper phase is mostly composed of IL and water.

Figure 2.1.3 depicts the extraction efficiencies (EE%) of the investigated IL-based ABS for the 3 antioxidants (phenolic acids), as well as their chemical structures. Extraction efficiencies correspond to the percentage weight amount of each phenolic acid in the IL-rich phase in respect to that present in both phases. Results given in partition coefficients (concentration of each phenolic acid in the IL-rich phase in respect to that in the carbohydrate-rich phase) are provided in the Appendix A1 (Table A.1.9).

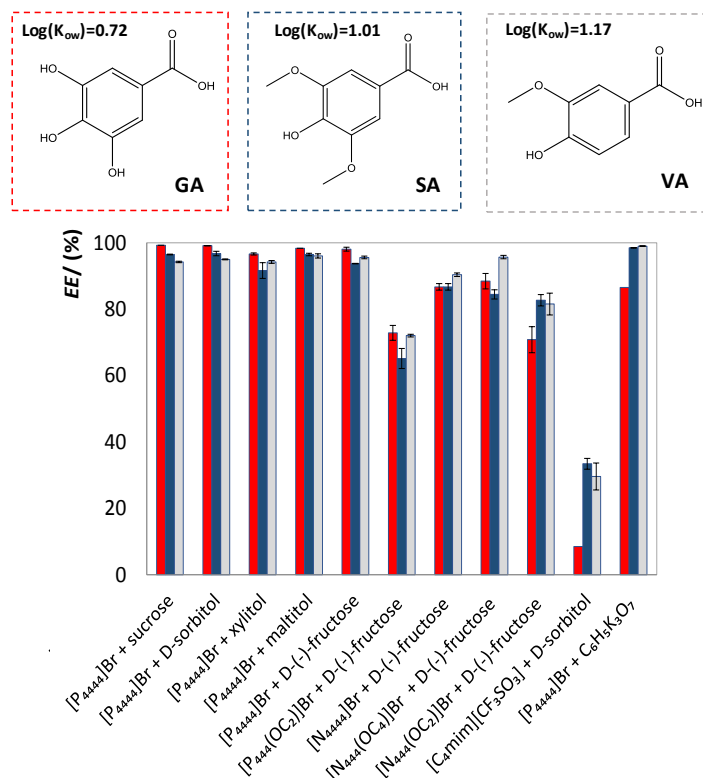


Figure 2.1.3 Extraction efficiencies ($EE\%$) of the studied systems for phenolic acids at 25 °C. ■■■ correspond to gallic acid (GA), syringic acid (SA), and vanillic acid (VA), respectively. Chemical structures and $\log(K_{ow})$ values of the studied antioxidants are also presented²⁷.

With the novel systems identified in this work, single-step extraction efficiencies of all antioxidants to the IL-rich phase ranging between 65 and 99% were obtained. Two trends on the performance of the studied ABS to extract phenolic acids were observed: gallic acid > vanillic acid > syringic acid (with phosphonium-based ILs) and vanillic acid > syringic acid > gallic acid (with ammonium-based ILs). According to the chemical structures displayed in Figure 2.1.3, it is patent that all antioxidants have a similar structure that differs in the substituents of the aromatic ring. With the ammonium-based ILs, the trend obtained follows the antioxidants $\log K_{ow}$ (octanol-water partition coefficient) values (provided in Figure 2.1.3). For these systems, the differences in hydrophobicity between the two phases seem to dominate the partition trend. Nevertheless, an inversion on the trend for gallic acid, the phenolic acid with a higher number of hydroxyl groups, was observed in phosphonium-based ABS, being this antioxidant that most extensively partitions into the IL-rich phase. In this case, specific interactions between gallic acid and the IL must be taking place, which given their chemical structures must correspond to hydrogen-bonding and dispersive-type interactions, and since electrostatic interactions do not play a role as discussed below.

Most of the studied systems are acidic in nature - *cf.* the Appendix A1 (Table A.1.8) with the pH values of the ABS coexisting phases - with pH values below the phenolic acids dissociation constants (Table 2.1.2)²⁶, meaning that antioxidants are being extracted in their protonated (neutral) form to the IL-rich phase. This fact suggests that electrostatic interactions are not taking place and are not responsible for the preferential migration of phenolic acids to the IL-rich phase.

Table 2.1.2 Dissociation constants of the studied phenolic acids²⁶.

Phenolic acid	pK_{a1} (-COOH)	pK_{a2} (-NH ₂)	pK_{a3} (-R)
VA	4.20	10.20	-
GA	4.40	9.40	11.00
SA	4.00	9.60	-

Overall, ABS formed by [P₄₄₄₄]Br and [N₄₄₄₄]Br perform better for the extraction of all antioxidants to the IL-rich phase than the respective [P₄₄₄(OC₂)]Br and [N₄₄₄(OC₂)]Br counterparts, where due to their higher polarity a small decrease on the extraction efficiencies is observed. An increase in the hydrophobicity of ILs seems to improve the extraction performance. On the other hand, when comparing all the [P₄₄₄₄]Br-based ABS, there is not a significant impact of the carbohydrate nature on the systems extraction efficiency.

The high extraction efficiencies achieved with the novel systems shown in this work are not common in ABS composed of ILs and carbohydrates. This is a main result of the weak salting-out ability of the sugar, in which only hydrophobic compounds, *e.g.* β -carotene, were previously observed to extensively partition to IL-rich phases¹⁷. To assert the higher potential of the studied ILs as novel phase-forming components of ABS for extraction purposes, the extraction abilities of ABS formed by imidazolium- and fluorinated-based ILs and carbohydrates ([C₄mim][CF₃SO₃] + D-sorbitol and [C₄mim][CF₃SO₃] + sucrose)¹⁷ were additionally investigated, for the same phenolic acids and similar mixture compositions. An ABS formed by ILs and salts ([P₄₄₄₄]Br + C₆H₅K₃O₇) was also investigated for comparison purposes (mixture composition: 25 wt% [P₄₄₄₄]Br + 38 wt% C₆H₅K₃O₇). The results obtained are depicted in Figure 2.1.3. With the systems formed by imidazolium-based ILs and carbohydrates, all phenolic acids preferentially partition to the carbohydrate-rich phase (*EE*% < 50%) – the opposite trend to that observed in ABS formed by phosphonium-/ammonium-based ILs. These data further support the idea that electrostatic interactions are not relevant since [C₄mim][CF₃SO₃]-based ABS display a higher pH (*cf.* the Appendix A1, Table A.1.8), and yet the charged phenolic acids still prefer to partition towards the low ionic strength phase (carbohydrate-rich).

Previous works have reported on the extraction of antioxidants using ABS formed by imidazolium-based ILs and inorganic salts^{27,28}. In some of these works it has been observed a significant effect of the pH of the medium and electrostatic interactions, thus allowing the design of switchable separation systems²⁹. To further clarify if the pH plays a significant role on the type of systems studied herein, the separation of the three antioxidants with the ABS composed of [P₄₄₄₄]⁺Br⁻ + D-(-)-fructose and [P₄₄₄₄]⁺Br⁻ + D-sorbitol at two additional pH values (5 and 6) were investigated – data shown in Figure 2.1.4.

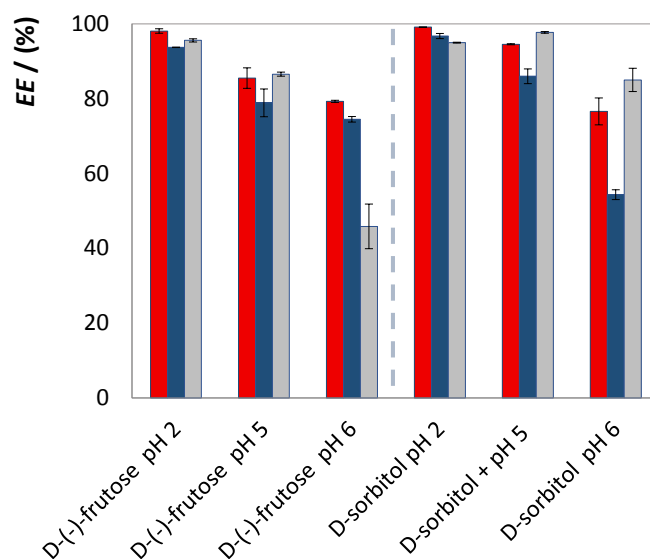


Figure 2.1.4 Extraction efficiencies (EE%) of the studied systems for phenolic acids in the ABS formed by [P₄₄₄₄]⁺Br⁻ + CH + H₂O at 25°C, at different pH values. ■ ■ ■ correspond to gallic acid (GA), syringic acid (SA) and vanillic acid (VA), respectively.

Although a small increase in the antioxidants partition to the IL-rich phase occurs as the pH decreases, the extraction efficiencies obtained with [P₄₄₄₄]⁺Br⁻-based ABS are still significantly higher than those obtained with ABS formed by ILs bearing imidazolium cations and fluorinated anions, and always preferentially migrating to the IL-rich phase (EE% > 50%). According to Figure 2.1.4, high extraction efficiencies (from 87 to 99%) were obtained with IL-salt-based ABS, demonstrating the preferential partition of phenolic acids to the IL-rich phase – an expected trend given the strong salting-out strength of the citrate-based salt used. ABS composed of polyethylene glycol (PEG), Na₂SO₄, and ILs as additives have been also reported in the literature in what concerns their ability to extract antioxidants²². For all systems it was observed the preferential partition of antioxidants to the PEG-rich phase (EE% > 90%), a result of the strong salt salting-out effect²². However, all these values are similar to those obtained with ABS formed

by phosphonium- and ammonium-based ILs and carbohydrates, reinforcing the competitive extraction performance of this set of more benign and lower ionic strength ABS.

An additional factor that can influence the extraction performance of IL-based ABS systems is temperature¹. However, in the studied systems, temperature, at least between 15 and 45 °C, has a negligible effect, leading to similar extraction efficiencies (Figure 2.1.5). This trend is in accordance with the almost negligible effect of temperature on the phase diagrams behaviour discussed above, thus not leading to changes in the phase's compositions.

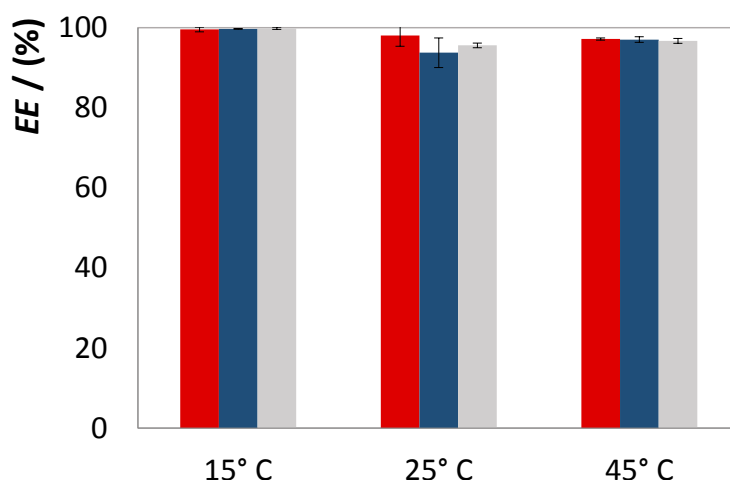


Figure 2.1.5 Extraction efficiencies ($EE\%$) of the studied systems for phenolic acids in the ABS formed by $[P_{4444}]\text{Br} + \text{D-(-)-fructose} + \text{H}_2\text{O}$ at different temperatures. ■ ■ ■ correspond to gallic acid (GA), syringic acid (SA) and vanillic acid (VA), respectively.

Recovery of phenolic acids and ABS components recyclability - Aiming at developing sustainable separation processes, we finally addressed the recovery of the studied phenolic acids from the IL-rich phase, and the phase-forming components recyclability for two times. We carried out the recovery of phenolic acids by solid-phase extraction (SPE), using previously identified effective cartridges for phenolic acids^{30,31}. The retention mechanisms of the used cartridges exhibits both hydrophilic and lipophilic retention characteristics³¹. We successfully eluted the IL and retained the phenolic acids by adsorption onto the column, which is finally recovered by a final elution step. With the $[P_{4444}]\text{Br} + \text{D-(-)-fructose}$ ABS, it is possible to recover between 98% and 100% of the initial content of gallic, syringic and vanillic acids at the IL-rich phase. The IL-rich solution was then subjected to evaporation under vacuum at room temperature, up to constant weight, and then used in the formation of new ABS and their extraction performance addressed (Figure 2.1.6).

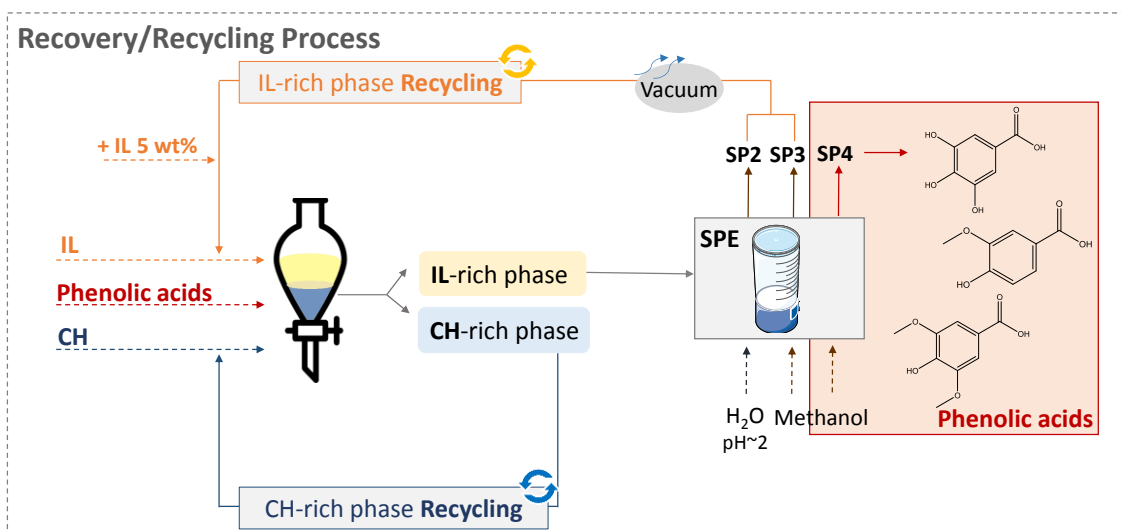


Figure 2.1.6 Scheme of the phenolic acids and ILs recovery, together with the IL recycling process.

The IL loss in each step is below 5 wt%, although we do believe that this value can be decreased by scaling-up the process. In the two subsequent extraction studies with the recycled IL, extraction efficiencies for gallic acid higher than 95% were obtained (Figure 2.1.7), confirming that the IL can be successfully recovered and reused without losses on the systems extraction performance.

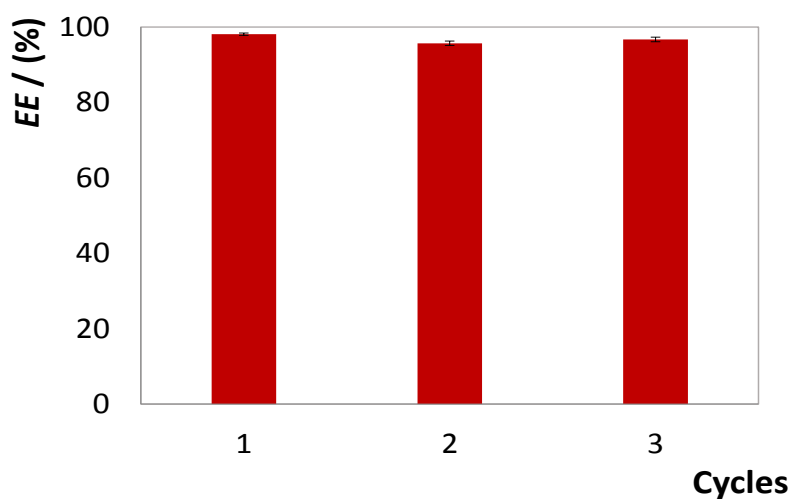


Figure 2.1.7 Extraction efficiencies (*EE*%) of the gallic acid in the ABS formed by [P₄₄₄₄]Br + D-(-)-fructose + H₂O in 3 cycles of extraction, where the last two correspond to the recycled IL.

Conclusions

All studies reported hitherto on the development of sustainable IL-based ABS by the use of carbohydrates focused on ILs constituted by aromatic cations combined with fluorinated anions - a crucial requirement given the weak salting-out of carbohydrates. Herein, we demonstrated the possibility of creating more sustainable ABS formed by carbohydrates and phosphonium- and ammonium-based ILs. Furthermore, these novel ABS display a significant performance to extract moderately hydrophilic compounds, such as phenolic acids, an unexpected behavior when compared with systems formed by carbohydrates and ILs previously reported. The novel systems disclosed in this work are competitive in terms of extraction performance, even when compared with ABS formed by ILs and strong salting-out salts. Finally, we demonstrated that phenolic acids can be recovered from the IL-rich phase, and that the employed IL can be recovered and reused with no losses on the ABS extraction performance.

References

1. M. G. Freire, A. F. M. Claudio, J. M. M. Araujo, J. A. P. Coutinho, I. M. Marrucho, J. N. C. Lopes and L. P. N. Rebelo, *Chem. Soc. Rev.*, 2012, 41, 4966-4995.
2. V. S. Anna, A. P. F. Correa, A. S. Motta and A. Brandelli, *Prep. Biochem. Biotechnol.*, 2016, 46, 838-843.
3. P. A. Albertsson, *Nature*, 1958, 182, 709-711.
4. K. E. Gutowski, G. A. Broker, H. D. Willauer, J. G. Huddleston, R. P. Swatloski, J. D. Holbrey and R. D. Rogers, *J. Am. Chem. Soc.*, 2003, 125, 6632-6633.
5. M. T. Z. Moattar and S. Hamzehzadeh, *Biotechnol Prog.*, 2011, 27, 986-997.
6. Q. Zeng, Y. Wang, N. Li, X. Huang, X. Ding, X. Lin, S. Huang and X. Liu, *Talanta*, 2013, 116, 409-416.
7. Z. Li, X. Liu, Y. Pei, J. Wang and M. He, *Green Chem.*, 2012, 14, 2941-2950.
8. Q. Liu, J. Yu, W. Li, X. Hu, H. Xia, H. Liu and P. Yang, *Sep. Sci. Technol.*, 2006, 41, 2849-2858.
9. J. Pang, C. Han, Y. Chao, L. Jing, H. Ji, W. Zhu, Y. Chang and H. Li, *Sep. Purif. Technol.*, 2015, 50, 1993-1998.
10. M. S. Noorashikin, S. Mohamad and M. R. Abas, *Anal. Methods*, 2014, 6, 419-425.
11. J. Zhang, Y. Zhang, Y. Chen and S. Zhang, *J. Chem. Eng. Data*, 2007, 52, 2488-2490.
12. M. D. Pérez, L. I. N. Tomé, M. G. Freire, I. M. Marrucho, O. Cabeza and J. A. P. Coutinho, *Sep. Purif. Technol.*, 2010, 72, 85-91.
13. E. V. Capela, M. V. Quental, P. Domingues, J. A. P. Coutinho and M. G. Freire, *Green Chem.*, 2017, 19, 1850-1854.
14. S. Noshadi and R. Sadeghi, *J. Phys. Chem. B*, 2017, 121, 2650-2664.
15. R. Sadeghi, N. Ebrahimi and M. D. Tehrani, *Polymer*, 2016, 98, 365-377.
16. Y. Chen, Y. Meng, J. Yang, H. Li and X. Liu, *J. Chem. Eng. Data*, 2012, 57, 1910-1914.
17. M. G. Freire, C. L. S. Louros, L. P. N. Rebelo and J. A. P. Coutinho, *Green Chem.*, 2011, 13, 1536-1545.
18. A. M. Ferreira, P. D. O. Esteves, I. B. Palheiros, A. B. Pereiro, L. P. N. Rebelo and M. G. Freire, *Green Chem.*, 2016, 18, 1070-1079.
19. M. G. Freire, C. M. S. S. Neves, I. M. Marrucho, J. A. P. Coutinho and A. M. Fernandes, *J. Phys. Chem. A*, 2010, 114, 3744-3749.
20. H. Wang, S. V. Malhotra and A. J. Francis, *Chemosphere*, 2011, 82, 1597-1603.
21. J. Chen, Y. Wang, Q. Zeng, X. Ding and Y. Huang, *Anal. Methods*, 2014, 6, 4067-4076.
22. Y. Gaetano, A. Mohamadou, S. Boudesocque, J. Hubert, R. P. Royon and L. Dupont, *J. Mol. Liq.*, 2015, 207, 60-66.
23. J. C. Merchuk, B. A. Andrews and J. A. Asenjo, *J. Chromatogr. B Biomed. Sci. Appl.*, 1998, 711, 285-293.
24. J. R. Hoffman, N. A. Ratamess, J. Kang, S. L. Rashti and A. D. Faigenbaum, *J. Int. Soc. Sports Nutr.*, 2009, 6, 7.
25. Z. F. Nsimba, M. Paquot, L. G. Mvumbi and M. Deleu, *Biotechnol. Agron. Soc. Environ.*, 2010, 14, 737-748.
26. Chemspider, The free chemical database, <http://www.chemspider.com> (accessed October 2017).

27. M. R. Almeida, H. Passos, M. M. Pereira, Á. S. Lima, J. A. P. Coutinho and M. G. Freire, *Sep. Purif. Technol.*, 2014, 128, 1–10.
28. A. F. M. Cláudio, A. M. Ferreira, C. S. R. Freire, A. J. D. Silvestre, M. G. Freire and J. A. P. Coutinho, *Sep. Purif. Technol.*, 2012, 97, 142–149
29. A. F. M. Claudio, C. F. C. Marques, I. B. Palheiros, M. G. Freire and J. A. P. Coutinho, *Green Chem.*, 2014, 16, 259-268.
30. M. N. Irakli, V. F. Samanidou, C. G. Biliaderis and I. N. Papadoyannis, *J. Sep. Sci.*, 2012, 35, 1603-1611.
31. A. Michalkiewicz, M. Biesaga and K. Pyrzynska, *J. Chromatogr. A*, 2008, 1187, 18-20.

2.2. Separation of aromatic and aliphatic amino acids mixtures using ionic-liquid-based aqueous biphasic systems

Based on the communication:² Emanuel V. Capela[§], Maria V. Quental[§], Pedro Domingues, João A. P. Coutinho and Mara G. Freire. *Green Chem.*, 2017, 19, 1850-1854.

[§]equal contribution

Abstract

Based on the particular ability of aliphatic amino acids to form aqueous biphasic systems with ionic liquids (ILs), it is here shown how these systems can be used to selectively and efficiently separate mixtures of aliphatic and aromatic amino acids usually present in protein hydrolysates or in fermentation broths. To this end, phosphonium- and ammonium-based ILs have been investigated. These novel IL-based ABS allow, in a single step, extraction efficiencies of aromatic amino acids ranging between 40 and 85% to the IL-rich phase, and extraction efficiencies of aliphatic amino acids ranging between 91 and 98% to the opposite phase. Finally, it is shown amino acids can be recovered from the IL-rich phase, allowing the IL recyclability.

Introduction

Amino acids are the “building blocks” of proteins and play an important role in several physiological phenomena, such as metabolism, gene expression, signal transduction, and in cellular and extracellular structures. Therefore, amino acids are critical compounds in animal and human nutrition, being also employed as food additives, feed supplements and artificial sweeteners¹. In particular, aromatic amino acids, such as L-Phenylalanine (L-Phe), L-Tryptophan (L-Trp) and L-Tyrosine (L-Tyr), are amongst the most important for nutritional applications. L-Phe is a major component of the artificial sweetener aspartame, L-Trp is used in large quantities as an animal feed², and L-Tyr is used in diet supplements³. These compounds can be obtained by the hydrolysis of proteins, fermentation or synthesis⁴. With the exception of the latter, the remaining processes result in complex mixtures of amino acids, thus requiring additional separation and purification steps to obtain the target product with an adequate purity level. In spite of these difficulties, natural amino acids are still the preferred choice and seen as the more safe option for use in human nutrition.

The hydrolysis of natural proteins, such as casein or whey proteins, results in a wide variety of essential amino acids – Phe, Trp, Threonine (Thr), Valine (Val), Lysine (Lys), among others –

²Contributions: M.G.F. and J.A.P.C. conceived and directed this work. M.V.Q. and E.V.C. acquired the experimental data. M.V.Q., M.G.F., P.D. and J.A.P.C. interpreted the obtained experimental data. The manuscript was mainly written by M.V.Q., E.V.C. and M.G.F. with contributions from the remaining authors.

and non-essential amino acids – Alanine (Ala), Asparagine (Asn), Serine (Ser), Proline (Pro) and Tyrosine (Tyr)⁵. The same type of amino acids can be directly obtained from protein hydrolysates of fish processing by-products⁶, adding value to matrices that are secondary or residues from food industries. On the other hand, fermentation media are rich in a wide variety of nutrients, *e.g.* glucose or other sugars, as well as in other amino acids used as feedstocks or obtained as products^{7,8}. As an example, a mutant of the genus *Bacillus* is used for Trp production; yet, L-Phe, L-Leucine (L-Leu) and L-Methionine (L-Meth) must be added to the growth medium⁹. In the same line, when resorting to the modified pentose phosphate pathway by *Corynebacterium glutamicum*, amino acids such as Pro, Val, and Ala are the major by-products obtained (*ca.* 6% of the total amino acids)¹⁰. Despite their high interest and value, amino acids obtained by proteins hydrolysis or fermentation lack in high purity standards.

The downstream processing of natural-derived amino acids comprises several stages, such as the cells removal by centrifugation and/or filtration¹¹, followed by chromatographic¹² and/or concentration/crystallisation¹³ steps. However, these sequential methods are rather difficult to be transposed to a large-scale and require a high investment¹⁴. The recovery and purification costs of amino acids can reach up to 80% of the final product cost¹⁵. Therefore, there is a crucial demand on the development of cost-effective processes for their fractionation and selective separation aiming at obtaining amino acids with high purity levels.

The introduction of the “Green Chemistry” concept¹⁶ triggered the research on more benign solvents and processes; it is in this context that ionic liquids (ILs) have been under the spotlight. Although some controversy still exists, and features such as biodegradability, toxicity and full life-cycle analyses need to be fulfilled¹⁷, aprotic ILs are non-volatile solvents, and thus they do not contribute to atmospheric pollution. In addition to their non-volatile nature, one of their most important characteristics is related to their tailoring ability achieved by the large range of possible cation/anion combinations; as a result, effective ILs can be designed for a particular application. Along with their wide variety of applications, in the last decade, it was demonstrated that ILs form aqueous biphasic systems (ABS) when added to aqueous solutions of inorganic salts¹⁸.

Due to their water-rich media, ABS are adequate for liquid-liquid extraction processes, and have been used in the purification and concentration of cells, viruses, nucleic acids, proteins, antibiotics, among others^{19,20}. Albeit ABS composed of polymers have been largely investigated in the past six decades¹⁸, the use of ILs in these systems has led to enhanced extraction efficiencies and selectivity²¹. In addition to the most studied type of ABS comprising ILs and inorganic salts²¹, in 2007, Zhang et al.²² demonstrated that amino acids (Glycine (Gly), L-Ser, and

L-Pro) are also able to form IL-based ABS. One of their main advantages comprises the possibility of using natural-derived compounds coupled to a medium of low ionic strength.

In spite of their advantages, only two works^{22, 23} reported the use of amino acids to create IL-based ABS. This lacuna is a consequence of the low capacity of amino acids to induce the salting-out of ILs, and thus to create two-phase systems in aqueous media^{22, 23}. Previous works^{22, 23} demonstrated the possibility of ABS formation only with 1-Butyl-3-methylimidazolium dicyanamide ([C₄mim][DCA]), 1-Butyl-3-methylimidazolium trifluoromethanesulfonate ([C₄mim][CF₃SO₃]) and 1-Butyl-3-methylimidazolium tetrafluoroborate ([C₄mim][BF₄]). These imidazolium-based ILs are of a low benign character, relatively expensive due their fluorinated anions, and some of them are non-water-stable²⁴. To the best of our knowledge, there are no reports in the literature regarding the use of ILs with a higher biodegradability, lower toxicity and lower cost, such as ammonium- and phosphonium-based^{25, 26}, to form ABS with amino acids. Furthermore, as it is only possible to form ABS with ILs of low hydrogen-bond basicity and more hydrophilic aliphatic amino acids (aromatic amino acids do not form ABS with ILs)^{22, 23}, these systems can be foreseen as adequate platforms to selectively separate mixtures of aliphatic and aromatic amino acids, a possibility that has never been attempted and that is explored herein.

As a first step, a wide range of amino acids as phase-forming components of ABS was investigated and were further combined with aqueous solutions of several tetraalkylphosphonium- and tetraalkylammonium-based ILs. For the combinations in which it was possible to create ABS, the respective ternary liquid–liquid equilibrium phase diagrams were determined at 25 °C. Then, the ability of these systems to selectively separate aliphatic and aromatic amino acids was evaluated by the determination of the extraction efficiency of each amino acid to a given phase. Figure 2.2.1 depicts a schematic overview of the proposed process, as well as the chemical structures of the amino acids investigated.

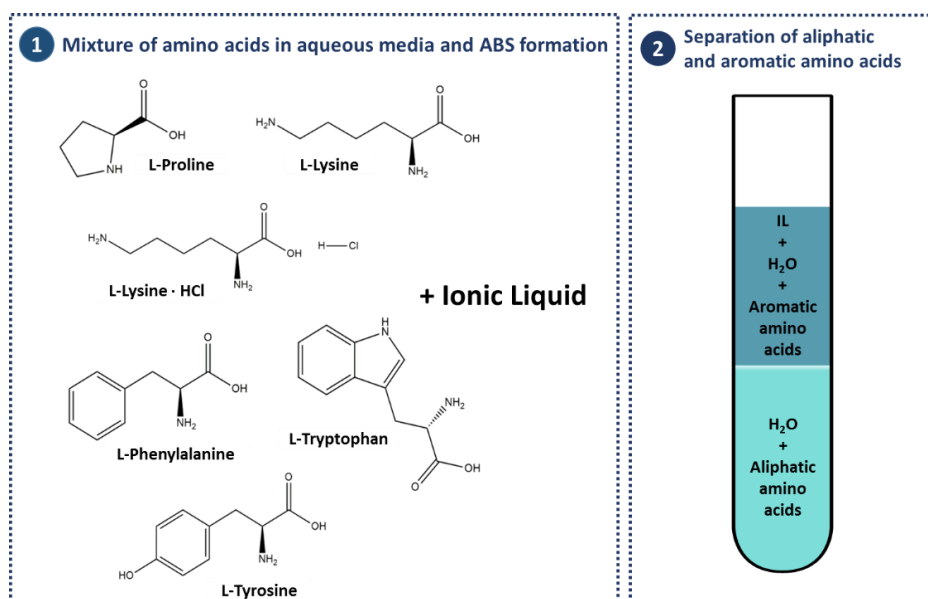


Figure 2.2.1 Chemical structures of the investigated amino acids and schematic view of the proposed process for the selective separation of aliphatic and aromatic amino acids mixtures.

Experimental Procedure

Materials - The phosphonium-based ILs investigated were the following: ethyl(tributyl)phosphonium diethylphosphate ([P₄₄₄₂][Et₂PO₄], purity > 95.0 wt%), tetrabutylphosphonium bromide ([P₄₄₄₄]Br, purity > 96.0 wt%), tetrabutylphosphonium chloride ([P₄₄₄₄]Cl, purity > 96.0 wt%), tri(isobutyl)methylphosphonium tosylate ([P_{ii(444)1}][TOS], purity > 99.0 wt%), tributyl(methyl)phosphonium methylsulfate ([P₄₄₄₁][MeSO₄], purity > 98.6 wt%), and tributyl(tetradecyl)phosphonium chloride ([P₄₄₄₍₁₄₎]Cl, purity > 97.0 wt%). All phosphonium-based ILs were kindly provided by CYTEC Industries, Inc. The ammonium-based ILs investigated were tetrapropylammonium bromide ([N₃₃₃₃]Br, purity > 98.0 wt%), tetrabutylammonium bromide ([N₄₄₄₄]Br, purity > 98.0 wt%), and tetrabutylammonium chloride, ([N₄₄₄₄]Cl, purity > 97.0 wt%). [N₄₄₄₄]Br was supplied by Fluka, while [N₃₃₃₃]Br and [N₄₄₄₄]Cl were obtained from Sigma-Aldrich. For the extraction studies, 1-butyl-3-methylimidazolium trifluoromethanesulfonate ([C₄mim][CF₃SO₃], purity ≥ 99 wt%), and 1-butyl-3-methylimidazolium dicyanamide ([C₄mim][DCA], purity > 98 wt%), both purchased from Iolitec, were also used. Ammonia aqueous solutions at ca. 25 wt% were from CHEM-LAB.

The following aliphatic amino acids were used: L-Proline (L-Pro, Acros, purity > 99 w/w%), L-Lysine monohydrated (L-Lys, Acros, purity > 99 w/w%), L-Lysine hydrochloride (L-Lys·HCl, Sigma, purity > 99 w/w%), L-Arginine (L-Arg, Merck, purity > 99 w/w %), D-L-Aspartic Acid (D-L-Asp, Fluka, purity > 99 w/w%), L-Asparagine monohydrated (L-Asn, Fluka, purity > 99 w/w%), L-Valine (L-Val, Fluka, purity > 99 w/w %), L-Isoleucine (L-Ile, Merck, purity > 99 w/w%), L-Alanine (L-Ala,

Biochemical, purity > 99 w/w%) and L-Cysteine (L-Cys, Biochemicals, purity > 99 w/w %). The studied aromatic amino acids were the following: L-Tryptophan (L-Trp, Sigma, purity > 99 w/w%), L-Tyrosine (L-Tyr, Fluka, purity > 99 w/w %) and L-Phenylalanine (L-Phe, Sigma, purity > 99 w/w %). A Dowex 50W X8 (20 to 50 mesh) cation exchange resin was purchased from DOW. Figures A.2.1 and Figure A.2.2 depict the chemical structures of the aliphatic and aromatic amino acids investigated in this work, although only the hydrophobic ones displayed in Figure 2.2.1 are able to form ABS with the investigated ILs.

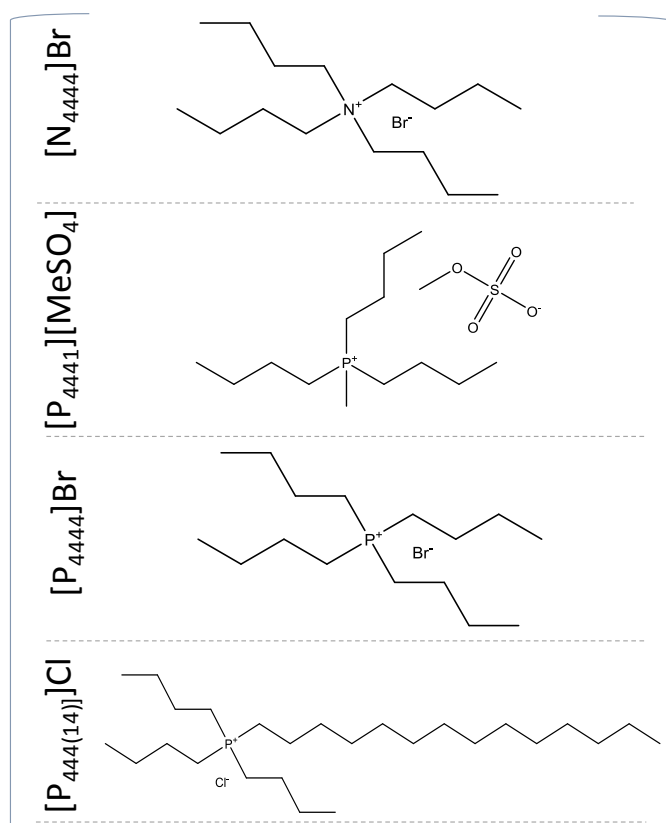


Figure 2.2.2 Chemical structure of the studied ILs.

ABS phase diagrams - The ternary phase diagrams (IL + amino acid + water) were determined with the following ILs: $[P_{4442}][Et_2PO_4]$, $[P_{4444}]Br$, $[P_{4444}]Cl$, $[P_{i(444)1}][TOS]$, $[P_{4441}][MeSO_4]$, $[P_{444(14)}]Cl$, $[N_{3333}]Br$, $[N_{4444}]Br$ and $[N_{4444}]Cl$, combined with the aliphatic amino acids L-Pro, L-Lys and L-Lys-HCl. The IL with the higher ability to be salted-out, was also tested with the remaining aliphatic amino acids, namely L-Arg, DL-Asp, L-Asn, L-Val, L-Ile, L-Ala and L-Cys. The binodal curves of each ABS were determined by the cloud point titration method at $(25 \pm 1)^\circ C$, as described in Chapter 2, Section 2.1. Aqueous solutions of aliphatic amino acids at ≈ 50 wt% and aqueous solutions of the different hydrophilic ILs at variable concentrations (from 50 wt% to 100 wt%) were gravimetrically prepared and used for the determination of the binodal curves.

The tie-lines (TLs) of each phase diagram, and at the mixtures compositions for which the extraction of aromatic amino acids was carried out, were determined by a gravimetric method originally described by Merchuk et al.²⁷, as described in Chapter 2.1 (Section 2.1).

Separation of amino acids - In order to avoid discrepancies in the results which could arise from the different compositions of the phases, all the partitioning studies were performed at a constant TLL. The mixture compositions which correspond to a TLL of ≈ 80 are the following: 42.81 wt% of $[P_{4444}]\text{Br}$ + 19.78 wt% of L-Lys + 37.41 wt% of H_2O ; 39.17 wt% of $[P_{4441}][\text{MeSO}_4]$ + 29.12 wt% of L-Lys + 31.71 wt% of H_2O ; 36.53 wt% of $[P_{4444}]\text{Br}$ + 31.73 wt% of L-Pro + 31.74 wt% of H_2O ; 40.03 wt% of $[\text{C}_4\text{mim}][\text{CF}_3\text{SO}_3]$ + 20.15 wt% of L-Lys + 39.82 wt% of H_2O ; and 51.50 wt% of $[\text{C}_4\text{mim}][\text{DCA}]$ + 20.80 wt% of L-Lys + 27.7 wt% of H_2O . For the $[P_{4444}]\text{Br}$ + L-Lys-HCl ABS a different TLL was used due to the smaller liquid-liquid region of this system, which corresponds to the following initial ternary mixture composition: 42.09 wt% of $[P_{4444}]\text{Br}$ + 11.40 wt% of L-Lys-HCl + 46.01 wt% of H_2O .

For the amino acids separation studies, instead of water, the systems were loaded with aqueous solutions containing the aromatic amino acids. Each mixture was vigorously stirred, centrifuged for 30 min, and left to equilibrate for at least 5 min at $25 (\pm 1)^\circ\text{C}$ to achieve the complete partitioning between the two phases. After a careful separation of both phases, the quantification of each amino acid in the two phases was carried by UV-spectroscopy, using a SYNERGY|HT microplate reader, BioTek, at a wavelength of 275 nm (for L-Trp and L-Tyr) or 255 nm (for L-Phe). At least three individual experiments were performed in order to determine the average in the extraction efficiency, as well as the respective standard deviations. The interference of the amino acids and ILs with the quantification method was ascertained and blank control samples were used. The pH of each aqueous phase was determined at $(25 \pm 1)^\circ\text{C}$ using an HI 9321 Microprocessor pH meter (HANNA instruments).

Percentage extraction efficiencies of amino acids ($EE_{aa}\%$) correspond to the percentage ratio between the amount of each amino acid in a given phase and that in the total mixture. The partition coefficients (K_{aa}) of each amino acid were determined by the ratio of concentrations of each amino acid in the IL-rich phase to that in the opposite phase, and the selectivity was determined as the ratio between the K_{aa} values for aromatic and aliphatic amino acids, as described in a previous work²⁸.

The extraction studies at different pH values were attained using aqueous solutions of NaOH at different concentrations to prepare the IL solutions at pH = 7, 10, and 11. The pH of each aqueous phase was determined at $25 (\pm 1)^\circ\text{C}$ using an HI 9321 Microprocessor pH meter (HANNA instruments).

Recovery of amino acids - The separation of the aromatic amino acids from the IL-rich phase was performed by solid-phase extraction, by cation exchange, with a Dowex-50 X8 (20 to 50 mesh) resin. The resin was initially washed with methanol (8 volumes), followed by 8 volumes of an ammonia aqueous solution at 4 wt% (pH *ca.* 11-12). Then, the IL-amino acid aqueous mixtures (corresponding to the IL-rich phase) were passed through the column. The column was finally regenerated with methanol. All fractions were collected, and the amino acid quantified by UV-Vis spectroscopy using calibration curves previously established and the IL quantified by ^1H NMR spectroscopy (Bruker AMX 300) operating at 300 MHz, using benzene as an internal reference.

Results and Discussion

ABS phase diagrams - The following amino acids as phase-forming components of ABS were investigated, namely L-Proline (L-Pro), L-Lysine (L-Lys), L-Lysine·HCl (L-Lys·HCl), L-Arginine (L-Arg), DL-Aspartic Acid (DL-Asp), L-Valine (L-Val), L-Isoleucine (L-Ile), L-Cysteine (L-Cys), L-Alanine (L-Ala) and L-Asparagine (L-Asn). These were combined with aqueous solutions of several tetraalkylphosphonium- and tetraalkylammonium-based ILs, *viz.* $[\text{P}_{4442}][\text{Et}_2\text{PO}_4]$, $[\text{P}_{4444}]\text{Br}$, $[\text{P}_{4444}]\text{Cl}$, $[\text{P}_{i(444)1}][\text{TOS}]$, $[\text{P}_{4441}][\text{MeSO}_4]$, $[\text{P}_{444(14)}]\text{Cl}$, $[\text{N}_{3333}]\text{Br}$, $[\text{N}_{4444}]\text{Br}$ and $[\text{N}_{4444}]\text{Cl}$. Not all amino acids and ILs combinations tested are able to form ABS - a detailed list of the systems able (or not) to form ABS is given in the Table A.2.1, Appendix A2. It was found that only combinations of ILs with a more hydrophobic character and amino acids with a more hydrophilic nature or higher affinity for water are able to form ABS, meaning that amino acids act as salting-out species. The experimental data corresponding to the ternary phase diagrams determined in this work, as well as the respective correlations, are presented in Tables A.2.3-A.2.7 in the Appendix A2.

The ternary phase diagrams of the IL-amino acid mixtures that form ABS are depicted in Figure 2.2.3 (the respective phase diagrams in molality units are reported in the at Figure A.2.3 Appendix A2). For mixture compositions above each solubility curve there is the formation of a two-phase system, while mixture compositions below the same curve result in the formation of a homogeneous solution with no phase-separation. We have found nine IL—amino acid pairs able to create ABS, namely those formed by L-Pro + $[\text{P}_{4444}]\text{Br}$, L-Pro + $[\text{P}_{4441}][\text{MeSO}_4]$, L-Pro + $[\text{P}_{444(14)}]\text{Cl}$, L-Lys + $[\text{P}_{4444}]\text{Br}$, L-Lys + $[\text{P}_{4441}][\text{MeSO}_4]$, L-Lys + $[\text{P}_{444(14)}]\text{Cl}$, L-Lys·HCl + $[\text{P}_{4444}]\text{Br}$, L-Lys·HCl + $[\text{P}_{444(14)}]\text{Cl}$ and L-Lys·HCl + $[\text{N}_{4444}]\text{Br}$. These results confirm that appropriate ammonium- and phosphonium-based ILs can form ABS with amino acids, overcoming therefore the need of using less benign fluorinated imidazolium-based fluids.

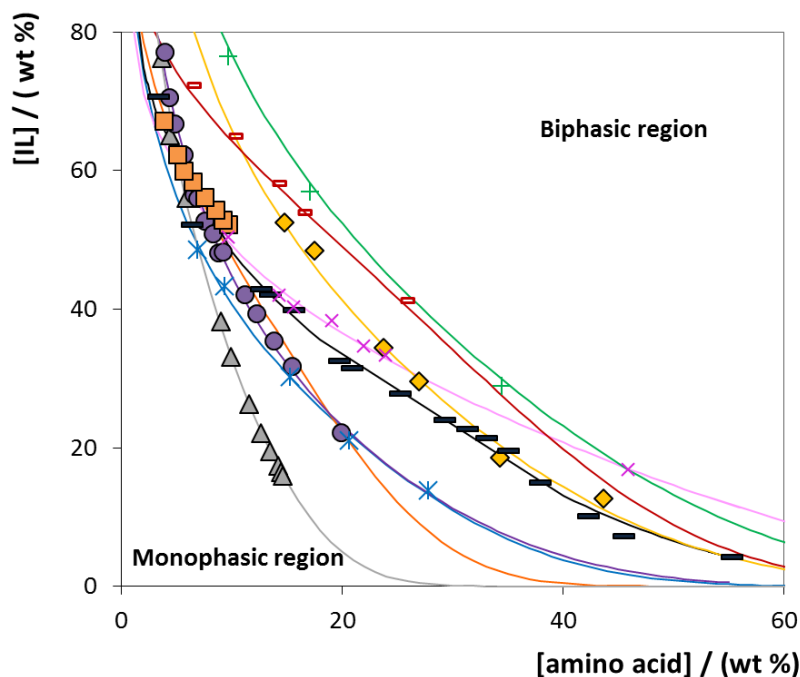


Figure 2.2.3 Phase diagrams of ABS composed of ILs + amino acids + H₂O at 25 °C: [P₄₄₄₍₁₄₎]Cl + L-Lys·HCl (▲); [P₄₄₄₄]Br + L-Lys·HCl (●); [N₄₄₄₄]Br + L-Lys·HCl (■); [P₄₄₄₄]Br + L-Pro (◆); [P₄₄₄₍₁₄₎]Cl + L-Pro (-); [P₄₄₄₁][MeSO₄] + L-Pro (+); [P₄₄₄₍₁₄₎]Cl + L-Lys (-); [P₄₄₄₄]Br + L-Lys (*); [P₄₄₄₁][MeSO₄] + L-Lys (×).

For a given IL, the ability of amino acids to create ABS follows the order: L-Lys·HCl > L-Lys > L-Pro (Figure 2.2.3). This trend is in accordance with their octanol-water partition coefficients and solubility in water - cf. the Appendix A2 (Table A.2.1), confirming therefore their salting-out aptitude over ILs in aqueous media. On the other hand, the ILs ability to form ABS in presence of a given amino acid is as follows: [P₄₄₄₍₁₄₎]Cl > [P₄₄₄₄]Br > [N₄₄₄₄]Br > [P₄₄₄₁][MeSO₄]. Although composed of an anion with a high hydrogen-bond basicity²⁹, [P₄₄₄₍₁₄₎]Cl is amongst the best ILs to form ABS with amino acids, a result of the high hydrophobic nature of the cation derived from the long tetradecyl alkyl chain. Contrarily, [P₄₄₄₁][MeSO₄] is constituted by shorter alkyl side chains at the cation coupled to an anion with high hydrogen-bond basicity²⁹, and thus displays a higher affinity for water, further reflected in the need of higher amounts of amino acid to create two-phase systems. The same phenomenon is behind the ABS formation ability of [N₄₄₄₄]Br versus [N₄₄₄₄]Cl (the former being not able to form ABS as described in the Table A.2.1 at Appendix A2). In general, the higher the IL hydrophilic nature or affinity for water, the lower it is its ability to form ABS with amino acids - following the trend observed in IL-salt ABS²¹.

Separation of amino acids - Given the capability of aliphatic amino acids to form ABS with phosphonium- and ammonium-based ILs against the non-ability of aromatic ones, these liquid-liquid platforms were further evaluated in what concerns their performance to separate

mixtures of amino acids. Figure 2.2.4 depicts the extraction efficiencies of the investigated IL-based ABS for aromatic and aliphatic amino acids. For comparison purposes, imidazolium-based ABS reported in the literature^{22, 23} were also tested. All extractions were carried out at a common tie-line length (≈ 80) to avoid discrepancies in the extraction efficiencies which could arise from differences between the compositions of the coexisting phases. Detailed values and respective uncertainties are given in the Table A.2.8, Appendix A2.

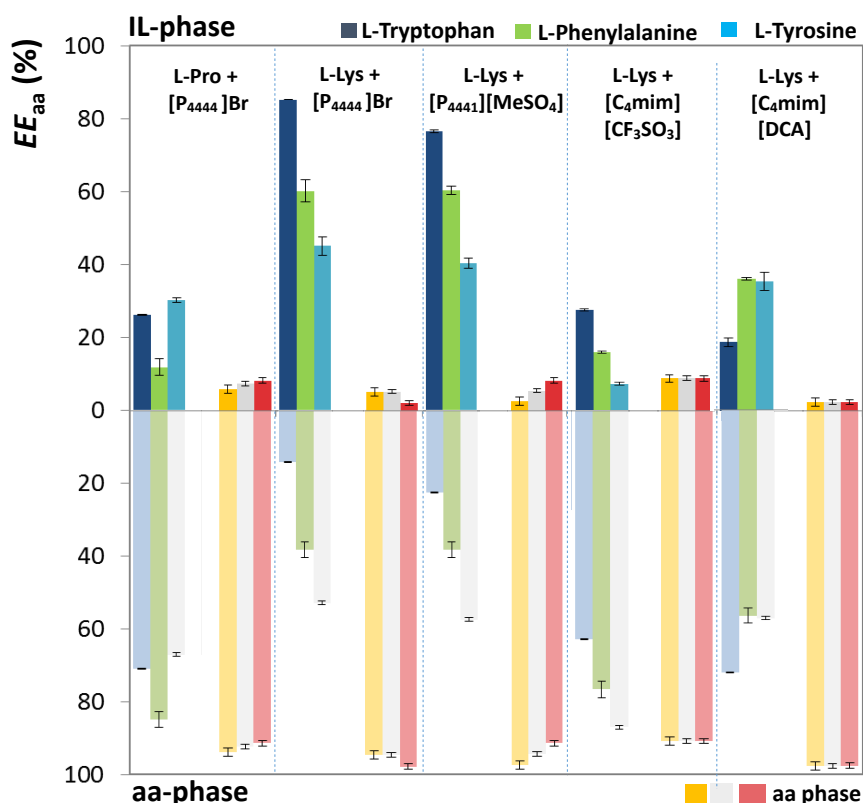


Figure 2.2.4 Extraction efficiencies of amino acids ($EE_{aa}\%$) in the studied systems at 25 °C. ■ ■ ■ represents the $EE_{aa}\%$ of aliphatic amino acids to the IL-rich opposite phase.

With the exception of the L-Pro + [P₄₄₄₄]Br ABS, amongst the phosphonium-based ABS there is the preferential migration of aromatic amino acids to the IL-rich phase while aliphatic amino acids are enriched in the opposite layer, hence allowing their effective separation. Within the best systems identified, $EE_{aa}\%$ of the IL-rich phase for aromatic amino acids ranging between 40 and 85%, and $EE_{aa}\%$ of the opposite phase for aliphatic amino acids ranging between 91 and 98%, were obtained in a single-step. The higher the extraction efficiency values to opposite phases, the higher the selective separation of aromatic/aliphatic amino acids mixtures. In fact, phosphonium-based ABS appear as remarkable separation techniques when compared with ABS formed by imidazolium-based fluids. The selectivity values of IL-based ABS to separate aromatic

amino acids from aliphatic ones are provided in the Appendix A2 (Table A.2.9). The selectivity values for phosphonium-based ILs range between 1.5 and 121, corresponding to significantly higher values than those found with imidazolium-based systems (from 0.01 to 0.07).

Amongst the ABS investigated, the $[P_{4444}]\text{Br}$ + L-Lys system provides the best results in what concerns the selective separation of amino acids mixtures. With this system it is possible to recover L-Trp in one-step with an extraction efficiency higher than 85% to the IL-rich, whereas L-Lys is almost completely enriched in the opposite phase ($EE_{aa}\%$ higher than 90%). In addition to the high ability of the IL-rich phase to extract aromatic amino acids, it should be remarked the almost null cross-contamination of this phase with aliphatic amino acids ($EE_{aa}\%$ of the IL-rich phase lower than 9% for all aliphatic amino acids, in all systems investigated). The obtained results, in terms of separation performance, are comparable to those obtained with conventional techniques^{30,31}, and that usually are more complex processes and require the use of less benign compounds and more expensive equipment.

According to the results depicted in Figure 2.2.4, the IL nature has a relevant influence through the partition behaviour of aromatic amino acids and a more negligible effect on the partition trend of aliphatic ones. While almost all systems are able to effectively separate mixtures of aliphatic and aromatic amino acids, the trend obtained for the extraction efficiencies is also related to the salting-out aptitude of the aliphatic amino acid. For instance, the system constituted by the strongest salting-out amino acid (L-Lys, according to Figure 2.2.4) is the one that displays the best performance in terms of selective separation. Furthermore, electrostatic interactions established between charged amino acids and ILs can also play a role on the amino acids partition and cannot be neglected. The pH of the coexisting phases of the L-Pro + $[P_{4444}]\text{Br}$ system is ≈ 5 , corresponding to the system with the lowest selectivity (Table A.2.9). On the other hand, both $[P_{4444}]\text{Br}$ + L-Lys and $[P_{4441}][\text{MeSO}_4]$ + L-Lys systems, have aqueous phases with pH values ranging from 10 to 11, and both systems provide better extraction efficiencies for aromatic amino acids. The pH of the coexisting phases of all ABS investigated is presented in the Appendix A2, Table A.2.7. The isoelectric points (pI) of the aromatic amino acids investigated are 5.89 for L-Trp, 5.48 for L-Phe, and 5.66 for L-Tyr³², indicating that electrostatic interactions between amino acids and ILs decrease at pH values *ca.* 5.

To address the relevance of electrostatic interactions, we carried out the separation of L-Lys and L-Trp with the ABS composed of $[P_{4444}]\text{Br}$ at several pH values, and explored the ability of the ABS formed by $[P_{4444}]\text{Br}$ and L-Lys·HCl, that will be more acidic in nature, for the separation of aromatic and aliphatic amino acids. The results obtained for both sets of experiments are shown in Figure 2.2.5.

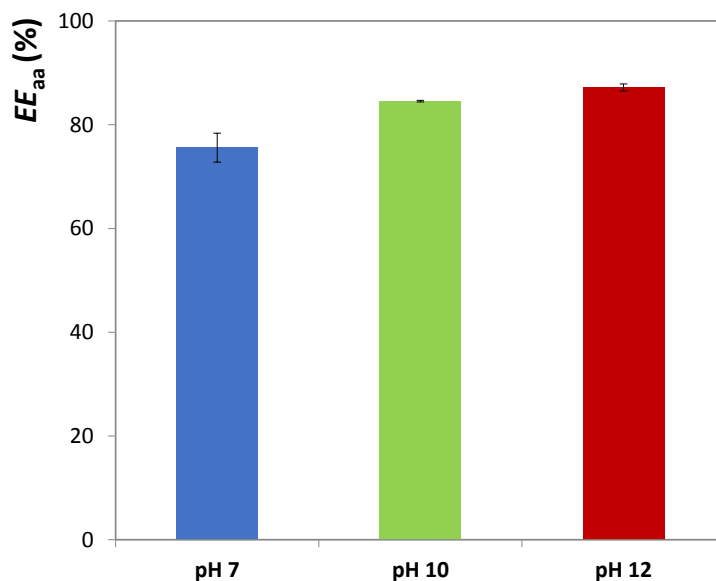


Figure 2.2.5 Extraction efficiency ($EE_{aa}\%$) of L-Trp in the system formed by $[P_{4444}]\text{Br} + \text{L-Lys} + \text{H}_2\text{O}$ (TLL ≈ 80), at different pH values (7, 10 and 12).

In general, an increase in the pH leads to an increase of the L-Trp partitioning to the IL-rich phase, and therefore confirms the relevance of electrostatic interactions in the performance of the systems investigated. In fact, $EE_{aa}\%$ of the IL-rich phase for L-Trp up to 87%, and $EE_{aa}\%$ of the opposite phase for L-Lys up to 95%, were obtained in a single-step at pH 12. In the same line, a lower separation performance was observed with the L-Lys·HCl-based system, as a result of its more acidic character (the pH of the coexisting phases is *ca.* 3). This dependence on the pH can be additionally used to further improve the selective separation ability of the investigated IL-based ABS.

Wang et al.³⁴ demonstrated the selective separation of L-Trp with imidazolium-based ILs, finding that this amino acid could be effectively separated from a fermentation broth, although requiring multiple steps. However, most studies reported in the literature on similar topics address the extraction of only one aromatic amino acid (*e.g.*, the selectivity toward other amino acids were not evaluated) while using less “benign” ILs³⁵⁻³⁹.

Recovery of amino acids- Most works on IL-based ABS have mainly focused on the evaluation of their extraction performance²¹. However, and although scarcely investigated, the products recovery from the IL-rich phase is a crucial task aiming at proving the “real” utility of these separation systems. In this context, we further evaluated the possibility of separating the aromatic amino acids from the ILs that constitute the ABS IL-rich-phase. To this end we used a solid-phase extraction approach, by means of a cation exchange column³³, able to retain the IL cation. The elution of the IL-rich phase was conducted at a high pH value (*ca.* 12) to avoid the amino acids adsorption. At the optimized conditions we successfully eluted the aromatic amino acid and retained the IL by adsorption onto the column, allowing thus its removal from the original aqueous phase. With the [P₄₄₄₄]Br + L-Lys ABS enriched in L-Trp, we were able to recover 93% of the aromatic amino acid and to remove 79% of the IL present in the original IL-rich phase. Even though these are already very promising results, we believe that by further optimizing the mobile phase composition, for instance the pH and ionic strength, and other operation variables, such as bed volume, an even better chromatographic performance will be reached. In addition to the amino acid/IL separation, this strategy also allows the IL recovery and reuse towards the development of cost-effective and more sustainable technologies.

Conclusions

In this work we demonstrate the ability of IL-based ABS for the separation of two classes of amino acids usually present in proteins hydrolysates or fermentation broths, and that more benign and non-fluorinated ILs can be efficiently used for such purpose. To this end, phosphonium and ammonium-based ILs have been investigated. These novel IL-based ABS allow extraction efficiencies of aromatic amino acids ranging between 40 and 85% to the IL-rich phase, and extraction efficiencies of aliphatic amino acids ranging between 91 and 98% to the opposite phase, in a single-step. Finally, it is demonstrated that amino acids can be recovered from the IL-rich phase, allowing the IL recyclability.

References

1. R. K. Murray, D. Bender, K. M. Botham and P. J. Kennelly, *Harpers Illustrated Biochemistry*, McGraw-Hill Education, 2012.
2. Y. Li, B. Kerr, M. Kidd and H. Gonyou, *J. Anim. Sci.*, 2006, 84, 212-220.
3. F. J. Spronsen, M. Rijn, J. Bekhof, R. Koch and P. G. Smit, *Am. J. Clin. Nutr.*, 2001, 73, 153-157.
4. R. Patnaik, R. R. Zolandz, D. A. Green and D. F. Kraynie, *Biotechnol. Bioeng.*, 2008, 99, 741-752.
5. J. Farup, S. K. Rahbek, A. C. Storm, S. Klitgaard, H. Jørgensen, B. M. Bibby, A. Serena and K. Vissing, *SpringerPlus*, 2016, 5, 382-383.
6. K. S. Ojha, C. Alvarez, P. Kumar, C. P. O'Donnell and B. K. Tiwari, *Food Sci. Technol.*, 2016, 68, 470-476.
7. J. Wang, L. K. Cheng, J. Wang, Q. Liu, T. Shen and N. Chen, *Appl. Microbiol. Biotechnol.*, 2013, 97, 7587-7596.
8. E. Faghfuri, J. Fooladi, S. Sepehr and S. Z. Moosavi-Nejad, *J. Jundishapur Microbiol.*, 2013, 6, 1-5.
9. M. Ikeda, *Appl. Microbiol. Biotechnol.*, 2006, 69, 615-626.
10. M. Ikeda and R. Katsumata, *Appl. Environ. Microbiol.*, 1999, 65, 2497-2502.

11. M. Li, Z.-Q. Zhu and A. E. Rodrigues, *Ind. Eng. Chem. Res.*, 2002, 41, 251-256.
12. S. Blackburn, *Amino acid determination - methods and techniques*, M. Dekker, 1978.
13. K. Drauz, I. Grayson, A. Kleemann, H. P. Krimmer, W. Leuchtenberger and C. Weckbecker, *Ullmann's Encyclopedia of Industrial Chemistry*, Wiley-VCH Verlag GmbH & Co. KGaA, 2000.
14. T. Hermann, *J. Biotechnol.*, 2003, 104, 155-172.
15. H. Itoh, M. Thien, T. Hatton and D. Wang, *Biotechnol. Bioeng.*, 1990, 35, 853-860.
16. P. T. Anastas and J. C. Warner, *Green Chemistry: Theory and Practice*, Oxford University Press, 2000.
17. B. Peric, E. Marti, J. Sierra, R. C. Terradas and M. A. Garau, *Recent advances in pharmaceutical sciences II*, Transworld Research Network, 2012.
18. K. E. Gutowski, G. A. Broker, H. D. Willauer, J. G. Huddleston, R. P. Swatloski, J. D. Holbrey and R. D. Rogers, *J. Am. Chem. Soc.*, 2003, 125, 6632-6633.
19. P. Å. Albertsson, *Partition of cell particles and macromolecules: separation and purification of biomolecules, cell organelles, membranes, and cells in aqueous polymer two-phase systems and their use in biochemical analysis and biotechnology*, Wiley New York, 1986.
20. B. Y. Zaslavsky, *Aqueous two-phase partitioning: physical chemistry and bioanalytical applications*, CRC Press, 1994.
21. M. G. Freire, A. F. M. Claudio, J. M. Araujo, J. A. Coutinho, I. M. Marrucho, J. N. C. Lopes and L. P. N. Rebelo, *Chem. Soc. Rev.*, 2012, 41, 4966-4995.
22. J. Zhang, Y. Zhang, Y. Chen and S. Zhang, *J. Chem. Eng. Data*, 2007, 52, 2488-2490.
23. M. D. Pérez, L. I. Tomé, M. G. Freire, I. M. Marrucho, O. Cabeza and J. A. Coutinho, *Sep. Purif. Technol.*, 2010, 72, 85-91.
24. M. G. Freire, C. M. Neves, I. M. Marrucho, J. A. Coutinho and A. M. Fernandes, *J. Phys. Chem. A*, 2009, 114, 3744-3749.
25. M. Taha, F. A. e Silva, M. V. Quental, S. P. Ventura, M. G. Freire and J. A. Coutinho, *Green Chem.*, 2014, 16, 3149-3159.
26. J. Chen, Y. Wang, Q. Zeng, X. Ding and Y. Huang, *Anal. Methods*, 2014, 6, 4067-4076.
27. J. C. Merchuk, B. A. Andrews and J. A. Asenjo, *J. Chromatogr. B Biomed. Sci. Appl.*, 1998, 711, 285-293.
28. F. A. Vicente, L. P. Malpiedi, F. A. e Silva, A. Pessoa, J. A. Coutinho and S. P. Ventura, *Sep. Purif. Technol.*, 2014, 135, 259-267.
29. F. M. Cláudio, L. Swift, J. P. Hallett, T. Welton, J. A. Coutinho and M. G. Freire, *Phys. Chem. Chem. Phys.*, 2014, 16, 6593-6601.
30. M. Kumar, B. P. Tripathi and V. K. Shahi, *J. Chem. Technol. Biotechnol.*, 2010, 85, 648-657.
31. C. Hirs, S. Moore and W. Steine, *J. Biol. Chem.*, 1952, 195, 669-683.
32. D. L. Nelson, A. L. Lehninger and M. M. Cox, *Lehninger principles of biochemistry*, Macmillan, 2008.
33. P. M. Cummins, K. D. Rochfort and B. F. O'Connor, *Protein Chromatography: Methods and Protocols*, Springer, 2017.
34. J. Wang, Y. Pei, Y. Zhao and Z. Hu, *Green Chem.*, 2005, 7, 196-202.
35. A. Luís, T. B. Dinis, H. Passos, M. Taha and M. G. Freire, *Biochem. Eng. J.*, 2015, 101, 142-149.
36. C. Li, Z. Li, A. Wang, J. Yin, J. Wang, H. Li and Q. Liu, *RSC Adv.*, 2013, 3, 6356-6361.
37. Y. Fan, X. Dong, Y. Li, Y. Zhong, J. Miao, S. Hua and Y. Sun, *Ind. Eng. Chem. Res.*, 2015, 54, 12966-12973.
38. L. I. Tomé, V. R. Catambas, A. R. Teles, M. G. Freire, I. M. Marrucho and J. A. Coutinho, *Sep. Purif. Technol.*, 2010, 72, 167-173.
39. Y. Xie, H. Xing, Q. Yang, Z. Bao, B. Su and Q. Ren, *ACS Sustain. Chem. Eng.*, 2015, 3, 3365-3372.

3. Extraction and purification of proteins using IL-based ABS

3.1. Purification of BSA using aqueous biphasic systems formed by self-buffering ionic liquids

Based on the published manuscript:³ Taha Mohamed[§], Maria V. Quental[§], Francisca A. e Silva, Emanuel V. Capela, Mara G. Freire, Sónia P. M. Ventura and João A. P. Coutinho. *J. Chem. Technol. Biotechnol.*, 2017, 92, 2287-2299.

[§]equal contribution

Abstract

A set of new IL based on the tetrabutylphosphonium cation ($[P_{4444}]^+$) and anions derived from Good Buffers (GBs) was synthesized and characterized. These ionic liquids display self-buffering characteristics and low toxicity towards the luminescent bacteria *Vibrio fischeri*. The ability of the GB-ILs to form ABS with the potassium citrate salt was investigated, and ternary phase diagrams, tie-lines and tie-line lengths were determined. These systems were then evaluated to extract and purify BSA from bovine serum samples. Extraction efficiencies of $100 \pm 5\%$ of BSA to the GB-IL-rich phase were obtained in a single-step. In addition, good recovery yields ($59.4 \pm 0.8\%$ to $80.1 \pm 0.7\%$) and purity levels ($75.0 \pm 0.3\%$ to $92 \pm 1\%$) of BSA were obtained. BSA keeps its secondary structure in the IL-rich phase, revealing the protein-friendly nature of the synthesized GB-ILs.

Introduction

Aqueous biphasic systems (ABS) are benign alternatives to replace the conventional liquid–liquid extractions using organic volatile solvents aiming the efficient separation of biomolecules, in which proteins and enzymes are included^{1, 2}. ABS are claimed as greener extraction techniques, minimizing the consumption of volatile organic solvents, which could be not only harmful to the environment and human resources, but also for proteins since they could cause their denaturation³. Several techniques such as electrophoresis, membrane separation, gel filtration, and affinity chromatography are adopted in protein separation. However, some are expensive processes and are associated to several limitations, namely their scale-up potential⁴. Traditional ABS consist of aqueous solutions of two polymers (*e.g.* polyethylene glycol and dextran) or a polymer and a salt. They have been established as an economical method making part of diverse downstream processes. These are claimed as methods exhibiting low-energy consumption, high performance, high biocompatibility and suitability for large scale production.

³Contributions: T. M., M.G.F., and J.A.P.C. conceived and directed this work. M.V.Q., F. A. S. and T. M. acquired the experimental data. T. M performed all computational studies. M.V.Q., M.G.F., T.M., S.P.M.V. and J.A.P.C. interpreted the obtained experimental data. The manuscript was mainly written by T. M., M.V.Q., M.G.F. and J.A.P.C. with contributions from the remaining authors.

Consequently, ABS have been extensively studied for the separation and purification of different biological products. As promising substitutes for conventional organic solvents, ionic liquids (ILs) have become ubiquitous in the recent literature due to their diverse properties, which are responsible for them to be useful in a plethora of different applications^{5, 6}. ILs are salts composed of a bulky, unsymmetrical organic cation and an inorganic or organic anion, which have a melting point below 100 °C. The wide structural diversity of ILs allows to adjust their properties, which could improve the protein stability and activity⁷⁻¹⁰. On the other hand, a variety of hydrophilic ILs was found to form ABS when mixed with aqueous solutions of inorganic or organic salts^{5, 11-13}, and proved to be efficient in the separation of proteins and enzymes^{4, 14-29}. Moreover, and behind the efficiency of IL-based ABS as separation techniques, their many advantages over the conventional polymer-based systems are their lower viscosity and a higher difference in the phases' polarity^{4, 14-29}, making them a more attractive purification tool. IL-based ABS have been applied as purification techniques of a large range of macromolecules, including enzymes like horseradish peroxidase (HRP), *Thermomyces lanuginosus* lipase, *Candida antarctica* lipase A, and *Candida antarctica* lipase B^{21, 23, 30, 31}, and proteins, namely BSA, cytochrome c, myoglobin, ovalbumin, hemoglobin, trypsin, cytochrome c, γ -globulins, among others^{4, 14-20}. When considering the previously reported works, it is clear that IL-based ABS provide a higher extraction efficiency regarding proteins if compared with the most conventional polymer-based systems.

Some parameters are defined as important conditions driving the migration of proteins, namely the potential formation of aggregates, or some particular interactions, like electrostatic, dispersive and hydrogen-bonding interactions^{4, 14-29}. In the studies reported in the last two decades, phosphate salts are still the most applied as salting-out agents. The phosphate buffer has been used to adjust the pH of the systems considering some specific proteins/enzymes and ABS³²⁻³⁴. However, and contrarily to the pH control by means of the added salt, buffered IL-based ABS can be created with ILs with self-buffering characteristics. For this purpose, we and the MacFarlane's group^{35,36} recently developed a series of self-buffering and biocompatible ILs (Good's buffer ionic liquids, GB-ILs) in which five Good's buffers (GBs, namely TRICINE, TES, MES, HEPES, and CHES) acted as anions and 1-ethyl-3-methylimidazolium ([C₂mim]⁺), alkylammonium ([N_{nnnn}]⁺), and cholinium ([Ch]⁺) acted as cations³⁶⁻³⁸. GBs are N-substituted glycine or taurine compounds that are frequently used in different fields of application³⁹, including diverse biological systems. To expand the range of available GB-based ABS and to better understand their potential in separation processes, in this work, five new GB-ILs with self-buffering characteristics were synthesized by the conjugation of a wide variety of GB's anions and the tetrabutylphosphonium cation ([P₄₄₄₄]⁺). These were characterized in terms of their toxicity

against the luminescent bacteria *Vibrio fischeri*⁴⁰, and further used to form GB-IL-based ABS with the biodegradable potassium citrate salt. The phosphonium cation ($[P_{4444}]^+$) was selected because it has an enhanced aptitude to form ABS⁴¹, and thus lower amounts of phase-forming components will be required to create two-phase systems. After the determination of the corresponding phase diagrams, the BSA partition between both aqueous phases was evaluated and compared with that of tetrabutylphosphonium chloride ($[P_{4444}]\text{Cl}$). Moreover, and having determined and optimized the weight compositions to promote the complete migration of BSA towards the GB-IL-rich phase, the purification of BSA from a bovine serum sample was evaluated. The stability of BSA was also addressed and the molecular-level mechanisms controlling the BSA extraction to the IL-rich phase were ascertained by COSMO-RS and molecular docking studies. The chemical structure of $[P_{4444}]\text{Cl}$ and of the GB-ILs synthesized in this work are depicted in Figure 3.1.1 (the synthetic pathway to prepare the later is shown in Figure B.1.1 in the Appendix B1).

Experimental Procedure

Materials - N-[tris(hydroxymethyl)methyl]glycine (TRICINE, purity > 99 wt%), 2-[(2-hydroxy-1,1-bis(hydroxymethyl)ethyl)amino]ethane sulfonic acid (TES, purity > 99 wt%), 2-(N-morpholino) ethanesulfonic acid (MES, purity > 99 wt%), 2-[4-(2-hydroxyethyl)piperazin-1-yl]ethanesulfonic acid (HEPES, purity > 99.5 wt%), 2-(cyclohexylamino)ethanesulfonic acid (CHES, purity > 99 wt%), and $[P_{4444}][\text{OH}]$ (45 wt% in water) were purchased from Sigma–Aldrich. Sodium hydroxide pellets were supplied from Eka Chemicals. BSA (fraction V) was obtained from Acros Organics. Methanol (HPLC grade, purity > 99.9 wt%) was obtained from Fisher Scientific (UK). Acetonitrile (purity > 99.7 wt%) was supplied from Lab-Scan. Purified water passed through a reverse osmosis and a Milli-Q plus 185 water purifying system was used in all experiments. Sodium nitrate (purity > 99.5 wt%) was obtained from Himedia Labs. Potassium nitrate (purity > 98.0 wt%), nitric acid (purity > 65 wt%), and potassium hydrogen phthalate (purity > 99.8 wt%) were purchased from Panreac. The bovine serum sample used was obtained from Sigma-Aldrich (B9433 Sigma), USA, sterile-filtered and stored at $-20\text{ }^{\circ}\text{C}$.

GB-IL synthesis and characterization - The synthesis of the GB-ILs tested in this work follows the protocol described elsewhere⁴². Briefly, an aqueous solution of $[P_{4444}][\text{OH}]$ was added dropwise to a GB aqueous solution with a slight equimolar excess. The solution was stirred at room temperature during 12 h; then, the reaction mixture was evaporated at $60\text{ }^{\circ}\text{C}$ under vacuum. A mixture of acetonitrile and methanol (1:1) was added to the viscous liquid previously obtained,

stirred vigorously at room temperature for 1 h until the precipitation of the unreacted buffer, which was posteriorly removed by filtration. The solvent (acetonitrile + methanol) was evaporated and GB-ILs were dried under vacuum ($\sim 10^{-3}$ mbar) for 3 days at room temperature (25 °C). The water content of each GB-IL prepared (less than 0.05 wt%) was measured by Karl–Fischer titration (Metrohm Ltd., model 831). The chemical structures of the GB-ILs were confirmed by ^1H and ^{13}C NMR spectroscopy (Bruker AMX 300) operating at 300.13 and 75.47 MHz, respectively. Figure 3.1.1 displays the chemical structures of the herein studied ILs. The melting points of GB-ILs were measured by differential scanning calorimetry (DSC), with a Perkin Elmer DSC-7 instrument (Norwalk, CT), at a heating rate of $5\text{ }^\circ\text{C}\cdot\text{min}^{-1}$ and under a N_2 flow of $40\text{ mL}\cdot\text{min}^{-1}$. These data (NMR data and melting points) are presented in Table B.1.1 in the Appendix B1.

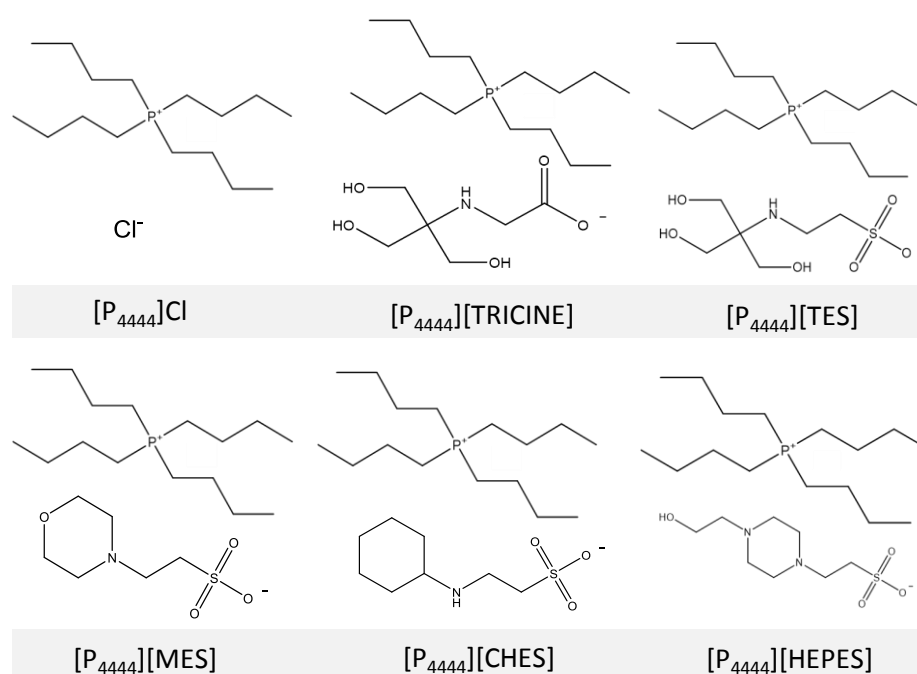


Figure 3.1.1 Chemical structure of the studied $[\text{P}_{4444}]\text{Cl}/[\text{P}_{4444}][\text{GB}]$ ILs.

Potentiometric titrations - The pH-potentiometric measurements were carried out in a 70 cm^3 double-walled glass vessel using an automatic titrator (Metrohm 904) equipped with a 801 magnetic stirrer, Dosino buret model 683, and a pH glass electrode (Metrohm 6.0262.100) with a precision of ± 0.001 . The temperature of the titration cell was controlled at $25.0 \pm 0.1\text{ }^\circ\text{C}$ by a thermostatic water bath. The titration cell was equipped with a lid with various openings for insertion of the electrode, burette tip, Pt 1000/B/2 (Metrohm 6.1114.010), and gas inlet and outlet. The titroprocessor was coupled to a personal computer and the titration software Tiamo 2.3 was used to control and record the titration process.

pH profiles - 10 mL of GB-ILs (0.05 M) were titrated with 0.1 mol·dm⁻³ of NaOH/HCl under continuous magnetic stirring. The pH electrode was calibrated using three standard buffer solutions of pH 4.01, 7.00, and 9.21.

Determination of protonation constants of GB/GB-ILs - The glass electrode was calibrated considering the hydrogen ion concentrations instead of activities, by means of a strong acid-strong base titration. In this titration, 2 cm³ of 0.1 M of HNO₃ and 50 cm³ of 0.1 M of a KNO₃ solution were titrated with a 0.1 M of carbonate-free NaOH solution. The concentration of NaOH was determined by standardization with potassium hydrogen-phthalate. The purified water was degassed under vacuum using a rotary evaporator at 70 °C and cooled under a stream of nitrogen. The titration cell was kept under a small positive pressure of nitrogen gas to eliminate the effect of atmospheric carbon dioxide. The nitrogen gas was purged for 15 min before starting the titration to expel any dissolved oxygen or carbon dioxide present. The values of volume added (cm³) and electrode potential (mV) were analyzed with the GLEE software⁴³. This computer program uses a (non-linear) least-squares refinement to fit a modified Nernst equation, described by Equation 1,

$$E = E^{\circ} + sl \log [H^{+}] \quad (\text{Equation 1})$$

where E refers to the potential of the glass electrode, E° and sl are the standard electrode potential and slope, and $[H^{+}]$ is the hydrogen ion concentration. In the acid region, the hydrogen ion concentration, T_H , is obtained from Equation 2, that is, $\text{Log}[H^{+}] = \log(T_H)$

$$T_H = \frac{a_H v_0 + \gamma b_H}{v_0 + v_1 + v} \quad (\text{Equation 2})$$

where a_H is the acid concentration (mol·dm⁻³) and v_0 (cm³) is the initial volume added to the titration vessel. b_H is the base concentration (mol·dm⁻³) in the burette (with negative sign), and γ is a correction factor for the base concentration. v is the volume (cm³) of base added from the burette, and v_1 (cm³) is the volume of the electrolyte solution.

In the alkaline region, the hydrogen ion concentration, T_H , is given by Equation 3, where $\log[H^{+}] = -pK_w - \log(-T_H)$, v_e^a is the volume (cm³) at the acid equivalence point, and v_e^b is the volume (cm³) at the alkali equivalence point.

$$T_H = \frac{a_H v_0 + \gamma \frac{v_e^a}{v_e} b_H v}{v_0 + v_1 + v} \quad (\text{Equation 3})$$

The Gran plot was used to estimate the carbonate contamination in the titrant and a typical Gran plot is shown in Figure B.1.2 in Appendix B1. The product of water $pK_w = 13.778$ at 25 °C and ionic strength = 0.1 mol·dm⁻³ KNO₃ were maintained constant during the refinements⁴⁴.

Titration for protonation constant calculations were performed by combining 0.003 M of HNO₃, 0.1 M of NaNO₃, and 0.001 M of GB/GB-ILs (total volume of 50 cm³) and titrated with the NaOH solution under carefully controlled experimental conditions, as described in the glass electrode calibration procedure. Each titration was repeated at least three times (more than 100 data points for each one). The determination of the protonation constants were computed using the HYPERQUAD program (Version 2008)⁴⁵. This computer program treats the protonation equilibria of ligand as overall association constants; *e.g.* the protonation equilibria of H₂A which can be expressed as,



The stepwise acid dissociation constants of H₂A is given by



Since $pK_a = -\log(1/K_a)$, the pK_a 's values are given by $pK_{a2} = \log\beta_1$ and $pK_{a1} = \log\beta_2 - \log\beta_1$.

Standard Microtox® liquid-phase assays - The luminescence inhibition of the marine bacteria *Vibrio fischeri* (strain NRRL B-11177) was measured after contacting with each [P₄₄₄₄][GB] at 15 °C. The protocol followed in this work (81.9% standard test) is described elsewhere in detail⁴⁵. Also in this work the effective concentration yielding 50% of inhibition of the bacteria luminescence (EC₅₀) along with the corresponding 95% confidence limits were determined through the Microtox® Omni™ Software version 4.1⁴⁶, to evaluate the toxicity of each GB-IL.

Dynamic light scattering (DLS) measurements - The hydrodynamic radius (R_H) values of the protein were measured at different temperatures using a Zetasizer Nano ZS equipment (Malvern

Instruments Ltd., UK). The average R_H was calculated from the scattering intensity data using the instrument software. The light source of the instrument is He-Ne laser light (4mW) with a wavelength (λ) = 633 nm, and the scattering angle were fixed at 173°. The instrument is provided with a thermostatic sampling chamber which controls the temperature in the range from 0 °C to 90 °C. The samples were prepared with 20 mg·cm⁻³ of BSA in (0.05 and 0.5) M of GB/GB-ILs/[P₄₄₄₄]Cl, and at pH= 7.4. The samples were incubated at 25 °C for 4 h to achieve the equilibrium. Around 1.3 cm³ bubble free sample in a square glass cuvette (PCS8501) was used for the DLS measurements.

Infrared measurements - Attenuated total reflectance (ATR) Fourier transform infrared (FTIR) spectra of 30 mg BSA in (0.05 and 0.5) M of GB/GB-ILs/[P₄₄₄₄]Cl solutions were measured using an ABB MB3000 FTIR spectrometer equipped with PIKE MIRacle™ and a single reflection diamond/ZnSe crystal plate. The spectral region was 400-4000 cm⁻¹ with a resolution of 4 cm⁻¹ and 100 scans. At least 5 measurements were performed for each sample. Second-derivative spectra of the amide I (~1652 cm⁻¹) region were used as peak position guides for the Gaussian curve-fitting analysis. The second-derivative and the curve fitting were done using PeakFit v4.0 (AISN software Inc.). The relative amount of α -helices, β -sheets, and turns was estimated by calculating the areas of the bands assigned to a particular substructure.

ABS phase diagrams - The binodal curve of each phase diagram was determined through the cloud point titration method at 25 (\pm 1) °C and at atmospheric pressure, as detailed elsewhere⁴². The tie-lines (TLs) of each phase diagram, including the mixtures compositions for which the extraction of BSA was carried out, were determined by a gravimetric method originally described by Merchuk et al⁴⁷. In this section, the same procedures described in the experimental sections of Chapters 2.1 and 2.2 were adopted.

Extraction and purification of BSA - The biphasic systems used for the extraction of BSA were gravimetrically prepared at a fixed common mixture composition: (39.4 \pm 0.7) wt% of GB-IL/IL + (15.1 \pm 0.9) wt% of salt + water. The aqueous solution added to complete the mixture composition contained BSA at a concentration of ca 0.5 g·L⁻¹. BSA was quantified by SE-HPLC using an analytical column Shodex Protein KW-802.5 (8 mm \times 300 mm). Phosphate buffer pH 7.0 with 0.3 M NaCl was run isocratically with a flow rate of 0.5 mL min⁻¹ with an injection volume of 25 μ L. The wavelength was set at 280 nm, whereas the retention time of BSA in the HPLC chromatograms was found to be 9.31 min within an analysis time of 24 min, using the external standard calibration method in the range of 0.001 to 1 g·L⁻¹ of BSA. In this work, three

ABS of each IL were prepared, and three samples of each phase were properly quantified. Blank controls were always used.

The extraction efficiency of BSA, EE_{BSA} (%), was calculated to evaluate the success of each ABS to the extraction of BSA. This parameter describes the ratio between the amount of protein quantified in the IL-GB-rich phase and the sum of the amount of the protein in both phases, as defined in Equation 8

$$EE_{BSA} (\%) = \frac{[BSA]_{IL} \times w_{IL}}{[BSA]_{IL} \times w_{IL} + [BSA]_{Salt} \times w_{Salt}} \times 100 \quad (\text{Equation 8})$$

where [BSA] is the concentration of protein quantified, w is the weight of each phase, and the subscripts IL and salt represent the IL- and potassium-citrate-rich phases, respectively.

After optimizing the extraction with pure BSA, it was carried out the extraction and purification of BSA from real bovine serum samples. The same extraction mixture point was used and the bovine serum was diluted at 1:5 (v/v). Each mixture was mixed using a Vortex mixer, centrifuged (10 min at 1000 rpm), in order to achieve the complete partitioning of serum content between the two phases. After the two phase's separation, the BSA monomer and remaining proteins (mostly BSA dimer) were quantified by SE-HPLC, as described above. The extraction efficiency was determined according to Equation 8. The yield and purity of BSA monomer to the IL-rich phase were determined according to following equations:

$$Y_{BSA} (\%) = \frac{w_{BSA}^{IL}}{w_{BSA}^{initial}} \times 100 \quad (\text{Equation 9})$$

$$P_{BSA} (\%) = \frac{peak\ Area_{BSA}^{IL}}{total\ peak\ Area_{proteins}^{IL}} \times 100 \quad (\text{Equation 10})$$

where w_{BSA}^{IL} , $w_{BSA}^{initial}$, $peakArea_{BSA}^{IL}$, and $total\ peak\ Area_{proteins}^{IL}$ are the weight of BSA monomer in the IL-rich phase, weight of BSA monomer in the initial mixture, HPLC peak area of BSA monomer and the total area of all peaks corresponding to all proteins present at the IL-rich phase, respectively. All extractions were carried out in duplicate.

COSMO-RS modelling - The detailed theory of the “Conductor-like Screening Model for Real Solvents” (COSMO-RS) was described in detail by Klamt⁴⁸. This model integrates concepts from quantum chemistry, continuum solvation model (COSMO), electrostatic interaction and extends to statistical thermodynamics, which are recurrently used for predicting the thermodynamic

properties of fluids and liquid mixtures. COSMO-RS is used to analyse the electrostatic ($E_{\text{misfit}}(\sigma$ and $\sigma')$), H-bonding (E_{HB}) and van der Waals (E_{vdW}) interaction energies of interacting species in terms of the screening charge densities (σ , σ') of the respective surface segments - Equations 11-13⁴⁹,

$$E_{\text{misfit}}(\sigma, \sigma') = a_{\text{eff}} \frac{\alpha'}{2} (\sigma + \sigma')^2 \quad (\text{Equation 11})$$

$$E_{\text{HB}} = a_{\text{eff}} c_{\text{hb}} \min(0, \sigma \sigma' + \sigma_{\text{hb}}^2) \quad (\text{Equation 12})$$

$$E_{\text{vdW}} = a_{\text{eff}} (\tau_{\text{vdW}} + \tau'_{\text{vdW}}) \quad (\text{Equation 13})$$

where a_{eff} refers to the effective contact area, α' is a general constant, c_{hb} is the strength coefficient, σ_{hb} represent the polarization charge density threshold for hydrogen bond, and τ_{vdW} and τ'_{vdW} are the element-specific parameter for dispersion parameters. The 3D distribution of the polarization charges, σ , of each molecule is converted into a surface composition function, named as sigma profile (σ -profile), by the COSMOtherm program version C30_1401^{50, 51}. The σ -profile depicts the surface charge density distribution on the molecular surface, which provides quantitative information about the polarity of the molecules^{49,50}. The σ -profiles of [P₄₄₄₄][GB]/[P₄₄₄₄][Cl] were computed at the RI-DFT BP/SVP level, as implemented in the TURBOMOLE 6.1 program package⁵², and the interaction energies were calculated using the COSMOtherm software version C30_1401.

Logarithm of the octanol-water partition coefficient calculation ($\log K_{\text{OW}}$) - The DFT/COSMO calculations of GBs were computed using the TURBOMOLE 6.1 program with RI-BP/TZVP method⁵². The $\log K_{\text{OW}}$ (octanol-water partition coefficients) values of all GBs were determined by the COSMOtherm software, version C30_1401^{49,50}. The K_{OW} is obtained through the computation of the ratio of the activity coefficient of the buffer at infinite dilution (γ_i^∞) in the water- and octanol-rich phases, as indicated in Equation 14.

$$K_{\text{OW},i} = 0.1505 \frac{\gamma_i^{\infty, \text{W}}}{\gamma_i^{\infty, \text{O}}} \quad (\text{Equation 14})$$

where the superscripts “W” and “O” refer to the water-rich and the octanol-rich (0.726 mole fraction of octanol) phases, respectively.

QSAR-serum albumin binding model, logK(HSA) - The molecular geometries of [P₄₄₄₄][GB]/[P₄₄₄₄]Cl were first computed with the AM1 semi-empirical method with Polak-Rebriere algorithm to reach a 0.01 root mean square gradient as implemented in the HyperChem (Version 8.0.7, Hypercube, Inc, USA, <http://www.hyper.com>) program. The COSMO files of these ILs were then obtained by single point calculations at the RI-DFT BP/SVP level using the TURBOMOLE 6.1 program package⁵¹. The QSAR-logK(HSA) values were computed using these COSMO files with the COSMOtherm software, version C30_1401^{49, 50}.

Molecular docking – The molecular docking between BSA and the diverse [P₄₄₄₄][GB] ions was performed using the Auto-dock Tools vina 1.5.4 program⁵³ and the three-dimensional structures of BSA (PDB, 3v03)⁵⁴. The lowest binding model was searched out from 9 different conformers for each ligand based on the one with the lowest objective function, which includes electrostatic interactions, hydrogen bonding, short range vdW, and solvation energies terms.

Results and Discussion

The acid-base behavior of GB-ILs - Good's buffers are zwitterionic compounds with two protonation states, the carboxylic/sulfonic (pK_{a1}) and the amino (pK_{a2}) groups. The first acidic sites of Good's buffers are released below *ca.* pH 3.0, while the second protonation constants are included in the physiological pH region of pH 6 to 9. The pH-profiles of these GB-ILs were measured in aqueous solution (Figure 3.1.2 A) to identify their buffering action, through which it is possible to show their buffering-like region, described by the moderate slope length appearing before the inflection point at high pH. Their buffer capacity is a measure of a buffer's ability to resist changes in pH upon the addition of an acid or base. Mathematically, the buffer capacity (β) is normally defined *according to* Equation 15,

$$\beta = \frac{dC_b}{d(pH)} = - \frac{dC_a}{d(pH)} \quad (\text{Equation 15})$$

where C_b and C_a , are the number of moles of strong base or acid added per liter.

The buffer capacity of the GB-ILs in aqueous solution is shown in Figure 3.1.2 B. The buffer capacities of GB-ILs are relatively high and offer a wide range of pH values. The buffering regions of [P₄₄₄₄][MES], [P₄₄₄₄][TES], [P₄₄₄₄][HEPES], [P₄₄₄₄][TRICINE], and [P₄₄₄₄][CHES], are 4.7–7.3, 6.2–8.7, 6.2–8.8, 6.6–9.7 and 7.7–10.7, respectively. The pH at the middle of the buffering region is equal to the pK_{a2}, and thus the buffering capacity is, at this point, the highest.

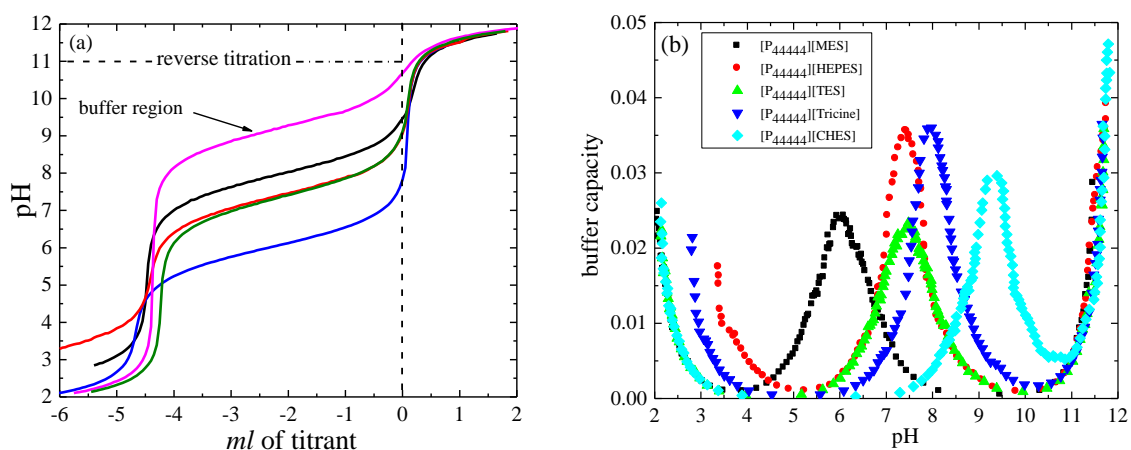


Figure 3.1.2 A Plots of pH vs. mL of 0.1 mol·dm⁻³ of NaOH/HCl added to 10.0 mL of 0.05 mol·dm⁻³ of GB-IL ([P₄₄₄₄][MES] (blue line), [P₄₄₄₄][TES] (green line), [P₄₄₄₄][HEPES] (red line), [P₄₄₄₄][CHES] (magenta line), and [P₄₄₄₄][TRICINE] (black line)) in water at (25.0 ± 0.1) °C; the reverse titration region is for mL of 0.1 mol·dm⁻³ of HCl added to 10.0 mL of 0.05 mol·dm⁻³ of GB-IL. **B** Buffer capacity as a function of pH for 0.05 M of GB-IL titrated with 0.1 mol·dm⁻³ of HCl/NaOH at (25.0 ± 0.1) °C.

The (acid + base) equilibria of GBs and GB-ILs (*e.g.*, MES and [P₄₄₄₄][MES], respectively) are represented in Figure 3.1.3. The pK_{a1} and pK_{a2} values of the investigated Good's buffers at 25 °C and the ionic strength of 0.1 M of NaNO₃, as well as the corresponding GB-ILs, are reported in Table 3.1.1.

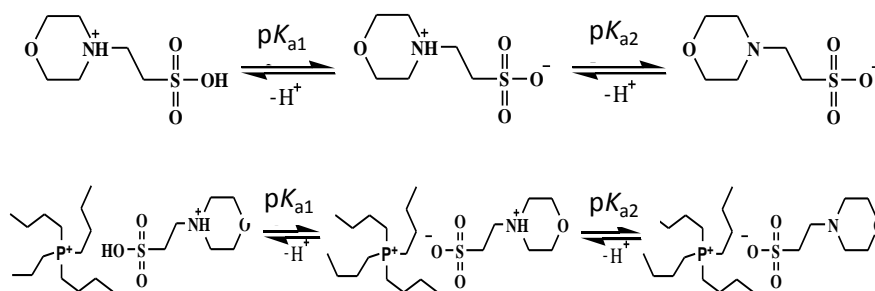


Figure 3.1.3 Protonation equilibria of MES and [P₄₄₄₄][MES].

Table 3.1.1 Protonation constants of GB/GB-ILs in water at 25 °C and $I = 0.1$ M of NaNO_3 .

GB/GB-ILs	$\text{p}K_{a1}$	$\text{p}K_{a2}$
MES	2.28 ± 0.07	$6.12 (6.07)^{55} \pm 0.02$
$[\text{P}_{4444}][\text{MES}]$	2.21 ± 0.10	5.91 ± 0.06
TES	3.05 ± 0.02	$7.30 (7.42)^{55} \pm 0.01$
$[\text{P}_{4444}][\text{TES}]$	—	7.21 ± 0.03
TRICINE	$2.68 (2.40)^{55} \pm 0.03$	$8.08 (8.00)^{55} \pm 0.02$
$[\text{P}_{4444}][\text{TRICINE}]$	2.39 ± 0.05	7.82 ± 0.01
HEPES	$3.17 (3.0)^{55} \pm 0.04$	$7.35 (7.45)^{55} \pm 0.04$
$[\text{P}_{4444}][\text{HEPES}]$	2.77 ± 0.10	7.23 ± 0.02
CHES	1.76 ± 0.03	9.13 ± 0.01
$[\text{P}_{4444}][\text{CHES}]$	—	8.93 ± 0.05

The $\text{p}K_{a1}$ values of MES, TES, and CHES, are here reported for the first time. The $\text{p}K_{a2}$ values obtained in this work are in good agreement with those found in the literature⁵⁵. Representative potentiometric fitted profiles of MES and $[\text{P}_{4444}][\text{MES}]$ using the HYPERQUAD 2008 program⁴³ are shown in Figure 3.1.4 A. The distribution diagrams of species computed with the HySS program⁵⁶ for MES and $[\text{P}_{4444}][\text{MES}]$ as a function of pH, are presented in Figure 3.1.4 B.

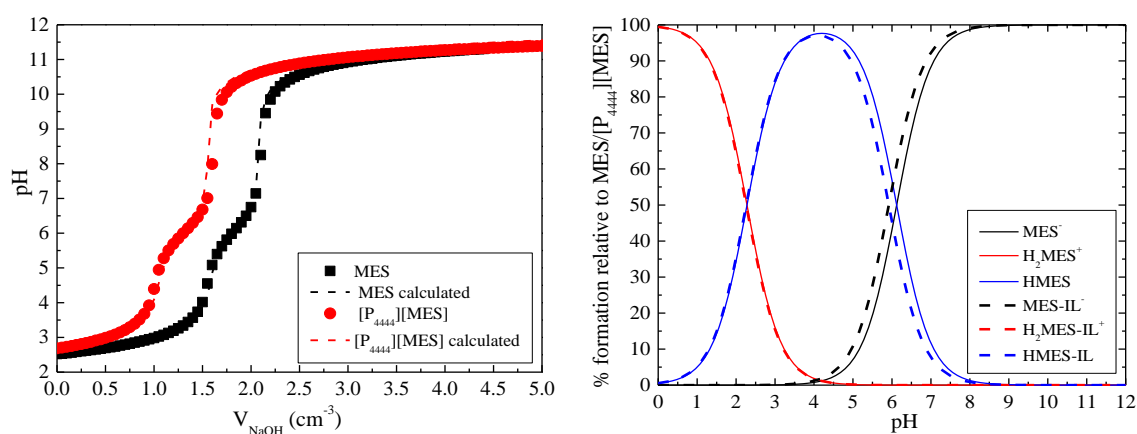


Figure 3.1.4 A pH titration curves of $1 \cdot 10^{-3}$ M of MES and $[\text{P}_{4444}][\text{MES}]$ at 25 °C and $I = 0.1$ M of NaNO_3 . The dashed lines are the calculated pH from the refinement operations. **B** Species-distribution diagrams of $1 \cdot 10^{-3}$ M of MES and $[\text{P}_{4444}][\text{MES}]$ at 25 °C and $I = 0.1$ M of NaNO_3 .

The potentiometric profiles and distribution diagrams of the species for the other investigated GB/GB-ILs are given in Figure B.1.3 in the Appendix B1. From the obtained results (potentiometric profiles and species distribution diagrams) it can be gauged that GB-ILs are more easily deprotonated than the corresponding GBs, as confirmed by the lower $\text{p}K_a$ values of the

former (Table 3.1.1). It should be remarked that it was not possible to determine the pK_{a1} value of $[P_{4444}][TES]$ and $[P_{4444}][CHES]$. The observed decrease in the pK_{a1} and pK_{a2} values of GB-ILs can be attributed to a higher stabilization of their free conjugated bases by electrostatic interactions with the tetrabutylphosphonium cation.

To determine the optimum pH of a protein function, different buffers are used to maintain the solution buffer capacity. However, the available universal buffers are scarce and have drawbacks since their anions interact or chelate metal-ions. The biological buffers MES, HEPES, and CHES are compatible with systems containing metal ions due to their negligible affinity to metal ions, and thus they are used to formulate biocompatible universal buffers in aqueous solution (Figure 3.1.5). The universal Good's buffer composed of $[P_{4444}][MES]$ + $[P_{4444}][HEPES]$ + $[P_{4444}][CHES]$ presents a linear behaviour in the pH range from 5.5 to 10.5, and can be seen as a promising option.

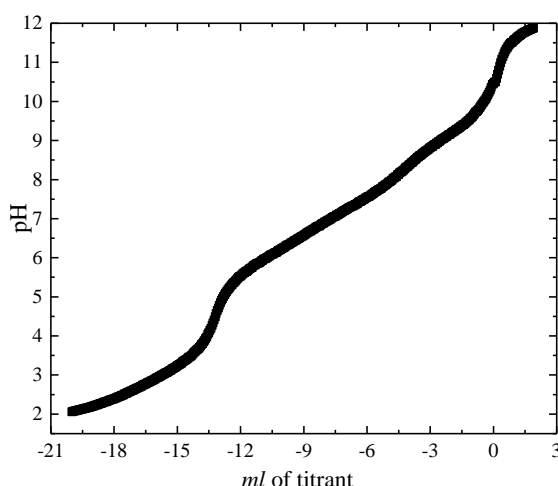


Figure 3.1.5 Plots of pH vs. mL of 0.1 mol·dm⁻³ of NaOH/HCl added to a mixture of 10.0 ml of 0.05 mol·dm⁻³ $[P_{4444}][MES]$ + $[P_{4444}][HEPES]$ + $[P_{4444}][CHES]$ at (25.0 ± 0.1) °C.

Toxicities of $[P_{4444}][GB]$ against the marine bacteria *Vibrio fischeri* - To evaluate the ecotoxicity of the five $[P_{4444}][GB]$ ILs, the Microtox® Acute toxicity test⁴⁰ was used. Table 2.3.6 reports the EC₅₀ values determined along with the 95% limits of confidence. The toxic character of $[P_{4444}][GB]$, as well as that of $[P_{4444}][Cl]$, was assessed after 30 min of the bacteria exposure, ensuring enough time to verify their effect in the luminescence inhibition⁵⁷. The results show that the $[P_{4444}][GB]$ species present a toxicity that is similar or lower than the toxicity obtained for the $[P_{4444}][Cl]$. In this sense, the EC₅₀ values can be ranked as follows: $[P_{4444}][MES]$ > $[P_{4444}][HEPES]$ > $[P_{4444}][CHES]$ > $[P_{4444}][Cl]$ (the commercial IL) > $[P_{4444}][TRICINE]$ > $[P_{4444}][TES]$. This tendency indicates that $[P_{4444}][MES]$ is the most benign compound, while $[P_{4444}][TES]$ is the one

with the highest toxicity. The $[P_{4444}][GB]$ (with the exception of $[P_{4444}][TES]$ which belongs to the category “acute 3” – $10 \text{ mg} \cdot \text{L}^{-1} < EC_{50} \leq 100 \text{ mg} \cdot \text{L}^{-1}$) can be classified as non-hazardous substances ($EC_{50} > 100 \text{ mg} \cdot \text{L}^{-1}$), according to the laws imposed by the European Legislation for the aquatic compartment⁵⁸. The trend for the effect of $[GB]^-$ anions on toxicity here observed is in general distinct from that observed before for other types of $[GB]^-$ ILs³⁶, suggesting a stronger impact of the $[P_{4444}]^+$ cation (Table 3.1.2). Nevertheless, by finely-tuning the $[GB]^-$ anion, it is possible to design self-buffering $[P_{4444}][GB]^-$ based ILs with similar or lower toxicity than the non-buffering $[P_{4444}]\text{Cl}$.

Table 3.1.2 EC_{50} values after 30 min of exposure time with the 95% confidence limits (within brackets) for $[P_{4444}][GB]$ and $[P_{4444}]\text{Cl}$.

Compound	$EC_{50} \text{ (mg L}^{-1}\text{) at 30 min (lower limit; upper limit)}$
$[P_{4444}]\text{Cl}$	110.26 (96.57; 123.95)
$[P_{4444}][\text{MES}]$	231.25 (204.72; 257.78)
$[P_{4444}][\text{TES}]$	85.98 (72.48; 99.48)
$[P_{4444}][\text{CHES}]$	154.31 (137.56; 171.07)
$[P_{4444}][\text{TRICINE}]$	107.82 (86.08; 129.55)
$[P_{4444}][\text{HEPES}]$	185.58 (174.07; 197.10)

ABS phase diagrams - The formation of an ABS depends on the IL type and its concentration, salt type and its concentration, temperature and pH. The intensity of the phase-forming ability in each IL-based system relies on the basis of the complex and competing nature of the interactions occurring between the solutes (*e.g.*, ions from the inorganic salt and IL) and water or between the phase-forming components⁵⁹. The phase diagrams provide information about the concentration of the phase-forming components needed for the design of purification processes using ABS. The experimental data corresponding to the ternary phase diagrams determined in this work, as well as the respective correlations, are presented in Tables B.1.2-B.1.4 in the Appendix B1. For all ABS studied, the top phase corresponds to the IL-rich aqueous layer while the bottom phase is salt enriched. Figure 3.1.6 depicts the phase diagrams obtained for several $[P_{4444}][GB]/[P_{4444}]\text{Cl}$ and $\text{K}_3\text{C}_6\text{H}_5\text{O}_7$ systems. Table B.1.5 in Appendix B1 presents additional data regarding the phase diagrams description, namely tie-lines (TLs) and respective tie-line lengths (TLL).

The $[P_{4444}]^+$ cation is already known for its high ability to form ABS with different salts, which easily justifies the easy formation of ABS with all the GB-ILs prepared in this work. The formation of ABS using these GB-ILs is driven by the low affinity of the phosphonium cation for water, since

it has a highly positive shielded charge that is surrounded by four hydrophobic alkyl chains. The smaller the affinity for water and/or the higher hydrophobic nature of the IL, the more prone it is to be salted-out⁵⁹ by the other phase-forming component, in this case, the potassium citrate salt. Since potassium citrate is a strong salting-out salt⁶¹, it has a higher affinity for water and thus the GB-ILs are strongly salted-out from the aqueous solution and create a two-phase system.

In Figure 3.1.7 B, the binodal curves are plotted on a molality scale, together with the data for the ABS composed of $[P_{4444}]\text{Cl} + \text{K}_3\text{C}_6\text{H}_5\text{O}_7$ obtained from literature⁶² for comparison purposes. It can be seen that the phase-forming ability of all GB-ILs is higher than $[P_{4444}]\text{Cl}$, meaning that lower amounts of both GB-IL and salt are required to form ABS. If compared to more traditional and commercially available ILs, these have the benefits of reducing the cost and simultaneously increase the biocompatible nature of these systems when applied as purification/fractionation platforms. The GB-IL anions ability to form ABS, for instance at $1.0 \text{ mol}\cdot\text{kg}^{-1}$ of $\text{K}_3\text{C}_6\text{H}_5\text{O}_7$, follows the order: $[\text{CHES}]^- > [\text{MES}]^- > [\text{HEPES}]^- > [\text{TES}]^- > [\text{TRICINE}]^-$. At a first glance, this trend can be interpreted in the light of each anion chemical structure (*cf.* Figure 3.1.1): *i)* the $[\text{TRICINE}]$ and $[\text{TES}]$ anions' weakest ABS formation ability is a consequence of the presence of three hydroxyl groups that enhance their hydrogen-bonding capacity with water, turning the salting-out process by the citrate-based salt a more difficult task; *ii)* $[\text{HEPES}]^-$, with one hydroxyl group, is ranked in an intermediate position; *iii)* and finally $[\text{MES}]^-$ and $[\text{CHES}]^-$, with no hydroxyl groups, are the most hydrophobic GB-ILs investigated and thus the strongest to promote two-phases. Meanwhile, the hydrophobic character of the $[\text{CHES}]$ anion arises from the cyclohexyl group present in its structure (Figure 3.1.1), which allows the easiest phase separation.

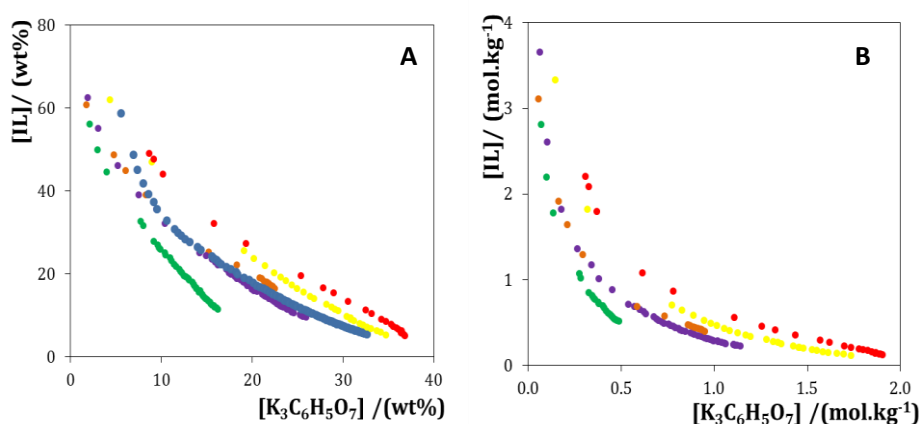


Figure 3.1.6 A Ternary phase diagrams for the systems composed of IL + $\text{K}_3\text{C}_6\text{H}_5\text{O}_7$ + water at 25 °C and atmospheric pressure in wt% **B** and in $\text{mol}\cdot\text{kg}^{-1}$ (right): (●) $[P_{4444}][\text{TRICINE}]$, (●) $[P_{4444}][\text{MES}]$, (●) $[P_{4444}][\text{HEPES}]$, (●) $[P_{4444}][\text{TES}]$, (●) $[P_{4444}][\text{CHES}]$, and (●) $[P_{4444}]\text{Cl}$.

The hydrophobic character of GBs can be evaluated through their water-octanol partition coefficients, $\log(K_{ow})$. The higher the value of $\log(K_{ow})$ the higher their solubility in the octanol-rich phase and, consequently, the lower the GB polarity. Therefore, higher $\log(K_{ow})$ values correspond to anions that are more easily salted-out and form two-phase systems (ABS). The $\log(K_{ow})$ values of CHES, MES, HEPES, TES, and TRICINE are, respectively, 2.04, 0.27, 0.12, -0.51, and -0.69, which is consistent with their phase-forming ability.

Figure B.1.4 in Appendix B1 shows a comparison between the effect of $[P_{4444}]^+$ and $[N_{4444}]^+$ -based ILs on the ABS formation with potassium citrate. It can be seen that $[P_{4444}]^+$ is a better phase-forming agent than $[N_{4444}]^+$ for all cation-anion combinations studied in this work. Although both types of compounds are composed of four alkyl chains of similar length, there are also some contributions derived from the central atom. Similar results were obtained in ABS constituted by more conventional ILs and potassium phosphate⁴¹, sodium carbonate⁶⁰ and potassium citrate⁶² as salting-out agents. In these studies, the results suggested that phosphonium-based ILs are also more effective in promoting ABS when compared with their ammonium-based congeners. Recently, the influence of the cation's central atom of some ammonium- and phosphonium-based ILs were investigated through experimental and theoretical studies. The authors observed that the ammonium cations are more polar than the corresponding phosphonium-based ILs, which is again consistent with the higher ABS phase-forming ability observed for phosphonium-based GB-ILs.

Extraction and purification of BSA using GB-IL-based ABS - The partition of commercial BSA was first studied aiming at understanding its preferential migration towards the GB-IL or salt-rich phases. Table 3.1.3 presents the BSA extraction efficiency data obtained for the IL-GB-rich phase at a fixed composition and for which the respective phases' compositions are given in Table B.1.5 in the Appendix B1. From the results presented in Table 3.1.3, it is observed that the extraction of BSA to the IL-rich phase is complete ($EE_{BSA} = 100\%$), without significant losses of protein, either by precipitation or denaturation (conclusion obtained by the mass balance results). The preferential migration of BSA and other macromolecules to the IL-rich phase was already described for GB-IL-based ABS^{37, 38}, which could be justified by specific interactions taking place between BSA and the (GB)-ILs³⁸, although the strong salting-out effect of the salt used cannot be discarded. Despite the results obtained in this and other works^{37, 38}, in which the protein preferentially migrates to the IL-rich phase, in other works the opposite migration behaviour was also verified^{23, 23}.

Table 3.1.3 Extraction efficiencies of serum bovine albumin, EE_{BSA} (%), in the ABS composed of $[P_{4444}][GB] + K_3C_6H_5O_7$ at 25 °C, and at the described mixture compositions.

GB-ILs/ILs	Weight fraction composition wt%		EE_{BSA} (%)
	IL	$K_3C_6H_5O_7$	
$[P_{4444}][TRICINE]$	38.7 ± 2.1	15.02 ± 1.8	100
$[P_{4444}][HEPES]$	39.4 ± 0.3	13.7 ± 0.1	100
$[P_{4444}][CHES]$	38.0 ± 5.5	13.5 ± 2.3	100
$[P_{4444}][MES]$	38.9 ± 0.1	16.3 ± 0.9	100
$[P_{4444}][TES]$	39.5 ± 0.1	14.4 ± 0.3	100
$[P_{4444}][Cl]$	38.9 ± 0.1	13.9 ± 1.2	100

BSA stability in GB-ILs - The stability of the protein conformation when in contact with the $[P_{4444}][GB]/[P_{4444}][Cl]$ was studied in this work through ATR-FTIR, in particular to determine the protein conformation integrity regarding the secondary structure of proteins^{63, 64}. The IR spectra of the amide I group of BSA in presence of (0.05 and 0.5) M of $[P_{4444}][TRICINE]/[P_{4444}][TES]/[P_{4444}][HEPES]/[P_{4444}][Cl]$ were measured at pH 7.4, since at this pH these three GB-ILs present good buffer capacity. The presence of the amide I band is due to carbonyl stretching vibration which appears at $\sim 1653 \text{ cm}^{-1}$. In order to analyse the BSA secondary structure, curve fitting was used for the amide I. The bands at (1615, 1631, 1653, 1675, and 1697) cm^{-1} correspond to inter and intra-molecular β - sheets, α -helix, turns, and antiparallel β -sheets, respectively^{63, 64}. The α -helix value of BSA in a buffer solution is consistent with those previously reported⁶⁵. The secondary structure of BSA in the studied GB-ILs as well as in the conventional $[P_{4444}][Cl]$, is listed in Table 3.1.4. The Gaussian curve-fitting analysis of the amide I spectra of BSA in 0.05 M $[P_{4444}][Cl]$ and $[P_{4444}][TES]$ are shown in Figure 3.1.7, as examples. The α -helices of BSA in GB-ILs are higher than the corresponding GBs. The α -helix contents of BSA in the studied ILs follow the order: $[P_{4444}][TES] > [P_{4444}][HEPES] > [P_{4444}][Cl] > [P_{4444}][TRICINE]$. It is important to mention that no buffer is used to adjust the pH of the protein solution in the GB-ILs presence, while 0.05 M of HEPES buffer was used for the analysis with the $[P_{4444}][Cl]$.

Table 3.1.4 Secondary structure analysis (infrared spectra) of BSA in conventional $[P_{4444}][GBs]/[P_{4444}]Cl$ at pH 7.4.

Amide I components	TES	HEPES	TRICINE	$[P_{4444}]Cl$		$[P_{4444}][TES]$		$[P_{4444}][HEPES]$		$[P_{4444}][TRICINE]$	
	0.05	0.05	0.05	0.05	0.5	0.05	0.5	0.05	0.5	0.05	0.5
	M	M	M	M	M	M	M	M	M	M	M
Inter β -sheet	—	—	2.4 ³⁶	—	—	—	—	—	—	—	—
Intra β -sheet	24.3 ³⁸	26.4 ³⁸	25.0 ³⁶	28.8	29.7	25.7	24.3	25.4	25.8	24.4	23.6
α -helix	59.8 ³⁸	58.3 ³⁸	57.6 ³⁶	60.6	61.2	64.9	65.9	61.2	62.9	59.9	60.5
turn	15.9 ³⁸	25.3 ³⁸	14.2 ³⁶	10.6	9.1	9.4	9.8	13.4	11.3	15.7	15.9
antiparallel β -sheet	—	—	0.8 ³⁶	—	—	—	—	—	—	—	—

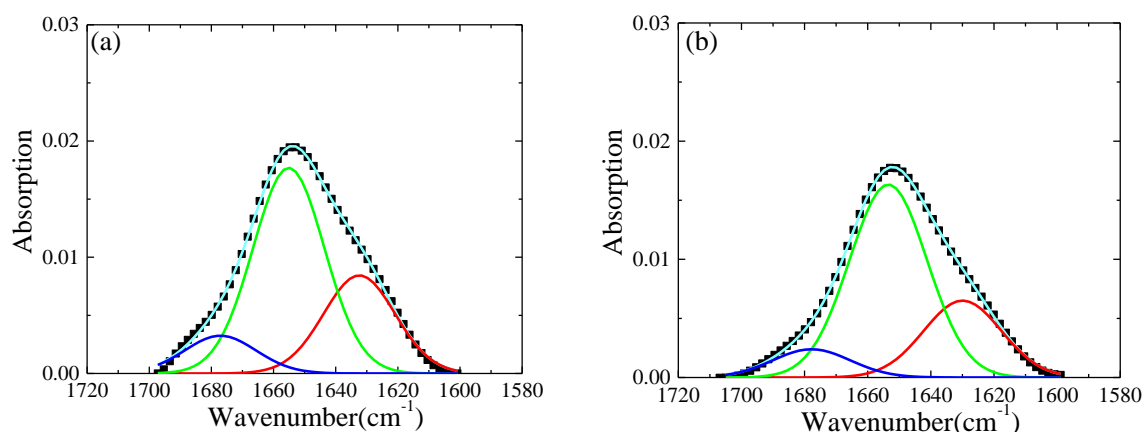


Figure 3.1.7 Gaussian curve-fitting analysis of amide I spectra of BSA in 0.05 M of $[P_{4444}]Cl$ (a) and in 0.05 M of $[P_{4444}][TES]$ at pH 7.4.

The evaluation of the BSA aggregation in aqueous solutions of ILs is an important factor to be studied to understand the stabilizing/destabilizing effect of the synthesized ILs through proteins. The effect of increasing the concentration of $[P_{4444}][GB]/[P_{4444}]Cl$ on BSA using DLS at pH 7.4 at 25 °C is presented in Figure 3.1.8. The size distribution curves of the studied ILs show that the BSA in the presence of 0.05 M of GB-ILs exhibited two peaks at $RH = 3.7$ nm and $RH \geq 100$ nm. The peak of small particles which appears with a major population is due to the native state of BSA. Meanwhile, the other peak with lower intensity is showing that BSA forms aggregates in these conditions. The size of BSA was increased while increasing the IL concentration from 0.05 M to 0.5 M (Figure 3.1.8). This indicates that with the increase of the IL concentration, the BSA molecules aggregate forming oligomeric species. However, these

oligomeric species are formed without unfolding as observed from the increase of the α -helices of BSA in the (GB-)ILs.

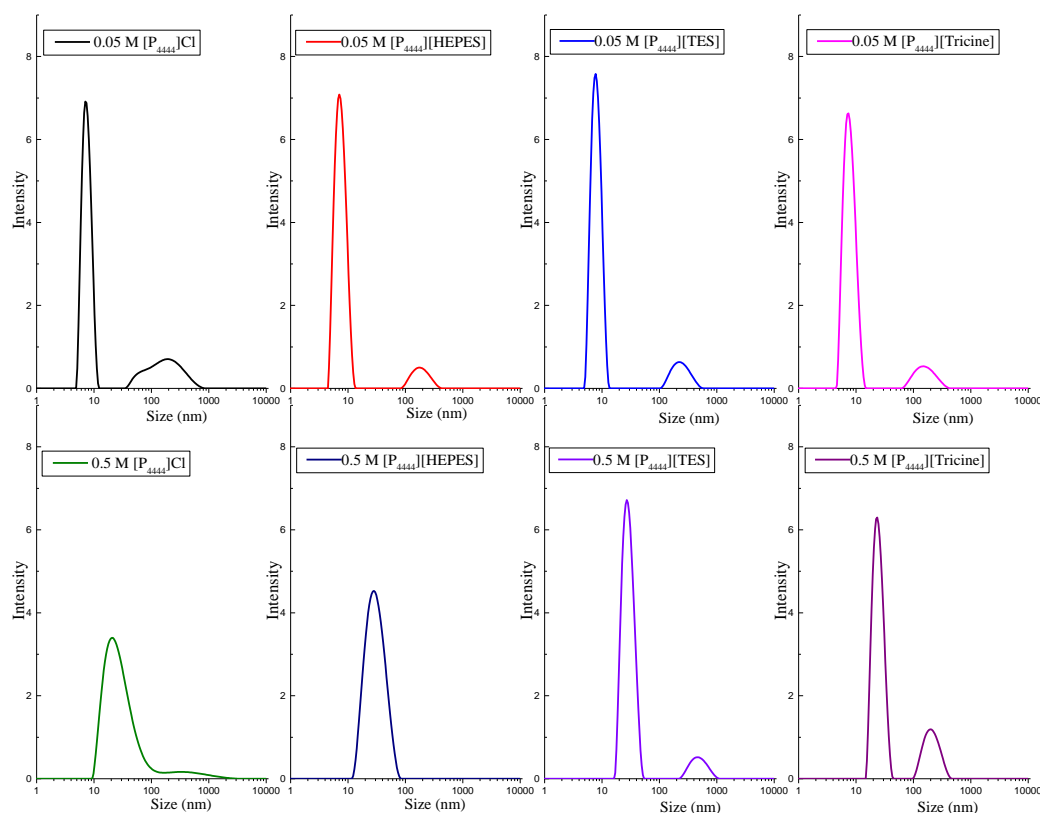


Figure 3.1.8 The intensity distribution graph of BSA in (0.05 and 0.5) M of $[P_{4444}]\text{Cl}/[P_{4444}][\text{TES}]/[P_{4444}][\text{TRICINE}]/[P_{4444}][\text{HEPES}]$, at pH 7.4 and 25 °C.

In order to calculate the binding between $[P_{4444}]\text{Cl}/[P_{4444}][\text{GB}]$ and BSA, the binding model quantitative structure-activity relationship (QSAR)-human serum albumin', $\log K(\text{HSA})$, was used to predict the binding affinity of $[P_{4444}]\text{Cl}/[P_{4444}][\text{GB}]$ to HSA⁶⁶. This model can be used also to predict the binding of the investigated ILs to BSA because both proteins (HSA and BSA) are similar in terms of their amino acid sequence⁶⁷. The $\log K(\text{HSA})$ values of $[P_{4444}]\text{Cl}$, $[P_{4444}][\text{TES}]$, $[P_{4444}][\text{TRICINE}]$, and $[P_{4444}][\text{HEPES}]$ are, respectively, 0.4438, 0.3112, 0.5754, and 0.8292. These phosphonium-based ILs show a binding affinity to BSA, thus confirming the complete extraction of BSA with no losses as discussed before. It is well known that BSA has different binding sites for a variety of biomaterials (*e.g.* fatty acids) with thermal stabilizing effect⁶⁸, where the hydrophobicity and polarity play a significant role in the binding. The polarity of the synthesized ILs can be qualitatively evaluated from the σ -profiles of their ions. The σ -profile is divided into three regions (Figure 3.1.9): H-bond donor, H-bond acceptor, and a non-polar region between

them. The H-bond cut-off is $0.079 \text{ e}\cdot\text{\AA}^{-2}$, and the hydrogen bonding is the weakest up to $0.01 \text{ e}\cdot\text{\AA}^{-2}$.

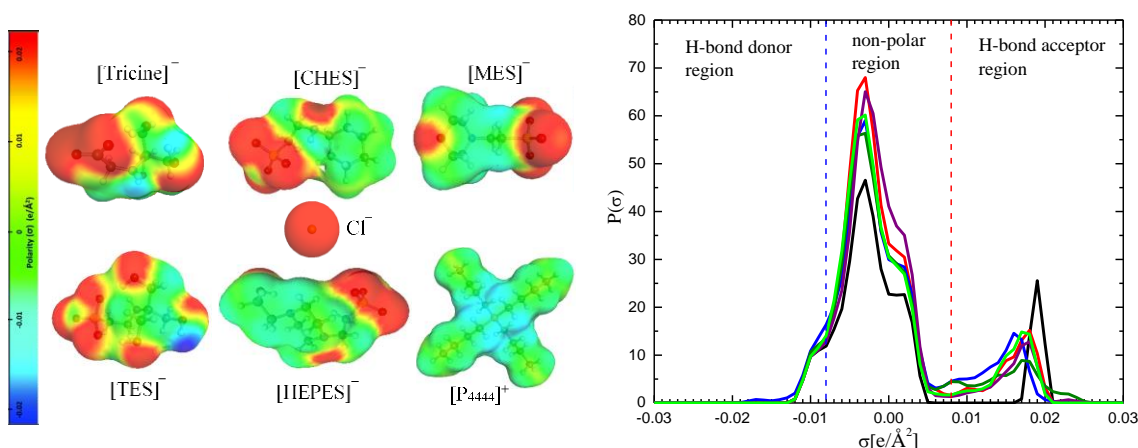


Figure 3.1.9 σ -profiles of $[P_{4444}]\text{Cl}$ (black line), $[P_{4444}][\text{HEPES}]$ (red line), $[P_{4444}][\text{TES}]$ (blue line), $[P_{4444}][\text{TRICINE}]$ (green line), $[P_{4444}][\text{CHES}]$ (purple line), and $[P_{4444}][\text{MES}]$ (green line).

It is clear from Figure 3.1.9 that GB-ILs show strong negative polar peaks over $(0.01 \text{ to } 0.025) \text{ e}\cdot\text{\AA}^{-2}$ (deep red) arising from the oxygen's sulfonic/carboxylic/morpholine groups and hydroxyl groups, as well as, the nitrogen's amine groups, in which they can provide hydrogen bonds with H-bond donor groups such as protein or water. On the other side, only $[P_{4444}][\text{TES}]$ shows positive polar peaks at $-0.015 \text{ e}\cdot\text{\AA}^{-2}$ (deep blue) arising from one hydroxyl's hydrogen of $[\text{TES}]^-$, while the others two hydroxyl's hydrogens formed intramolecular hydrogen bonds with the sulfonic group. The hydroxyl's hydrogens of $[\text{TRICINE}]^-$ do not show any positive peaks because they form intramolecular hydrogen bonds with themselves and the oxygen's carboxylic group. The hydroxyl's hydrogen of $[\text{HEPES}]^-$ forms intramolecular hydrogen bonds with the nearby tertiary amine group. Furthermore, the amine's hydrogens of $[\text{TES}]^-$, $[\text{TRICINE}]^-$, and $[\text{CHES}]^-$ form intramolecular hydrogen bonds with oxygen's sulfonic and carboxylic groups. Therefore, GBs' anions show weak hydrogen bond donor fragments due to the intramolecular hydrogen bond formations. The sharp negative peak of $[P_{4444}]\text{Cl}$ is a result of the chloride ion while the broad peak in the non-polar area arises from the aliphatic groups of $[P_{4444}]^+$. This non-polar peak becomes broader in case of GB-ILs due to the methylene groups of the GB's anion, further supporting the higher ability of GB-ILs to form ABS. Table 3.1.5 reports the total mean interaction energy (E_i), electrostatic interaction energy ($E_{i,\text{misfit}}$), hydrogen bond interaction energy ($E_{i,\text{HB}}$), and van der Waals interaction energy ($E_{i,\text{vdW}}$) of the pure GB-ILs derived from COSMO-RS computations.

Table 3.1.5 Interaction energies of $[P_{4444}][GB]/[P_{4444}]Cl$ at 25 °C .

$[P_{4444}][GB]/[P_{4444}]Cl$	E_i	$E_{i,MF}$	$E_{i,HB}$	$E_{i,vdW}$
	kcal·mol ⁻¹			
$[P_{4444}]Cl$	-6.75	16.25	-2.38	-20.62
$[P_{4444}]^+$	-8.20	10.75	-1.20	-17.75
Cl^-	1.45	5.50	-1.18	-2.87
$[P_{4444}][TRICINE]$	-12.78	14.11	-2.22	-24.67
$[P_{4444}]^+$	-9.65	8.04	-1.07	-16.62
$[TRICINE]^-$	-3.13	6.07	-1.15	-8.05
$[P_{4444}][TES]$	-18.75	12.23	-5.31	-25.68
$[P_{4444}]^+$	-10.26	7.04	-0.72	-16.58
$[TES]^-$	-8.49	5.19	-4.59	-9.10
$[P_{4444}][HEPES]$	-13.25	16.43	-2.04	-27.64
$[P_{4444}]^+$	-9.49	8.27	-1.00	-16.76
$[HEPES]^-$	-3.76	8.16	-1.04	-10.88
$[P_{4444}][MES]$	-11.51	16.08	-1.95	-25.64
$[P_{4444}]^+$	-9.19	8.55	-0.98	-16.77
$[MES]^-$	-2.32	7.53	-0.97	-8.873
$[P_{4444}][CHES]$	-14.71	14.39	-1.95	-27.16
$[P_{4444}]^+$	-10.05	7.77	-0.98	-16.84
$[CHES]^-$	-4.66	6.62	-0.97	-10.32

The electrostatic-misfit interaction energy arises from the dissimilarity and mismatching between the hydrogen bond donors and acceptors among ILs ions, as it is evident from the results of the σ -profiles. The data in Table 3.1.5 show strongly negative values of van der Waals interaction energy, indicative of their expected strong dispersive interactions with protein. The hydrogen bond energy values are also found to be negative. The electrostatic-misfit contributions are positive due to their lack of H-bond donors, which in turn, show the expected attraction towards the H-donors sites of the protein. The total mean interaction energies of the investigated ILs were found to be negative. Thus, the van der Waals and hydrogen bond interactions between BSA and these ILs play an important role in the protein migration pattern in $[P_{4444}][GB]/[P_{4444}]Cl$ -based ABS. We have previously identified the hydrogen bond interactions between TRICINE³⁶, TES³⁸, and HEPES³⁸ anions with BSA using molecular docking. The TRICINE anion has found to form five hydrogen bonds with Leu346, Glu353, and Arg208 amino acid residues of BSA³⁶. TES anion forms two hydrogen bonds with Arg198, while the HEPES anion forms only one hydrogen bond with Ser428³⁸. Herein, we also carried out molecular docking to

predict the binding sites of MES^- , CHES^- , and $[\text{P}_{4444}]^+$ to BSA as shown in Figure 3.1.10. The MES^- anion forms three hydrogen bonds with Ser428, Arg458, and His 45. CHES^- anion forms two hydrogen bonds with Arg458 and His145. The residues found next to the $[\text{P}_{4444}]^+$ are Thr 190, Ser 428, and Leu 454. The binding free energies of the $[\text{MES}]^-$, and $[\text{P}_{4444}]^+$ are (-5.0, -5.6, and -5.0) $\text{kcal}\cdot\text{mol}^{-1}$, respectively.

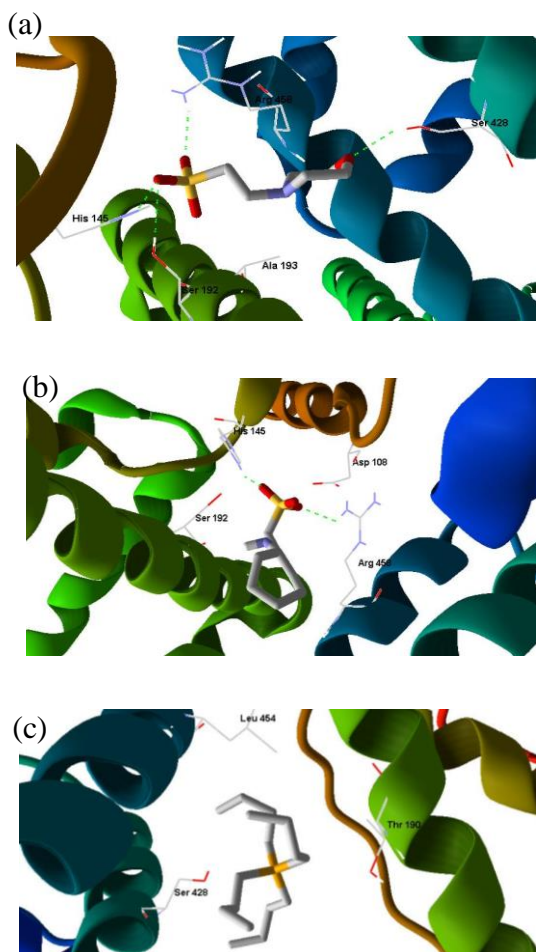


Figure 3.1.10 Molecular docking of BSA with **A** $[\text{MES}]^-$, **B** $[\text{CHES}]^-$, and **C** $[\text{P}_{4444}]^+$.

Purification of BSA from a bovine serum sample using GB-IL-based ABS - Proteins are usually present in an original complex media, and in order to evaluate the potential applicability of the IL-based ABS investigated, these systems were finally applied to purify BSA from a bovine serum sample. The GB-ILs-based ABS were evaluated regarding their capacity to extract BSA into the GB-IL-rich phase and to simultaneously remove contaminant macromolecules to the opposite aqueous phase. The analysed bovine serum sample is mostly composed of two different structural forms of BSA, the monomer (target molecule of this study) and a BSA aggregate (the main contaminant identified in this matrix). Based on the results obtained according to the HPLC

chromatograms), and considering the monomer as the target protein, the determined purity of BSA monomer (Figure 3.1.11) in the serum sample is *ca.* 45 %.

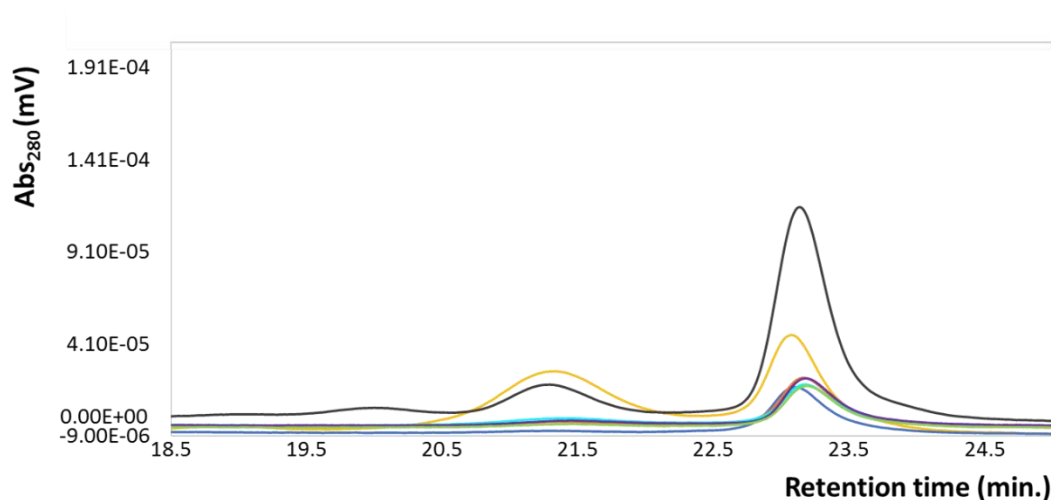


Figure 3.1.11 Size exclusion chromatograms of a BSA solution in PBS (0.5 g L^{-1}) (—), Bovine serum solution (—), top phase of $[P_{4444}][\text{TRICINE}] + \text{K}_3\text{C}_6\text{H}_5\text{O}_7$ (—), top phase of $[P_{4444}][\text{TES}] + \text{K}_3\text{C}_6\text{H}_5\text{O}_7$ (—), top phase of $[P_{4444}][\text{HEPES}] + \text{K}_3\text{C}_6\text{H}_5\text{O}_7$ (—), top phase of $[P_{4444}][\text{MES}] + \text{K}_3\text{C}_6\text{H}_5\text{O}_7$ (—), top phase of $[P_{4444}][\text{CHES}] + \text{K}_3\text{C}_6\text{H}_5\text{O}_7$ (—).

Following the same quantification protocol previously applied to study the commercial BSA, the BSA monomer was additionally quantified by SE-HPLC (Figure 3.1.11), indicating that the commercial BSA has a purity of $88 \pm 2 \%$ (Table 3.1.5). Table 3.1.6 provides the results of extraction efficiency, recovery yield and purity of the BSA monomer at the GB-IL-rich phase.

Table 3.1.6 Recovery efficiencies of serum bovine albumin from serum sample, EE_{BSA} (%), BSA Purity, $Purity_{BSA}$ (%), and BSA yield, $Yield_{BSA}$ (%), in the ABS composed of $[P_{4444}][GB]$ + $C_6H_5K_3O_7$ at 25 °C.

IL	EE_{BSA} (%)	$Purity_{BSA}$ (%)	$Yield_{BSA}$ (%)
$[P_{4444}][TRICINE]$	100	92.38 ± 1.48	80.09 ± 0.66
$[P_{4444}][TES]$	100	88.63 ± 2.28	73.15 ± 0.28
$[P_{4444}][HEPES]$	100	74.96 ± 0.31	68.84 ± 7.56
$[P_{4444}][CHES]$	100	85.85 ± 1.66	64.17 ± 0.48
$[P_{4444}][MES]$	100	84.69 ± 2.02	59.41 ± 0.83
Serum sample	–	45.33 ± 1.97	–
BSA commercial	–	88.36 ± 1.84	–

As previously observed with the commercial BSA, all GB-IL-based ABS lead to the complete migration of the BSA monomer from the serum samples to the GB-IL-rich phase, *e.g.* extraction efficiencies of 100%. Remarkably, all the studied systems lead to a decrease on the amount of the BSA aggregates at the IL-rich phase, which results in BSA with a higher purification level when compared to the serum sample - the BSA purity increases from $45 \pm 2\%$ to $92 \pm 1\%$. Moreover, good recovery yields (from 60 to 80%) have been obtained, as presented in Table 3.1.5. Thus, GB-IL-based ABS can be seen as potential purification platforms for BSA by eliminating protein aggregates and/or other contaminants from complex matrices.

Conclusions

The synthesis and characterization of new self-buffering ILs, based on the $[P_{4444}]^+$ cation and GB's anions (TES, HEPES, CHES, MES, and TRICINE), was here addressed. These ILs demonstrated a high capacity to form ABS with organic salts. In this sense they can be considered as remarkable platforms for the separation and purification of proteins, namely BSA from a bovine serum sample. Moreover, most of these ILs can be classified as non-hazardous substances (as gauged from the EC_{50} results for *Vibrio fischeri*). The effect of the studied ILs on the BSA structure was investigated using IR absorption spectroscopy, and their binding affinity towards the protein was determined by the QSAR-logK(HSA) model. The $[P_{4444}][GB]$ ILs were found to exhibit a stabilizing effect over the BSA structure as compared with the commercial IL $[P_{4444}][Cl]$. COSMO-RS and molecular docking were used to address the polarity of the ILs and to better interpret the

extraction process. Based on these studies, van der Waals and hydrogen-bonding interactions show to play an important role in the protein partitioning.

References

1. J. Benavides and M. R. Palomares. *J. Chem. Technol. Biotechnol.*, 2008, 83, 133-142.
2. J. A. Asenjo and B. A. Andrews, *J. Chromatogr. A*, 2011, 1218, 8826-8835.
3. S. H. Krishna, N. D. Srinivas, K. S. M. S. Raghavarao and N. G. Karanth, *History and Trends in Bioprocessing and Biotransformation*, Springer, 2002.
4. Y. Pei, J. Wang, K. Wu, X. Xuan and X. Lu, *Sep. Purif. Technol.*, 2009, 64, 288-295.
5. M. G. Freire, A. F. M. Claudio, J. M. M. Araujo, J. A. P. Coutinho, I. M. Marrucho, J. N. C. Lopes and L. P. N. Rebelo, *Chem. Soc.*, 2012, 41, 4966-4995.
6. T. Welton, *Chem. Rev.*, 1999, 99, 2071-2084.
7. S. Cantone, U. Hanefeld and A. Basso, *Green Chem.*, 2007, 9, 954-971.
8. A. Kumar and P. Venkatesu, *Chem. Rev.*, 2012, 112, 4283-4307.
9. N. Debeljuh, C. J. Barrow, L. Henderson and N. Byrne, *Chem. Commun.*, 2011, 47, 6371-6373.
10. L. J. Huang, M. E. Noss, K. M. Schmidt, L. Murray and M. R. Bunagan, *Chem. Commun.*, 2011, 47, 8007-8009.
11. A. F. M. Cláudio, A. M. Ferreira AM, A. J. D. Silvestre, M. G. Freire and J. A. P. Coutinho, *Sep. Purif. Technol.*, 2012, 97, 142-149.
12. H. Passos, A. C. A. Sousa, M. R. Pastorinho, A. J. A. Nogueira, L. P. N. Rebelo, J. A. P. Coutinho and M. G. Freire, *Anal. Methods*, 2012, 4, 2664-2667.
13. J. F. B. Pereira, F. Vicente, V. C. Santos-Ebinuma, J. M. Araújo, A. Pessoa, M. G. Freire and J. A. P. Coutinho, *Process Biochem.*, 2013, 48, 716-722.
14. Z. Du, Y. L. Yu and J. H. Wang, *Chem. Eur. J.*, 2007, 13, 2130-2137.
15. M. J. R. Angel, V. Pino, S. C. Broch and A. Berthod, *J. Chromatogr. A*, 2007, 1151: 65-73.
16. Q. Cao, L. Quan, C. He, N. Li, K. Li and F. Liu, *Talanta*, 2008, 77, 160-165.
17. S. Dreyer and U. Kragl, *Biotech. Bioeng.*, 2008, 99, 1416-1424.
18. S. Dreyer, P. Salim and U. Kragl, *Biochem. Eng. J.*, 2009, 46, 176-185.
19. Y. Pei, Z. Li, L. Liu, J. Wang and H. Wang, *Sci. China Chem.*, 2010, 53, 1554-1560.
20. Y. Lu, W. Lu, W. Wang, Q. Guo and Y. Yang, *Talanta*, 2011, 85, 1621-1626.
21. F. J. Deive, A. Rodríguez, A. B. Pereiro, J. M. M. Araujo, M. A. Longo, M. A. Z. Coelho, J. N. C. Lopes, J. M. S. S. Esperanca, L. P. N. Rebelo and I. M. Marrucho, *Green Chem.*, 2011, 13, 390-396.
22. S. P. M. Ventura, S. G. Sousa, M. G. Freire, L. S. Serafim, A. S. Lima and J. A. P. Coutinho, *J. Chromatogr. B*, 2011, 879, 2679-2687.
23. S. P. M. Ventura, R. L. F. Barros, J. M. P. Barbosa, C. M. F. Soares, A. S. Lima and J. A. P. Coutinho, *Green Chem.*, 2012, 14, 734-740.
24. F. J. Deive, A. Rodríguez, L. P. N. Rebelo and I. M. Marrucho, *Sep. Purif. Technol.*, 2012, 97, 205-210.
25. U. Novak, A. Pohar, I. Plazl and P. Znidarsic-Plazl, *Sep. Purif. Technol.*, 2012, 97, 172-178.
26. X. Lin, Y. Wang, Q. Zeng, X. Ding and J. Chen, *Analyst.*, 138, 6445-6453.
27. Q. Zeng, Y. Wang, N. Li, X. Huang, X. Ding, X. Lin, S. Huang and X. Liu, *Talanta*, 2013, 116, 409-416.
28. R. K. Desai, M. Streefland, R. H. Wijffels and H. M. Eppink, *Green Chem.*, 2014, 16, 2670-2679.
29. X. Ding, Y. Wang, Q. Zeng, J. Chen, Y. Huang and K. Xu, *Anal. Chim. Acta*, 2014, 815, 22-32.
30. E. G. Arnillas, F. J. Deive, M. A. Sanromán and A. Rodríguez, *Bioresour. Technol.*, 2015, 186, 303-308.
31. R. L. Souza, R. A. Lima, J. A. P. Coutinho, C. M. F. Soares and A. S. Lima, *Sep. Sci. Technol.*, 2015, 155, 118-126.
32. S. R. L. Souza, S. P. M. Ventura, C. M. F. Soares, J. A. P. Coutinho and A. S. Lima, *Green Chem.*, 2015, 17, 3026-3034.
33. R. K. Desai, M. Streefland, R. H. Wijffels and H. M. Eppink, *Green Chem.*, 2014, 16, 2670-2679.
34. S. Moreira, S. C. Silvério, E. A. Macedo, A. M. F. Milagres, J. A. Teixeira and S. I. Mussatto, *Chromatogr. A*, 2013, 1321, 14-20.
35. D. R. MacFarlane, R. Vijayaraghavan, H. N. Ha, A. Izgorodin, K. D. Weaver and G. D. Elliott, *Chem. Comm.*, 2010, 46, 7703-7705.
36. M. Taha, F. A. Silva, M. V. Quental, S. P. M. Ventura, M. G. Freire and J. A. P. Coutinho, *Green Chem.*, 2014, 3149-3159.
37. M. Taha, M. R. Almeida, F. A. Silva, P. Domingues, S. P. M. Ventura, J. A. P. Coutinho and M. G. Freire, *Chem. Eur. J.*, 2015, 21, 4781-4788.
38. M. Taha, M. V. Quental, I. Correia, M. G. Freire and J. A. P. Coutinho, *Process Biochem.*, 2015, 50, 1158-1166.
39. R. T. K. Kumar, I. G. D. Mello, D. Kinnamon, D. C. Rodrigues, C. P. Frizzo and S. Prasad, *RSC Adv.*, 2016, 6, 22594-22603.
40. S. M. Steinberg, E. J. Poziomek, W. H. Engelmann and K. R. Rogers, *Chemosphere*, 1995, 30: 2155-2197.

41. C. L. S. Louros, A. F. M. Cláudio, C. M. S. S. Neves, M. G. Freire, I. M. Marrucho, J. Pauly and J. A. P. Coutinho, *Int. J. Mol. Sci.*, 2010, 11, 1777-1791.
42. S. Y. Lee, F. A. Vicente, F. A. e Silva, T. E. Sintra, M. Taha, I. Khoiroh, J. A. P. Coutinho, P. L. Show and S. P. M. Ventura, *ACS Sustain. Chem. Eng.*, 2015, 3, 3420-3428.
43. P. Gans, B. O'Sullivan, *Talanta*, 2000, 51, 33-37.
44. R. F. Jameson and M. F. Wilson, *J. Chem. Soc.*, 1972, 2607-2610.
45. P. Gans, A. Sabatini, A. Vacca, *Talanta*, 1996, 43, 1739-1753.
46. B. T. J., *Environmental A, Microtox manual*. Carlsbad CA, 1998.
47. J. C. Merchuk, B. A. Andrews and J. A. Asenjo, *J. Chromatogr. B*, 1998, 711, 285-293.
48. A. Klamt, *COSMO-RS from Quantum Chemistry to Fluid Phase Thermodynamics and Drug Design*, Elsevier, 2005.
49. A. Klamt and F. Eckert, *Fluid Phase Equilib.*, 2000, 172, 43-72.
50. A. Klamt, *J. Phys. Chem. A*, 1995, 99, 2224-2235.
51. A. Klamt, V. Jonas, T. Bürger and J. C. W. Lohrenz, *J. Phys. Chem. A*, 1998, 102, 5074-5085.
52. A. Schafer, A. Klamt, D. Sattel, J. C. W. Lohrenz and F. Eckert, *Phys. Chem. Chem. Phys.*, 2000, 2, 2187-2193.
53. O. Trott and A. J. Olson, *J. Comp. Chem.*, 2010, 31, 455-461.
54. K. A. Majorek, P. J. Porebski, A. Dayal, M. D. Zimmerman, K. Jablonska, A. J. Stewart, M. Chruszcz and W. Minor, *Mol. Immunol.*, 2012, 52, 174-182.
55. R. N. Goldberg, N. Kishore and R. M. Lennen, *J. Phys. Chem. Ref. Data*, 2002, 31, 231-370.
56. L. Alderighi, P. Gans, A. Lenzo, D. Peters, A. Sabatini, A. Vacca, *Coord. Chem. Rev.*, 1999, 184, 311-318.
57. S. P. M. Ventura, C. S. Marques, A. A. Rosatella, C. A. M. Afonso, F. Gonçalves and J. A. P. Coutinho, *Ecotoxicol. Environ. Saf.*, 2012, 76, 162-168.
58. L. Li, J. Xie, S. Yu, Z. Su, S. Liu, F. Liu, C. Xie and B. Zhang, *RSC Adv.*, 2012, 2, 11712-11718.
59. M. G. Freire, A. F. M. Cláudio, J. M. M. Araújo, J. A. P. Coutinho, I. M. Marruch, J. N. C. Lopes, L. P. N. Rebelo, *Chem. Soc. Rev.*, 2012, 41, 4966-4995.
60. C. F. Marques, T. Mourao, C. M. Neves, A. S. Lima, I. Boal-Palheiros, J. A. Coutinho and M. G. Freire, *Biotechnol. Prog.*, 2013, 29, 645-654.
61. L. M. Pegram and M. T. Record, *J. Phys. Chem. B*, 2007, 111, 5411-5417.
62. H. Passos, A. R. Ferreira, A. F. M. Cláudio, J. A. P. Coutinho and M. G. Freire, *Biochem. Eng. J.*, 2012, 67, 68-76.
63. S. Seshadri, R. Khurana and A. L. Fink, Academic Press, 1999, 309, 559-576.
64. B. Shivu, S. Seshadri, J. Li, K. A. Oberg, V. N. Uversky and A. L. Fink, *Biochem.*, 2013, 52, 5176-5183.
65. S. Ghosh, S. Jana and N. Guchhait, *J. Phys. Chem. B*, 2011, 116, 1155-1163.
66. C. X. Xue, R. S. Zhang, H. X. Liu, X. J. Yao, M. C. Liu, Z. D. Hu and B. T. Fan, *J. Chem. Inf. Comput. Sci.*, 2004, 44, 1693-1700.
67. H. Benyamini, A. S. Peleg, H. J. Wolfson, B. Belgorodsky, L. Fadeev and M. Gozin, *Bioconjugate Chem.*, 2006, 17, 378-386.
68. A. Michnik, K. Michalik and Z. Drzazga, *J. Therm. Anal. Calorim.*, 2005, 80, 399-406.

3.2. Extraction and purification of immunoglobulin G using aqueous biphasic systems formed by bio-based ionic liquids

Based on the published manuscript:⁴ Dibyendu Mondal, Mukesh Sharma, Maria V. Quental, Ana P. M. Tavares, Kamallesh Prasad and Mara G. Freire, *Green Chem.*, 2017,92 , 6071-6081.

Abstract

In the past decade, remarkable advances in the production and use of antibodies as therapeutic drugs and in research/diagnostic fields have led to their recognition as value-added proteins. These biopharmaceuticals have become increasingly important, reinforcing the current demand for the development of more benign, scalable and cost-effective techniques for their purification. Typical polymer–polymer and polymer–salt aqueous biphasic systems (ABS) have been studied for such a goal; yet, the limited polarity range of the coexisting phases and their low selective nature still are their major drawbacks. To overcome this limitation, in this work, ABS formed by bio-based ionic liquids (ILs) and biocompatible polymers were investigated. Bio-based ILs composed of ions derived from natural sources, namely composed of the cholinium cation and anions derived from plants natural acids, have been designed, synthesized, characterized and used for the creation of ABS with polypropyleneglycol (PPG 400). The respective ternary phase diagrams were initially determined at 25 °C to infer on mixture compositions required to form aqueous systems of two phases, further applied in the extraction of pure immunoglobulin G (IgG) to identify the most promising bio-based ILs, and finally employed in the purification of IgG from complex and real matrices of rabbit serum. Remarkably, the complete extraction of IgG to the IL-rich phase was achieved in a single-step. With pure IgG a recovery yield of 100% was obtained, while with rabbit serum this value slightly decreased to *ca.* 85%. Nevertheless, a 58% enhancement in the IgG purity was achieved when compared with its purity in serum samples. The stability of IgG before and after extraction was also evaluated by size exclusion high-performance liquid chromatography (SE-HPLC), sodium dodecyl sulphate polyacrylamide gel electrophoresis (SDS-PAGE) and Fourier transform infrared spectroscopy (FTIR). In most ABS formed by bio-based ILs, IgG retained its native structure, without degradation or denaturation effects, supporting thus their potential as remarkable platforms for the purification of high-cost biopharmaceuticals.

⁴**Contributions:** D.M., K.P. and M.G.F. conceived and directed this work. M.V.Q. and A.P.M.T. acquired the experimental data related to ABS and IgG. M.S. and D.M. synthesized and characterized the studied ILs. M.V.Q., D.M. and M.G.F. interpreted the obtained experimental data. The manuscript was mainly written by M.V.Q., D. M. and M.G.F., with contributions from the remaining authors.

Introduction

Amongst several therapeutic agents in current clinical use, major technological advances in biopharmaceuticals demonstrated the high relevance of antibodies¹. Immunoglobulin G (IgG), a glycoprotein, is a widely used type of antibodies in a variety of biomedical applications². Antibodies have been used in the treatment of cancer, as transporters of toxins or radio labelled isotopes to cancerous cells and in the treatments of autoimmune diseases and neural disorders³⁻⁶. Due to the continuous increase in the use of IgG in various applications, there is thus a boost in demand for high quality/high purity IgG, not only for therapeutic applications but also for applications in cutting-edge diagnosis and research. However, the expensive antibodies available commercially turns to be the major bottleneck affecting substantially their wide spread applications. The purification of IgG is rather desired since current production techniques result in complex mixtures comprising the antibodies along with other compounds/proteins/contaminants⁷. Processes for the purification of IgG typically require various steps, *viz.* clarification, concentration and purification by chromatographic techniques (such as ion exchange, gel permeation or affinity chromatography)⁸⁻¹¹, which result in the expensive production of antibodies. On the other hand, solvents use represents *ca.* 60% of the overall energy in pharmaceuticals production and can lead to 50% of post-treatment greenhouse gas emissions¹²⁻¹³. Therefore, there is a high demand for developing cost-effective and sustainable techniques to obtain high quality IgG. In order to overcome these and other inadequacies associated with conventional methods, the extraction and purification of value-added biopharmaceuticals using aqueous biphasic systems (ABS) might be seen as a viable alternative¹⁴⁻¹⁶.

ABSs were proposed in the late 50's by Albertsson¹⁷ and they have been recognized as a biocompatible extraction technique mostly due to their high water content. Two aqueous-rich phases are spontaneously formed after mixing two structurally different and appropriate components in aqueous media, such as polymer-polymer, polymer-salt or salt-salt combinations¹⁸. Although these systems have been studied for at least the last five decades, the introduction of ionic liquids (ILs) in ABS formation (IL-based ABS)¹⁹, combined with salts or polymers allowed to overcome the major drawback of more traditional polymer-based systems – the restricted polarity difference in their coexisting phases which hampers their selective nature²⁰. IL-based ABS appeared as outstanding alternatives supported by the achievement of improved and tailored extraction efficiencies of a wide range of value-added biomolecules, including highly susceptible biomolecules such as proteins^{18,21}.

ABS formed by ILs and inorganic salts are the most widely investigated, since they are also the easiest to form due to the high salting-out capacity of inorganic salts^{18, 25-26}. On the other

hand, imidazolium-based ILs combined with halogens and fluorinated anions have been the preferred choice for a number of applications¹⁸. This combination raises however some environmental and biocompatibility concerns. To minimize these apprehensions, ABS formed by bio-based ILs, preferably derived from natural sources, and biodegradable and biocompatible polymers, such as polypropylene glycol, polyethylene glycol, natural polysaccharides, among others, represent the most relevant type of IL-based ABS. Apart from the commonly studied imidazolium-based fluids, many of them toxic to organisms and poorly biodegradable, in the past few years, advances on the ILs field allowed the synthesis of ILs derived from natural sources, such as from amino acids, carbohydrates and phenolic acids²⁷⁻³¹. Fukaya et al.³² have demonstrated that bio-based ILs not only have a more benign character but also exhibit higher hydrogen bonding abilities when compared to more conventional ILs. It was also demonstrated the DNA/RNA dissolution with long term structural stability and isolation of polysaccharides using bio-ILs³³⁻³⁵. These findings therefore foster the potential of bio-based ILs in the extraction of sensitive biomacromolecules, such as proteins and antibodies. It is known that the proteins function and activity is directly dependent of their three-dimensional structure³⁶. In this context, when developing techniques to purify value-added proteins, it is required to guarantee that they maintain their biological activity and native structure, and here bio-based ILs appear as promising candidates for such applications.

Herein, a series of new bio-based ILs have been synthesized and characterized. The novel ILs are composed of the cholinium cation combined with anions derived from plants natural acids. Amongst the ten bio-based ILs studied herein, six are reported for the first time. The suitability of these bio-based ILs towards the formation of polymer-IL based ABS was explored thereafter. Polypropylene glycol with a molecular weight of 400 g mol⁻¹ (PPG 400) was used as the second phase-forming component due to its biocompatible nature and high biodegradability³⁷. After addressing the possibility of forming ABS with the set of bio-based ILs investigated and PPG, these were then investigated for the extraction of pure IgG and finally for the purification of IgG from rabbit serum. The structural stability of IgG before and after extraction was also studied to guarantee that the developed purification platform displays protein-friendly features.

Experimental Procedure

Materials - For the synthesis of bio-based ILs, cholinium bicarbonate (80 wt% aqueous solution) and D-(+)-galactouronic acid were purchased from Sigma-Aldrich Pvt. Ltd., USA. Glycolic, pyruvic, abietic, L-ascorbic, 2,5-dihydroxybenzoic (Gentisic acid) and D-(-) quinic acids were purchased from TCI Chemicals, Tokyo, Japan. Indole-3-acetic acid and indole-3-butyric acid

were purchased from SRL Chemicals, Mumbai, India. Lactic acid was procured from Riedel-de-Haën. Cholinium chloride ([Ch]Cl, purity > 98% pure) and cholinium acetate ([Ch][Ac], purity > 99%) were obtained from Sigma-Aldrich and Acros Organics, respectively, for comparative studies. The phase-forming component polypropylene glycol of average molecular weight 400 g·mol⁻¹ was purchased from Sigma Aldrich. All chemicals used were of analytical grade and used as received. Phosphate buffered saline (PBS) pellets (Sigma-Aldrich) were used to prepare the solutions of IgG. Purified IgG was obtained from rabbit serum (reagent grade, purity ≥ 95%) obtained as a lyophilized powder from Sigma-Aldrich, which was stored at -20 °C. The rabbit serum used was obtained from Sigma Aldrich, having a total protein concentration between 40-70 mg·mL⁻¹ (determined by Biuret). This product was provided as a liquid containing 0.01% thimerosal as preservative and was stored at -20 °C. The water used was double distilled, passed through a reverse osmosis system and further treated with a Milli-Q plus 185 water purification apparatus.

IL synthesis - Bio-based ILs were synthesized using a metathesis reaction reported earlier³³, where the corresponding acid was added into a round bottom flask containing aqueous cholinium bicarbonate (80 wt% in water) in an equimolar ratio (1:1) with continuous stirring under inert atmosphere. After the complete addition of each acid, the reaction mixture was refluxed at 60 °C for 12 h under a N₂ atmosphere. Finally, synthesized ILs were washed with ethyl acetate to remove unreacted starting materials. The ILs obtained were dried under reduced pressure and stored under dry conditions. The structure of the synthesized ILs was confirmed by ¹H NMR and electrospray ionization-mass spectrometry (ESI-MS). ¹H NMR spectra were recorded on a Bruker Avance II (500 MHz), in which *ca.* 15 mg of each IL were dissolved in D₂O/d₆-DMSO. Electrospray ionization-mass spectra (ESI-MS) of all ILs were recorded on a Q-TOF Micro Mass Spectrometer. Mass fragmentation patterns of all bio-based ILs were recorded in both positive mode (ESI⁺) and negative mode (ESI⁻) in the range of m/z 50-500 and data were processed using the Masslynx 4.0 software (Waters corp.) (Appendix B2, Figures B.2.1-B.2.10). Thermo-gravimetric analysis (TGA) was carried out on a NETZSCH TG 209F1 Libra TGA209F1D-0105-L machine using a temperature programmer 30-450 °C at a heating rate 5 °C·min⁻¹, under nitrogen gas atmosphere. Differential Scanning Calorimetry (DSC) was measured on a NETZSCH DC 209F1 Libra DCA209F1D-0105-L equipment from -100 to 100 °C, at a heating rate of 2 °C·min⁻¹, under nitrogen gas atmosphere. The zero shear viscosity of all ILs was recorded on Anton Paar, Physica MCR 301 Rheometer USA, using parallel plate PP50/P-PTD200 geometry (49.971 mm diameter, 0.1 mm gap). The zero shear viscosity was measured employing the shear rates 0.01, 1 and 10 s⁻¹ at 25 °C. The optical rotation of the studied bio-based ILs was measured

on a Rudolph Instrument DigiPol DP781 Polarimeter, using a Polarimeter tube with 100 mm path length. Optical rotation was measured at 589 nm at 25 °C. Before their use in the formation of ABS, all ILs samples were subjected to a further drying step under high vacuum to remove traces of water.

ABS phase diagrams - To ascertain on mixture compositions required to form two phases and to be able to use ABS as extraction/purification platforms, the respective ternary phase diagrams were initially determined. The binodal curve of each ABS was determined through the cloud point titration method at (25 ± 1) °C and atmospheric pressure. The experimental procedure adopted has been validated in a previous work³⁸. Briefly, pure PPG 400 and aqueous solutions of different ILs (*ca.* 90 wt%) were prepared gravimetrically. Each mixture composition was determined by the weight quantification of all components added within $\pm 10^{-4}$ g (Mettler Toledo Excellence XS205 Dual Range). The tie-lines (TLs), which give the composition of each phase for a given mixture composition, were determined gravimetrically at 25 °C according to the original method reported by Merchuk et al.³⁹. The experimental binodal curves were fitted by Equation 1³⁹:

$$[\text{PPG}] = A \exp[(B[\text{IL}]^{0.5}) - (C[\text{IL}]^3)] \quad (\text{Equation 1})$$

where [PPG] and [IL] are the PPG 400 and IL weight fraction percentages, respectively, and the coefficients *A*, *B*, and *C* are fitting parameters. The parameters were determined using the Sigma Plot 11.0 software.

Tie-lines (TLs) and tie-line lengths (TLLs) were determined according to the procedure described in the experimental section of Chapter 2.1.

Extraction and purification of IgG - ABS consisting of 25 wt% of different ILs, 30 wt% of PPG 400 and 45 wt% of an aqueous solution containing IgG at $1 \text{ mg} \cdot \text{mL}^{-1}$ were prepared by weight ($\pm 10^{-4}$ g). Only for the system composed of Choline-indole-3-acetate a different mixture composition was used, namely 40 wt% IL, 40 wt% of PPG 400 and 20 wt% of an aqueous solution containing IgG at $1 \text{ mg} \cdot \text{mL}^{-1}$, due to the more restricted biphasic regime of this IL as discussed below. Each ABS was mixed in a vortex, centrifuged (10 min at 1000 rpm), and then left at (25 ± 1) °C for 4 h. The upper and lower phases were then carefully separated and used for the determination of the IgG concentration in each phase. The IgG contents in both top and bottom phases were determined by size exclusion high-performance liquid chromatography (SE-HPLC). Before injection in the SE-HPLC, each phase was diluted at a 1:10 (v:v) ratio in PBS buffer (10

mM, pH = 7.4). A Chromaster HPLC system (VWR Hitachi) equipped with a binary pump, column oven, temperature controlled auto-sampler and DAD detector was used. SE-HPLC was performed using an analytical column Shodex Protein KW- 802.5 (8 mm x 300 mm). A 100 mM phosphate buffer pH 7.0 with NaCl 0.3 M was run isocratically with a flow rate of 0.5 ml·min⁻¹ with injection volume of 25 µL. The wavelength was set at 280 nm whereas the retention time of IgG was found to be *ca.* 15.6 min within an analysis time of 30 min. Pure IgG from a rabbit source was used for the calibration curve. The percentage extraction efficiency of IgG ($EE_{IgG}\%$) and IgG recovery yield ($Y_{IgG}\%$) were determined by the following Equations,

$$EE_{IgG}\% = \frac{e_{IgG}^{IL}}{w_{IgG}^{PPG} + w_{IgG}^{IL}} \times 100 \quad (\text{Equation 2})$$

$$Y_{IgG}\% = \frac{w_{IgG}^{IL}}{w_{IgG}^{Initial}} \times 100 \quad (\text{Equation 3})$$

where w_{IgG}^{PPG} , w_{IgG}^{IL} and $w_{IgG}^{Initial}$ are the total weight of IgG in the PPG-rich phase, in the IL-rich phase, and in the initial mixture, respectively.

After identifying the best ABS constituted by bio-based ILs for the extraction of IgG, carried out with pure IgG as described before, they were then applied for the extraction and purification of IgG from real rabbit serum samples. ABS formed by 25 wt% of ILs + 30 wt% of PPG 400 + 45 wt% of rabbit serum (diluted at 1:10 (v/v); pH \approx 7) were used. Each mixture was mixed using a Vortex mixer, centrifuged (10 min at 1000 rpm), and left for 4h at (25 \pm 1) °C in order to attain the complete partitioning of IgG and remaining proteins between the two phases. After the separation of the two phases, the IgG and remaining proteins were quantified by SE-HPLC, as described above. The percentage extraction efficiency and recovery yield of IgG to the IL-rich phase were determined according to Equations 2 and 3, respectively, whereas the percentage purity of IgG was calculated dividing the HPLC peak area of IgG by the total area of all peaks corresponding to all proteins present at the IL-rich phase. All extractions were carried out in triplicates.

Stability of IgG - The stability of IgG before and after extraction with the studied ABS was investigated by SE-HPLC, Sodium Dodecyl Sulphate Polyacrylamide Gel Electrophoresis (SDS-PAGE) and Fourier Transform Infrared Spectroscopy (FTIR). Although SE-HPLC was used to quantify IgG as mentioned before, at the same time, the structural integrity of the protein was monitored. The aggregation/degradation of IgG can be studied by SE-HPLC since it affects its

retention time. SDS-PAGE analysis of IgG after extraction was carried out using ABS and pure IgG ($1 \text{ mg} \cdot \text{mL}^{-1}$) in PBS buffer (10 mM, pH 7.4) for comparative analysis. The detailed process for SDS-PAGE analysis is reported elsewhere⁴⁰. Before loading in the gel wells, all samples were diluted in Laemmli sample buffer in order to load $ca. 200 \text{ } \mu\text{g}$ of IgG mL^{-1} per lane. These solutions were heated at $95 \text{ }^{\circ}\text{C}$ for 5 min for denaturation followed by the loading into the wells of the SDS-PAGE gel containing 20% polyacrylamide. SDS-PAGE molecular weight markers from VWR were used. Gels were electrophoresed for 1.5 h at 135 V on polyacrylamide gels (stacking 4%; resolving 20%) with a running buffer constituted by 250 mM Tris-HCl, 1.92 M glycine and 1% SDS. After the run, gels were stained with Coomassie Brilliant Blue G-250 0.1% (w/v), methanol 50% (v/v), acetic acid 7% (v/v) and water 42.9% (v/v) for 3-4 h at room temperature in an orbital shaker. Gels were then de-stained in a solution of acetic acid at 7% (v/v), methanol at 20% (v/v) and water at 73% (v/v) in an orbital shaker at 50 rpm for 3-4 h at $40 \text{ }^{\circ}\text{C}$. Mixtures composed of 45 wt% of aqueous solutions containing IgG ($1 \text{ mg} \cdot \text{mL}^{-1}$), 30 wt% of PPG 400 and 25 wt% of different bio-based ILs were prepared and used to perform the stability studies by FTIR. Pure IgG ($1 \text{ mg} \cdot \text{mL}^{-1}$) in an aqueous solution of PBS buffer (10 mM, pH 7.4) was taken as the control sample for comparison purposes. FTIR spectra were obtained in the wavelength range from 1800 to 1200 cm^{-1} , and recorded using a Perkin Elmer Spectrum Bx spectrometer with a resolution of 4 cm^{-1} and 64 scans. All spectra were fitted at amide I region (1600 - 1700 cm^{-1}) and deconvoluted using the Origin 8.5 software.

Results and Discussion

Synthesis and characterization of bio-based ILs - All bio-based ILs studied herein were synthesized by metathesis reaction as reported earlier³². In all cases, cholinium act as the cation and different bioactive natural acids act as sources of anions. Figure 3.2.1 shows the chemical structure of the bio-based ILs used in this study.

In general, ILs having cholinium (Ch) as cation and plant growth regulators based anions, such as indole-3-acetic acid ([A]) and indole-3-butyric acid (IB), are liquid at room temperature. Similar liquid appearance at room temperature was observed for ILs prepared with anions derived from glycolic acid (Gly), pyruvic acid (Pyr), abietic acid (Abt), L-ascorbic acid (Asc), galactouronic acid (Gal) and quinic acid (Qui). However, ILs prepared with anions derived from coumarine-3-carboxylic acid (C3C) and 2,5-dihydroxy benzoic or genistic acid (Gen) are highly viscous and semi-solid in appearance. Amongst the ten synthesised bio-based ILs, four of them, namely [Ch][IA], [Ch][IB], [Ch][Gly] and [Ch][Pyr] were reported earlier for the dissolution and stabilisation of salmon DNA³³ and for the extraction of the protein bovine serum albumin (BSA)⁴¹. ^1H NMR and ESI-MS were recorded for all ILs. For instance, the various peaks (D_2O , 500 MHz,

δ /ppm relative to TMS) for the IL [Ch][IA] are assigned as 2.62 (s, 9H, $-\text{CH}_3$), 2.88 (t, 2H, $-\text{CH}_2-\text{N}^+$), 3.22 (s, 1H, $-\text{OH}$), 3.47 (s, 2H, $-\text{CH}_2-\text{CO}-$), 3.60 (t, 2H, $-\text{O}-\text{CH}_2-$), 7.08 (d, 1H, $=\text{CH}-\text{N}-$), 6.96-7.51 (m, 4H, aromatic protons), and 10.04 (s, 1H, $-\text{HN}-$) (Figure B.2.1 in the Appendix B2). In ESI-MS experiments, the m/z was found to be 174.06 which further confirm the structure of this IL. The structure of the remaining bio-based ILs was also confirmed by ^1H NMR and ESI-MS (Figures B.2.2-B.2.10 in the Appendix B2). NMR and ESI-MS results support the structure and purity of all ILs synthesized and shown in Figure 3.2.1.

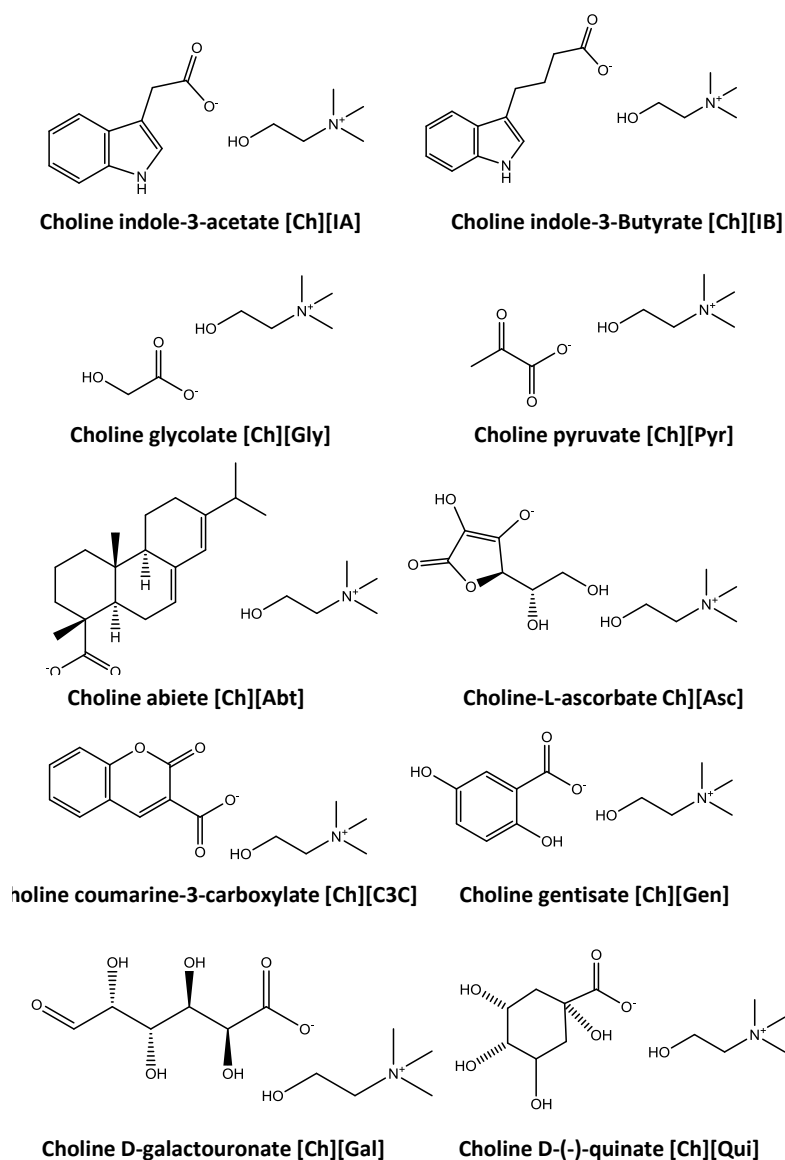


Figure 3.2.1 Chemical structures of the synthesized bio-based ILs.

Some physicochemical properties of the synthesized ILs are shown in Table 3.2.1. Glass transition temperatures were observed between $-63.3\text{ }^{\circ}\text{C}$ for [Ch][Gal] to $-98.8\text{ }^{\circ}\text{C}$ for [Ch][Pyr]. [Ch][Abt] displays the lowest melting temperature ($-20.5\text{ }^{\circ}\text{C}$) while [Ch][Gen] presents the

highest one (52.4 °C). In general, all synthesized ILs display melting temperatures lower than 100 °C and thus fit within the IL melting temperature based definition⁴². [Ch][Qui] displays the highest temperature of decomposition (330 °C) while the IL with the indole-3-butyrate derived anion decomposes at 220 °C. Based on these results it is safe to admit that all ILs are relatively stable up to high temperatures and can be used in a wide variety of applications. The apparent viscosities are widely different depending on the nature of IL anion, with apparent viscosities ranging from 0.02 Pa·s for [Ch][IB] up to 6290 Pa·s for [Ch][C3C].

Table 3.2.1 Physicochemical properties of the synthesized bio-based ionic liquids.

IL	T _g / °C	T _m / °C	T _{dec} / °C	[α] _D	η/ (Pa.s)
[Ch][IA]	---	---	300	NS	3.34
[Ch][IB]	---	---	220	NS	0.02
[Ch][Gly]	-98.4	16.0	256	NS	0.18
[Ch][Pyr]	-98.8	16.6	230	NS	0.21
[Ch][Abt]	-46.3	-20.5	314	-39.4	107
[Ch][Asc]	-70.1	15.3	251	35.6	1.18
[Ch][C3C]	-88.3	17.3	261	NS	6290
[Ch][Gen]	-66.5	52.4	279	NS	---
[Ch][Gal]	-63.3	50.1	245	40.15	3.02
[Ch][Qui]	-76.3	18.8	330	-5.83	0.23

Note: T_g = Glass transition temperature; T_m = Melting temperature; T_{dec} = Decomposition temperature; [α]_D = Optical rotation; NS = Not studied; η = Zero shear viscosity measured at 0.01 s⁻¹ and 25 °C.

After confirming the chemical structures and physicochemical properties of all bio-based ILs, they were further tested for their water miscibility at 25 °C. All synthesized ILs are completely water-soluble at 25 °C, and were used thereafter to explore their suitability towards formation of biocompatible ABS with PPG 400. Ternary phase diagrams were determined for each bio-based IL + PPG 400 + H₂O at 25 °C under atmospheric pressure, whose results are shown in Figure 3.2.2. The solubility curves are presented both in weight fraction and molality units [moles of PPG per·kg of (IL + water) vs moles of IL per·kg of (PPG + water)]. Ternary mixtures with compositions above each binodal curve result in the formation of a two-phase system, while initial mixtures with compositions below this curve result in the formation of a homogenous and completely miscible solution. The experimental weight fraction data corresponding to each phase diagram are provided in the Appendix B2, Table B.2.2-B.2.3. The experimental binodal data were further fitted by the empirical relationship described by Equation 1, and shown in Figure 3.2.2 (right). The regression parameters and corresponding standard deviations (σ) are

provided in the Table B.2.4 (Appendix B2). In general, good correlation coefficients were obtained for all systems, which mean that these fittings can be used to predict the phase diagram in a region where no experimental results are available. The experimental tie-lines (TLs) useful to ascertain on the coexisting phases compositions for a given initial mixture in which the extractions were carried) and their respective tie-line length (TLL) were also determined and are given in Table B.2.4 in Appendix B2.

The first set of solubility curves (Figure 3.2.2, right) is useful for defining their applicability and mixture compositions for a given extraction/purification step while the use of molality units allows a better understanding of the impact of each species on the phase diagrams behaviour (Figure 3.2.2, left). Amongst all studied ILs, [Ch][Gly], [Ch][Qui], [Ch][Gal], [Ch][Pyr], [Ch][Asc] and [Ch][IA] are able to form two-phase systems with PPG 400.

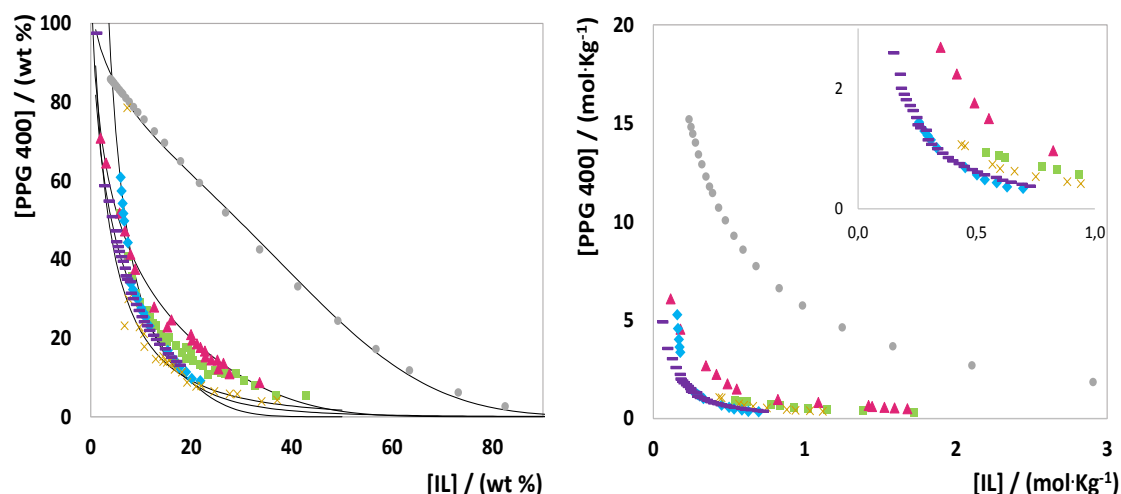


Figure 3.2.2 Phase diagrams for ABS composed of PPG 400 + bio-based ILs + H₂O in wt% (left) and in molality units (right) at 25 °C and under atmospheric pressure. [Ch][Gly] (×); [Ch][Qui] (♦); [Ch][Gal] (—); [Ch][Pyr] (■), [Ch][Asc] (▲); [Ch][IA] (●). Lines correspond to the fitting of the experimental data using Equation 1.

All bio-based ILs investigated in this work share the same cation; therefore, the ability to form ABS with PPG 400 depends on the anion counterpart. [Ch][IB], [Ch][Abt], [Ch][C3C] and [Ch][Gen] are not able to form ABS with PPG 400, being these the ones that present the higher octanol-water partition coefficients (Table 3.2.2)⁴³. Octanol-water partition coefficients correspond to the partition of a particular solute between octanol and water (hydrophobic and hydrophilic layer). This means that ILs with lower affinity for water are more hydrophobic in nature and have a lower propensity to be hydrated, being weaker salting-out species to salt-out PPG 400 from aqueous media and to induce the formation of ABS. An exception to this pattern

was observed with [Ch][IA], which may indicate that other types of interactions may govern the phase behaviour, particularly relevant when dealing with IL-polymer-based ABS in which the interactions between all pairs of phase-forming components cannot be discarded and may play a significant role⁴⁴.

Table 3.2.2 Logarithm of octanol-water partition coefficients ($\text{Log}K_{\text{ow}}$) of the acids used to synthesize bio-based ILs⁴³.

Acids	$\text{Log}K_{\text{ow}}$
Indole-3-Butyric acid	2.60
Indole-3-acetic acid	1.71
Glycolic acid	-1.07
Pyruvic acid	0.07
Abeitic acid	4.95
Ascorbic acid	-1.26
Coumarine-3-carboxylic acid	1.37
Gentisic acid	1.67
Galacturonic acid	-2.61
Quinic acid	-2.70

Among the ILs able to form ABS, their ability to form two phases in presence of ~90 wt% of PPG 400 is as follows: $[\text{Ch}][\text{Qui}] \simeq [\text{Ch}][\text{Gal}] > [\text{Ch}][\text{Gly}] > [\text{Ch}][\text{Pyr}] > [\text{Ch}][\text{Asc}] > [\text{Ch}][\text{IA}]$. This trend closely correlates with the octanol-water partition values of each acid (Table 3.2.2) and thus with the IL hydration aptitude and/or affinity for water. This behaviour is in accordance with what has been observed with ABS formed by polymers and inorganic salts^{44,20}, in which salts with higher charge density more easily promote the formation of two phase systems. Hence, the investigated cholinium-based ILs which forms ABS seems to act as salting-out species over PPG 400 in aqueous media. An unique exception was observed with [Ch][Asc]. Based on its octanol-water partition coefficient, this IL should better induce the two phase formation or at least in a similar way to that displayed by [Ch][Gly]. However, and as stated before, in polymer-IL-based ABS, the phenomenon can be more complex since polymer-IL interactions cannot be discarded⁴⁴.

Extraction and purification of IgG - After identifying the bio-based ILs able to act as phase-forming components of ABS, the potential of these systems for the extraction and purification of IgG was studied. As a first attempt, extractions with pure IgG were carried out in order to

ascertain on the most promising systems which are able to efficiently extract and recover antibodies. In order to compare the performance of the novel bio-based ILs with more conventional cholinium-based counterparts, the partitioning of pure BSA was also addressed in ABS formed by PPG 400 and cholinium acetate ([Ch][Ac]), cholinium lactate ([Ch][Lac]) and cholinium chloride ([Ch]Cl)⁴¹. IgG was quantified by SE-HPLC and the obtained chromatograms are depicted in Figure 3.2.3. The percentage extraction efficiency (EE_{IgG} %) and recovery yield (Y_{IgG} %) are presented in Table 3.2.3. For [Ch][Ac] and [Ch][Lac] systems it was observed the preferential partitioning of IgG into the bottom phase (IL-rich phase), whereas for [Ch]Cl no IgG was detected in both phases. These results are in good agreement with a previous work where the same systems were studied for the extraction of BSA, and where a higher loss of the protein was observed with the system formed by [Ch]Cl⁴¹. In the ABS constituted by [Ch]Cl the antibody completely precipitated at the interface meaning a recovery yield of 0%, while with [Ch][Ac]- and [Ch][Lac]-based ABS the protein partially precipitated with a consequent negative impact on the recovery yield of IgG (Y_{IgG} % of 82 and 65%, respectively). Remarkably, and contrarily to more conventional cholinium-based ABS, the systems formed by most of the bio-based ILs synthesized in this work, namely [Ch][Gly], [Ch][Pyr], [Ch][Asc], [Ch][Gal] and [Ch][Qui] allow the complete extraction and complete recovery of IgG in a single-step, *e.g.* EE_{IgG} % of 100% and Y_{IgG} % of 100 %. In fact, no IgG was detected at the PPG-400-rich phase (top phase) and no losses of IgG, either by visible precipitation or quantification were perceived. In these ABS, IgG completely migrated to the more hydrophilic phase (IL-rich phase).

Table 3.2.3 Extraction efficiencies of IgG (EE_{IgG} %) and IgG recovery yield (Y_{IgG} %) in ABS formed by an aqueous solution containing IgG at 1 mg·mL⁻¹.

IL	Y_{IgG} %	EE_{IgG} %	Observation
[Ch]Cl	0	0	Precipitation
[Ch][Ac]	82 ± 9	100	Partial precipitation
[Ch][Lac]	65 ± 5	100	Partial precipitation
[Ch][IA]	0	0	Precipitation
[Ch][Qui]	100	100	No precipitation
[Ch][Asc]	100	100	No precipitation
[Ch][Gly]	100	100	No precipitation
[Ch][Pyr]	100	100	No precipitation
[Ch][Gal]	100	100	No precipitation

No IgG peak was detected in both phases of the [Ch][IA]-based ABS, suggesting that IgG was completely degraded or denatured during extraction. In fact, and contrary to the remaining

systems, in this particular case it was witnessed the existence of precipitated protein at the interface. According to the phase diagrams shown in Figure 3.2.2, [Ch][IA] is the IL which presents a smaller two-phase regime meaning that it is the most hydrophobic IL investigated. For this particular IL, a different mixture composition was used (40 wt% of IL + 40 wt% of PPG 400 + 20 wt% of an aqueous solution containing IgG at $1 \text{ mg}\cdot\text{mL}^{-1}$) due to the more restricted biphasic regime of [Ch][IA]. Therefore, this particular IL-based ABS has a lower content of water which reflects into a lower amount of water in the respective coexisting phases— *cf.* TL data in the Appendix B2, Table B.2.4. This lower content of water seems thus responsible for the loss of stability of the antibody.

With the exception of [Ch][IA], the newly developed IL-based ABS are outstanding platforms for the complete extraction of IgG in a single-step with no losses of the protein. Previous studies^{9, 45} with ABS composed of polyethylene glycol (PEG) with molecular weights of 6000 and 3350 $\text{g}\cdot\text{mol}^{-1}$ and a phosphate-based salt have led to extraction efficiencies of IgG of 90% from both Chinese Hamster Ovary (CHO) and hybridoma cell culture supernatants, whereas the recovery yields were 90 % and 88 %, respectively. Since these ABS are formed by polymers with high molecular weights, they also display high viscosities at the coexisting phases which can be seen as a major drawback when considering the scale-up of the technology. Wu et al.⁴⁶ also investigated different ABS formed by PEG and hydroxypropyl starch for IgG extraction. Despite the high extraction yields (99.2 %), the authors have reported the co-precipitation of the protein in all tested systems. More recently, an integrated method of polymer-polymer- based ABS and a hybrid combination of ABS with magnetic particles resulted in 84% and 92% recovery yield of IgG, respectively^{47, 48}. Most of the studies regarding the IgG extraction addressed the use of PEG, mostly due to its more hydrophilic character, high biodegradability, low toxicity and low cost. The use of PPG 400 in the present study, having a more hydrophobic character (due to the additional methyl group at the side chain) enhances the ABS separation and the water content at the coexisting phases, which can be beneficial for the extraction of products with biological activity. It should be taken into consideration that in our work IgG preferentially migrates to the IL-rich phase and not to the polymer-rich phase as typically observed with more conventional polymer-based ABS^{9, 45}.

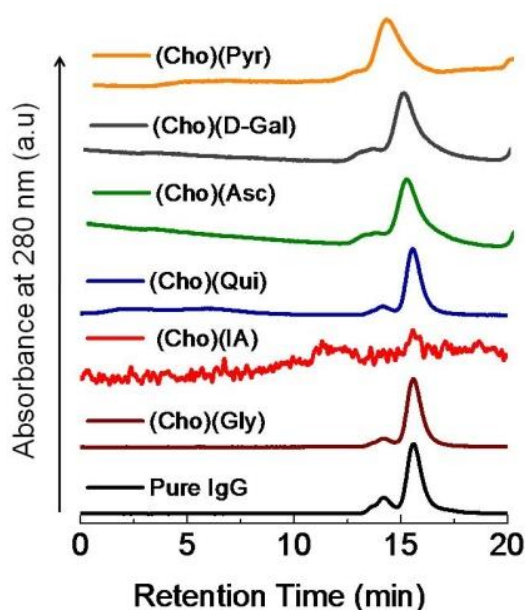


Figure 3.2.3 Size-exclusion chromatograms of pure IgG and IgG obtained in the bottom phases (IL-rich phases) after extraction and purification by ABS. IgG peak is characterized by a retention time around 15.6 min.

After identifying the most promising ILs for the extraction of IgG, these were employed for the extraction/purification of IgG directly from rabbit serum. ABS formed by [Ch][Gly], [Ch][Pyr], [Ch][Asc] and [Ch][Qui] at the mixture compositions described before and used for the extraction of pure IgG were investigated. In this approach it was possible to evaluate whether the presence of other contaminant proteins in serum influence the extraction of IgG and how these systems perform in terms of purification. Figure 3.2.4 depicts the results on the purification, recovery yield and extraction efficiency of IgG from rabbit serum (Table B.2.5 in the Appendix B2 presents detailed data). The quantification was carried out by SE-HPLC (Figure B.2.11 in the Appendix B2).

For all studied systems, IgG completely migrates to the IL-rich phase in a single-step – extraction efficiency of 100% - following the behaviour found with the pure antibody (Table B.2.5 in Appendix B2). However, a lower recovery yield of IgG was obtained when carrying out extractions from real serum samples. It was found that contaminant proteins also preferentially partition into the IL-rich phase, although not completely, thus allowing the enhancement on the purification factor of IgG as discussed below. The migration of other proteins to the IL-rich phase is thus the major cause of this decrease in the recovery yield of IgG, either because there is a competition between all proteins to migrate to the IL-rich phase or because the phase saturation can be reached. From the bio-IL-based ABS evaluated, the system composed of [Ch][Asc] appears as the most promising with an IgG extraction efficiency of 100% and a recovery yield of

85%. A previous study reported a pilot-scale purification of IgG from goat serum with a 58% recovery yield by modified ion-exchange chromatography⁴⁹, thus supporting the good results obtained here. IgG with the highest purity level, defined as the ratio between the IgG content and the total proteins content in the IL-rich phase, was obtained with the ABS constituted by [Ch][Asc].

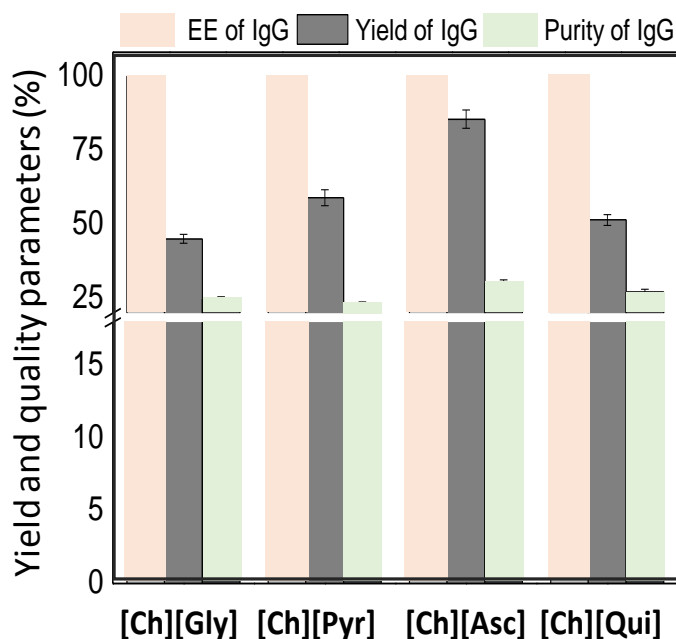


Figure 3.2.4 Extraction efficiencies of IgG (EE_{IgG} %), IgG recovery yield (Y_{IgG} %) and IgG percentage purity (%) from rabbit serum in ABS composed of PPG 400 (30 wt%) + bio-based IL (25 wt%) + 45 wt% of rabbit serum (diluted at 1:10 (v/v); pH \approx 7).

Enhancements on the IgG purity of 22.5%, 30.4% and 12.2% from serum sample were achieved with [Ch][Asc] as compared to [Ch][Gly], [Ch][Pyr] and [Ch][Qui], respectively. This best system allowed an enrichment of 58 % on the IgG purity when compared against the IgG present in rabbit serum. The enhanced purity of IgG in the IL-rich phase is a result of the migration of major contaminant protein (albumin) to the polymer-rich phase. Thus, and although further optimization studies are still required, the introduction of bio-based ILs in ABS can be foreseen as a promising alternative for the purification and recovery of high-cost IgG from real matrices.

As evident from previous results, bio-IL-based ABS not only allow the complete extraction of IgG in a single-step, but also enhance the purity of IgG extracted from a real and complex matrix. However, and taking into consideration the therapeutic, diagnostic and research applications of IgG²⁻⁶, it is important to guarantee the chemical and biological stability of the antibody after extraction and purification steps. Some aqueous solutions of ILs have been reported as adequate media for the dissolution and stabilization of proteins, such as cytochrome-c⁵⁰. In an additional

work, it was demonstrated that the native conformation of cytochrome-c is preserved in 50-70 wt% IL aqueous solutions⁵¹. Jha et al.⁵⁴, have proved that structure of globular proteins remains intact in presence of ammonium-based ILs. Dreyer and Kragl⁵⁵ have demonstrated that IL-based ABSs can be used to extract and stabilize enzymes. [Ch][Gly]-based ABS have been reported as an efficient extraction platform d able to maintain the structural stability of BSA⁴¹. Based on these works, it seems suitable that the bio-based ILs investigated herein can be used to purify and to maintain the structural integrity of proteins. Even so, no studies were found in the literature in what concerns the effect of the investigated bio-based ILs on the stability of proteins or antibodies.

Stability of IgG - Although SE-HPLC was used as the quantification technique, simultaneously, it can be used to address the conformational and structural stability of IgG, as typically carried out with other proteins⁵⁶. SE-HPLC chromatograms of the pure IgG in PBS buffer and those after the extraction step with each ABS are shown in Figure 3.2.3. For both standard IgG and IgG after extraction with bio-based ABS, with the exception of the system with [Ch][IA] where the complete precipitation of the protein was observed, a sharp peak at a retention time of ~15.6 min is noticed. Moreover, no other peaks at lower retention times were observed, being an indication on the absence aggregates, or at higher retention times, which are an indication of IgG degradation. The structural stability of IgG was also evaluated by FTIR spectroscopy and SDS-PAGE – results depicted in Figure 3.2.5. The secondary structure of IgG in an aqueous solution of PBS (10 mM, pH 7.4) was studied for comparative analyses (Figure 3.2.5 A). At its native state, IgG contains 64% of β -sheet, 3% of α -helix, 28% of β -turn and 5% of random coil⁵⁷. As shown in Figure 3.2.5 A, the amide I region in the FTIR spectra of pure IgG in PBS buffer absorbs in the region of 1600-1690 cm^{-1} , which corresponds to the β -sheet (~1635 cm^{-1}), random coil (~1645 cm^{-1}), α -helix (~1660 cm^{-1}) and β -turn (~1670 cm^{-1}). However, the amide I region of IgG in presence of [Ch][IA] deviates (Figure 3.2.5 B), meaning that all the random coil and α -helix structures were transformed into β -sheet, which facilitates the protein fibrillation and precipitation. These results are in full agreement with the respective SE-HPLC chromatograms and macroscopic identification of protein precipitation with this IL. On the other hand, in presence of [Ch][Gly] and [Ch][Asc] (Figures 3.2.5 C and 3.2.5 D) there are no major changes in the amide I region of IgG, which further corroborate the results gathered by SE-HPLC. Still, in presence of [Ch][Pyr] (Figure 3.2.5 E), a small structural deformation was recorded, although no precipitation was observed, which thus suggest the partial denaturation of the IgG structure.

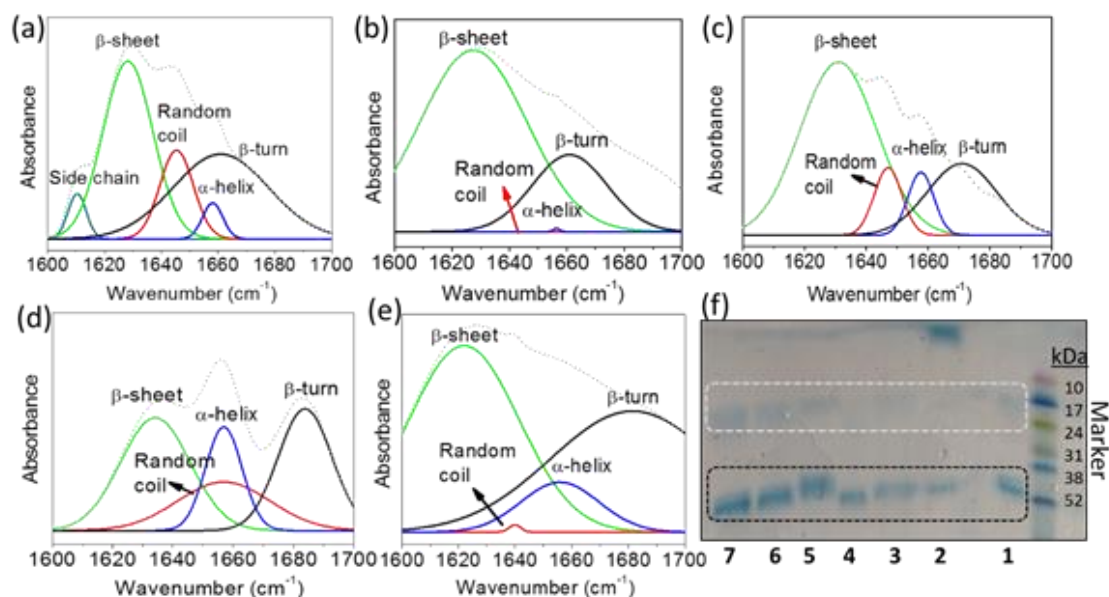


Figure 3.2.5 FTIR spectra of IgG in presence of **A** 10 mM PBS (pH 7.4), **B** 25 wt% [Ch][IA] + 30 wt% PPG 400 + H₂O, **C** 25 wt% [Ch][Gly] + 30 wt% PPG 400 + H₂O, **D** 25 wt% [Ch][Asc] + 30 wt% PPG 400 + H₂O and **E** 25 wt% [Ch][Pyr] + 30 wt% PPG 400 + H₂O. **F** SDS-PAGE of IgG at a 200 μ g/mL concentration *per* lane in: PBS buffer 10 mM, pH 7.4 (1), [Ch][IA] (2), [Ch][Gly] (3), [Ch][Pyr] (4), [Ch][Asc] (5), [Ch][Qui] (6) and [Ch][Gal] with 25 wt% of each IL.

SDS-PAGE analysis was also employed to cover the effect of bio-based ILs on IgG (Figure 3.2.5 F). In presence of PBS buffer (10 mM, pH 7.4,) as shown in Figure 3.2.5 F, lane 1, the two bands corresponding to the light chain and heavy chain of IgG, with a molecular weight \sim 20 kDa and \sim 50 kDa, respectively, are clearly identified. These two bands are also identified in presence of most of the bio-based ILs investigated, indicating therefore that there is no degradation of IgG, except in presence of [Ch][IA] (lane 2 of Figure 3.2.5 F). In summary, amongst all bio-based ILs studied, [Ch][IA] was the only one found to be unable to maintain the structural integrity of IgG and which reflects the 0% of recovery yield gathered during the extraction steps. Remarkably, all remaining bio-IL-based ABSs are suitable for the extraction/purification of IgG from complex serum samples, since they allow the complete extraction of IgG to the IL-rich phase in a single-step, a recovery yield of at least 85% and an enhancement in the purity level of *ca.* 58%, while maintaining the structural integrity of the antibody. Further investigations on the purification of IgG are ongoing, particularly on the optimization of mixture compositions and on the incorporation of these ABS in centrifugal partition chromatography to ascertain on their scale-up viability.

Conclusions

A new set of bio-based ILs, constituted by the cholinium cation and anions derived from plant natural acids, were synthesized and characterized. All bio-based ILs display melting temperatures below 100 °C, ranging from -20.5 to 52.4 °C, and high decomposition temperatures, at least up to 220 °C. All ILs are completely miscible with water, and out of ten, six are able to form ABS with PPG 400. The respective phase diagrams were determined to ascertain the mixture compositions required to form two-phase systems, and their extraction and purification performance for IgG was then evaluated. With pure IgG samples, and with the exception of the [Ch][IA]-based ABS, all remaining systems lead to a 100% extraction efficiency and 100% recovery yield of IgG into the IL-rich phase. These newly developed ABS proved to be better systems for the extraction of IgG when compared to ABS formed by more traditional cholinium-based ILs.

The most promising systems were thereafter applied to the extraction and purification of IgG from real rabbit serum samples. With real samples, the extraction efficiency of 100% of IgG in a single-step was achieved, although with a small compromise on the recovery yield (85%). Even so, and taking into consideration the current high cost of IgG at a high purity level, it was found that the best ABS leads to an enhancement of 58% in the IgG purity level (against its purity in the original serum sample).

Since IgG is currently used in therapeutic, diagnostic and research applications, it is crucial to guarantee its stability after purification. IgG was found to maintain its native structure in presence of most of the studied bio-based ILs, except for [Ch][IA]. This indicates that most of the synthesized bio-based ILs are protein-friendly and that their incorporation in ABS, given the obtained extraction efficiencies, recovery yields and purity levels, is a promising option for the recovery and purification of IgG from real matrices, while envisaging the widespread applicability of biopharmaceuticals at a lower cost.

References

1. M. M. Aragón, E. L. V. Goetheer and A. B. Haan, *Sep. Purif. Technol.*, 2009, 65, 73–78.
2. N. S. Lipman, L. R. Jackson, L. J. Trudel and F. Weis-Garcia, *ILAR J.*, 2005, 46, 258–268.
3. M. Leenaars and C. F. M. Hendriksen, *ILAR J.*, 2005, 46, 269–279.
4. A. Buchacher and G. Iberer, *Biotechnol. J.*, 2006, 1, 148–163.
5. A. Zhiqiang, *Trends in Bio/Pharma. Ind.*, 2008, 2, 24–29.
6. S. M. Andrew and J. A. Titus, *Current Protocols in Cell Biology*, John Wiley & Sons Inc., 2001.
7. M. Azevedo, P. A. Rosa, I. F. Ferreira and M. R. A. Barros, *J. Biotechnol.*, 2007, 132, 209–217.
8. D. Low, R. O’Leary and N. S. Pujar, *J. Chromatogr., B: Biomed. Appl.*, 2007, 848, 48–63.
9. P. Rosa, A. Azevedo, S. Sommerfeld, M. Mutter, M. A. Barros and W. Bäcker, *J. Biotechnol.*, 2009, 139, 306–313.
10. B. Weiner, M. SáRa, G. Dasgupta and U. B. Sleytr, *Biotechnol. Bioeng.*, 1994, 44, 55–65.
11. G. Corthier, E. Boschetti and J. Charley-Poulain, *J. Immunol. Methods*, 1984, 66, 75–79.
12. V. K. Ahluwalia, *Green chemistry: Environmentally benign reaction*, Taylor & Francis, 2010.
13. P. J. Dunn, *Chem. Soc. Rev.*, 2012, 41, 1452–1461.

14. R. R. G. Soares, A. M. Azevedo, J. M. V. Alstine and M. R. A. Barros, *Biotechnol. J.*, 2015, 10, 1158–1169.
15. J. A. Asenjo and B. A. Andrews, *J. Chromatogr., A*, 2011, 1218, 8826–8835.
16. M. V. Quental, M. Caban, M. M. Pereira, P. Stepnowski, J. A. P. Coutinho and M. G. Freire, *Biotechnol. J.*, 2015, 10, 1457–1466.
17. P.-Å. Albertsson, *Nature*, 1958, 182, 709–711.
18. M. G. Freire, A. F. Claudio, J. M. Araujo, J. A. Coutinho, I. M. Marrucho, J. N. Canongia Lopes and L. P. Rebelo, *Chem. Soc. Rev.*, 2012, 41, 4966–4995.
19. K. E. Gutowski, G. A. Broker, H. D. Willauer, J. G. Huddleston, R. P. Swatloski, J. D. Holbrey and R. D. Rogers, *J. Am. Chem. Soc.*, 2003, 125, 6632–6633.
20. J. F. B. Pereira, L. P. N. Rebelo, R. D. Rogers, J. A. P. Coutinho and M. G. Freire, *Phys. Chem. Chem. Phys.*, 2013, 15, 19580–19583.
21. M. Azevedo, P. A. J. Rosa, I. F. Ferreira, A. M. M. O. Pisco, J. de Vries, R. Korporaal, T. J. Visser and M. R. A. Barros, *Sep. Purif. Technol.*, 2009, 65, 31–39.
22. J. P. Hallett and T. Welton, *Chem. Rev.*, 2011, 111, 3508–3576.
23. N. Meine, F. Benedito and R. Rinaldi, *Green Chem.*, 2010, 12, 1711–1714.
24. S. Ahrens, A. Peritz and T. Strassner, *Angew. Chem. Int. Ed.*, 2009, 48, 7908–7910.
25. B. Jiang, Z. Feng, C. Liu, Y. Xu, D. Li and G. Ji, *J. Food Sci. Technol.*, 2015, 52, 2878–2885.
26. B. Erickson, J. E. Nelson and P. Winters, *Biotechnol. J.*, 2012, 7, 176–185.
27. H. Ohno and K. Fukumoto, *Acc. Chem. Res.*, 2007, 40, 1122–1129.
28. V. Kumara, C. Peib, C. E. Olsenc, S. J. C. Schäfferd, V. S. Parmarb and S. V. Malhotra, *Tetrahedron: Asymmetry*, 2008, 19, 664–671.
29. T. E. Sintra, A. Luís, S. N. Rocha, A. I. M. C. L. Ferreira, F. Gonçalves, L. M. N. B. F. Santos, B. M. Neves, M. G. Freire, S. P. M. Ventura and J. A. P. Coutinho, *ACS Sustai. Chem. Eng.*, 2015, 3, 2558–2565.
30. K. Kundu, B. K. Paul, S. Bardhan and S. K. Saha, in *Ionic Liquid-Based Surfactant Science: Formulation, Characterization, and Applications*, John Wiley & Sons Inc., 2015.
31. R. Hajipour and F. Rafiee, *Org. Prep. Proced. Int.*, 2015, 47, 249–308.
32. Y. Fukaya, Y. Iizuka, K. Sekikawa and H. Ohno, *Green Chem.*, 2007, 9, 1155–1157.
33. M. Sharma, D. Mondal, N. Singh, N. Trivedi, J. Bhatt and K. Prasad, *RSC Adv.*, 2015, 5, 40546–40551.
34. R. R. Mazid, U. Divisekera, W. Yang, V. Ranganathan, D. R. MacFarlane, C. Cortez-Jugo and W. Cheng, *Chem. Commun.*, 2014, 50, 13457–13460.
35. R. Patel, M. Kumari and A. B. Khan, *Appl. Biochem. Biotechnol.*, 2014, 172, 3701–3720.
36. M. Sharma, J. P. Chaudhary, D. Mondal, R. Meena and K. Prasad, *Green Chem.*, 2015, 17, 2867–2873.
37. R. J. West, J. W. Davis, L. H. Pottenger, M. I. Banton and C. Graham, *Environ. Toxicol. Chem.*, 2007, 26, 862–871.
38. M. R. Almeida, H. Passos, M. M. Pereira, Á. S. Lima, J. A. P. Coutinho and M. G. Freire, *Sep. Purif. Technol.*, 2014, 128, 1–10.
39. J. C. Merchuk, B. A. Andrews and J. A. Asenjo, *J. Chromatogr., B: Biomed. Appl.*, 1998, 711, 285–293.
40. M. M. Pereira, R. A. P. Cruz, M. R. Almeida, A. S. Lima, J. A. P. Coutinho and M. G. Freire, *Process Biochem.*, 2016, 51, 781–791.
41. M. V. Quental, M. Caban, M. M. Pereira, P. Stepnowski, J. A. P. Coutinho and M. G. Freire, *Biotechnol. J.*, 2015, 10, 1457–1466.
42. N. V. Plechkova and K. R. Seddon, *Chem. Soc. Rev.*, 2008, 37, 123–150.
43. ChemSpider – The free chemical database, <http://www.chemspider.com>.
44. M. G. Freire, J. F. B. Pereira, M. Francisco, H. Rodriguez, L. P. N. Rebelo, R. D. Rogers and J. A. P. Coutinho, *Chem. – Eur. J.*, 2012, 18, 1831–1839.
45. M. S. S. Neves, S. Shahriari, J. Lemus, J. F. B. Pereira, M. G. Freire and João A. P. Coutinho, *Phys. Chem. Chem. Phys.*, 2016, 18, 20571–20582.
46. H. Wu, S. Yao, G. Qian, T. Yao and H. Song, *J. Chromatogr. A*, 2015, 1418, 150–157.
47. M. Azevedo, P. A. J. Rosa, I. F. Ferreira and M. R. A. Barros, *J. Biotechnol.*, 2007, 132, 209–217.
48. Q. Wu, D. Q. Lin and S. J. Yao, *J. Chromatogr., B: Biomed. Appl.*, 2013, 928, 106–112.
49. M. F. Silva, A. F. Platzgummer, M. R. A. Barros and A. M. Azevedo, *Sep. Purif. Technol.*, 2014, 132, 330–335.
50. V. L. Dhadge, S. A. Rosa, A. Azevedo, R. A. Barros and A. C. Roque, *J. Chromatogr., A*, 2014, 1339, 59–64.
51. P. R. Levison, M. L. Koscielny and E. T. Butts, *Bioseparation*, 1990, 1, 59–67.
52. Y. Kohno, S. Saita, K. Murata, N. Nakamura and H. Ohno, *Polym. Chem.*, 2011, 2, 862–867.
53. W. Wei and N. D. Danielson, *Biomacromolecules*, 2011, 12, 290–297.
54. Jha and P. Venkatesu, *Phys. Chem. Chem. Phys.*, 2015, 17, 20466–20484.
55. S. Dreyer and U. Kragl, *Biotechnol. Bioeng.*, 2008, 99, 1416–1424.
56. P. Hong, S. Koza and E. S. P. Bouvier, *J. Liq. Chromatogr. Relat. Technol.*, 2012, 35, 2923–2950.
57. S. Wi, P. Pancoska and T. A. Keiderling, *Biospectroscopy*, 1998, 4, 93–106.

4. Preservation and separation of nucleic acids using IL aqueous solutions and ABS

4.1. Aqueous solutions of cholinium-based Good's buffers as preservation media for recombinant small RNAs

Based on the published manuscript: ⁵ Augusto Q. Pedro, Patrícia Pereira, M. V. Quental, André P. Carvalho, Sérgio M. Santos, João A. Queiroz, Fani Sousa. *ACS Sustainable Chem. Eng.*, 2018, 612, 16645-16656.

Abstract

RNA is a biopolymer of high relevance in the biopharmaceuticals field and in fundamental and applied research; however, the preservation of the RNA stability is still a remarkable challenge. Herein, we demonstrate the enhanced potential of aqueous solutions of self-buffering cholinium-based Good's buffers ionic liquids (GB-ILs), at 20 and 50 wt%, as alternative preservation media of recombinant small RNAs. The thermal stability of RNA is highly enhanced by GB-ILs, with an increase of 14 °C in the biopolymer melting temperature - the highest increase observed up to date with ILs. Most GB-ILs investigated improve the stability of RNA at least up to 30-days, both at 25 °C and at 4 °C, without requiring the typical samples freezing. Molecular dynamics simulations were applied to better understand the molecular-level mechanisms responsible for the observed RNA improved stability. The number of IL cations surrounding the RNA chain is similar, yet with differences found for the IL anions, which are responsible for the overall charge of the biopolymer first solvation sphere. No cytotoxicity of the studied solutions containing RNA and ILs at 20 wt% was observed onto two distinct human cell lines, reinforcing their potential to act as preservation media when foreseeing biopharmaceutical applications. Finally, RNA was successfully recovered from the ILs aqueous solutions, without changes in its structural integrity, and the ILs successfully recycled.

Introduction

For a long time, RNA has been considered a biopolymer of high interest, regarded as an intermediate between DNA and proteins. However, the milestones discoveries of catalytic RNAs in the early 80's and RNA interference (RNAi) in the late 90's changed the RNA landscape to a dynamic and versatile biopolymer that regulates many functions related with gene expression and cellular mechanisms¹. The RNAi technology² involves some small RNAs – microRNAs (miRNAs) and small interfering RNAs (siRNAs) - that act as regulators of the messenger RNA (mRNA) expression. This fact led to the development of novel therapeutic strategies based on

⁵Contributions: F.S., J. A. Q. and M.G.F. conceived and directed this work. M.V.Q., A.Q.P. and P.P. acquired the experimental data. A.P.C and S.M.S. performed the molecular dynamic simulations. All authors interpreted the obtained experimental data. The manuscript was mainly written by A.Q.P., P.P., M.V.Q. and M.G.F. with contributions from the remaining authors.

RNA, where siRNAs and miRNAs have shown promising outcomes in clinical trials, streamline drug discovery and development beyond protein therapeutics^{3,4}. However, the understanding of the biological role of RNAs or their use as biotherapeutic agents require pure and intact RNA with adequate integrity, stability and biological activity⁵. It is known that the stability of nucleic acids depends on a balance of features, such as base pairing, electrostatic interactions, and hydration capacity, with impact on their structure and function, in which the decrease of their lifetime occurs by the bases hydrolysis (deamination, depurination)⁶⁻⁹. The RNA required for most biomolecular applications may be obtained by *in vitro* transcription and chemical synthesis¹⁰. Still, natural RNAs obtained by *in vivo* procedures are better in retaining their structure and function, and have improved safety characteristics. Therefore, their recombinant production using bacterial-adapted cells has been a hot topic of research¹⁰. Regardless of the approach used to produce RNA, the final product has always to be purified, mainly to remove contaminants (plasmid DNA template, enzymes, free nucleotides, salts or buffers, chemicals, genomic DNA or proteins)¹⁰⁻¹², which is traditionally achieved using highly selective chromatographic techniques¹³. Nevertheless, the peculiar three-dimensional compaction and structural instability of RNA are still crucial challenges, as the biological activity and integrity are easily compromised during the extraction and purification procedures⁵. To overcome this drawback, general approaches to work with RNA, mostly focusing on the inactivation of ribonucleases, have been reported^{5,12}. In addition to the purification and recovery steps, the RNA short-term storage is usually accomplished using high purity water or sterile phosphate buffered saline (PBS) solutions at temperatures below 4 °C, while lyophilization and temperatures below -80 °C are required for the long-term storage of RNA¹⁴; at this temperature, RNA is stable when stored as an ethanol precipitate¹⁵. Prior to any application, RNA may be dissolved in aqueous solutions of buffers, either sterile water or modified Tris buffer (10 mM Tris, 0.1 mM EDTA, overall pH 7.5)¹⁵. Highly purified 100% formamide may also be used for RNA long-term storage¹⁶, although it limits the subsequent applications of this biopolymer. In general, divalent cations such as Mg²⁺, monovalent cations (*e.g.* K⁺, Na⁺), and polycationic amines (polyamines such as spermidine) increase the RNA stability by shielding negative phosphates in the backbone and coordinating 2' hydroxy groups¹⁷. Alternative strategies focused on enhancing the RNA stability comprise chemical modifications¹⁸, and the application of the tRNA scaffold approach for bacterial RNA constructs¹⁹. Based on the exposed, it is of paramount relevance to develop simple and sustainable strategies and protocols to maintain or increase the RNA stability and biological activity during the manufacturing and storage steps, ideally using less extreme temperatures and more benign solvents, and for which aqueous solutions of ionic liquids (ILs) may be considered as potential solvents for both the RNA

purification and preservation steps. ILs, commonly described as molten salts at temperatures below 100 °C, and composed of large and unsymmetrical organic cations and organic or inorganic anions, have been reported as appropriate stabilizing media for proteins and enzymes²⁰⁻²². During the last years, ILs have also been applied to improve some properties of nucleic acids, mainly of DNA, such as solubility, stability and bioavailability²³⁻²⁹. Despite its high importance, few reports dealing with ILs and RNA are available^{14,23}. In these works, cholinium dihydrogen phosphate and cholinium chloride were investigated. However, it is known that the stability, structure and functionality of RNA depend on the concentration and chemical identity of the ions in solution⁷, justifying a more intensive search on adequate IL ions, which is even of higher relevance given the ILs designer ability. Recently, we proposed a novel class of self-buffering imidazolium- and tetraalkylammonium-based ILs containing anions derived from biological buffers (Good's buffers) – GB-ILs³⁰. These ILs display high stabilizing effects over proteins and allow their complete extraction from aqueous media when used as phase-forming components of liquid-liquid systems³¹. Cholinium chloride is a water-soluble nutrient, and appropriate cholinium-based ILs usually present high biodegradability, low toxicity, and are able to maintain the structure and function of proteins and/or other labile biomolecules³¹. Based on the exposed and considering that nucleic acids are not stable in extreme ranges of pH values¹², aqueous solutions of GB-ILs comprising the cholinium cation seem thus to be an attractive and biocompatible milieu to maintain the integrity and improve the stability of RNA. Furthermore, the use of self-buffering ILs can avoid the need of adding an additional buffer. Accordingly, in this work, we synthesized several cholinium-based GB-ILs and evaluated their performance to stabilize a recombinant *Escherichia coli* small RNAs fraction (sRNAs) containing a microRNA precursor (pre-miR-29). The integrity, structural stability, cytotoxicity, and superficial charge of RNA in aqueous solutions comprising 20 and 50 wt% of each IL were evaluated, as well as the medium-term storage stability of RNA in these aqueous solutions. Zeta potential measurements and molecular dynamics simulations were used to appraise the ILs effects on the RNA stability. Finally, it was demonstrated that the dissolved RNA can be successfully recovered from the aqueous solutions of ILs, further allowing the IL recycling.

Experimental Procedure

Materials - Cholinium hydroxide solution (46%, wt in methanol), 2-(N-morpholino)ethanesulfonic acid (MES, purity > 99 wt%, 2-[(2-hydroxy-1,1-bis(hydroxymethyl)ethyl)amino]ethane sulfonic acid (TES, purity > 99 wt%, 2-[4-(2-hydroxyethyl)piperazin-1-yl]ethanesulfonic acid (HEPES, purity > 99.5 wt%, and N-

[tris(hydroxymethyl)methyl]glycine (TRICINE, purity >99 wt% were supplied by Sigma-Aldrich. Sodium hydroxide was purchased from Eka Chemicals. Methanol (HPLC grade, purity > 99.9 wt%) was supplied from Fisher Scientific, and acetonitrile (purity > 99.7%) was from LabScan. Hyper Ladder I (Bioline) was used as DNA molecular weight marker. All materials used in the experimental assays were RNase-free. Ultrapure reagent-grade water (Mili-Q system, Milipore/Waters) was treated with 0.05% diethyl pyrocarbonate (DEPC, Sigma-Aldrich).

ILs synthesis - GB-ILs were synthesized through the neutralization of cholinium hydroxide with Good's buffers, as described elsewhere³¹. The following ILs have been synthesized: cholinium 2-[4-(2-hydroxyethyl)piperazin-1-yl]ethanesulfonate ([Ch][HEPES]), cholinium 2-(N-morpholino)ethanesulfonate ([Ch][MES]), cholinium N-[tris(hydroxymethyl)methyl]glycinate ([Ch][TRICINE]), and cholinium 2-[(2-hydroxy-1,1-bis(hydroxymethyl)ethyl)amino]ethanesulfonate ([Ch][TES]). Briefly, a slight excess of equimolar buffer aqueous solution was added dropwise to the cholinium hydroxide solution. The mixture was stirred continuously for at least 12 h at ambient conditions. The mixture was then evaporated at 60 °C under reduced pressure, yielding viscous liquids. A mixture of acetonitrile and methanol (1:1, v/v) was added and then vigorously stirred at room temperature for 1 h to precipitate any excess of buffer. The solutions were filtrated to remove the precipitated solids, and further dried under vacuum (10 Pa) at room temperature. The chemical structure of each GB-IL was confirmed by ¹H and ¹³C NMR spectroscopy, showing to be > 98 wt% pure. Cholinium dihydrogen phosphate ([Ch][DHP]) acquired from Iolitec was also evaluated, as well as buffered cholinium dihydrogen phosphate (Buff[Ch][DHP]), which was obtained by adjusting the pH of [Ch][DHP] to 7.0 with cholinium hydroxide.

Small RNA biosynthesis and small RNA isolation - A cell culture of *Escherichia coli* (*E. coli*) DH5 α strain modified with plasmid pBHSR1-RM containing the sequence of human pre-miR-29b was used for the sRNA production, namely transfer RNA (tRNA), pre-miR-29b and 6S RNA. Growth was carried out in shake-flasks of 1 L, containing 250 mL of Terrific Broth medium (12 g/L Tryptone, 24 g/L Yeast extract, 4 ml/L glycerol, 0.017 M KH₂PO₄ and 0.072 M K₂HPO₄) supplemented with 30 μ g/mL of kanamycin, in a rotary shaker at 37 °C and 250 rpm. Cell growth was evaluated by optical density of the culture medium, carried out at a wavelength of 600 nm. The cultivated cells of *E. coli* DH5 α were then recovered by centrifugation at 4500 g for 20 min at 4 °C, and the pellets stored at -20 °C.

The isolation of sRNA was carried out according to the acid guanidinium thiocyanate-phenol-chloroform extraction method described by Chomczynski and co-workers³², with some

modifications. Bacterial pellets were resuspended in 5 mL of denaturing cell lysis solutions (4 M guanidinium thiocyanate; 25 mM sodium citrate, pH 4.0; 0.5% (w/v) N-lauroylsarcosine and 0.1 M β -mercaptoethanol to perform the lysis. After incubating on ice for 10 min, cellular debris, genomic DNA and proteins were precipitated by gently adding and mixing 5 mL of water-saturated phenol and 0.5 mL of 2 M sodium acetate (pH 4.0). The sRNA isolation was achieved by adding 1 mL of chloroform/isoamyl alcohol (49:1, v:v), and by vigorously mixing until two immiscible phases were obtained. The upper aqueous phase, which contains mostly RNA, was recovered and concentrated by the addition of 5 mL of ice-cold isopropanol. Precipitated molecules were recovered by centrifugation at 10,000 g for 20 min at 4 °C, and resuspended in 1.5 mL. sRNA molecules were concentrated again with 1.5 mL of ice-cold isopropanol. After centrifugation for 10 min, at 10,000 g (4 °C), the RNA pellet was washed with 7.5 mL of 75% ethanol and incubated at room temperature for 10 min, followed by a 5 min centrifugation at 10,000 g (4 °C). The air-dried RNA pellet was solubilized in 1 mL of 0.05% DEPC-treated water. Finally, 260 and 280 nm absorbance of the samples was measured using a Nanodrop spectrophotometer to assess the RNA quantity, and an agarose gel electrophoresis was performed to assess the RNA purity.

ILs aqueous solutions as preservation media of RNA - The sRNA samples were dissolved in aqueous solutions of the different ILs, at 20 and 50 wt% (ILs structures are displayed in Figure C.1.1 at Appendix C1). The mixtures were incubated for different periods, namely 1 h, and 15 and 30 days at room temperature (25 ± 1) °C and at 4 °C. After the incubation period, RNA was precipitated by adding 2 volumes of pure ethanol, incubated for 2 h at -80 °C, and recovered by centrifugation at 15,000 g for 30 min at 4 °C. Finally, the nucleic acids pellets were air-dried for 10 min at room temperature and solubilized in 0.05% DEPC-treated water.

Electrophoretic analysis - The integrity and identification of sRNAs recovered after incubation with ILs for 1 h at 4 °C were evaluated using denaturing urea polyacrylamide gel electrophoresis and agarose gel electrophoresis. 20 μ L of sRNA corresponding to 48 μ g was analyzed by horizontal electrophoresis using 0.8% of agarose gel (Hoefer). Agarose electrophoresis was carried out at 110 V, for 30 min, with TAE buffer (40 mM Tris base, 20 mM acetic acid and 1 mM EDTA, pH 8.0). 10 μ L corresponding to 24 μ g of sRNA was also analyzed by vertical electrophoresis using an Amersham Biosciences system (GE Healthcare) with 10% polyacrylamide gel. Polyacrylamide electrophoresis was carried out at 125 V for 90 min with TBE buffer (0.84 M Tris base, 0.89 M boric acid and 0.01 M EDTA, pH 8.3). sRNA samples were previously denatured with 97.5% formamide, and denatured conditions were kept in the gel

owing to the presence of 8 M urea. In both electrophoresis, the bands corresponding to sRNA molecules were visualized in the gel using the UVIttec FireReader system (UVIttec) after staining with 0.01% GreenSafe Premium from NZYtech.

Molecular Dynamics Simulations - All molecular dynamics simulations were performed with GROMACS 2016.³³ Parameters for RNA were taken from the Amber99SB forcefield³⁴ and partial charges for [DHP]⁻ and [MES]⁻ were calculated by the Restrained Electrostatic Potential (RESP) method²⁹, using optimized geometries at the B3LYP/6-31G* level, using Gaussian-09³⁶; remaining parameters were taken from the GAFF GAFF (General Amber Force Field forcefield³⁷; description of [Ch]⁺ was made according to Gontrani et al.³⁸. Simulations started with the insertion of a linear single random RNA chain (AGCGAACGCAUCUCGAGUUC) into a box of water containing *ca.* 430 [Ch][DHP] or [Ch][MES] pairs and 18k water molecules, leading to a final IL concentration of 20 wt%, in simulation boxes with volumes *ca.* 85x85x85 Å³. The overall negative charge of the simulation box was neutralized upon addition of 19 Na⁺ cations. Prior to all MD simulations, the overall configurations were geometry optimized to remove bad contacts using a combination of steepest-descent and conjugate-gradient minimizers. A short 1 ns equilibration in the NVT ensemble at 300K, followed by 1 ns of NPT equilibration at 1 atm, were used to ensure proper temperature and pressure equilibration, respectively. Both thermodynamic quantities remained stable at the reference value during the last 500 ps of the equilibration stages. Finally, 20 ns NPT production runs were obtained. Simulations used a 12 Å nonbonded cutoff with long range electrostatic interactions calculated using the PME method; the integration timestep was 2 fs; hydrogen involving bonds were constrained using LINCS; temperature was controlled using the v-rescale and Berendsen thermostats in the equilibration and production stages, respectively; pressure was controlled with the isotropic Berendsen barostat.

Circular Dichroism (CD) spectroscopy - CD experiments were performed in a Jasco J-815 spectropolarimeter (Jasco), using a Peltier-type temperature control system (model CDF-426S/15). CD spectra were acquired at a constant temperature of 25 °C using a scanning speed of 10 nm/min, with a response time of 1 s over wavelengths ranging from 210 to 320 nm. The recording bandwidth was of 1 nm with a step size of 1 nm using a quartz cell with an optical path length of 1 mm. Three scans were averaged per spectrum to improve the signal to-noise ratio and the spectra were smoothed by using the noise-reducing option in the operating software. CD melting experiments were performed in the temperature range from 10 to 110 °C, with a heating rate of 1 °C/min, by monitoring the ellipticity at 265 nm. Data were converted into fraction folded (Θ) plots using the following equation:

$$\theta = \frac{CD_{\lambda} - CD_{\lambda}^{\min}}{CD_{\lambda}^{\max} - CD_{\lambda}^{\min}} \quad (\text{Equation 1})$$

where CD is the ellipticity of the monitored wavelength at each temperature, and CD^{\min} and CD^{\max} are the lowest and highest ellipticity, respectively. Data points were then fitted to a Boltzmann distribution (OriginPro 2015) and the melting temperatures (T_m) determined from the two-state transition model used, using the first derivative method. Total RNA concentration was 150 $\mu\text{g/mL}$, and distinct incubation periods and temperatures of sRNA with ILs were performed.

Zeta potential - The zeta potential of RNA samples, with and without ILs, were determined by dynamic light scattering (DLS) using a Zetasizer Nano ZS particle analyzer (Malvern Instruments, Worcestershire, UK), equipped with a He-Ne laser, at 25 °C. Zeta potential measurements were performed in disposable capillary cells and computed using the Henry's [F(Ka) 1.5] and Smoluchowsky models. All data were treated with the Zetasizer software v7.03. Experiments were performed in triplicate and an average of 30 measurements was acquired for each sample. The sRNA was incubated with ILs during 1 h at 4 °C, and the total RNA concentration was 200 $\mu\text{g/mL}$. Values given represent the average of three independent samples (average \pm SD, $n = 3$).

Cell viability - The cellular viability of the different IL-RNA formulations was assessed by the MTS assay using the Cell Titer 96® Aqueous Non-Radioactive Cell Proliferation Assay from Promega, according to the manufacturer's instructions. Human fibroblasts and cervical cancer cells (HeLa) were cultured at 37 °C, in a humidified atmosphere containing 5 % CO_2 . Three passages of each cell line were seeded at a density of 1×10^4 cells per mL in a 96-well plate; after 24 h, the cell culture medium was replaced by serum-free culture medium. After 12 h, 10 μL of a mixture containing 200 $\mu\text{g/mL}$ sRNA and 20 wt% or 50 wt% IL was used to transfect each well, corresponding to a final concentration of 20 $\mu\text{g/mL}$ sRNA and 2 wt% or 5 wt%. Transfection was carried out for 24 h, and subsequently the culture medium was exchanged by fresh medium and a mixture of MTS/phenazine metasulfate (PMS) was added to each well, and cells were incubated for 2 h at 37 °C in a humidified atmosphere containing 5 % CO_2 , protected from light. Following incubation, absorbance measurements of the soluble brown formazan produced by MTS were performed in a microplate reader purchase from Bio-Rad, at 490 nm. Moreover, cells incubated with absolute ethanol were used as positive control for cytotoxicity, while untreated

cells were used as negative control. The values given correspond to the average percentage values relative to the untreated cells and standard error in 3 independent experiments (ANOVA, mean \pm SD).

Results and Discussion

The milestone discoveries related with catalytic RNAs and RNA interference mechanism¹ changed the RNA landscape to a versatile biopolymer, leading to the development of novel RNA-based therapeutics, and to their widespread use in fundamental and applied research. However, and in contrast with DNA, the higher flexibility and folding heterogeneity of RNAs, coupled with their increased susceptibility to degradation by naturally occurring nucleases¹¹, demand for improved protocols for their manipulation and adequate formulations for their storage. ILs have been described as biocompatible media, being able to enhance the stability of DNA, proteins and siRNA³⁹; however, limited attention has been given to RNA^{14,23}, which may be due to its poor stability and inherent complex manipulation. Hitherto, the majority of the published works dealing with nucleic acids have focused on cholinium dihydrogen phosphate¹⁴ and cholinium chloride²³ and, to the best of our knowledge, no studies were reported concerning the stability of recombinant sRNA fractions in aqueous solutions of ILs, nor the effect of the IL anion was ascertained with the same RNA type.

Small RNAs integrity and structure in aqueous solutions of ILs - The sRNA fraction profile obtained from *E. coli* DH5 α by the phenol-chloroform method includes a well-defined band with a low molecular weight visualized by agarose electrophoresis (*cf.* the Appendix C1, Figure C.1.2). Furthermore, the increased resolution offered by polyacrylamide electrophoresis allows the identification of three bands corresponding to three classes of RNAs, namely 6S RNA, pre-miR-29 and tRNA, in a decreasing order of molecular weight (Figure 4.1.1).

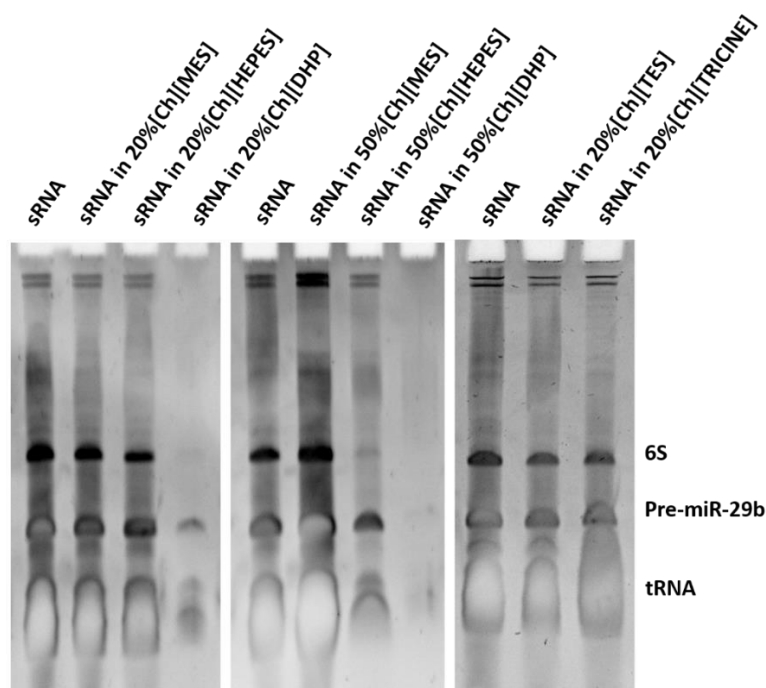


Figure 4.1.1 Polyacrylamide gel electrophoresis of sRNA in the presence of aqueous solutions of 20 and 50 wt% of the following ILs: [Ch][DHP], [Ch][MES], [Ch][HEPES], [Ch][TES], and [Ch][TRICINE]. RNA control samples without ILs are also included.

Several cholinium-based GB-ILs were synthesized, by neutralization of cholinium hydroxide with Good's buffers (MES, TES, HEPES and TRICINE). Aqueous solutions of these ILs and of non- and buffered cholinium dihydrogen phosphate, at 20 and 50 wt%, were then used to appraise their potential as preserving media of RNA. To this end, the sRNA fraction was mixed with the several aqueous solutions of ILs, incubated for 1 h at room temperature ($25 \pm 1^\circ\text{C}$), and further characterized in terms of integrity, structural stability, and charge.

To avoid interferences of ILs in the electrophoretic runs, RNA was precipitated from the ILs aqueous solutions and further solubilized in DEPC (diethyl pyrocarbonate)-treated water. The results obtained are depicted in Figure C.1.2 in Appendix C1. The agarose gel electrophoresis results reveal that for the lowest concentration of IL (20 wt%), the structural integrity of RNA is maintained in all investigated ILs, with the exception of the non-buffered [Ch][DHP]. Although no RNA was observed in agarose electrophoresis with [Ch][DHP], the higher detection limit of polyacrylamide electrophoresis allowed to confirm the presence of RNA and to demonstrate that the biopolymer suffers degradation when incubated with this IL, as shown in Figure 4.1.1. On the other hand, for higher concentrations of ILs (50 wt%), different trends were observed. The structural integrity of RNA is maintained with [Ch][MES], but highly impaired in presence of non-buffered [Ch][DHP]. In this set of results, the pH values of the respective aqueous solutions

play a significant role. According to the data shown in Table C.1.1 in the Appendix C1, aqueous solutions of the non-buffered [Ch][DHP] are acidic (pH ranging between 3.54 and 4.17) whereas the pH values of aqueous solutions of GB-ILs range between 8.62 and 12.38, demonstrating that alkaline solutions are beneficial to maintain the RNA integrity.

In particular, [Ch][HEPES] selectively stabilizes pre-miR-29 over the other host RNAs - Figure 4.1.1. This behavior may be due to the stem-loop structure of pre-miR-29¹¹, contrasting with the linear structure of other host RNAs. These hairpin loops represent short secondary structural folds, which are formed in single-stranded nucleic acids and consist of a base-paired stem and a loop sequence with unpaired nucleotide bases⁴⁰. Hydrogen-bonding is relevant in base pairing, while base stacking between adjacent bases through van der Waals interactions may contribute to the stabilization of RNA structural motifs. Amongst the diverse ILs anions investigated, [HEPES]⁻ has been described as the most polar anion according to their dipole moment values³¹, which can further justify its higher polarity and ability to establish hydrogen bonds with the RNA nitrogen bases and that may be responsible for the enhanced stabilization of stem-loop RNAs. At higher IL concentrations we were unable to efficiently remove [Ch][TES] and [Ch][TRICINE] and their analysis by electrophoresis could not be performed correctly. Even so, the best results in terms of RNA integrity were obtained with aqueous solutions of cholinium-based GB-ILs at 20 wt%.

To address the sRNA structural stability, CD spectra were recorded for all mixtures of sRNA and aqueous solutions of ILs - shown in Figure 4.1.2 and Figure C.1.3 in the Appendix C1.

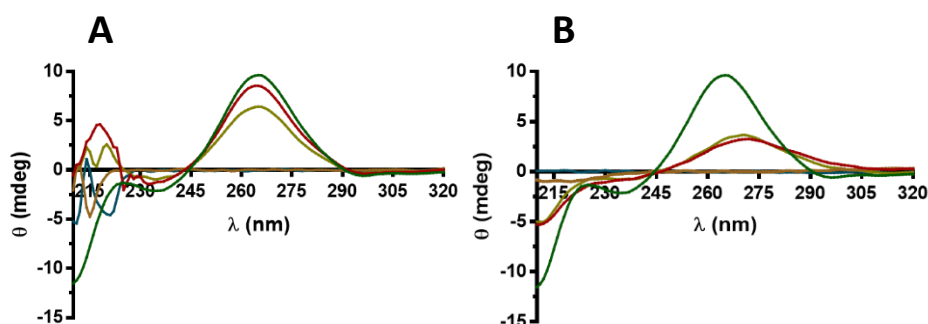


Figure 4.1.2 CD spectra (200 – 320 nm) of sRNA in the absence and presence of ILs: (A) 20 and 50 wt% of [Ch][MES]; (B) 20 and 50 wt% of [Ch][DHP]. For each set, the dark green line represents RNA, the red line corresponds to RNA in 20 wt% IL, the brown line to 20 wt% IL, the light green line to RNA in 50 wt% IL, and the blue line to 50 wt% IL. sRNA was incubated for 1 h at 4 °C.

The typical CD spectrum of the studied sRNA sample (dark green line) comprises two major peaks of ellipticity: a maximum at 265 nm (positive band) and a minimum at 215 nm (negative band). From the analysis of the CD spectra of all aqueous solutions and sRNA, it is clear that ILs

largely interfere with the CD signal below 230 nm. However, through the analysis of the CD spectra of sRNA-IL at 20 wt% (red line in Figure 4.1.2 and Figure C.1.3 in the Appendix C1) and 50 wt% (light green line in Figure 4.1.2 and Figure C.1.3 in the Appendix C1) for wavelengths above 230 nm, it is possible to conclude that there is a shift in the maximum ellipticity with [Ch][DHP], at both IL concentrations, indicating that this IL causes the destabilization of the RNA structure. On the other hand, the structure of sRNA is maintained in all GB-ILs investigated, thus reinforcing their ability to stabilize RNAs. As discussed above, and at least for an incubation period of 1h, the pH value of the aqueous solutions plays a significant role over the RNA stability. Specifically, and as shown in Table C.1.2 (Appendix C1), the pH of 20 and 50 wt% aqueous solutions of unbuffered [Ch][DHP] is highly acidic (below 4). As RNA tends to hydrolyse at room temperature and at pH values below 5¹², we further explored if the adjustment of the pH of the [Ch][DHP] aqueous solution with cholinium hydroxide up to 7 – Buff[Ch][DHP] – would enhance the stability of RNA. Cholinium hydroxide was added to [Ch][DHP] up to pH 7 and was chosen to maintain the same species in solution. As shown in Figure C.1.3 in the Appendix C1, the sRNA structure is also maintained with 20 and 50 wt% of Buff[Ch][DHP]. Although no results were yet reported on a recombinant sRNA fraction and ILs. Mazid et al.¹⁴ previously studied the influence of aqueous solutions of buffered [Ch][DHP] on a siRNA sample. Buffered [Ch][DHP] was indeed identified as an efficient stabilizer of a double-stranded RNA¹⁴, and it is here additionally proved that this buffered IL is also able to stabilize *E. coli* sRNAs. In general, and at least for an incubation period of 1h, the RNA stability in the selected ILs strongly depends on the pH and is enhanced at neutral to alkaline pH values.

Thermal denaturation experiments were performed to infer the stability of the secondary structure of RNA in the presence/absence of ILs, assessed by the RNA melting temperature (T_m). The CD T_m was determined at 265 nm since ILs do not interfere with the RNA ellipticity at this wavelength. According to Figure 4.1.3, the melting temperature of RNA dissolved in high-purity water is 43.7 °C. Nevertheless, a remarkable enhancement in the T_m of sRNA was observed in presence of GB-ILs. For the lowest concentration of IL (20 wt%), [Ch][MES], [Ch][TES], [Ch][HEPES], [Ch][TRICINE], and Buff[Ch][DHP] lead to an increase of *ca.* 14 °C in the sRNA T_m , indicating that it is significantly more stable in aqueous solutions of appropriate ILs than in high-purity water. The same protection effect was observed with 50 wt% of GB-ILs, increasing the sRNA T_m values up to 58.1, 57.8 and 59.3 °C for [Ch][MES], [Ch][HEPES] and [Ch][TES], respectively. In general, and taking into account the associated standard deviations, no significant differences are observed between the GB-ILs comprising the [MES]⁻, [TES]⁻, and [HEPES]⁻ anions. The T_m obtained with [Ch][TRICINE] is lower for both concentrations of IL, and for 50 wt% it leads to a decrease of 11.5 °C when compared with the RNA in high-purity water,

indicating that RNA samples are not stable in high amounts of this particular IL. This result is in accordance with the electrophoresis data, where the RNA integrity is compromised in presence of [Ch][TRICINE] at higher concentrations (Figure 4.1.1). With the exception of [TRICINE]⁻ that contains a terminal carboxylic group, all the remaining GB-ILs present a negatively charged sulphonate group which seems to be of high relevance to improve the RNA stability. For [Ch][DHP], at 20 and 50 wt%, a sRNA T_m similar to sRNA in high-purity water was obtained (44.1 and 46.5 °C, respectively), being this a main effect of the acidic pH afforded by non-buffered [Ch][DHP] aqueous solutions. These results correlate with those obtained from the CD spectra, where the RNA destabilization was identified in non-buffered [Ch][DHP] (Figure 4.1.3).

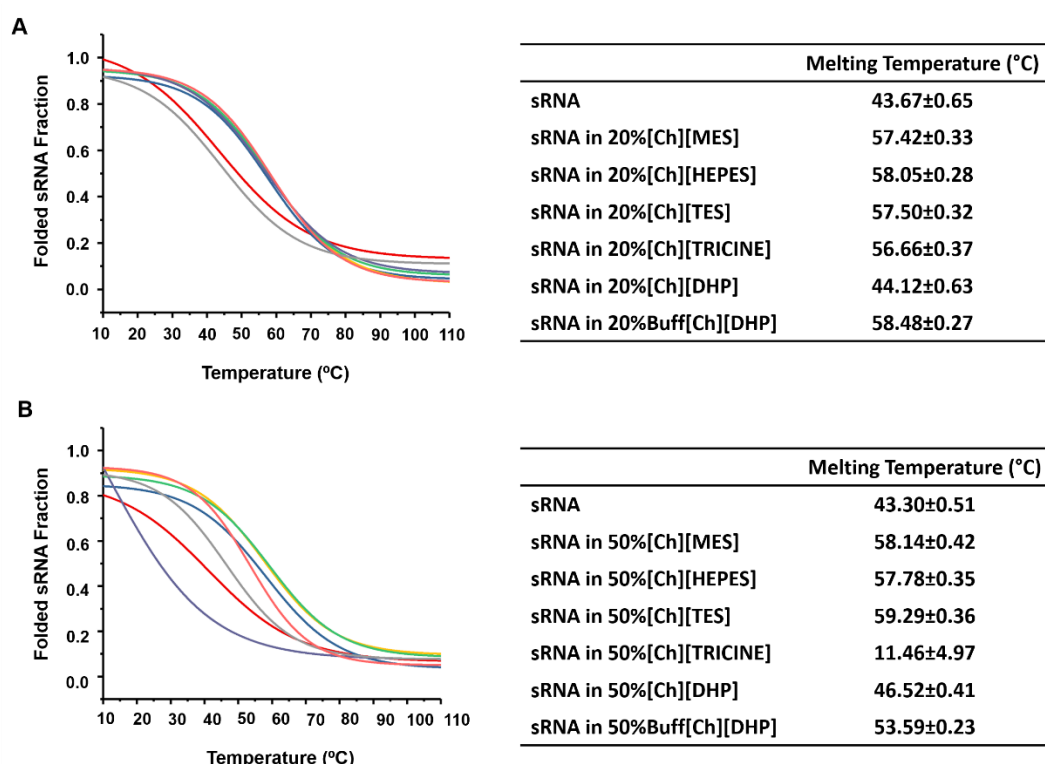


Figure 4.1.3 CD melting curves (265 nm) of a sRNA fraction from *E. coli* DH5 α . sRNA was incubated for 1 h at 4 °C with (A) 20 wt% IL, and (B) 50 wt% IL: absence of IL (red); [Ch][MES], blue; [Ch][TES], green; [Ch][HEPES], yellow; [Ch][TRICINE], purple; [Ch][DHP], grey; and Buff[Ch][DHP], pink.

Aqueous solutions of GB-ILs and Buff[Ch][DHP] at 20 wt% are outstanding solvents for preserving the RNA integrity and to enhance its stability. Contrarily to most ILs investigated (including Buff[Ch][DHP]), GB-ILs display self-buffering characteristics^{30,31} and there is no need to add additional buffers to control the pH, as carried out with [Ch][DHP]. Other advantages of GB-ILs include their high solubility in water, their inability to chelate with metal-ions, and their high chemical stability and resistance to enzymatic degradation^{30,39}.

Superficial charge and molecular dynamics simulations - Aiming at better understanding the overall enhanced performance afforded by GB-ILs to preserve the sRNA integrity and enhance its stability, zeta potential measurements were performed, allowing us to conclude on the solution effective charge density. The results obtained are depicted in Figure 4.1.4 As polyanionic biopolymers, the typical zeta potential of sRNA at 200 $\mu\text{g/mL}$ is approximately -40 mV. All mixtures of sRNA and aqueous solutions at 20 or 50 wt% of ILs also display negative zeta potential values, although less negative than the isolated RNA. This trend may be attributed to the presence of cholinium cations in the outer shell of RNA – also discussed below based on molecular dynamics simulations. On the other hand, the charge of the IL alone is less negative than when complexed with RNA. Altogether, these observations confirm that all ILs employed in this study effectively surround sRNA. Furthermore, sRNA in presence of [Ch][TRICINE] displays the most negative zeta potential values. The presence of a higher number of [TRICINE]⁻ anions in close proximity to RNA may account for this behavior, thus justifying the poorer performance of this GB-IL to keep the RNA integrity. Our results agree with those previously reported by Satpathi et al.⁴¹ using calf thymus DNA and a guanidinium-based IL (Gua-IL). The authors⁴¹ reported that DNA presents a negative charge in the presence of distinct concentrations of Gua-IL (0.1 – 100 mM), becoming less negative as the IL concentration increases.

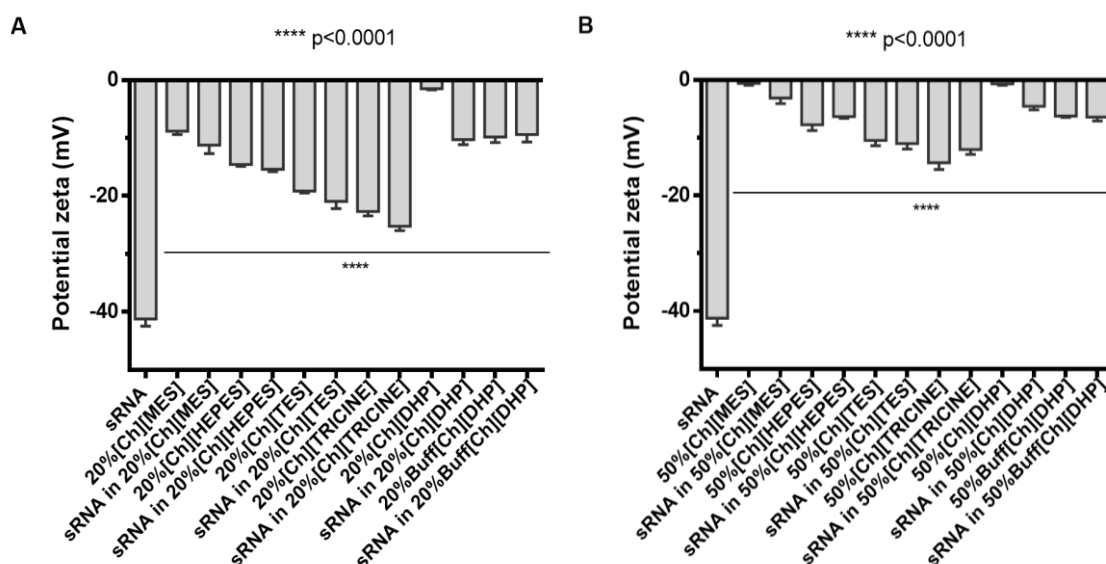


Figure 4.1.4 Average zeta potential (mV) of sRNA, ILs in aqueous solution, and ILs with the sRNA fraction from *E. coli*, at distinct IL concentrations: (A) 20 wt%, and (B) 50 wt%.

Molecular dynamics simulations were performed to gain insights into the molecular-level mechanisms ruling the outstanding performance of GB-ILs to stabilize and maintain the integrity of sRNA. A random 20-residue long single chain of RNA was assembled and simulated, in

presence of aqueous solutions containing 20 wt% of IL. To this end, [Ch][DHP] and [Ch][MES] were considered: the first as a well-studied IL and the latter as a GB-IL representative. According to the snapshots provided in Figure 4.1.5 (see also Figures C.1.4-C.1.6 in the Appendix C1 for a full depiction of the simulation boxes), which are representative of the overall dynamical behavior of the systems, the number of IL anions near the sRNA chain (consistent with the first IL solvation-like layer) is lower in [Ch][MES] than in [Ch][DHP]. This means that the chain first solvation layer has an overall more negative charge in presence of [Ch][DHP] than in presence of [Ch][MES]. The number of cations ([Ch]⁺) is however similar in both environments (Figures C.1.4-C.1.6 in the Appendix C1), implying that electrostatic interactions between the negatively charged RNA chain and [Ch]⁺ do not depend on the IL anion type. As highlighted, differences are however observed for the number of IL anions at the RNA first hydration layer. Taking 4 Å as the cutoff (*e.g.* the distance between any atom of the RNA chain and a representative atom of the ion: N for [Ch]⁺, S for [MES]⁻ and P for [DHP]⁻), the average number of cations obeying this threshold is 14.16 and 14.50 for [Ch][MES] and [Ch][DHP], respectively, whereas for the anions the averages are 8.92 and 12.14. The smaller size and higher charge density of [DHP]⁻ suggests that it is more likely to be found closer to the IL cation (stronger IL cation-anion interactions) and thus to the nucleic acid chain than [MES]⁻, facing thus more repulsive electrostatic interactions with the negatively charged nucleic acid. Similar trends are observed for cutoff distances up to 8 Å (see Figures C.1.4-C.1.6 in the Appendix C1). It is interesting to note that the -SO₃ group of [MES]⁻, which bears most of the negative charge of this anion, has a size similar to that of [DHP]⁻, but yet fails to be accommodated in an analogous fashion. Therefore, the stability of the sRNA chain is higher in presence of [Ch][MES] because the global charge of the overall complex (RNA chain + first solvation layer) is less negative than in presence of [Ch][DHP].

It should be noted that the correlation of these results with the measured zeta potential is not straightforward because the former is a macroscopic measure of the electrostatic potential at the interface of the solvated complex (with its multiple solvation spheres in which solvent molecules are not fully mobile) and bulk solvent. Still, the second solvation shell of the complex should accommodate more cations in the case of [Ch][DHP] because of its higher negative charge, in contrast with [Ch][MES], which ultimately should lead to a more neutral total charge of the full complex in the former case, and consistent with the zeta potential measurements. The solvation structure of the RNA chain would be visible through analysis of spatial distribution functions, although not possible because of the large size and mobility of the RNA chain.

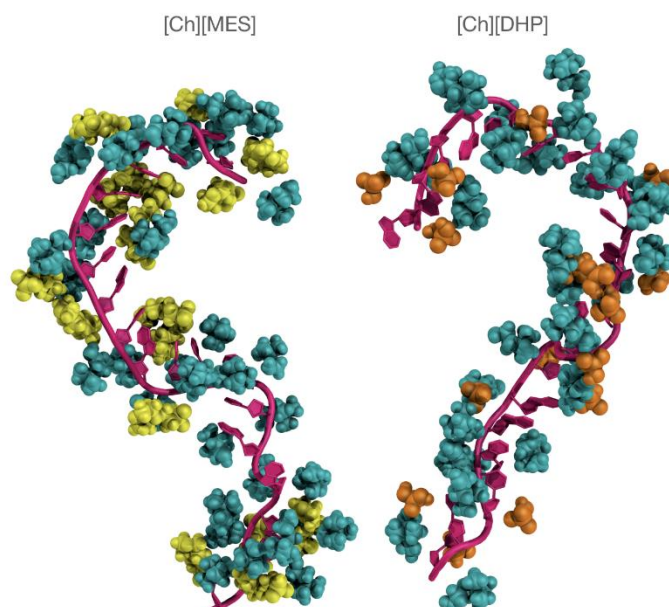


Figure 4.1.5 Snapshot of a 20-residue long linear sRNA chain in [Ch][MES] and [Ch][DHP] (left and right, respectively). The RNA chain is depicted as purple cartoon and the IL components as teal, yellow and orange spheres for [Ch]⁺, [MES]⁻ and [DHP]⁻, respectively. Only ions at a distance up to 4 Å from the chain surface are shown.

Medium-term stability of small RNAs in ILs aqueous solutions, cytotoxicity, and IL recyclability

- Following the previously described assays with 1 h of incubation at 4 °C, and to ascertain if GB-ILs are suitable to be used as preservation media for RNAs storage, experiments with longer incubation periods - 15 and 30 days – at temperatures at which RNA is only marginally stable (room temperature and 4 °C) were performed. These studies were carried out with aqueous solutions of ILs at 20 wt%, a concentration chosen given the results discussed before. This lower concentration of IL also results in a more economical and sustainable approach. The obtained results are summarized in Figure 4.1.6.

The behavior and stability of sRNA in the absence and presence of GB-ILs is quite different, being their stability particularly enhanced in aqueous solutions of [Ch][MES], [Ch][HEPES] and Buff[Ch][DHP]. The sRNA T_m in aqueous solutions of [Ch][TES] is 57 °C after 15 days of storage at room temperature and at 4 °C. However, after 30 days at room temperature, it decreases down to 44 °C, similarly to the result obtained with RNA in high-purity water. This trend indicates that for longer storage periods at room temperature, [Ch][TES] is not an effective stabilizer for sRNA. Even so, based on the RNA melting temperature experiments, [Ch][MES], [Ch][HEPES], and Buff[Ch][DHP] are remarkable sRNA stabilizers, at least up to 30 days.

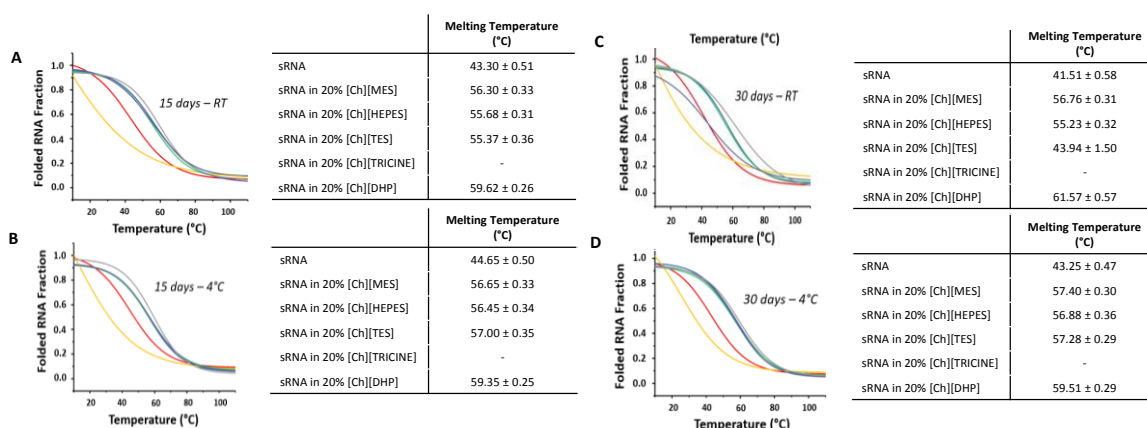


Figure 4.1.6 CD melting curves (265 nm) of a sRNA fraction from *E. coli* DH5α at different incubation periods and distinct temperatures. (A) sRNA incubated with 20 wt% of ILs for 15 days at room temperature (25 ± 1 °C); (B) for 15 days at 4 °C; (C) for 30 days at room temperature (25 ± 1 °C); and (D) for 30 days at 4 °C: absence of IL (red); [Ch][MES], blue; [Ch][TES], purple; [Ch][HEPES], green; [Ch][TRICINE], yellow; and Buff[Ch][DHP], grey.

The chemical structures of the selected ILs are shown in Figure C.1.1 in the Appendix C1. If on one hand all ILs share the same cholinium cation, they are composed of different anions. [TES]⁻ and [TRICINE]⁻ anions present multiple hydroxyl groups, which may be responsible for the lower RNA stability due to a stronger hydrogen-bonding with RNA nitrogen bases, thus resulting in a higher number of IL anions at the RNA first hydration layer as discussed above with the MD simulations, and in base-pairing disruption mediated by intramolecular hydrogen. This mechanism may be similar to that reported for the destabilization of RNA by urea, attributed to the disruption of base-pair interactions by direct hydrogen-bonding of urea with the RNA bases⁴². Moreover, it has also been shown that polyols, containing multiple hydroxyl groups, induce the thermal destabilization of double stranded DNA⁴³. On the other hand, RNA is stable after one-month storage at room temperature (see Figure 4.1.6) in Buff[Ch][DHP], [Ch][MES], and [Ch][HEPES]. The observed enhanced stability in presence of these GB-ILs is, at least in part, due to the shielding of negative phosphates in the backbone and coordinating 2' hydroxy groups by the cholinium cation, similar to what was previously reported for divalent and monovalent cations and polycationic amines¹⁷.

To ensure the sustainable character of GB-ILs aqueous solutions as stabilizing and preservation media of sRNA, both the safety profile of the complexes sRNA-IL and the ILs reusability are important criteria. Previously, Taha et al.³¹ determined the ecotoxicity of several GB-ILs towards *Vibrio fischeri* and found that the investigated ILs present non-toxic character as indicated by their high EC₅₀ values. According to the same standard assay, [Ch][DHP] was described as “practically harmless”⁴⁴. However, no cytotoxicity studies involving human cell

lines have yet been performed for GB-ILs, essential assays given the RNA biological role or when used as a therapeutic. Figure 4.1.7 shows the viability of human cell lines, namely human fibroblasts and a cervical cancer cell line (HeLa), in the presence of sRNA in aqueous solutions of ILs, at 20 and 50 wt%. These cell lines were selected based on the rationale that both cell lines are physiologically distinct entities, and therefore present different reactivity to external stimulus. Moreover, both are human cell lines, a relevant factor when envisaging the use of sRNA as alternative biopharmaceuticals.

As depicted in Figure 4.1.7 A, and by comparison with untreated cells, aqueous solutions of both non- and buffered-[Ch][DHP] highly impair the viability of fibroblasts, with only *ca.* 20% of viable cells. On the other hand, non- and buffered [Ch][DHP] at 20 and 50 wt% and [Ch][TRICINE] at 50 wt% affect the HeLa viability, with *ca.* 50, 25, 20 and 30% of viable cells, respectively. Previously, Weaver et al.⁴⁵ determined the [Ch][DHP] EC₅₀ for a J774 murine macrophage cell line and observed that this IL exceeds the buffer capacity of the complemented media at high concentrations (≥ 50 mM), but it is not clearly apparent whether toxicity can be attributed to pH effects. These effects were however observed in this work for [Ch][DHP] and Buff[Ch][DHP] ILs. Therefore, the use of this IL, at the described concentrations, at least in biological assays or for biologics storage purposes is not advisable, unless they could be previously removed. The same applies to [Ch][TRICINE] at 50 wt%. Despite these results, promising ILs were however identified, namely [Ch][MES], [Ch][TES], [Ch][TRICINE] and [Ch][HEPES] at 20 wt%. Their non-cytotoxic profile combined with their ability to maintain the integrity and enhance the thermal stability of sRNA, allow us to conclude that these self-buffering ILs are appropriate solvents for RNA preservation.

In the pursuit of developing sustainable processes and media for preserving RNA, we finally evaluated the possibility of recycling the ILs used, after the proper RNA recovery from the IL aqueous solution. A scheme of the overall process is depicted in Figure 4.1.8. Before any application, sRNA can be successfully recovered from the IL aqueous solutions by precipitation with ethanol (after a 2h incubation period at -80 °C, followed by a centrifugation step at 15,000 g). Then, the IL can be recovered and reused again as preservation media of sRNA. This possibility was experimentally addressed with two ILs, namely [Ch][MES] and [Ch][HEPES] and repeated for 3 times. In general, sRNA can be recovered, without compromising its structural integrity, and the IL reused. At the laboratory scale, a maximum loss of 3 wt% of IL in each cycle of IL recovery/reuse was registered, which is mainly due to the transference process between different vials. Since ethanol (well-known anti-solvent for RNA) was used for RNA precipitation and no degraded RNA was observed in the agarose gel electrophoresis (Figure 4.1.8), it is safe to admit that there are no significant losses of RNA among the different cycles. In all recycling

steps, RNA was recovered with high-integrity, and the IL was reused. This strategy, comprising both the RNA recovery and the IL recycling, is a step forward in the demand for effective RNA stabilizing and preservation solvents, which not only leads to less hazardous solvent wastes, but from an economical point of view is also less expensive.

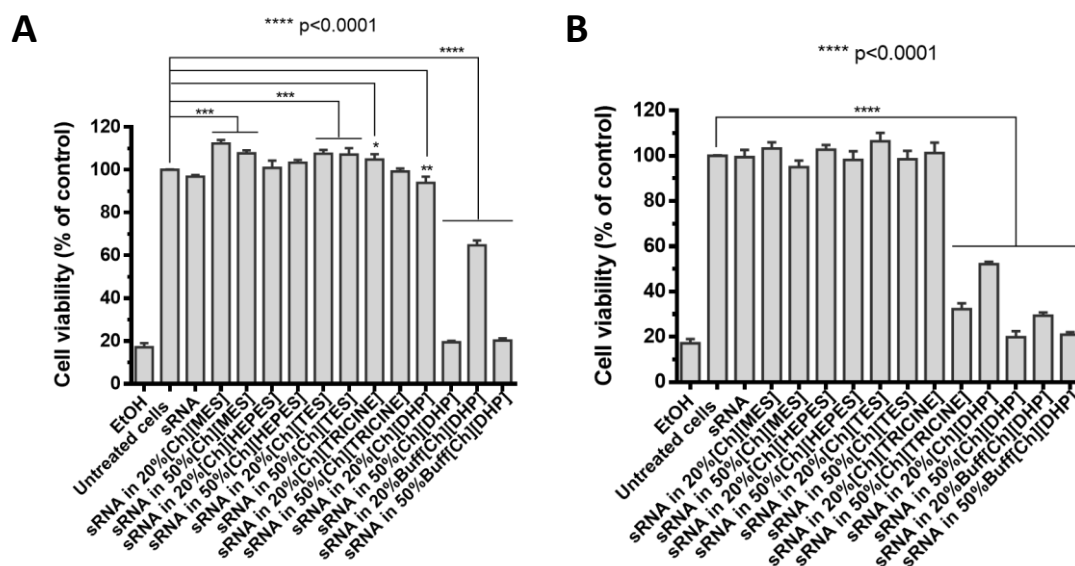


Figure 4.1.7 Viability of two human cell lines in presence of sRNA-IL aqueous solutions: (A) Fibroblasts, and (B) HeLa cells. Cell viability was measured using the MTS assay, and is shown as percentage of control (%).

Overall, aqueous solutions of adequate GB-ILs are enhanced solvents for the stabilization of recombinant sRNA, being able to maintain the sRNA integrity and to promote an increase of *ca.* 14 °C in its melting temperature, even after a medium-term storage of 1 month. In comparison with volatile organic solvents, the use of non-volatile ILs as RNA stabilizers eliminates organic solvent losses to the atmosphere³⁴, decreasing both the environmental footprint and the cost of the process. The sustainability of this strategy is also reinforced not only by the low environmental impact of appropriate GB-ILs (low toxicity to *Vibrio fischeri* and low cytotoxicity to human cell lines), as well as by the ILs recycling possibility without compromising the sRNA integrity.

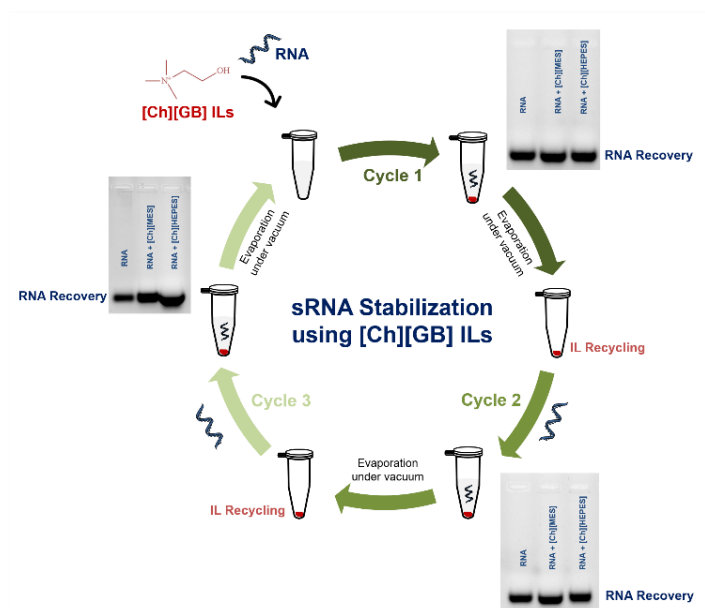


Figure 4.1.8 Scheme describing the recovery of recombinant *E. coli* sRNAs from aqueous solutions of GB-ILs and the IL recycling. 3 cycles were successfully carried out with [Ch][MES] and [Ch][HEPES] for mixtures incubated during 1 h.

Conclusions

Nucleic-acid-based products have been identified as promising biopharmaceuticals and as relevant biomolecules in biological assays. Nevertheless, nucleic acids are highly susceptible to nuclease cleavage, and although RNA is more prone to degradation than DNA, most studies aiming at finding adequate preservation media focused on improving the stability of DNA. Based on this lacuna, we evaluated the potential of self-buffering and biological-based ILs for extending the shelf life of a recombinant sRNA fraction derived from *E. coli*, containing the therapeutically relevant pre-miR-29. To the best of our knowledge, this is the first study that successfully reports the enhanced stability of a recombinant *E. coli* sRNA fraction containing a pre-miRNA in aqueous solutions of ILs.

It was found that ILs comprising the cholinium cation combined with anions derived from Good's buffers are able to maintain the sRNA stability, at least up to 30 days, thereby increasing the RNA shelf life. From the ILs investigated, [Ch][MES], [Ch][HEPES] and Buff[Ch][DHP] are the most suitable for maintaining the integrity and stability of sRNA. Molecular dynamics simulations allowed to better understand the molecular-level phenomena responsible for the observed improved stability of RNA, in which the overall charge of the biopolymer first solvation sphere plays a primary role.

Amongst the most suitable ILs that improve the sRNA stability, [Ch][HEPES] and [Ch][MES] were additionally identified as non-cytotoxic to human cell lines, which is particularly relevant

when envisaging the use of RNA as therapeutics. The sustainability of GB-ILs solvents and preservation approach to RNA is reinforced not only by their low environmental impact and low cytotoxicity, but also by the possibility of the ILs recycling without compromising the RNA integrity, as demonstrated.

In summary, aqueous solutions of [Ch][MES] and [Ch][HEPES] are remarkable stabilizing and storage media of recombinant sRNAs at room temperature, without requiring the typically carried out samples freezing, thus reinforcing their effectiveness in RNA bioprocessing.

References

1. J. C. Burnett, J. J. Rossi, *Chem. Biol.*, 2012, 19, 60-71.
2. A. Fire, S. Xu, M. K. Montgomery, S. A. Kostas, S. E. Driver, C. C. Mello, *Nature*, 1998, 391, 806-811.
3. M. S. Singh, D. Peer, *Curr. Opin. Biotechnol.*, 2016, 39, 28-34.
4. S. V. Ho, J. M. McLaughlin, B. W. Cue, P. J. Dunn, *Green. Chem.*, 2010, 12, 755-766.
5. R. Martins, J. A. Queiroz, F. Sousa, *J. Chromatogr. A.*, 2014, 1355, 1-14.
6. N. Sugimoto, *Chemical biology of nucleic acids. RNA technologies*, Springer, 2014.
7. A. Benedetto, P. Ballone, *Philos. Mag.*, 2016, 96, 870-894.
8. N. Sugimoto, *Int. Rev. Cell. Mol. Biol.*, 2014, 307, 205-273.
9. N. Singh, M. Sharma, D. Mondal, M. M. Pereira, K. Prasad, *ACS. Sustainable. Chem. Eng.*, 2017, 5, 1998-2005.
10. P. Pereira, A. Q. Pedro, J. A. Queiroz, A. R. Figueiras, F. Sousa, *Bioengineered*, 2017, 8, 670-677.
11. P. A. Pereira, J. F. Tomás, J. A. Queiroz, A. R. Figueiras, F. Sousa, *Sci. Rep.*, 2016, 6, 19946.
12. F. T. Edelmann, A. Niedner, D. Niessing, *Methods*, 2014, 65, 333-341.
13. P. Pereira, A. Sousa, J. A. Queiroz, I. Correia, A. Figueiras, F. Sousa, *J. Chromatogr. B. Analyt. Technol. Biomed. Life. Sci.*, 2014, 951-952, 16-23.
14. R. R. Mazid, U. Divisekera, W. Yang, V. Ranganathan, D. R. MacFarlane, C. Cortez-Jugo, W. Cheng, *Chem. Commun.*, 2014, 50, 13457-13460.
15. R. E. Farrell, Ed. *RNA methodologies: A laboratory guide for isolation and characterization*, Academic Press New York, 2010.
16. P. Chomczynski, *Nucleic. Acids. Res.* 1992, 20, 3791-3792.
17. R. Silvers, H. Keller, H. Schwalbe, M. Hengesbach, *Chem. Biochem.*, 2015, 16, 1109-1114.
18. G. F. Deleavey, M. J. Damha, *Chem Biol.* 2012, 19, 937-954
19. L. Ponchon, F. Dardel, 2011, 54, 267-273
20. K. E. Gutowski, G. A. Broker, H. D. Willauer, J. G. Huddleston, R. P. Swatloski, J. D. Holbrey, R. D. Rogers, *J. Am. Chem. Soc.*, 2003, 125, 6632-6633.
21. S. Y., Lee, S. Y., F. Vicente, F. A. Silva, T. E. Sintra, M. Taha, I. Khoiroh, J. A. P. Coutinho, P. L. Show, S. P. M. Ventura, *ACS. Sustainable Chem. Eng.*, 2015, 3, 3420-3428.
22. C. P. Song, R. N. Ramanan, R. Vijayaraghavan, D. R. MacFarlane, E. S. Chan, C. W. Ooi. *ACS. Sustainable. Chem. Eng.*, 2015, 3, 3291-3298.
23. I. Mamajanov, A. E. Engelhart, H. D. Bean, Hud. N. V., *Angew. Chem. Int.*, 2010, 49, 6310-6314.
24. H. T. Karimata, N. Sugimoto, *Angew. Chem. Int.*, 2012, 51, 1416-1419.
25. H. T. Karimata, N. Sugimoto, *Nucleic. Acids. Res.*, 2014, 42, 8831-8844.
26. R. Vijayaraghavan, A. Izgorodin, V. Ganesh, M. Surianarayanan, D. R. MacFarlane, *Angew. Chem. Int.*, 2010, 49, 1631-1633.
27. K. Jumbri, M. B. Abdul Rahman, E. Abdulmalek, H. Ahmadab, N. M. Micaelo, *Phys. Chem. Chem. Phys.*, 2014, 16, 14036-14046.
28. M. Marušič, H. T. Karimata, N. Sugimoto, J. Plavec, *Biochimie*, 2015, 108, 169-177.
29. A. Haque, I. Khan, S. I. Hassan, M. S. Khan. *J. Mol. Liq.*, 2017, 237, 201-207.
30. M. Taha, F. A. Silva, M. V. Quental, S. P. M. Ventura, M. G. Freire, J. A. P. Coutinho, *Green. Chem.*, 2014, 16, 3149-3159.
31. M. Taha, A. R. Almeida, F. A. Silva, P. Domingues, S. P. Ventura, J. A. Coutinho, M. G. Freire, *Chem. Eur. J.*, 2015, 21, 4781-4788.
32. P. Chomczynski, N. Sacchi, *Anal. Biochem.*, 1987, 162, 156-159.
33. M. J. Abraham, T. Murtola, R. Schulz, S. Páll, J. C. Smith, B. Hess, E. Lindahl, *SoftwareX*, 2015, 1, 19-25.
34. V. Hornak, R. Abel, A. Okur, B. Strockbine, A. Roitberg, C. Simmerling, *Proteins*, 2006, 65, 712-725.
35. C. I. Bayly, P. Cieplak, W. Cornell, P. A. Kollman, *J. Phys. Chem.*, 1993, 97, 10269-10280.
36. Gaussian, Revision, M. J. Frisch, G. W. Trucks, H. B. Schlegel, G. E. Scuseria, M. A. Robb, J. R. Cheeseman, G. Scalmani, V. Barone, B. Mennucci and G.A. Petersson, Gaussian, Inc., Wallingford CT, 2009.

37. J. Wang, R. M. Wolf, J. Caldwell, P. A. Kollman, D. A. Case, *J. Comput. Chem.*, 2004, 25, 1157-1174
38. M. Campetella, E. Bodo, R. Caminiti, A. Martino, F. D'Apuzzo, S. Lupi, L. Gontrani, *J. Chem. Phys.*, 2015, 142, 234502.
39. S. P. M. Ventura, F. A. Silva, M. V. Quental, D. Mondal, M. G. Freire, J. A. P. Coutinho, *Chem. Rev.*, 2017, 117, 6984-7052.
40. J. B. Swadling, K. Ishii, T. Tahara, A. Kitao. *Phys. Chem. Chem. Phys.*, 2018, 20, 2990-3001.
41. S. Satpathi, A. Sengupta, V. M. Hridya, K. Gavvala, R. K. Koninti, B. Roy, P. Hazra, *Sci. Rep.*, 2015, 5, 9137.
42. U. D. Priyakumar, C. Hyeon, D. Thirumalai, Jr. A.D. Mackerell, *J. Am.Chem. Soc.*, 2009, 131, 17759-17761.
43. P. Del Vecchio, D. Esposito, L. Ricchi, G. Barone. *Int. J. Biol. Macromol.*, 1999, 24, 361-369.
44. S. P. Ventura, F. A. e Silva, A. M. Gonçalves, J. L. Pereira, F. Gonçalves, J. A. Coutinho, *Ecotoxicol. Environ. Saf.*, 2014, 102, 48-54.
45. K. D. Weaver, H. J. Kim, J. Sun, D. R. MacFarlane, G. D. Elliott, *Green Chem.*, 2010, 12, 507-513.

4.2. Integrated extraction-preservation strategies for RNA using aqueous biphasic systems formed by ionic liquids

Based on the published manuscript:⁶ Maria V. Quental, Augusto Q. Pedro, Patrícia Pereira, Mukesh Sharma, João A. Queiroz, João A. P. Coutinho, Fani Sousa and Mara G. Freire. *ACS Sustainable Chem. Eng.*, 2019, 710, 9439-9448.

Abstract

The ubiquitous instability of RNA along with issues associated to its purity degree have been preventing its widespread use as low-cost biotherapeutics. Based on the well-known capacity of amino acids to specifically interact with RNA when used as chromatographic ligands, a set of amino-acid-based ionic liquids (AA-ILs) was herein investigated, both to act as preservation media and as phase-forming agents of aqueous biphasic systems (ABS) to carry out the biopolymer extraction from real matrices. AA-ILs comprising the cholinium cation and anions derived from L-lysine ([Ch][Lys]), L-arginine ([Ch][Arg]), L-glutamic acid ([Ch][Glu]) and DL-aspartic acid ([Ch][Asp]) were studied. It is shown that the stability of RNA is preserved in aqueous solutions of AA-ILs, even in presence of ribonucleases (RNases). Foreseeing the application of RNA as an alternative biopharmaceutical, it is further demonstrated that the investigated AA-ILs display no cytotoxicity onto two distinct human cell lines. After ensuring the stability of RNA in presence of AA-ILs and protection against RNases, ABS formed by AA-ILs and polypropylene glycol with a molecular weight of 400 g·mol⁻¹ (PPG 400) were investigated as extraction media of RNA from a bacterial lysate sample, being shown that RNA can be successfully extracted to the IL-rich phase without compromising the biopolymer integrity and stability. Based on these results, an integrated extraction-preservation process for RNA is proposed and demonstrated. RNA is initially extracted from the raw material using ABS, after which the IL-rich phase can be used as the preservation medium of RNA up to its use. It is further demonstrated that RNA can be easily recovered from the IL-rich phase by ethanol precipitation, and the ABS phase-forming components recovered and reused. The approach here reported represents a step forward in the development of sustainable processes to supply the critical demand of high-quality/high-purity RNA to be used as biotherapeutics.

⁶**Contributions:** M.G.F., J.A.P.C., J.A.Q. and F.S. conceived and directed this work. M.V.Q., A.Q.P. and P.P. acquired the experimental data. All authors interpreted the obtained experimental data. The manuscript was mainly written by M.V.Q and M.G.F. with contributions from the remaining authors.

Introduction

Ribonucleic acid (RNA) is an essential biopolymer in various biological functions, such as in coding, decoding, regulation, and expression of genes¹. Recent studies allowed the identification of new RNA classes with unanticipated functions², as well as of new types of RNA modifications, unexpected multiplicity of alternative transcripts, and widespread transcription of extragenic regions².

Nucleic acids are powerful biological tools in several fields², ranging from fundamental to applied research. For instance, RNA is a target of study in: (1) the quantification of transcript and protein levels of target genes, which are essential for understanding gene regulatory mechanisms and to develop drugs that regulate gene expression³; (2) structural studies using biophysical methods, to further understand RNA functions⁴; and (3) the development of RNA-based therapeutics⁵. In all these biological-based applications, the methods and solvents used for extracting and purifying RNA from various types of cells or other biological matrices, and respective preservation, are critical issues³.

RNA research studies and RNA-based therapeutics applications require large amounts of high-purity/high-quality RNA⁶. Thus, the RNA synthesis by chemical, enzymatic and, more recently, by recombinant technologies (using prokaryotic hosts such as *Escherichia coli* and *Rhodovulum Sulfidophilum*) has become an indispensable tool⁶. In 1968, Kirby et al.⁷ reported the pioneering work on RNA isolation from cells by the well-known phenol-chloroform method⁷. Up to date, two methods for isolating RNA prevail, namely this extraction method based on phenol and chloroform and solid-phase extraction (SPE) using silica-based materials^{8,9}. In addition to these recovery protocols, other purification steps including chromatography¹⁰ and denaturing polyacrylamide gel electrophoresis¹¹ are applied to remove process-associated impurities¹².

In RNA bioprocessing, besides high purity, other parameters are essential, namely the biopolymer integrity and biological activity. Both features are particularly relevant for their use as biotherapeutics, which should fulfil the requirements of regulatory authorities¹⁰. RNA is a highly labile polymer with inherent chemical instability and can suffer rapid degradation by nucleases¹. Therefore, RNA is normally preserved in high-purity water or sterile phosphate buffered saline (PBS) aqueous solutions under refrigeration at temperatures below 4 °C or at -80 °C for short- and long-term applications, respectively¹.

Based on the exposed, it is of paramount relevance to develop effective and sustainable recovery processes and to identify novel preservation media, where ionic liquids (ILs) can play a role in both approaches. Some published works in the past few years described the strong affinity between ILs and different biomolecules, showing that ILs are solvents with a high

potential for biomolecules preservation and extraction¹³, including nucleic acids¹⁴. However, in most of these studies, no extractions from raw materials have been performed, and DNA is usually the target. This preference is mainly due to the conditions required to work with RNA, as consequence of its poor stability (short half-life) when compared to DNA and ubiquitous presence of ribonucleases (RNases)¹.

Amongst the few reports comprising ILs and RNA, Mazid et al.¹⁵ proved that aqueous solutions of cholinium dihydrogen phosphate ([Ch][DHP]) are able to prolong the shelf life of siRNA up to three months in presence of RNase A. Mamajanov et al.¹⁶ evaluated the stability of a duplex RNA, which adopts a A-form helix in several aqueous buffers. The authors¹⁶ showed that the RNA melting temperature in aqueous solutions of cholinium chloride is lower than in other salt aqueous solutions. Fister et al.¹⁷ successfully used imidazolium-based ILs to disintegrate virus particles and isolate RNA. In summary, these works dealing with ILs and RNA are focused on two strategies: (i) to use ILs as alternative solvents to maintain or increase the stability and integrity of RNA; or (ii) to use ILs as alternative media to disintegrate biological systems to recover the target nucleic acid. The exploration of integrated systems, *e.g.* by using the same solvent in both the recovery and purification steps and as preservation media, was not attempted hitherto.

ILs can be used to form liquid-liquid systems to be used in separation processes, in which aqueous biphasic systems (ABS) are a promising alternative when dealing with biologically active products¹⁸. Contrarily to liquid-liquid systems formed by hydrophobic ILs and water, ABS are ternary systems formed by water, water-soluble ILs and a third component that can exert the salting-out of the IL or be salted-out by the IL, *e.g.* a salt or polymer¹⁸. ABS are mainly composed of water, and thus may offer a more biocompatible environment to deal with nucleic acids¹³. Albeit ABS have been described as biocompatible separation systems, most of the studied IL-based ABS are formed by imidazolium ILs¹⁸, which often are deleterious for biomacromolecules. This fact prompted the research on ILs based on natural feedstocks; for instance, biocompatible ILs formed by the cholinium cation and anions derived from essential amino acids were reported in 2005 by Ohno and co-workers²⁰. After this pioneering work, an increasing number of reports focusing on their properties, including viscosity²¹, thermal stability²² and toxicity²³ have emerged. However, cholinium amino-acid-based ILs (AA-ILs) have been scarcely applied in the development of separation processes. AA-ILs have been combined with inorganic salts (K_3PO_4 and K_2CO_3)²⁴ and polypropylene glycol²⁵ to form IL-based ABS, where a comprehensive characterization of the respective phase diagrams was performed. In two of these works it was evaluated the extraction capacity of ABS for two model proteins (bovine serum albumin and

trypsin²⁵) and for phenylalanine enantiomers²⁶. Still, the performance of these systems was not appraised in the separation of target compounds from real matrices.

As result of the high affinity between amino acids and RNA²⁷, amino-acid-based affinity chromatography is highly used to purify this biopolymer^{10, 28,29}. In addition, amino acids may have an important role in RNA loop recognition through a base-flipping process²⁷. This well-known preferential affinity, together with the fact that in general amino-acid-based ILs are non-toxic, biodegradable and biocompatible³⁰, motivated us to investigate the use of aqueous solutions of amino-acid-based ILs as alternative solvents to stabilize and protect RNA from nucleases coupled to their use in the formation of ABS, envisioning the development of integrated preservation-extraction strategies. In affinity chromatography, hydrophilic amino acids (*e.g.* arginine) are usually used as ligands to improve the RNA biorecognition^{10,28,29}. Accordingly, in this work, we selected two hydrophilic amino acids (arginine and lysine) and two hydrophobic amino acids (aspartic and glutamic acids) from the aliphatic amino acids group to be used as IL anions. This selection allowed us to evaluate the amino acids chemical features, and thus explore preferential interactions, required to improve the selectivity for RNA. Based on the exposed, AA-ILs composed of the cholinium cation combined with the anions L-lysinate, L-argininate, L-glutamate and DL-aspartate were synthesized and characterized by us. Their protective effect (aqueous solutions containing 20 wt% of IL) towards RNA, even in presence of RNases, and respective cytotoxicity onto two human cell lines were evaluated. Zeta potential measurements were additionally carried out to perceive the mechanisms behind the RNA stabilization. The best identified AA-ILs were then investigated as phase-forming components of ABS combined with polypropylene glycol with a molecular weight of 400 g·mol⁻¹ (PPG 400) to extract RNA from a bacterial lysate sample. Finally, the recovery of the RNA from the IL-rich phase and reuse of the ABS phase-forming agents was addressed, demonstrating that amino-acid-based ILs can be used in the development of integrated processes comprising both the extraction and preservation steps.

Experimental Procedure

Materials - Four cholinium-based salts were synthesized, namely 2-hydroxyethyl)trimethylammonium 2,6-diaminohexanoate ([Ch][Lys]), 2-hydroxyethyl)trimethylammonium (2S)-2-amino-5-guanidinopentanoate ([Ch][Arg]), (2-hydroxyethyl)trimethylammonium 2-aminopentanedioic ([Ch][Glu]), and (2-hydroxyethyl)trimethylammonium (2S)-2-aminobutanedioic acid ([Ch][Asp]). The following amino acids were used to synthesize the ILs: purity > 99 wt%), L-lysine monohydrated (Lys, Acros,

purity > 99 wt%), L-arginine (Arg, Merck, purity > 99 wt%), glutamic acid (Glu, Riedel de Haen, purity > 99 wt%) and DL-aspartic Acid (Asp, purity > 99 wt%). Their full name, acronym and chemical structure are depicted in Figure 4.2.1. Cholinium hydroxide (Sigma Aldrich, 45 wt%), acetonitrile (Sigma Aldrich, 99 wt%) and methanol (VWR, HPLC grade) were also used. All the reagents used for RNA extraction as well as fluorescein isothiocyanate isomer 1 (FITC) were acquired from Sigma Aldrich. The ABS studied herein were determined using polypropylene glycol with an average molecular weight of $400 \text{ g}\cdot\text{mol}^{-1}$ (PPG 400), supplied by Aldrich, and used as received. All the materials used in the experiments were RNase-free. Ultrapure reagent-grade water (Mili-Q system, Milipore/Waters) was treated with 0.05 % diethyl pyrocarbonate (DEPC, Sigma-Aldrich).

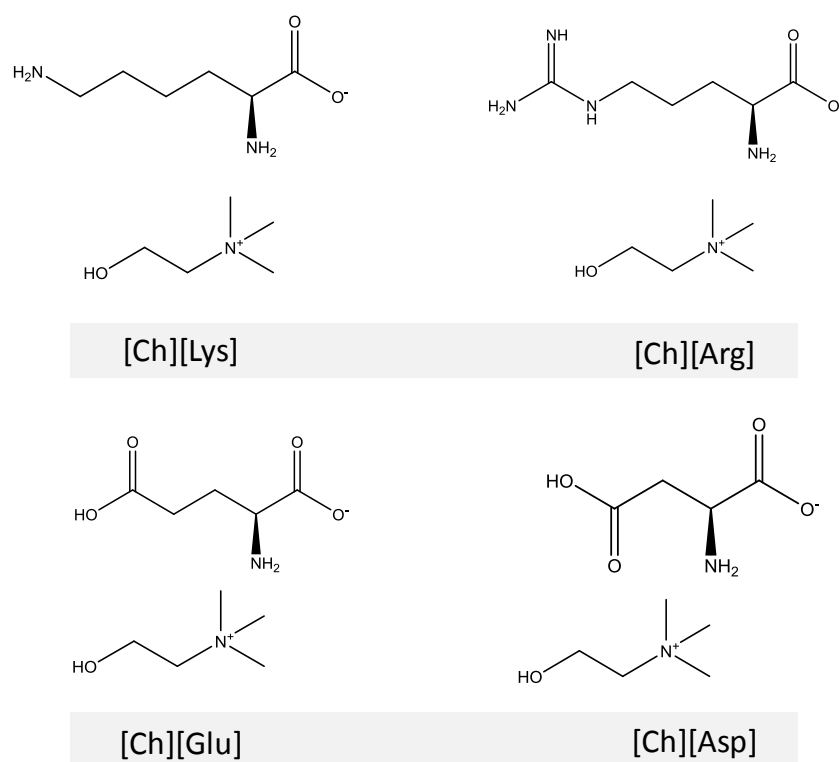


Figure 4.2.1 Chemical structures of the studied [Ch][AA] ILs.

Synthesis of [Ch][AA]-based ILs - ILs containing the cholinium cation and anions derived from amino acids, namely L-lysine, L-arginine, DL-aspartic acid and L-glutamic acid, were synthesized by neutralization of cholinium hydroxide (in methanol solution at 45 wt%) with amino acids²⁰. In a typical reaction, 1:1.05 mole of both cholinium hydroxide (45 wt% in methanol) and amino acids, respectively, were mixed at ambient conditions. The reaction mixture was kept at room temperature (25 °C) under inert atmosphere with continuous stirring for at least 24 h. Methanol was then removed under reduced pressure at 60 °C. The synthesized ILs were washed with

acetonitrile/methanol (7:3, v/v) to remove unreacted amino acids. Excess solvent and water were then removed under reduced pressure using a rotary evaporator (60 °C, 2 h) and under high vacuum (60 °C, 72 h). The dried ILs were finally collected and stored under dark and cool place. The purity and structure of the synthesized ILs were confirmed by ^1H NMR spectroscopy and elemental analysis.

Small RNA biosynthesis and isolation - In this section, the same procedure described in the experimental section of Chapter 4 (Section 4.1) was adopted.

Aqueous solutions of ionic liquids as preservation media for RNA - RNA was dissolved in aqueous solutions of different ILs, at 20 wt%, and the mixtures incubated at room temperature ($25 \pm 1^\circ\text{C}$) for different periods, namely 1 h and 15 days. Subsequently, RNA was precipitated by adding 2 volumes of pure alcohol (butanol in the case of [Ch][Arg], and ethanol for the remaining), and further incubation for 2 h at -80°C , until it was recovered by centrifugation at 15,000 g for 30 min at 4°C . Finally, the nucleic acids pellets were air-dried for 10 min at room temperature and solubilized in 0.05% DEPC-treated water.

Agarose gel electrophoresis, Zeta potential and cell viability - The integrity and identification of sRNAs recovered after incubation with ILs for 1 h at 4°C were evaluated using agarose gel electrophoresis (*cf.* the experimental section in Chapter 4 (Section 4.1) for the protocol). The Zeta potential and cell viability assays follow the procedure described in the experimental section in Chapter 4 (Section 4.1).

Circular Dichroism (CD) spectroscopy - CD experiments were performed in a Jasco J-815 spectropolarimeter (Jasco, USA), using a Peltier-type temperature control system (model CDF-426S/15). The same protocol described in experimental section 3.1 was performed. Data were converted into fraction folded (Θ) as detailed in the literature³¹. Data points were then fitted to a Boltzmann distribution (OriginPro 2015) and the melting temperatures (T_m) were determined from the two-state transition model used, using the first derivative method³².

ABS phase diagrams - Aiming to explore the ability of [Ch][AA] to undergo ABS formation in the presence of PPG 400, the binodal curve of each ABS was determined by the cloud point titration method at 25°C and atmospheric pressure. Aqueous solutions of [Ch][AA] in the range of ≈ 50 wt% to 70 wt% and aqueous solutions of PPG 400 (from 50 wt% to 80 wt%) were gravimetrically prepared and used for the determination of the binodal curves. These

determinations as well as the tie-lines determinations follow the procedure described in the experimental section in Chapter 2 (Section 2.1).

Extraction of RNA using IL-based ABS - The ternary mixtures used in the partitioning experiments of RNA were gravimetrically prepared at the follow common mixture composition: 20 wt% of PPG 400 + 20 wt% of [Ch][AA] + 60 wt% of DEPC-treated water. This fixed mixture composition was selected considering the biphasic region of all the studied systems. Moreover, by previously setting a mixture composition it is possible to determine which is the adequate amount of RNA to introduce in each system, and thus do the direct comparison of the extraction efficiencies of all ABS under study. Initially, the partitioning of sRNA was ascertained, from a 400 µg/mL RNA aqueous. All mixtures were carefully stirred and centrifuged for 5 min at 25 °C (5000 g). Then, a precise separation of the phases was performed, and the RNA recovered from both phases by alcohol precipitation, as described above. Then, the preferential location and partitioning of nucleic acids in IL-ABS was ascertained by agarose gel electrophoresis. After demonstrating the favourable RNA extraction to the IL-rich phase with these systems and studied mixture composition, new experiments were carried out envisaging the purification of RNA directly from a bacterial lysate sample (detailed experimental information on sample preparation is given in the Appendix C2). The ABS chosen are composed of 20 wt% of PPG 400, 20 wt% of AA-IL and 60 wt% of lysate. Each mixture composition was weighed, mixed and centrifuged for 5 min (5000 g). RNA evaluation was carried out as described before.

Recovery of RNA and recyclability of the ABS phase-forming components - The recovery of RNA from the IL-rich phase was performed by ethanol precipitation, as described above. Then, the solvent present in the IL-rich phase was evaporated under vacuum at room temperature, up to constant weight since only the IL and PPG400 are the non-volatile species. The volatile solvents present in the IL-rich phase were evaporated under vacuum at room temperature, up to constant weight, leaving only the IL and PPG 400 as the non-volatile species. The recovered PPG 400 and AA-IL were then reused (two more times) in the creation of novel ABS, and their impact on the integrity of RNA after a new extraction step was assessed by agarose gel electrophoresis. The recovered phase-forming components aqueous solutions were also evaluated in terms of their feasibility for keeping the RNA stability and integrity toward the development of integrated extraction-preservation processes.

Results and Discussion

Although extraction, purification, and storage of nucleic acids are required for biological-based research³, RNA of high quality and high purity is particularly relevant when foreseeing its use as biotherapeutics. However, RNA is known for being an extremely unstable and labile biopolymer, being critical the research on novel stabilization solvents and purification strategies³³. The current work addresses the use of aqueous solutions of bio-based ionic liquids composed of the cholinium cation and anions derived from amino acids as alternative solvents able to maintain and improve the stability of RNA. All ILs used, namely [Ch][Lys], [Ch][Arg], [Ch][Glu] and [Ch][Asp], were synthesized in this work. Their chemical structure are shown in Figure 4.2.1. Details on their characterization and purity are given in the Appendix C2 (*cf.* Figures C.2.1-C.2.4). These ILs were designed and synthesized based on the specific affinity between amino acids and RNA and their previous use on amino acid-based affinity chromatography for RNA purification^{28, 29} coupled to the fact that amino-acid-based ILs are non-toxic, biodegradable and biocompatible³⁰. Based on these features, the selected ILs may thus be used as alternative solvents to stabilize and protect RNA from nucleases and applied in the formation of ABS to carry out its extraction from the media in which it is produced. The combination of both possibilities allows the development of integrated preservation-extraction strategies.

Integrity, stability and cytotoxicity of RNA in presence of aqueous solutions of ILs - Initial studies on the integrity of RNA at 25 °C in presence of aqueous solutions of [Ch][Lys], [Ch][Arg], [Ch][Glu] and [Ch][Asp] at 20 wt% were carried out by agarose gel electrophoresis in order to address the potential of the synthesized ILs to act as alternative preservation media. The results obtained are depicted in Figure 4.2.2, where a well-defined band with a low molecular weight is shown, corresponding to the recombinant RNA fraction extracted from *E. coli*. To avoid interferences of ILs in the electrophoretic run, alcohol-induced precipitation of RNA was applied in all samples. Different alcohols (propan-2-ol, ethanol, propanol, and butanol) were tested in what concerns to their ability to precipitate RNA, and distinct behaviours were observed (shown in Figure C.2.5 in the Appendix C2). Although discussed here with a different purpose, the identification of appropriate solvents for the induced precipitation of RNA is valuable when considering the RNA and ILs recovery proposed below.

The results shown in Figure 4.2.2 correspond to RNA precipitated with the best identified alcohols, namely butanol for the [Ch][Arg] aqueous solution and ethanol for the remaining ILs aqueous solutions. Depending on the original media, either ethanol or isopropanol have been reported for the precipitation of nucleic acids³⁴. Ethanol and butanol are however more benign and less hazardous alcohols than isopropanol³⁵; therefore, the efficient recovery of RNA from

ILs aqueous solutions with these alcohols further reinforces the sustainability of the proposed recovery strategy in comparison with processes based on isopropanol.

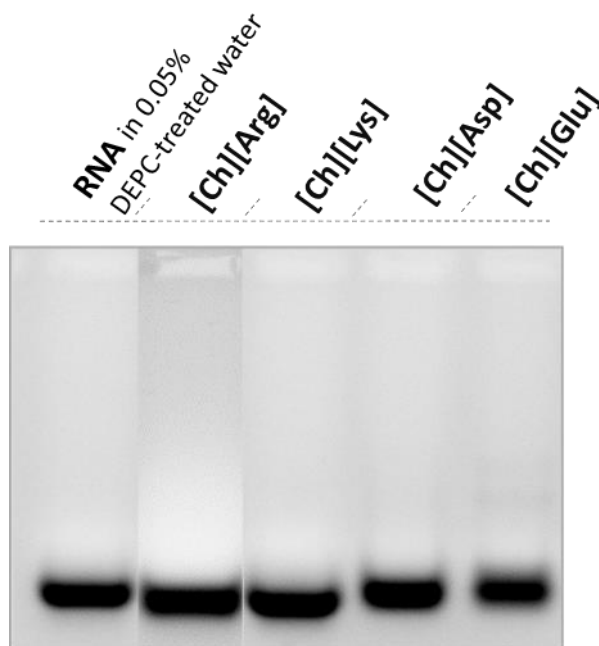


Figure 4.2.2 Electrophoretic analysis of the integrity of RNA in 0.05 % DEPC-treated water and RNA in presence of aqueous solutions of 20 wt% of the studied ILs.

It is well-known that RNA secondary structure elements and global folding patterns are temperature dependent³⁶. Accordingly, RNA melting studies were performed in the absence and presence of different aqueous solutions of 20 wt% of ILs. The typical CD spectrum of RNA includes a minimum ellipticity peak at 215 nm, and a maximum ellipticity peak at 265 nm; however, the investigated ILs interfere with the CD spectrum of RNA at lower wavelengths (*cf.* the representative CD spectrum of RNA in presence of [Ch][Arg] in Figure C.2.6 in the Appendix C2). The CD melting temperatures (T_m) of RNA were thus determined by addressing the changes in the RNA ellipticity at 265 nm in the temperature range from 10 to 110 °C. The obtained results corresponding to 1 h of incubation with each AA-ILs are given in Table 4.2.1 (the respective melting curves are depicted in Figure C.2.7 in the Appendix C2). T_m is defined as the temperature at which half of the molecules of a double-stranded species become single-stranded, where higher T_m values are an indicator of a higher RNA thermostability³⁷. The T_m of RNA dissolved in high-purity water is 45.8 °C, but it is lower in presence of [Ch][Lys] and [Ch][Arg] aqueous solutions (39.9 °C and 43.3 °C, respectively). Contrarily, a remarkable enhancement of *ca.* 15 °C (60.0 °C and 60.3 °C, respectively) in the T_m of RNA was observed in presence of aqueous solutions of [Ch][Glu] and [Ch][Asp], indicating that the thermal stability of RNA during 1 h of

incubation in AA-ILs is significantly enhanced with these two ILs. In addition to the high stabilizing effect and preservation of RNA afforded by the studied ILs for short-term periods, the results shown in Table 4.2.1 also demonstrate the potential of these two ILs as preservation agents even after 15 days of incubation. These results are in agreement with a previous work¹⁶, showing an increase of the RNA stability with buffered aqueous solutions of [Ch][DHP], although a lower enhancement, *ca.* 8.5 °C, was achieved.

Overall, this first set of results demonstrate that RNA is more stable in aqueous solutions of [Ch][Glu] and [Ch][Asp] than in 0.05 % DEPC-treated water, both for short-term and medium-term storage periods (1 h and 15 days). Thus, it seems that the anionic counterpart of ILs has a significant influence on the RNA structure and stability, which is discussed in more detail below.

Table 4.2.1 Melting temperature of RNA in 0.05 % DEPC-treated water and in AA-ILs (20 wt%) aqueous solutions after 1 h and 15 days of incubation at 25 °C.

	$T_m / ^\circ\text{C}$	$T_m / ^\circ\text{C}$
	after 1 h	after 15 days
RNA in 0.05 % DEPC-treated water	45.8 ± 0.5	46.0 ± 0.5
RNA in 20 wt% [Ch][Lys]	39.9 ± 0.5	29.5 ± 2.0
RNA in 20 wt% [Ch][Arg]	43.3 ± 0.7	32.4 ± 5.5
RNA in 20 wt% [Ch][Glu]	60.0 ± 0.3	56.4 ± 0.4
RNA in 20 wt% [Ch][Asp]	60.3 ± 0.3	56.2 ± 0.4

Aiming at better understanding the mechanisms behind the preservation and enhanced stability promoted by some of the investigated ILs, zeta potential measurements of RNA in pure water and in aqueous solutions of 20 wt% of ILs were carried out. Zeta potential corresponds to the electrostatic potential generated in an applied electric field due to the attraction between charged species and the oppositely charged electrode, thereby allowing to draw some conclusions on the solution effective charge density. Nucleotides are the building blocks of RNA, which comprise phosphate groups that confer to RNA a negative charge, resulting in a zeta potential of approximately – 40 mV, as shown in Figure 4.2.3. In all assays it was observed that when dissolved in aqueous solutions of ILs, RNA displays a less negative value, confirming that all ILs employed in this study interact with RNA. Since less negative zeta potential values are obtained when in presence of ILs, it is plausible to admit that when in aqueous solution the cholinium cation forms an outer shell around RNA, in agreement with previously reported molecular dynamics simulations results³⁸.

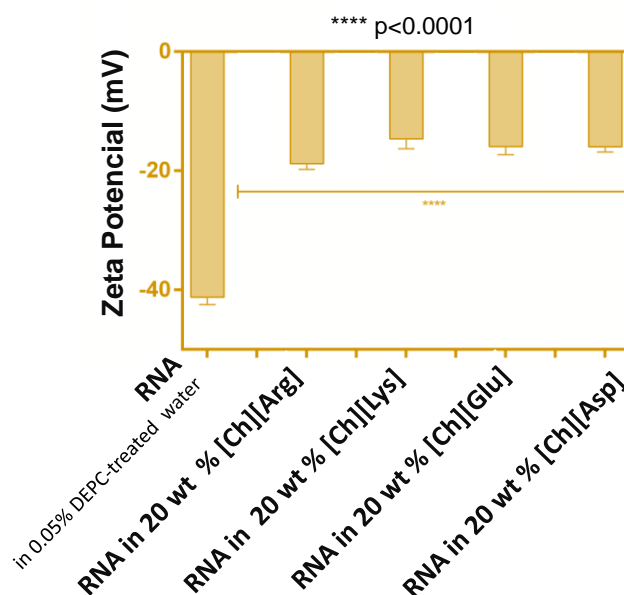


Figure 4.2.3 Average zeta potential (mV) of RNA dissolved in 0.05 % DEPC-treated water and in 20 wt% AA-ILs aqueous solutions.

Considering the application of AA-ILs as efficient preservation and stabilization media of RNA for biological assays or for its use as biopharmaceuticals, it is crucial to ascertain the RNA safety profile. Different studies already approached the ecotoxicity²³ and biodegradability³⁰ of AA-ILs. These studies demonstrated that AA-ILs display low ecotoxicity and high biodegradable character. In this work we addressed their impact onto different cell lines by cytotoxicity studies. Figure 4.2.4 depicts the effect of mixtures of RNA and ILs at 20 wt% in the viability of two human cell lines, namely fibroblasts and a cervical cancer cell line – HeLa. These two distinct cell lines were chosen since they are physiologically distinct entities and, therefore, present different reactivity to external stimulus. According to the results obtained, aqueous solutions of [Ch][Lys] greatly impair the viability of both cell lines. In contrast, the remaining AA-ILs tested ([Ch][Arg], [Ch][Glu], and [Ch][Asp] at 20 wt%) are harmless to both tested human cell lines, thereby confirming their non-cytotoxic character at the concentrations used.

Overall, [Ch][Glu] and [Ch][Asp] can increase the thermal stability of RNA and do not display cytotoxicity onto two human cell lines. However, the major factor affecting the RNA stability, and thereby causing its degradation, is the ubiquitous presence of RNases (active nucleases)⁴⁰. Thus, as the next step we appraised the protective effect of both [Ch][Glu] and [Ch][Asp] aqueous solutions against ribonuclease enzymatic activity. The CD ellipticity at 265 nm of RNA dissolved in high-purity water was monitored during different incubation periods (6, 12, 24, 36 and 48 h), and compared with the ellipticity of RNA in aqueous solutions of 20 wt% of [Ch][Glu] and [Ch][Asp]. 1 % (v/v) Fetal bovine serum (FBS), commonly added to mammalian cell culture

media to provide essential growth factors, was added to each solution, being the source of ribonuclease enzymatic activity. The results depicted in Figure C.2.8 in the Appendix C2 show that the RNA ellipticity decreases with the increase of the incubation period, indicating that the biopolymer is naturally degraded by RNases. In comparison with RNA in high-purity water, the ellipticity of RNA is higher in presence of [Ch][Asp], meaning that this IL is more effective on RNA protection from degradation by RNases. The beneficial role of [Ch][Asp] reinforces the idea that this IL is particularly relevant to be used as preservation and stabilization media for RNA, for instance for storage or to be used as an additive in biological assays.

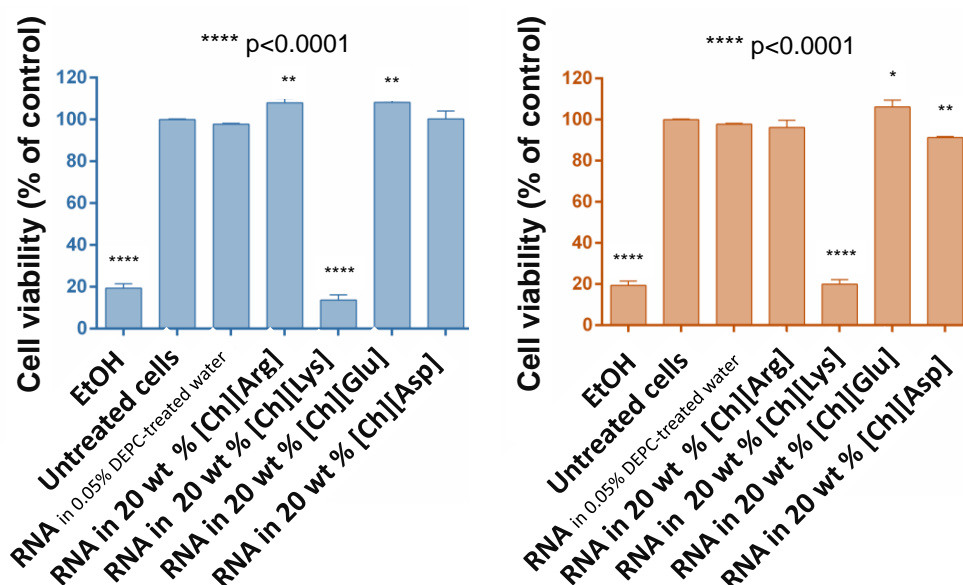


Figure 4.2.4 Cytotoxic effect of AA-ILs in two different human cell lines: Fibroblasts (left) and HeLa (right).

Extraction of RNA using IL-based ABS - The set of results presented above demonstrate that, amongst the ILs studied, [Ch][Glu] and [Ch][Asp] are the most promising ones to be employed in RNA bioprocessing. These AA-ILs do not disturb the RNA secondary structure, but instead increase their thermal stability and offer protection against RNase activity without signs of cytotoxicity. With the purpose of creating an integrated extraction-preservation process with AA-ILs, their ability to form ABS with PPG 400 for the extraction of RNA was investigated. In addition to these promising AA-ILs ([Ch][Glu] and [Ch][Asp]), the remaining studied AA-ILs were also tested as ABS phase-forming agents, whose results are shown in Figures C.2.9 and C.2.10 in the Appendix C2. To the best of our knowledge, only the ABS formed by PPG 400 + [Ch][Lys] + water was previously reported²⁵. The ternary phase diagram of the ABS formed by PPG 400 + [Ch][Lys] + water is in agreement with literature data²⁵, as depicted in Figure C.2.9 in the

Appendix C2. The experimental weight fraction data and corresponding regression parameters of the respective binodal curves of each ABS are reported in the Appendix C2 (Figure C.2.10 and Tables C.2.1-C.2.2). Tie-lines (TLs), along with their respective length (TLL), were also determined and are given in the Appendix C2 (Table C.2.3). These data and parameters are useful to characterize the monophasic/biphasic regimes of each ABS and the composition of the coexisting phases at the mixture point at which the extraction of RNA was carried out. In all studied ABS, the top phase corresponds to the PPG-rich phase, while the bottom phase is enriched in the IL (as confirmed by conductivity measurements). All ILs share a common cation (cholinium); thus, differences in the solubility curves shown in Figure C.2.11 in the Appendix C2, *e.g.* the amount of each phase-forming component required to form two-phase systems, is a result of the IL anion nature. As PPG 400 is a hydrophobic polymer, and given the trend obtained, it is plausible to admit that ILs act as salting-out agents over PPG 400 in aqueous media. More hydrophobic ILs, such as [Ch][Asp], require higher amounts of IL and/or PPG 400 to undergo liquid-liquid demixing and create two phases.

After determining the ABS phase diagrams, extraction studies of RNA with [Ch][Glu] and [Ch][Asp] were carried out. ABS with fixed compositions of 20 wt% of PPG 400 + 20 wt% of IL + 60 wt% of RNA in DEPC-treated water (at $400 \mu\text{g}\cdot\text{L}^{-1}$) were used. The preferential partitioning of RNA in the ABS phases was evaluated by agarose gel electrophoresis, whose results are shown in Figure 4.2.5. In the systems investigated, RNA completely partitions to the IL-rich phase (bottom phase) – complete extraction in one-step. No RNA was detected at the PPG 400-rich phase (top phase) and no losses of RNA by precipitation were perceived. Furthermore, according to the agarose gel electrophoresis profile, the structural integrity of RNA is preserved after the extraction step. Some studies already reported the use of ABS formed by ILs and PPG 400 for the extraction of other biomolecules, *e.g.* BSA²⁵, IgG⁴² and IgY⁴³, demonstrating their preferential partitioning to the IL-rich phase. However, and contrarily to what is typically observed in the extraction of proteins using systems with PPG where significant losses in yield are observed, in this work, no losses of RNA were detected. In amino-acid-based affinity chromatography, multiple interactions, such as electrostatic interactions, van de Waals forces, hydrogen bonding, and dispersive forces between amino acids and RNA occur³¹. In the same line, and since no salting-out effects by PPG dominate the partition behaviour, these favourable interactions must be responsible for the complete partition of RNA to the IL-rich phase.

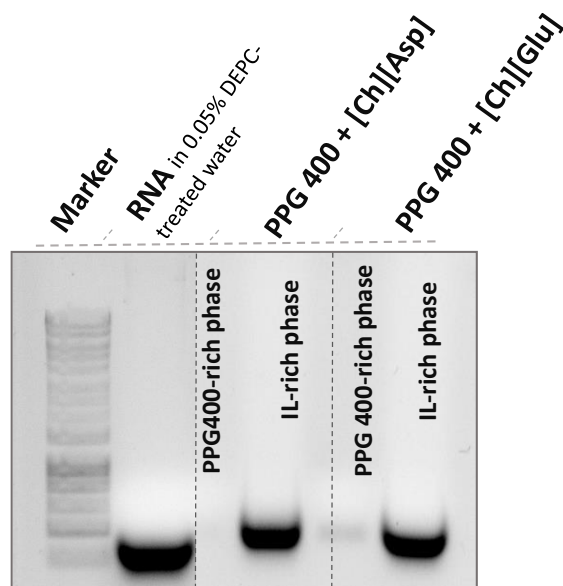


Figure 4.2.5 Agarose gel electrophoresis of the ABS coexisting phases at the mixture point: 20 wt% of PPG 400 + 20 wt% of AA-IL + 60 wt% of RNA in DEPC-treated water ($400 \mu\text{g}\cdot\text{L}^{-1}$). RNA in 0.05 % DEPC-treated water was used as control sample and a marker is also included.

After confirming the potential of AA-IL-based ABS to extract RNA, the same systems were employed in the extraction of RNA directly from a real sample - a recombinant bacterial lysate that contains RNA, genomic DNA, proteins and other impurities (*cf.* the Appendix C2 for the protocol on the lysate sample preparation). Similarly, to what occurred in the assays with pure RNA, the preferential partition of RNA to the IL-rich phase was observed. However, some RNA was also identified in the polymer-rich phase (Figure C.2.11 in the Appendix C2), indicating that there is a competition of other molecules present in the medium to partition to the IL-rich phase. Both gDNA and gDNA fragments (the first two bands with higher molecular weight shown in Figure C.2.11 in the Appendix C2) also preferentially partition to the IL-rich phase. Although additional studies are required to improve the selectivity of the investigated ABS for RNA, the structural integrity of RNA is still preserved after the extraction step from the original sample, reinforcing the potential of these systems to be used as purification platforms for RNA.

Recovery of RNA, recyclability of the ABS phase-forming components, and proposal of the integrated extraction-preservation process - The RNA integrity and stability are of crucial relevance when envisaging the development of processes in which RNA needs to be recovered for further use, *e.g.* in biopharmaceutical applications. Moreover, the sustainability of IL-based ABS processes can be improved not only by using more benign (low-toxicity and high biodegradability) ABS phase-forming components, such as amino-acid-ILs and polymers, but also

through their recycling and reuse. The main objective of this work is to develop an integrated strategy where RNA can be firstly extracted from the raw material without changes in its structure using ABS, after which the IL-rich phase can be used as the preservation medium of RNA up to use, and, if required, further recycled.

We firstly evaluated the integrity of RNA in the IL-rich phase, followed by its recovery from the IL-rich-phase and the IL/PPG recycle and reuse. The ABS formed by PPG 400 and [Ch][Glu] was used since it was one of the best systems identified according to the stability, extraction and cytotoxicity data discussed before. The proposed integrated preservation-extraction strategy includes 4 main steps: 1) RNA extraction from the lysate sample using ABS and RNA preservation in the IL-rich phase; 2) RNA recovery from the IL-rich phase by alcohol precipitation; 3) evaporation under vacuum of the ABS phase-forming components at room temperature up to constant weight; 4) formation of new ABS with the recovered non-volatile (IL and PPG) solvents for RNA extraction and preservation. Three cycles of this combined strategy were tested herein as a proof of concept, which is summarized in Figure 4.2.6. A maximum of 5 wt% of IL and PPG was lost in each cycle, mainly due to the transfer of solvents between vials. This value could be reduced by scaling-up the proposed process and by improving the operational conditions. The ABS phase-forming components were also successfully recovered and reused, without losses on the ABS extraction and RNA stabilization performance, as shown by the agarose gel electrophoresis results given in Figure 4.2.6.

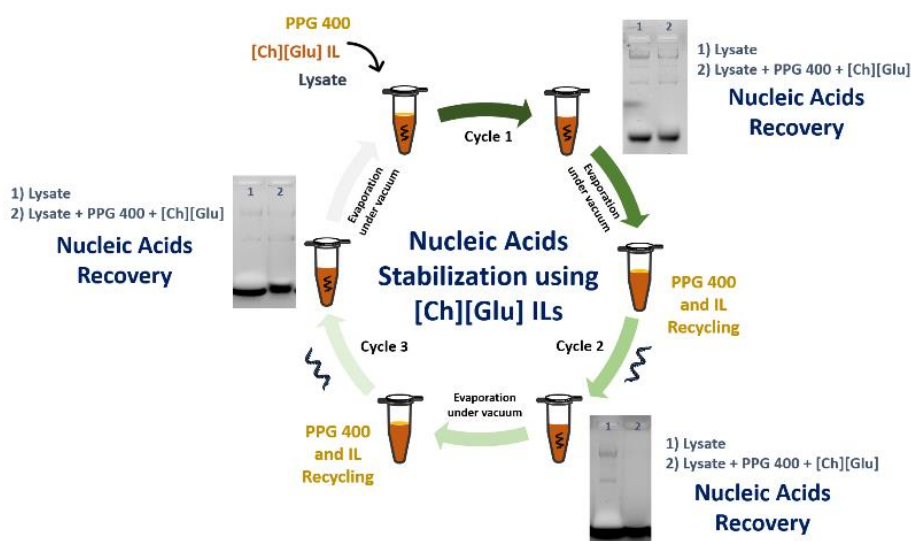


Figure 4.2.6 Agarose gel electrophoresis of the ABS coexisting phases at the mixture point: 20 wt% of PPG 400 + 20 wt% of AA-IL + 60 wt% of RNA in DEPC-treated water ($400 \mu\text{g}\cdot\text{L}^{-1}$). RNA in 0.05 % DEPC-treated water was used as control sample and a marker is also included.

Figure 4.2.7 depicts a schematic overview of the proposed integrated extraction-preservation process for RNA, targeting its use as biopharmaceuticals. To the best of our knowledge, this is the first study that successfully reports the development of an integrated extraction-preservation platform for RNA bioprocessing resorting to IL-based ABS.

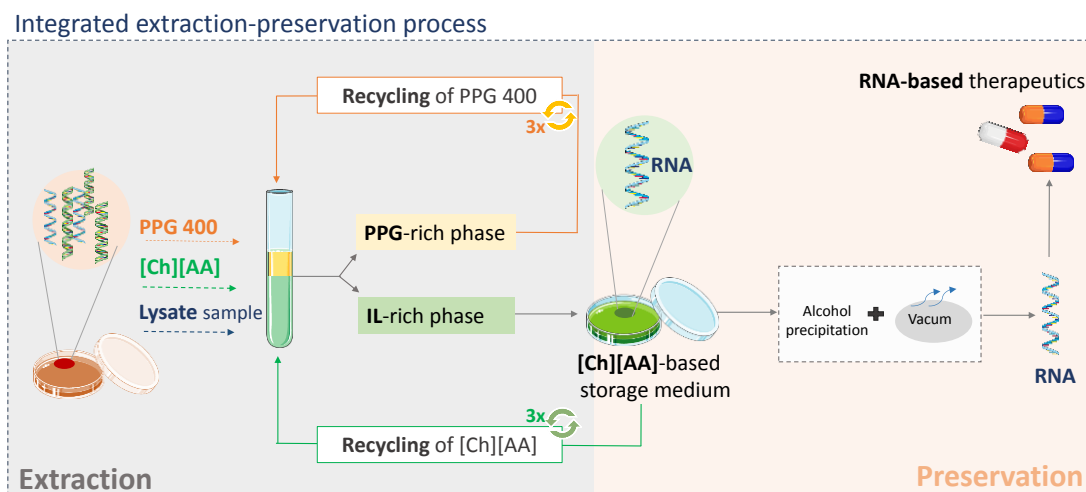


Figure 4.2.7 Schematic diagram of the proposed integrated extraction-preservation process of RNA, where all steps occur at *ca.* 25 °C, while foreseeing its use as biotherapeutic.

Conclusions

Based on the use of amino-acid-based chromatographic ligands in the purification of nucleic acids, in this work we propose the use of amino-acid-based ILs as phase-forming components of ABS to carry out the RNA extraction from original and complex matrices, followed by the use of the IL-rich phase as preservation medium of the biopolymer up to use.

The studied ABS allow the extraction of RNA from complex samples, without compromising its integrity. Further, the IL-rich phase can be used as the preservation medium, allowing to keep the RNA integrity and stability at temperatures close to room temperature, thus avoiding the need for freezing RNA-containing samples. The use of aqueous solutions of non-volatile ILs as RNA preservation media further eliminates volatile organic solvent losses to the atmosphere, decreasing both the environmental footprint and the cost of the process. Both features are also improved by the demonstrated possibility of recycling the ABS phase-forming components. Furthermore, the studied ILs display low cytotoxicity to human cell lines, supporting their use in biopharmaceutical applications. In summary, integrated and sustainable extraction-preservation process for nucleic acids can be designed by the application of adequate IL-based ABS, strongly contributing to the current critical demand of high-quality/high-purity biotherapeutics.

References

1. S. C. Tan and B. C. Yiap, J. J. Biomed. Biotechnol., 2009, 2009, 1-10.
2. J. Lieberman, Nat. Struct. Mol., 2018, 25, 357-364.
3. H. T. Karimata and N. Sugimoto, Biophys. Rev., 2018, 10, 931-940.
4. L. Baronti, H. Karlsson, M. Marusic and K. Petzold, Anal. Bioanal. Chem., 2018, 410, 3239-3252.
5. B. K. Muralidhara, R. Baid, S. M. Bishop, M. Huang, W. Wang and S. Nema, Drug Discov. Today, 2016, 21, 430-444.
6. P. Y. Ho and A. M. Yu, Wiley Interdiscip. Rev. RNA, 2016, 7, 186-197.
7. K. S. Kirby, Biochem. J., 1965, 96, 266-269.
8. P. Chomczynski and N. Sacchi, Nature protocols, 2006, 1, 581-585.
9. R. M. McCormick, Anal. Biochem., 1989, 181, 66-74.
10. R. Martins, J. A. Queiroz and F. Sousa, J. Chrom. A, 2014, 1355, 1-14.
11. F. S. Hagen and E. T. Young, Biochem., 1974, 13, 3394-3400.
12. P. Pereira, J. A. Queiroz, A. Figueiras, F. Sousa, J. Chrom. B., 2016, 1021, 45-56.
13. M. Taha, F. Silva, M. V. Quental, S.P.M. Ventura, M. G. Freire, J. A. P. Coutinho, Green Chem., 2014, 16, 3149-3159.
14. A. Beneditto, P. Ballone, ACS Sustain. Chem, 2016, 4, 392-412.
15. R. R. Mazid, U. Divisekera, W. Yang, V. Ranganathan, D. R. MacFarlane, C. Cortez-Jugo and W. Cheng, Chem. Comm., 2014, 50, 13457-13460.
16. I. Mamajanov, A. E. Engelhart, H. D. Bean and N. V. Hud, Angew. Chem., 2010, 49, 6310-6314.
17. S. Fister, S. Fuchs, P. Mester, I. Kilpeläinen, M. Wagner and P. Rossmanith, Sep. Sci. Technol., 2015, 155, 38-44.
18. M. G. Freire, A. F. M. Claudio, J. M. M. Araujo, J. A. P. Coutinho, I. M. Marrucho, J. N. C. Lopes and L. P. N. Rebelo, Chem. Soc. Rev., 2012, 41, 4966-4995.
19. J. Hulsbosch, D. E. Vos, K. Binnemans, R. Ameloot, ACS Sustain. Chem., 2016, 4, 2917-2931.
20. K. Fukumoto, M. Yoshizawa, H. Ohno, J. Am. Chem. Soc., 2005, 127, 2398-2399.
21. G. H. Tao, L. He, W. Liu, L. Xu, W. Xiong, T. Wanga, Y. Kou, Green Chem., 2006, 639-646.
22. S. Bhattacharyya and F. U. Shah, J. Mol. Liq., 2018, 266, 597-602.
23. A. Foulet, O. B. Ghanem, M. El-Harbawi, J. M. Lévêque, M. I. A. Mutalib and C. Y. Yin, J. Mol. Liq., 2016, 221, 133-138.
24. R. Wang, Y. Chang, Z. Tan and F. Li, J. Mol. Liq., 2016, 222, 836-844.
25. C. P. Song, R. N. Ramanan, R. Vijayaraghavan, D. R. MacFarlane, E. S. Chan and C. W. Ooi, ACS Sustain. Chem. Sustain. Chem., 2015, 3, 3291-3298.
26. D. Sun, R. Wang, F. Li, L. Liu and Z. Tan, Processes, 2018, 6, 212.
27. J. Iwakiri, H. Tateishi, A. Chakraborty, P. Patil and N. Kenmochi, Nucleic Acids Res., 2012, 40, 3299-3306.
28. P. Pereira, Â. Sousa, J. Queiroz, I. Correia, A. Figueiras and F. Sousa, J. Chrom. B, 2014, 951-952, 16-23.
29. P. Pereira, Â. Sousa, J. Queiroz, A. Figueiras and F. Sousa, J. Chrom. A, 2014, 1331, 129-132.
30. S. H. Baharuddin, N. A. Mustahil, A. A. Abdullah, M. Sivapragasam, M. Moniruzzaman, Procedia Eng., 2016, 148, 401-408.
31. J. Carvalho, T. Quintela, N. M. Gueddouda, A. Bourdoncle, J. L. Mergny, G. F. Salgado, J. A. Queiroz and C. Cruz, Org. Biomol. Chem., 2018, 16, 2776-2786.
32. J. Carvalho, J. Ferreira, P. Pereira, E. Coutinho, A. Guédin, P. Nottelet, G. F. Salgado, J. L. Mergny, J. A. Queiroz, F. Sousa, E. J. Cabrita and C. Cruz, Tetrahedron, 2016, 72, 1229-1237.
33. G. Brooks, Biotechnology in Healthcare: An Introduction to Biopharmaceuticals, Pharmaceutical Press, 1998.
34. M. R. Green and J. Sambrook, Cold Spring Harbor protocols, 2016.
35. S. W. Salyer, Essential Emergency Medicine, W.B. Saunders, 2007.
36. F. Haque, F. Pi, Z. Zhao, S. Gu, H. Hu, H. Yu and P. Guo, Wiley Interdiscip. Rev. RNA, 2018, 9, e1452.
37. Y. Wan, K. Qu, Z. Ouyang, M. Kertesz, J. Li, R. Tibshirani, D. L. Makino, R.C. Nutter, E. Segal and H. Y. Chang, Mol. Cell, 2012, 48, 169-181.
38. A. Q. Pedro, P. Pereira, M. V. Quental, P. Carvalho, S. M. Santos, J. A. Queiroz, F. Sousa, M. G. Freire, ACS Sustain. Chem. Eng., 2018, 6, 16645-16656.
39. X. D. Hou, Q. P. Liu, T. J. Smith, N. Li and M. H. Zong, PloS one, 2013, 8, e59145.
40. L. Buckingham, Molecular Diagnostics: Fund., Meth. Clin. Applic., F.A. Davis Company, 2012.
41. L. D. Olmo, I. L. Estebanez, R. López and J. M. G. Vega, J. Phys. B, 2016, 120, 10327-10335.
42. C. C. Ramalho, C. M. Neves, M. V. Quental, J. A. Coutinho and M. G. Freire, J. Chem. Technol. Biot., 2018, 93, 1931-1939.
43. M. Taha, M. R. Almeida, F. A. Silva, P. Domingues, S. P. Ventura, J. A. Coutinho and M. G. Freire, Chemistry, 2015, 21, 4781-4788.

5. Final remarks & future work

This thesis was focused on the potential of aqueous solutions of ILs and IL-based ABS for the stabilization, extraction and purification of different bioactive molecules. The design of cost-effective, sustainable and integrated preservation-recovery strategies was the major goal of this work. In Chapter 2.1 we took a step forward in the development of sustainable IL-based ABS by proving the use of tetraalkylammonium- and tetraalkylphosphonium-based ILs combined with carbohydrates to create ABS, avoiding the use of ILs comprising aromatic cations or fluorinated anions. These systems were demonstrated to have a high extraction performance for antioxidants, namely phenolic acids. Finally, the recovery of the phenolic acids from the IL-rich phase was carried out, allowing to recycle the employed IL without losses on the ABS extraction performance. In Chapter 2.2, still envisioning the sustainable character of IL-based ABS, IL-based ABS were created with aliphatic amino acids, demonstrating the possibility of using these systems for the separation of aromatic and aliphatic amino acids. A final solid-phase extraction was applied to recover amino acids from the IL-rich phase, allowing the IL to be recycled. In addition to simple molecules, IL-based ABS were further investigated as separation platforms for proteins from complex matrices. In Chapter 3.1, a novel class of ILs with self-buffering properties, namely GB-ILs, were used to create ABS with potassium citrate to carry out the extraction of BSA. Both extractions with the commercial protein and from bovine serum samples were carried out, allowing to increase the purity of BSA at the IL-rich phase. The protein structure was finally evaluated by spectroscopic assays. Still dealing with proteins, Chapter 3.2 refers to the use of bio-based ILs combined with PPG 400 for the extraction and purification of a high cost antibody, namely IgG. Assays with both the pure protein and with rabbit serum samples were carried out. Even in the presence of a high complex matrix, these systems maintained the extraction efficiency of 100% of IgG, although with a small compromise in the recovery yield (85%). The purity of the antibody increased by 58% in respect to the original sample, without compromising its stability. The last set of works presented are focused on the use of ILs aqueous solutions and IL-based ABS for the preservation and purification of RNA. Chapter 4.1 shows that cholinium-based ILs with self-buffering characteristics are enhanced media to preserve a recombinant *E. coli* sRNA fraction containing pre-miRNA. Among all the ILs tested, [Ch][MES] and [Ch][HEPES] show to be the most adequate solvents for this purpose, being able to improve the RNA stability after a 30-day period of incubation at 4° C and at room temperature. These ILs were also characterized as non-cytotoxic to human cell lines. Finally, RNA was recovered without comprising its integrity, and the IL recycled. Proved the possibility of using ILs aqueous solutions as RNA preservation media, the development of an integrated extraction-preservation strategy was accomplished. In Chapter 4.2 amino-acid-based ILs were

chosen due to the use of amino acids as ligands in chromatographic columns for RNA capture, and combined with PPG 400 to form ABS. All IL-based ABS allowed the RNA complete extraction to the IL-rich phase, although [Ch][Glu] and [Ch][Asp] proved to be the most suitable ILs to be used as ABS constituents for the remaining assays due to the observed RNA thermal stability enhancements. After the extraction of RNA from a bacterial lysate sample, the IL-rich phase can be used as the preservation media. Finally, it was proved that RNA can be recovered by induced precipitation with alcohols and the IL recycled.

Overall, a set of novel IL-based ABS was investigated in this thesis, demonstrating to be promising alternatives to extract, purify and preserve a series of compounds with relevant biological activities. Despite the promising results here disclosed, future work in this line of research should include:

- Research on new biological sources for ILs synthesis;
- Application of bio-based ILs as adjuvants in conventional polymer-polymer or polymer-salt ABS, not only to reach higher purification factors, but also due to the lower cost of these systems;
- Extension of similar studies to other complex matrices enriched in value-added compounds, like biomass extracts, cell culture media, fermentation broths, among others;
- Development of integrated strategies combining ILs aqueous solutions used in the extraction of value-added compounds from their natural sources (*e.g.* biomass extracts, cell culture media, fermentation broths) combined with their direct use in the formation of ABS for the purification step;
- Application of centrifugal partition chromatography (CPC) to enhance the separation performance and guarantee the scale-up of the developed processes.

List of publications

List of publications in the thesis

1. **Maria V. Quental**, Augusto Pedro, Patrícia Pereira, André Carvalho, João A. Queiroz, Fani Sousa and Mara G. Freire, "Integrated extraction-preservation strategies for RNA using bio-based ionic liquids". *ACS Sustainable Chemistry and Engineering*, 2019, 7, 10, 9439-9448.
2. Augusto Pedro, Patrícia Pereira, **Maria V. Quental**, André Carvalho, Sergio M. Santos, João A. Queiroz, Fani Sousa and Mara G. Freire, "Cholinium-Based Good's Buffers Ionic Liquids as Remarkable Stabilizers and Recyclable Preservation media for Recombinant Small RNAs". *ACS Sustainable Chemistry and Engineering*, 2018, 6, 12, 16645–16656.
3. **Maria V. Quental**, Matheus M. Pereira, Ana M. Ferreira, Sónia N. Pedro, Shahla Shahriari, Aminou Mohamadou, João A. P. Coutinho and Mara G. Freire, "Aqueous Biphasic Systems formed by Carbohydrates and non-Aromatic and non-Fluorinated Ionic Liquids: Competitive Separation Platforms". *Green Chemistry*, 2018, 20, 13, 2978–2983.
4. Emanuel V. Capela[§], **Maria V. Quental**[§], Pedro Domingues, João A. P. Coutinho and Mara G. Freire, "Effective separation of aromatic and aliphatic amino acid mixtures using ionic-liquid-based aqueous biphasic systems". *Green Chemistry*, 2017, 19, 8, 1850-1854, (§equal contribution), Green Chemistry Hot Articles and International Symposium on Green Chemistry 2017.
5. Mohamed Taha[§], **Maria V. Quental**[§], Francisca A. e Silva, Emanuel V. Capela, Mara G. Freire, Sónia P. M. Ventura and João A. P. Coutinho, "Good's Buffer Ionic Liquids as Relevant Phase-Forming Components of Self-Buffered Aqueous Biphasic Systems". *Journal of Chemical Technology and Biotechnology*, 2017, 92, 9, 2287-2299, (§equal contribution).
6. Dibyendu Mondal, Mukesh Sharma, **Maria V. Quental**, Ana P. M. Tavares, Kamalash Prasad and Mara G. Freire, "Suitability of bio-based ionic liquids for the extraction and purification of IgG antibodies". *Green Chemistry*, 2017, 18, 22, 6071–6081.

Other publications

1. Helena Passos, Teresa B. V. Dinis, Emanuel V. Capela, **Maria V. Quental**, Joana Gomes, Judite Resende, Pedro P. Madeira, Mara G. Freire and João A. P. Coutinho, "Mechanisms Ruling the Partition of Solutes in Ionic-Liquid-Based Aqueous Biphasic Systems – the Multiple Effects of Ionic Liquids". *Physical Chemistry Chemical Physics*, 2018, 20, 13, 8411 - 8422.
2. Catarina C. Ramalho, Catarina M. S. S. Neves, **Maria V. Quental**, João A. P. Coutinho and Mara G. Freire, "Separation of Immunoglobulin G Using Aqueous Biphasic Systems Composed of Cholinium-Based Ionic Liquids and Poly(Propylene Glycol)". *Journal of Chemical Technology and Biotechnology*, 2018, 93, 7, 1931-1939.

3. Sónia P. M. Ventura, Francisca A. e Silva, **Maria V. Quental**, Dibyendu Mondal Mara G. Freire and João A. P. Coutinho, "Ionic-Liquid-Mediated Extraction and Separation Processes for Bioactive Compounds: Past, Present, and Future Trends". ACS Sustainable Chemistry & Engineering, 2017, 117, 10, 6984–7052.
4. Jorge Fernando Brandão Pereira, Agnes Magri, **Maria V. Quental**, Maria Gonzalez-Miquel, Mara G. Freire and Joao A.P. Coutinho, "Alkaloids as Alternative Probes to Characterize the Relative Hydrophobicity of Aqueous Biphasic Systems". ACS Sustainable Chemistry & Engineering, 2016, 4, 3, 1512–1520.
5. **Maria V. Quental**, Helena Passos, Kiki A. Kurnia, João A. P. Coutinho, and Mara G. Freire, "Aqueous Biphasic Systems Composed of Ionic Liquids and Acetate-Based Salts: Phase Diagrams, Densities, and Viscosities". The Journal of Chemical Engineering Data, 2015, 60, 6, 1674–1682.
6. **Maria V. Quental**, Magda Caban, Matheus M. Pereira, Piotr Stepnowski, João A. P. Coutinho and Mara G. Freire, "Enhanced Extraction of Proteins Using Cholinium-Based Ionic Liquids as Phase-Forming Components of Aqueous Biphasic Systems". Biotechnology Journal, 2015, 10, 9, 1457–1466.
7. Matheus M. Pereira, Sónia N. Pedro, **Maria V. Quental**, Álvaro S. Lima, João A.P. Coutinho and Mara G. Freire, "Enhanced Extraction of Bovine Serum Albumin with Aqueous Biphasic Systems of Phosphonium- and Ammonium-Based Ionic Liquids". Journal of Biotechnology, 2016, 4, 206, 17-25.
8. Mohamed Taha, **Maria V. Quental**, Isabel Correia, Mara G. Freire and João A.P. Coutinho, "Extraction and Stability of Bovine Serum Albumin (BSA) using Cholinium-Based Good's Buffers Ionic Liquids". Green Chemistry, 2015, 50, 7, 1158–1166.
9. Kiki A Kurnia, **Maria V. Quental**, Luis B. Santos, Mara G. Freire and João A.P. Coutinho, "Mutual solubilities between water and non-aromatic sulfonium-, ammonium- and phosphonium-hydrophobic ionic liquids". Separation and Purification Technology, 2015, 17, 6, 4569 - 4577.
10. Mohamed Taha, Francisca A e Silva, **Maria V. Quental**, Mara G. Freire, Sónia P.M. Ventura and João AP Coutinho, "Good's buffers as a basis for developing selfbuffering and biocompatible ionic liquids for biological research". Green Chemistry, 2014,16, 6, 3149–3159.

Appendix A

A1.

Table A.1.1 Non-forming ABS composed of carbohydrates (CHs) and ionic liquids (ILs).

CHs	IL
D-(+)-maltose	[P ₄₄₄₄]Br
D-(+)-glucose	
D-(+)-xylose	
Sucrose	[P ₄₄₄₄]Cl
	[P ₍₄₄₄₁₎₁][MeSO ₄]
D-(+)-glucose	[P ₄₄₄ (OC ₂)]Br
D-(+)-mannose	
D-(+)-maltose	

Table A.1.2 Experimental weight fraction data for the ABS formed by [P₄₄₄₄]Br (w_1) + D-(-)-CH (w_2) + H₂O at 25 °C and atmospheric pressure.

D-(-)-fructose						Sucrose		Maltitol		Xylitol		D-sorbitol	
w_1	w_2	w_1	w_2	w_1	w_2	w_1	w_2	w_1	w_2	w_1	w_2	w_1	w_2
75.65	11.18	36.52	29.29	24.44	36.63	57.90	16.94	44.66	26.96	57.06	21.39	48.19	13.28
73.62	12.09	35.82	29.66	24.10	36.74	56.29	18.09	49.94	23.90	54.36	22.61	44.69	17.35
70.90	13.39	35.15	30.01	23.79	36.84	51.04	18.99	42.38	28.22	42.95	26.65	43.09	17.97
67.42	14.66	34.25	30.74	23.26	36.78	47.78	20.73	37.72	29.69	42.63	27.18	37.71	24.76
64.34	15.63	32.77	31.41	22.96	37.00	45.01	21.37	37.59	29.80	36.45	30.92	34.74	27.40
62.54	16.88	32.03	31.93	22.86	36.99	42.29	23.22	32.69	35.17	33.30	34.49	30.74	33.26
59.88	17.67	30.80	32.59	22.55	37.13	40.19	24.52	28.96	38.78	25.12	40.48	27.95	37.48
57.78	18.06	30.28	32.73	21.87	38.12	38.99	25.0			24.85	40.71	22.15	47.87
55.52	19.02	29.39	33.60	21.63	38.24	38.39	25.04					20.50	52.82
53.88	20.00	28.70	33.85	21.240	38.63	37.83	25.54						
52.09	20.84	28.19	34.12	20.99	38.75	37.72	26.22						
47.42	22.71	27.39	34.74	20.73	38.99	29.89	30.88						
46.17	23.49	26.97	35.02	20.30	39.30								
44.87	24.32	26.41	35.16	20.08	39.42								
43.56	25.21	25.96	35.47										
42.51	25.87	25.61	35.75										
41.41	26.53	25.08	36.26										
40.60	27.04	24.72	36.46										
39.47	27.26	24.44	36.63										
38.54	27.83	24.101	36.74										
37.81	28.19	23.79	36.84										

Table A.1.3 Experimental weight fraction data for the ABS formed by IL (w_1) + D-(-)-fructose (w_2) + H₂O at 25 °C and atmospheric pressure.

[P ₄₄₄ (OC ₂)]Br				[P ₄₄₄₁][MeSO ₄]	
w ₁	w ₂	w ₁	w ₂	w ₁	w ₂
67.24	23.58	19.39	44.13	83.97	4.16
66.47	24.12	18.69	45.08	74.93	11.00
59.63	25.86	18.09	45.21	74.58	11.86
53.39	26.97	17.73	45.58	61.66	20.57
53.33	27.80	17.39	45.86	61.58	20.78
46.78	29.74	16.36	46.53	56.19	23.98
46.22	31.80	16.29	46.81	51.99	26.95
41.33	32.91	14.99	47.91	45.85	31.27
35.56	35.90	14.32	48.40	40.76	35.33
35.48	36.45	13.69	49.40	37.18	37.82
32.49	37.45	13.30	49.47	28.92	41.74
32.13	37.71	12.79	49.69		
29.74	39.13	11.91	50.74		
29.10	39.18	10.34	52.81		
28.34	39.32	10.31	53.41		
26.77	40.34	9.46	54.66		
26.01	40.62	8.94	54.97		
24.99	40.77				
24.48	41.47				
23.42	41.54				
22.58	42.40				
21.52	42.62				
20.89	43.24				
20.45	43.27				

Table A.1.4 Experimental weight fraction data for the ABS formed by IL (w₁) + D-(-)-fructose (w₂) + H₂O at 25 °C and atmospheric pressure.

[N ₄₄₄₄]Br		[N ₄₄₄ (OC ₂)]Br	
w ₁	w ₂	w ₁	w ₂
58.02	22.92	56.61	28.57
44.12	31.36	52.81	30.78
39.42	34.63	31.22	43.25
34.05	38.68	27.85	45.55
30.08	41.57	24.16	49.26
27.07	43.79	19.30	54.61
23.95	46.25		

Table A.1.5 Experimental weight fraction data for the ABS formed by IL (w₁) + D-(-)-fructose (w₂) + H₂O at 25 °C and atmospheric pressure.

[P ₄₄₄₄][Oct]		[P ₄₄₄₄][Hex]		[P ₄₄₄₄][But]	
w ₁	w ₂	w ₁	w ₂	w ₁	w ₂
43.09	38.20	52.90	31.66	46.51	38.19
28.76	42.82	41.07	38.16	28.83	46.80
16.81	50.77	35.14	40.23	25.88	47.66
19.92	49.59	28.06	42.73	21.73	49.92
18.46	50.01	26.81	43.42		
16.81	50.77	20.72	46.85		
		18.70	48.01		

Table A.1.6 Experimental weight fraction data for the ABS formed by [P₄₄₄₄]Br (w₁) + D-(-)-fructose (w₂) + H₂O at different temperatures: 15, 35, 45 °C, and atmospheric pressure.

15 °C		35 °C		45 °C	
w ₁	w ₂	w ₁	w ₂	w ₁	w ₂
47.66	22.19	39.20	29.03	47.60	23.41
44.95	23.67	46.80	23.02	43.90	25.24
39.56	26.65	43.57	25.05	41.64	26.56
37.07	28.09	41.30	26.35	36.46	30.75
34.50	29.61	36.03	30.39		

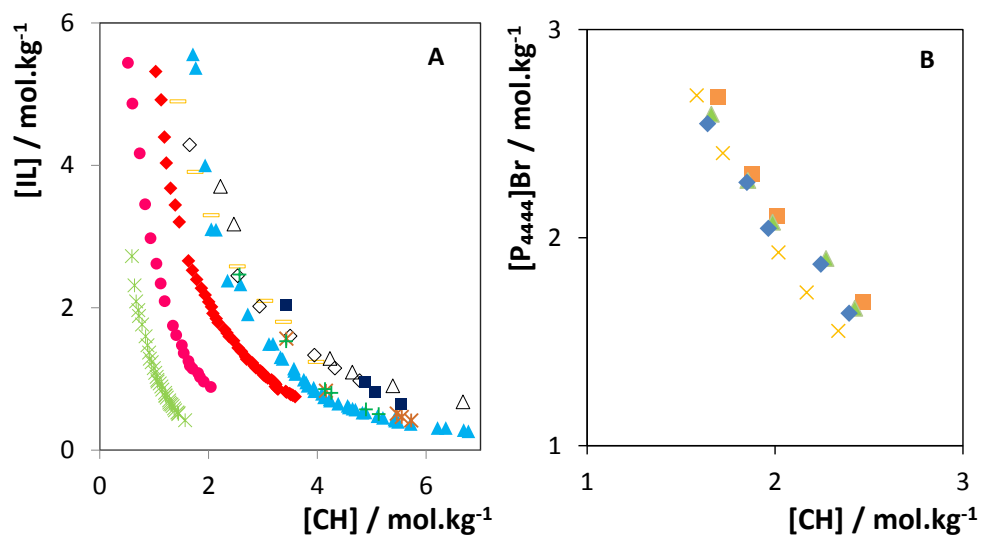


Figure A.1.1 A) Ternary phase diagrams for ABS formed by ILs and D-(-)-fructose at 25 °C and atmospheric pressure (in molality units): [C₂C₁py][C₄F₉SO₃] (x)¹; [C₄mim][CF₃SO₃] (•)²; [P₄₄₄₄]Br (♦); [P₄₄₄(OC₂)]Br (▲); [P₄₄₄₄][Oct] (★); [P₄₄₄₄][Hex] (+); [P₄₄₄₄][But] (■); [P₄₄₄₁][MeSO₄] (–); [N₄₄₄₄]Br (◇); [N₄₄₄(OC₂)]Br (Δ). **B)** Ternary phase diagrams for ABS formed by [P₄₄₄₄]Br and D-(-)-fructose at different temperatures and atmospheric pressure (in molality units): 15 °C (x), 25 °C (♦), 35 °C (▲) and 45 °C (■).

Table A.1.7 *A*, *B* and *C* parameters of the equation proposed by Merchuk et al.³ and respective correlation coefficients, R^2 , for the ABS formed by ILs + CH + H₂O at 25 °C and atmospheric pressure.

ABS					
IL	CHs	$A \pm \sigma$	$B \pm \sigma$	$10^5 (C \pm \sigma)$	R^2
[P ₄₄₄₄]Br	sucrose	392 ± 53	-0.47 ± 0.06	0.19 ± 0.27	0.950
	D-sorbitol	266 ± 35	-0.35 ± 0.02	0.47 ± 0.01	0.999
	maltitol	121 ± 29	-0.04 ± 0.00	0.00 ± 0.00	0.970
	xylitol	141 ± 18	-0.04 ± 0.01	0.00 ± 0.00	0.990
[P ₄₄₄₁][MeSO ₄]	D-(-)-fructose	124 ± 6	-0.16 ± 0.01	1.41 ± 0.09	0.999
		107 ± 34	-0.11 ± 0.08	0.93 ± 0.41	0.999
		230 ± 40	-0.25 ± 0.04	0.95 ± 0.75	0.999
		629 ± 278	-0.07 ± 0.01	0.00 ± 0.00	0.989
[P ₄₄₄ (OC ₂)]Br	D-(-)-fructose	359 ± 174	-0.06 ± 0.01	0.00 ± 0.00	0.966
[P ₄₄₄₄][Oct]		673 ± 411	-0.07 ± 0.01	0.00 ± 0.00	0.995
[P ₄₄₄₄][Hex]		137 ± 8E ⁻⁶	-0.17 ± 0.01	0.57 ± 0.05	0.950
[N ₄₄₄₄]Br		490 ± 2E ⁻⁶	-0.39 ± 0.01	0.21 ± 0.05	0.950
[N ₄₄₄ (OC ₂)]Br					

Table A.1.8 Weight fraction compositions for the IL + CH + H₂O systems at 25 °C, and respective values of tie-line length (TLL). Initial mixture compositions are represented as [CH]_M and [IL]_M whereas [CH]_{CH} and [IL]_{CH} are the composition of IL and carbohydrate at the IL-rich phase, respectively, and vice-versa.

IL	CHs	Weight fraction composition / wt%								
		[IL] _{IL}	[CH] _{IL}	pH	[IL] _M	[CH] _M	[IL] _{CH}	[CH] _{CH}	pH	TLL
[P ₄₄₄₄]Br	sucrose	58.47	16.57	1.52	39.83	35.13	20.02	54.88	1.57	54.27
	D-sorbitol	66.60	15.24	1.42	39.92	34.54	7.22	58.21	1.35	48.60
	maltitol	57.73	20.54	1.46	36.88	34.87	24.2	43.60	1.34	40.71
	xylitol	58.03	21.58	1.29	40.10	34.85	17.47	52.06	1.25	51.96
[P ₄₄₄₁][MeSO ₄]	D-(-)-fructose	89.09	3.93	2.20	24.88	49.6	0.51	66.72	1.95	109.28
		84.65	4.83	1.70	25.02	49.82	2.92	66.49	1.62	102.38
		79.09	17.01	4.01	25.12	50.03	2.69	63.75	3.92	89.56
		77.12	10.67	2.15	24.95	49.99	8.99	62.02	2.30	85.30
[N ₄₄₄₄]Br	D-(-)-fructose	42.47	35.76	4.67	25.03	50.11	17.92	55.98	3.95	31.81
[N ₄₄₄ (OC ₂)]Br										
[C ₄ mim][CF ₃ SO ₃]	sucrose	84.28	2.14	6.61	25.13	49.87	0.05	70.10	6.65	108.22
	D-sorbitol	96.08	0.16	6.68	24.95	49.80	0.00	66.51	6.67	115.64

Table A.1.9 Extraction efficiencies (*EE*%) and partition coefficients (*K*) of phenolic acids to the IL-rich phase at 25 °C.

ABS		Phenolic acids		
		VA	GA	SA
[P ₄₄₄₄]Br + sucrose	<i>EE</i> /%	94.2 ± 0.2	99.3 ± 0.0	96.5 ± 0.1
	<i>K</i>	14.0 ± 0.6	95.3 ± 1.2	34.6 ± 0.5
[P ₄₄₄₄]Br + D-sorbitol	<i>EE</i> /%	95.9 ± 0.4	99.1 ± 0.0	96.8 ± 0.7
	<i>K</i>	16.4 ± 1.0	92.7 ± 2.8	24.5 ± 2.9
[P ₄₄₄₄]Br + xylitol	<i>EE</i> /%	94.2 ± 0.1	96.6 ± 0.3	91.6 ± 2.4
	<i>K</i>	14.2 ± 0.1	15.1 ± 1.4	9.1 ± 1.8
[P ₄₄₄₄]Br + maltitol	<i>EE</i> /%	96.1 ± 0.6	98.3 ± 0.0	96.5 ± 0.4
	<i>K</i>	13.8 ± 0.2	29.3 ± 0.0	13.4 ± 2.0
[P ₄₄₄₄]Br + D-(-)-fructose	<i>EE</i> /%	95.6 ± 0.4	98.1 ± 0.6	93.7 ± 0.1
	<i>K</i>	58.9 ± 0.1	144.7 ± 42.2	40.6 ± 0.4
[P ₄₄₄₁][MeSO ₄] + D-(-)-fructose	<i>EE</i> /%	95.9 ± 0.0	94.5 ± 1.6	93.8 ± 1.5
	<i>K</i>	45.1 ± 0.2	41.5 ± 8.9	37.4 ± 4.1
[P ₄₄₄ (OC ₂)]Br + D-(-)-fructose	<i>EE</i> /%	72.0 ± 0.4	72.8 ± 2.2	65.1 ± 3.0
	<i>K</i>	6.4 ± 0.1	5.4 ± 0.4	3.6 ± 0.5
[N ₄₄₄₄]Br + D-(-)-fructose	<i>EE</i> /%	90.4 ± 0.5	86.7 ± 1.0	87.7 ± 1.0
	<i>K</i>	30.7 ± 1.8	21.4 ± 1.9	23.4 ± 1.0
[N ₄₄₄ (OC ₂)]Br + D-(-)-fructose	<i>EE</i> /%	81.5 ± 3.3	70.8 ± 3.9	82.7 ± 1.7
	<i>K</i>	11.5 ± 2.4	6.1 ± 1.1	11.9 ± 1.4
[C ₄ mim][CF ₃ SO ₃] + Sucrose	<i>EE</i> /%	6.7 ± 1.1	6.7 ± 0.7	12.2 ± 0.2
	<i>K</i>	0.2 ± 0.0	0.2 ± 0.0	0.4 ± 0.0
[C ₄ mim][CF ₃ SO ₃] + D-sorbitol	<i>EE</i> /%	29.6 ± 4.1	8.5 ± 0.7	33.4 ± 1.6
	<i>K</i>	1.1 ± 0.2	0.2 ± 0.0	1.3 ± 0.0
[P ₄₄₄₄]Br + C ₆ H ₅ K ₃ O ₇	<i>EE</i> /%	99.0 ± 0.1	86.6 ± 0.3	98.5 ± 0.1
	<i>K</i>	267.6 ± 8.8	17.3 ± 0.4	175.7 ± 8.9

Table A.1.10 Extraction efficiencies ($EE\%$) and partition coefficient (K) of phenolic acids to the IL-rich phase in $[P_{4444}]Br$ -based ABS at 25 °C at different pH values.

		Phenolic acids		
		VA	GA	SA
D-(-)-fructose pH 5	$EE/\%$	86.6 ± 0.5	85.9 ± 2.2	78.9 ± 3.7
	K	16.1 ± 0.8	18.8 ± 4.1	15.5 ± 0.3
D-(-)-fructose pH 6	$EE/\%$	45.8 ± 6.0	79.3 ± 0.3	74.5 ± 0.7
	K	2.7 ± 1.0	9.5 ± 0.2	7.3 ± 0.3
D-sorbitol pH 5	$EE/\%$	97.7 ± 0.2	94.5 ± 0.2	86.0 ± 2.0
	K	31.1 ± 3.2	13.0 ± 0.4	7.9 ± 0.5
D-sorbitol pH 6	$EE/\%$	85.0 ± 3.1	76.6 ± 3.6	54.3 ± 1.3
	K	7.8 ± 0.1	4.5 ± 0.9	1.5 ± 0.1

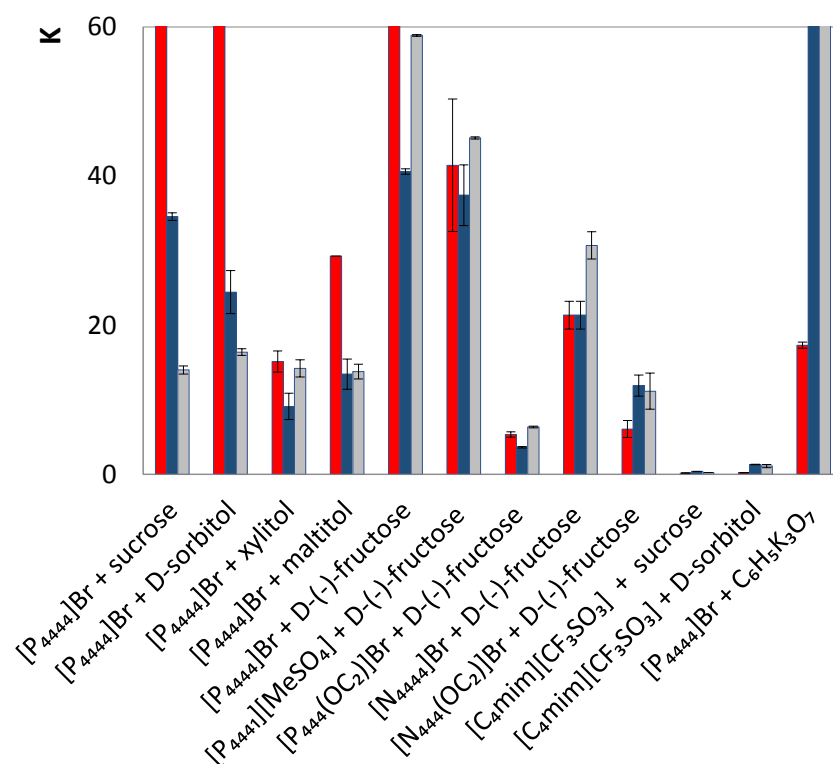


Figure A.1.2 Partition coefficients of phenolic acids (K) in the studied systems at 25°C. ■ ■ ■ correspond to gallic acid (GA), syringic acid (SA) and vanillic acid (VA), respectively.

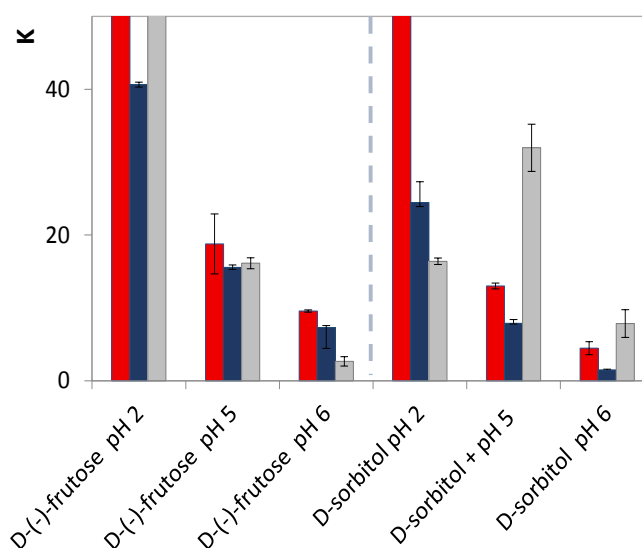


Figure A.1.3 Partition coefficients (K) of the studied systems for phenolic acids in the ABS formed by $[P_{4444}]\text{Br} + \text{CH} + \text{H}_2\text{O}$ at 25°C , at different pH values. ■ ■ ■ correspond to gallic acid (GA), syringic acid (SA) and vanillic acid (VA), respectively.

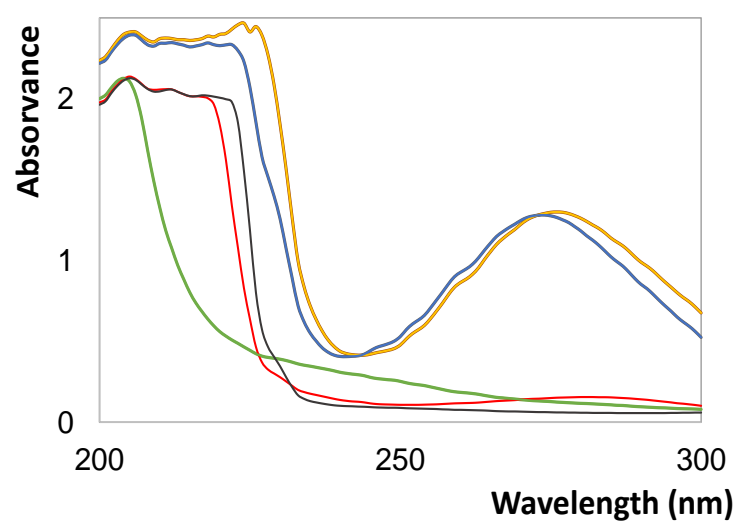


Figure A.1.4 UV-Vis spectra of the different fractions obtained in the SPE experiment. SPE1 fraction (—), SPE2 fraction (—), SPE3 fraction (—), SPE4 fraction (—), and initial IL-rich phase containing gallic acid (—).

References

1. A. M. Ferreira, P. D. O. Esteves, I. B. Palheiros, A. B. Pereiro, L. P. N. Rebelo and M. G. Freire, *Green Chem.*, 2016, 18, 1070-1079.
2. M. G. Freire, C. L. S. Louros, L. P. N. Rebelo and J. A. P. Coutinho, *Green Chem.*, 2011, 13, 1536-1545.
3. J. C. Merchuk, B. A. Andrews and J. A. Asenjo, *J. Chromatogr. B Biomed. Sci. Appl.*, 1998, 711, 285-293.

A2.

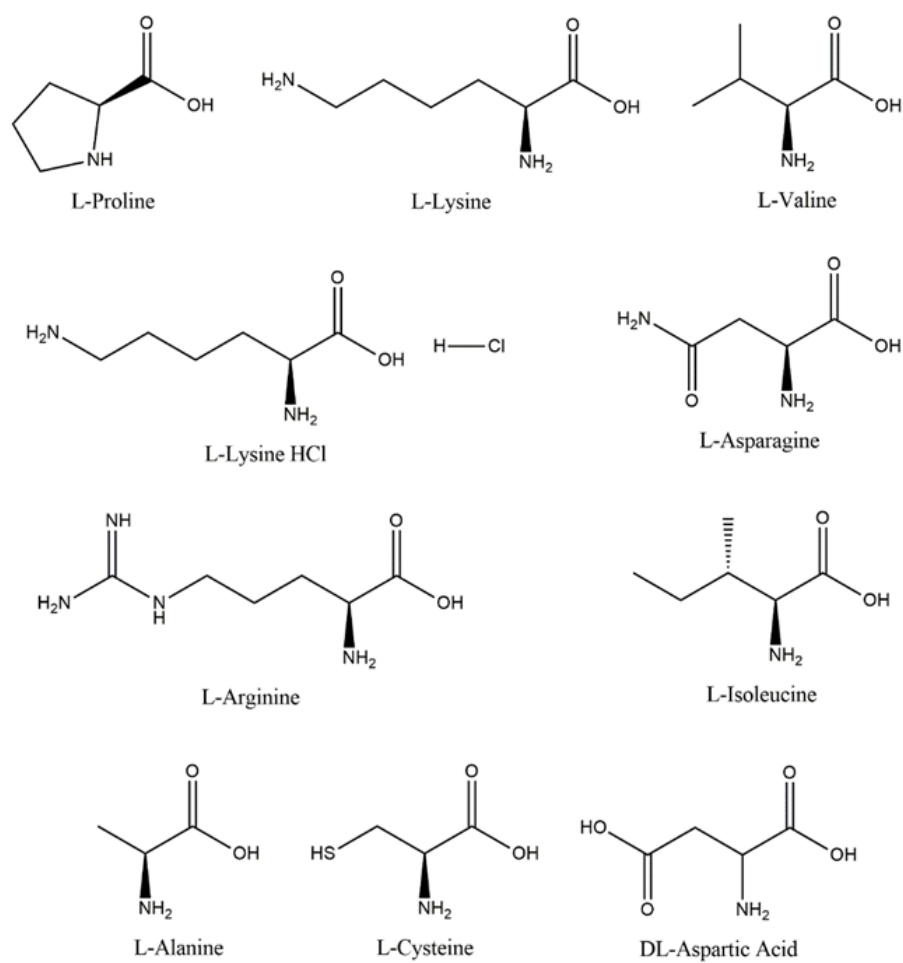
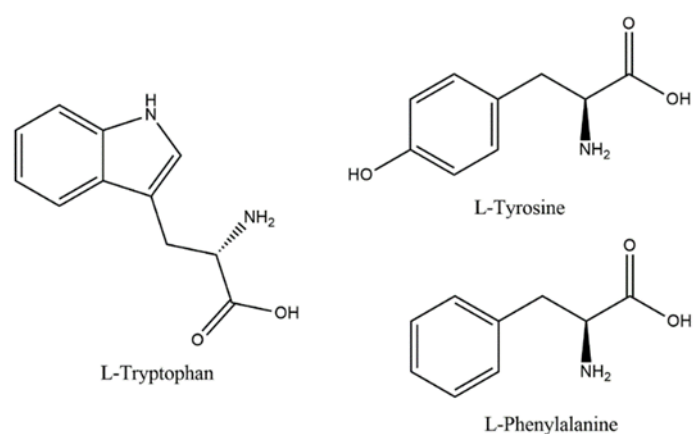
**Figure A.2.1** Chemical structure of the studied aliphatic amino acids.**Figure A.2.2** Chemical structure of the studied aromatic amino acids.

Table A.2.1 Log K_{ow} ¹ and solubility in water of aliphatic amino acids.

Amino acid	Log K_{ow}	Solubility in water (100 g ⁻¹)
L-Pro	-3.05	162.3
L-Lys	-2.54	Very soluble

Table A.2.2 Identification of the systems able (✓) and not able (×) to form ABS at 25 °C.

Amino acid	IL		Amino acid	IL	
L-Lys·HCl	[P ₄₄₄₍₁₄₎]Cl	✓	L-Lys	[P ₄₄₄₍₁₄₎]Cl	✓
	[P ₄₄₄₄]Br	✓		[P ₄₄₄₄]Br	✓
	[N ₄₄₄₄]Br	✓		[P ₄₄₄₁][MeSO ₄]	✓
	[P ₄₄₄₁][MeSO ₄]	×		[N ₄₄₄₄]Br	×
	[P ₄₄₄₂][Et ₂ PO ₄]	×		[P ₄₄₄₄][EtSO ₄]	×
	[P _{i(444)1}][TOS]	×		[P _{i(444)1}][TOS]	×
	[P ₄₄₄₄]Cl	×		[P ₄₄₄₄]Cl	×
	[N ₄₄₄₄]Cl	×		[N ₄₄₄₄]Cl	×
L-Pro	[N ₃₃₃₃]Br	×		[N ₃₃₃₃]Br	×
	[P ₄₄₄₍₁₄₎]Cl	✓	L-Arg		×
	[P ₄₄₄₄]Br	✓	D,L-Asp		×
	[P ₄₄₄₁][MeSO ₄]	✓	L-Asn		×
	[N ₄₄₄₄]Br	×	L-Val	[P ₄₄₄₄]Br	×
	[P ₄₄₄₄][EtSO ₄]	×	L-Ile		×
	[P _{i(444)1}][TOS]	×	L-Ala		×
	[P ₄₄₄₄]Cl	×	L-Cys		×
	[N ₄₄₄₄]Cl	×			
	[N ₃₃₃₃]Br	×			

Table A.2.3 Experimental weight fraction data for the ABS composed of IL (w_1) + L-Pro (w_2) + H₂O at (25 ± 1) °C and atmospheric pressure.

[P ₄₄₄₄]Br		[P ₄₄₄₍₁₄₎]Cl		[P ₄₄₄₁][MeSO ₄]	
w_1	w_2	w_1	w_2	w_1	w_2
52.44	14.80	81.28	2.54	76.50	9.67
48.43	17.45	72.17	6.10	57.00	17.04
34.38	23.71	64.84	9.88	28.95	34.45
29.51	26.94	58.05	13.84		
18.55	34.26	53.90	16.12		
12.61	43.65	41.17	25.41		

Table A.2.4 Experimental weight fraction data for the system composed of IL (w_1) + L-Lys (w_2) + H₂O (3) at (25 ± 1) °C and atmospheric pressure.

[P ₄₄₄₄]Br		[P ₄₄₄₁][MeSO ₄]		[P ₄₄₄₍₁₄₎]Cl	
w_1	w_2	w_1	w_2	w_1	w_2
48.57	6.90	50.35	9.70	70.69	3.30
43.26	9.37	42.07	14.25	52.28	6.37
21.11	20.58	40.35	15.60	42.88	12.65
30.27	15.23	38.29	19.06	42.08	13.47
13.78	27.73	34.71	21.92	39.85	15.61
		33.34	23.92	32.64	19.72
		16.88	45.86	31.57	20.84
				27.85	25.24
				24.12	29.29
				22.80	31.30
				21.39	33.07
				19.62	34.99
				14.98	37.93
				10.14	42.28
				7.35	45.47
				4.33	55.22

Table A.2.5 Experimental weight fraction data for the system composed of IL (w_1) + L-Lys·HCl (w_2) + H₂O at (25 ± 1) °C and atmospheric pressure.

[N ₄₄₄₄]Br		[P ₄₄₄₄]Br		[P ₄₄₄₍₁₄₎]Cl	
w_1	w_2	w_1	w_2	w_1	w_2
67.16	3.82	77.13	3.90	76.21	3.64
62.34	5.02	70.61	4.33	65.10	4.36
59.98	5.65	66.83	4.80	56.04	5.92
58.39	6.48	62.32	5.66	38.15	9.01
56.19	7.50	56.59	6.57	33.09	9.91
54.34	8.49	52.75	7.55	26.29	11.59
52.82	9.16	48.23	8.79	22.08	12.65
52.28	9.63	56.01	6.87	19.45	13.44
		50.95	8.26	17.37	14.20
		48.34	9.14	16.52	14.47
		42.21	11.16	15.89	14.63
		39.34	12.18	12.89	15.99
		35.51	13.70		
		31.75	15.43		

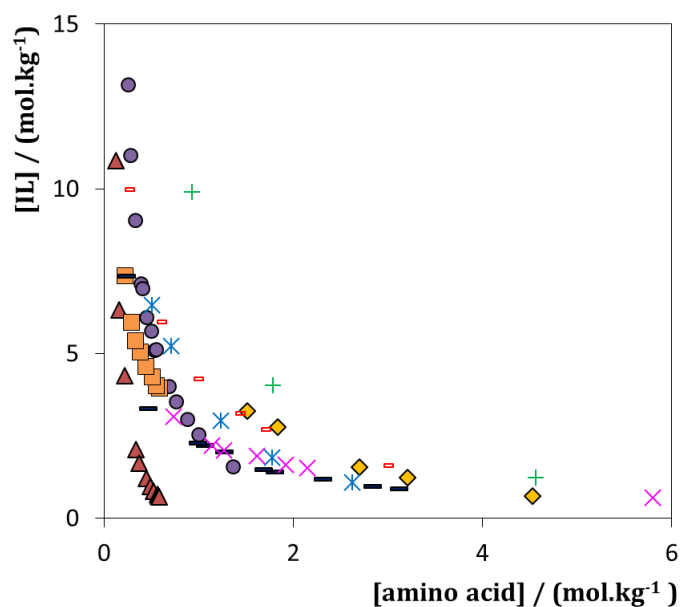


Figure A.2.3 Phase diagrams for ABS composed of IL + amino acid + H₂O, in molality units: [P₄₄₄₍₁₄₎]Cl + L-Lys·HCl (▲); [P₄₄₄₄]Br + L-Lys·HCl (●); [N₄₄₄₄]Br + L-Lys·HCl (■); [P₄₄₄₄]Br + L-Pro (◆); [P₄₄₄₍₁₄₎]Cl + L-Pro (—); [P₄₄₄₁][MeSO₄] + L-Pro (+); [P₄₄₄₍₁₄₎]Cl + L-Lys (—); [P₄₄₄₄]Br + L-Lys (*); [P₄₄₄₁][MeSO₄] + L-Lys (×).

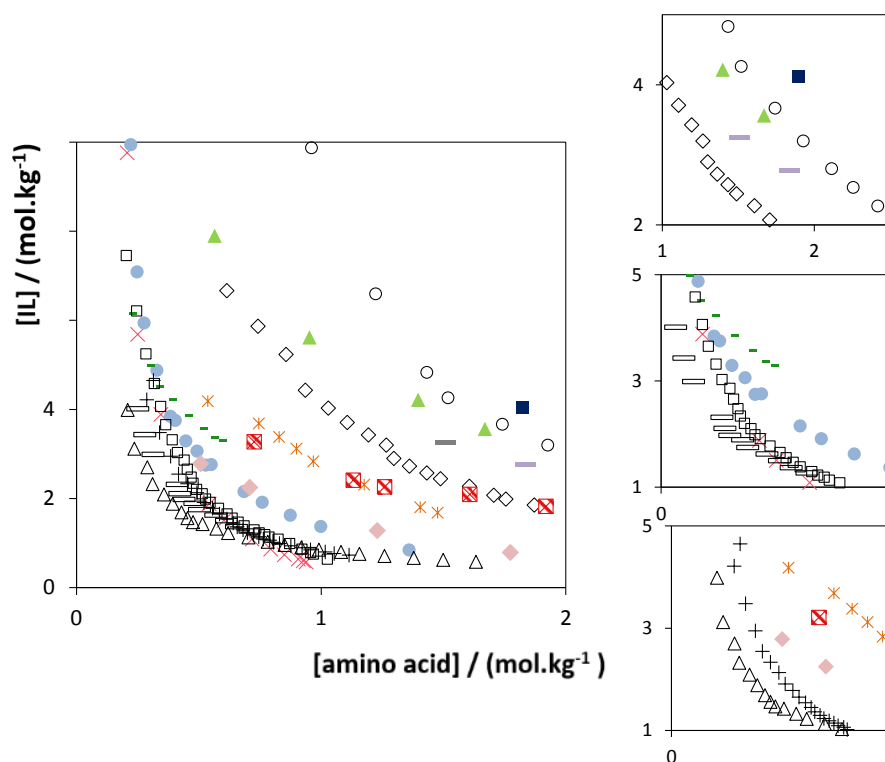


Figure A.2.4 Ternary phase diagrams determined in this work compared to those in the literature (amino acid + [C₄mim][CF₃SO₃] + H₂O and amino acid + [C₄mim][BF₄] + H₂O) at 25 °C and atmospheric pressure.²: L-Pro-based ABS ([C₄mim][CF₃SO₃] (○); [P₄₄₄₁][MeSO₄] (■); [P₄₄₄₄]Br (—); [P₄₄₄₁₄]Cl (▲); [C₄mim][BF₄] (□); L-Lys·HCl-based ABS ([N₄₄₄₄]Br (▪); [P₄₄₄₄]Br (●); [C₄mim][CF₃SO₃] (□); [C₄mim][BF₄] (=); [P₄₄₄₁₄]Cl (×)); L-Lys-based ABS ([P₄₄₄₁][MeSO₄] (⊠); [P₄₄₄₄]Br (◆); [P₄₄₄₁₄]Cl (*); [C₄mim][BF₄] (Δ); [C₄mim][CF₃SO₃] (+)).

Table A.2.6 Correlation parameters used to describe the experimental binodal data, determined by the method described by Merchuk et al.³, standard deviations (σ), and correlation coefficients (R^2).

IL	Amino Acid	$A \pm \sigma$	$B \pm \sigma$	$10^{-5} (C \pm \sigma)$	R^2
[P ₄₄₄₄]Br		227.8 ± 0.6	-0.37 ± 0.07	0.64 ± 0.33	0.994
[P ₄₄₄₁][MeSO ₄]	L-Pro	175.5 ± 0.0	-0.27 ± 0.00	0.60 ± 0.00	1.000
[P ₄₄₄₍₁₄₎]Cl		103.1 ± 1.7	-0.15 ± 0.01	1.14 ± 0.16	0.999
[P ₄₄₄₄]Br		117.6 ± 15.3	-0.33 ± 0.05	2.11 ± 0.78	0.997
[P ₄₄₄₁][MeSO ₄]	L-Lys	95.6 ± 6.8	-0.21 ± 0.02	0.32 ± 0.09	0.995
[P ₄₄₄₍₁₄₎]Cl		105.2 ± 5.6	-0.24 ± 0.02	0.79 ± 0.15	0.989
[P ₄₄₄₄]Br		181.1 ± 9.0	-0.45 ± 0.02	1.10 ± 1.48	0.995
[P ₄₄₄₍₁₄₎]Cl	L-Lys·HCl	205.3 ± 14.1	-0.53 ± 0.03	17.2 ± 2.35	0.998
[N ₄₄₄₄]Br		110.7 ± 4.2	-0.26 ± 0.02	6.19 ± 2.48	0.997

Table A.2.7 Experimental TLs and TLLs of the ABS investigated, where: $[IL]_{IL}$ and $[aa]_{IL}$ are, respectively, the IL and amino acid weight percentages in the IL-rich phase; $[IL]_{aa}$ and $[aa]_{aa}$ are, respectively, the IL and amino acid weight percentages in amino-acid-rich phase; $[IL]_M$ and $[aa]_M$ are, respectively, the IL and amino acid weight percentages in the initial mixture point; and pH_{IL} and pH_{aa} represent the pH value of the IL-rich phase and amino-acid-rich phase, respectively.

IL	Weight fraction composition / wt%								TLL
	[IL] _{IL}	[aa] _{IL}	pH _{IL}	[IL] _M	[aa] _M	[IL] _{aa}	[aa] _{aa}	pH _{aa}	
IL + L-Pro + H ₂ O									
[P ₄₄₄₄]Br	53.60	14.80	-	29.60	27.66	25.10	30.07	-	32.33
	77.75	8.35	5.31	36.53	31.73	9.08	47.31	4.69	78.95
[P ₄₄₄₍₁₄₎]Cl	74.64	4.86	-	59.53	17.93	0.77	68.73	-	97.65
	78.19	3.57	-	59.18	20.13	0.50	71.25	-	98.55
IL + L-Lys + H ₂ O									
[P ₄₄₄₄]Br	65.49	3.16	-	30.89	19.82	12.11	28.86	-	59.24
	77.96	1.56	10.16	42.81	19.78	3.83	39.97	10.2	83.49
[P ₄₄₄₁][MeSO ₄]	55.17	6.87	-	33.50	28.50	18.44	43.53	-	51.90
	63.36	3.86	10.71	39.17	29.12	9.30	60.33	10.4	78.17
[P ₄₄₄₍₁₄₎]Cl	56.40	6.50	-	29.92	30.29	6.24	51.56	-	67.43
	77.54	1.57	-	47.29	25.21	2.97	59.86	-	94.65
[C ₄ mim][CF ₃ SO ₃]	68.92	3.27	10.6	40.03	20.15	42.96	1.96	10.7	77.80
[C ₄ mim][DCA]	91.35	1.70	10.3	51.50	20.80	35.61	20.49	10.4	78.45
IL + L-Lys·HCl + H ₂ O									
[P ₄₄₄₄]Br	47.32	9.12	2.94	42.09	11.40	31.88	15.86	3.55	16.84

Table A.2.8 Extraction efficiencies of the aromatic amino acids to the IL-rich phase ($EE_{AR}\%$) and extraction efficiencies of aliphatic amino acids to the opposite phase ($EE_{AL}\%$).

Amino acid	ABS	L-Pro + [P ₄₄₄₄]Br	L-Lys + [P ₄₄₄₄]Br	L-Lys + [P ₄₄₄₁] [MeSO ₄]	L-Lys.HCl + [P ₄₄₄₄] Br	L-Lys + [C ₄ mim] [CF ₃ SO ₃]	L-Lys + [C ₄ mim] [DCA]
L-Trp	EE_{AR} (%)	26.26 ± 0.20	85.31 ± 0.09	76.63 ± 0.45	71.62 ± 1.27	29.42 ± 1.60	18.98 ± 1.12
	EE_{AL} (%)	93.83 ± 1.12	94.63 ± 0.41	97.36 ± 0.51	39.24 ± 1.66	90.79 ± 0.81	96.40 ± 0.80
L-Phe	EE_{AR} (%)	11.83 ± 2.30	60.20 ± 3.08	60.31 ± 1.11	67.29 ± 1.51	20.98 ± 0.86	36.44 ± 0.33
	EE_{AL} (%)	92.22 ± 0.61	94.54 ± 0.87	97.23 ± 0.87	34.50 ± 2.66	91.65 ± 0.080	95.85 ± 0.45
L-Tyr	EE_{AR} (%)	30.32 ± 0.61	45.07 ± 2.60	40.34 ± 1.50	60.87 ± 0.28	10.81 ± 0.93	35.77 ± 2.50
	EE_{AL} (%)	91.40 ± 0.72	95.26 ± 1.47	97.80 ± 0.040	34.64 ± 3.03	91.60 ± 0.025	95.85 ± 0.34

Table A.2.9 Partition coefficients (K_{aa}) of amino acids between the IL-rich and the opposite phase, and selectivity (S) of aromatic amino acids over aliphatic ones towards the IL-rich phase.

Amino Acid		L-Pro + [P ₄₄₄₄]Br	L-Lys + [P ₄₄₄₄]Br	L-Lys + [P ₄₄₄₁] [MeSO ₄]	L-Lys.HCl + [P ₄₄₄₁] [MeSO ₄]	L-Lys + [C ₄ mim] [CF ₃ SO ₃]	L-Lys + [C ₄ mim] [DCA]
L-Trp	K_{aa}	0.570	4.546	3.220	0.220	0.626	0.603
	S	4.144	120.892	121.279	2.396	0.048	0.029
L-Phe	K_{aa}	0.230	1.256	1.540	1.540	0.320	1.430
	S	1.672	29.930	59.795	1.513	0.024	0.069
L-Tyr	K_{aa}	0.655	2.714	0.750	0.910	0.160	1.500
	S	4.763	69.368	28.248	1.583	0.012	0.072

References

1. J. Sangster, Octanol-water partition coefficients: fundamentals and physical chemistry, John Wiley & Sons, 1997.
2. M. D. Pérez, L. I. Tomé, M. G. Freire, I. M. Marrucho, O. Cabeza and J. A. Coutinho, Sep. Purif. Technol., 2010, 72, 85-91
3. J. C. Merchuk, B. A. Andrews and J. A. Asenjo, J. Chromatogr. B Biomed. Sci. Appl., 1998, 711, 285-293.

Appendix B

B1.

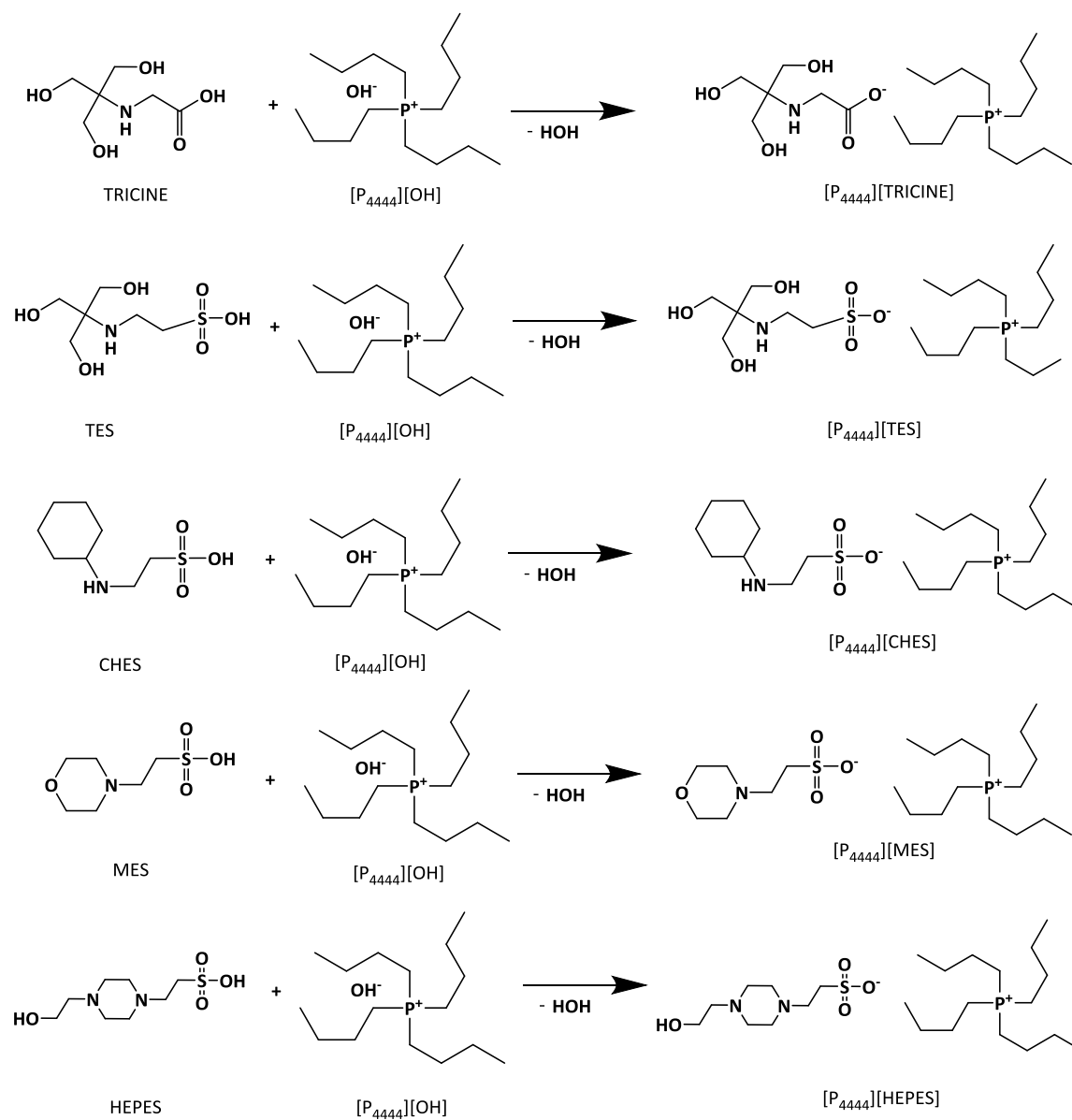
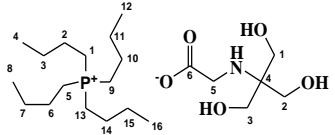
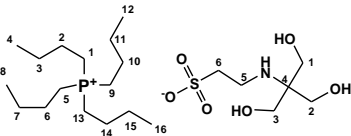
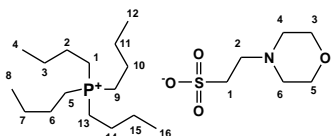
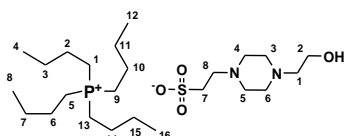
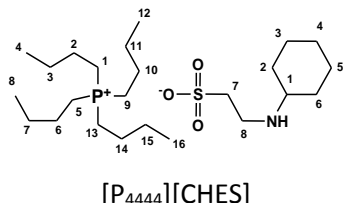
Figure B.1.1 The synthetic pathway for the synthesis of [P₄₄₄₄][GB] ILs.

Table B.1.1 Characterization of Good's buffer ionic liquids (GB-ILs).

<p>[P₄₄₄₄][TRICINE]: ¹H NMR (300 MHz, D₂O/TSP); δ [P₄₄₄₄], 0.77 (12H, t, C4C8C12C16's H), 1.27-1.44 (16H, m, C2C3C6C7C10C11C14C15's H), 2.00 (8H, m, C1C5C9C13's H); δ [TRICINE], 3.37 (6H, s, C1-C3's H), 3.12 (2H, s, C5's H). ¹³C NMR (75.47 MHz, D₂O/TSP); δ [P₄₄₄₄], 15.42 (C4C8C12C16), 20.15 (C3C7C11C15), 20.79 (C2C6C10C14), 26.28 (C1C5C9C13); δ [TRICINE], 62.97 (C4), 63.12 (C1-C3), 182.71 (C6), 47.68 (C5); melting point = 116°C.</p>	 <p style="text-align: center;">[P₄₄₄₄][TRICINE]</p>
<p>[P₄₄₄₄][TES]: ¹H NMR (300 MHz, D₂O/TSP); δ [P₄₄₄₄], 0.79 (12H, t, C4C8C12C16's H), 1.29-1.49 (16H, m, C2C3C6C7C10C11C14C15's H), 2.10 (8H, m, C1C5C9C13's H); δ [TES], 3.31 (6H, s, C1-C3's H), 2.82 (2H, t, C6's H), 2.57 (2H, t, C5's H). ¹³C NMR (75.47 MHz, D₂O/TSP); δ [P₄₄₄₄], 15.46 (C4C8C12C16), 20.17 (C3C7C11C15), 20.83 (C2C6C10C14), 26.28 (C1C5C9C13); δ [TES], 60.65 (C4), 57.63 (C1-C3), 51.58 (C6), 37.69 (C5); viscous liquid.</p>	 <p style="text-align: center;">[P₄₄₄₄][TES]</p>
<p>[P₄₄₄₄][MES]: ¹H NMR (300 MHz, D₂O/TSP); δ [P₄₄₄₄], 0.78 (12H, t, C4C8C12C16's H), 1.27-1.42 (16H, m, C2C3C6C7C10C11C14C15's H), 2.02 (8H, m, C1C5C9C13's H); δ [MES], 2.50 (4H, t, C4C6's H), 2.72 (2H, t, C2's H), 2.99 (2H, t, C1's H), 3.63 (4H, t, C3C5's H). ¹³C NMR (75.47 MHz, D₂O/TSP); δ [P₄₄₄₄], 15.44 (C4C8C12C16), 20.16 (C3C7C11C15), 20.80 (C2C6C10C14), 26.28 (C1C5C9C13); δ [MES], 50.02 (C4C6), 55.11 (C2), 55.44 (C1), 68.80 (C3C5); melting point = 92 °C.</p>	 <p style="text-align: center;">[P₄₄₄₄][MES]</p>
<p>[P₄₄₄₄][HEPES]: ¹H NMR (300 MHz, D₂O/TSP); δ [P₄₄₄₄], 0.79 (12H, t, C4C8C12C16's H), 1.28-1.45 (16H, m, C2C3C6C7C10C11C14C15's H), 2.03 (8H, m, C1C5C9C13's H); [HEPES], 2.46 (8H, t, C3C4C5C6's H), 2.67 (2H, t, C8's H), 2.94 (2H, t, C1's H), 2.97 (2H, t, C7's H), 3.59 (4H, t, C2's H). ¹³C NMR (75.47 MHz, D₂O/TSP); δ [P₄₄₄₄], 15.44 (C4C8C12C16), 20.16 (C3C7C11C15), 20.80</p>	 <p style="text-align: center;">[P₄₄₄₄][HEPES]</p>

<p>(C2C6C10C14), 26.29 (C1C5C9C13); δ [HEPES], 50.39 (C8), 54.19 (C4C5), 54.78 (C3C6), 55.02 (C1), 60.87 (C7), 61.59 (C2); melting point = 64 °C.</p>	
<p>[P₄₄₄₄][CHES]: ¹H NMR (300 MHz, D₂O/TSP); ¹H NMR (300 MHz, D₂O/TSP); δ [P₄₄₄₄], 0.78 (12H, t, C4C8C12C16's H), 1.28-1.45 (16H, m, C2C3C6C7 C10C11C14C15's H), 2.02 (8H, m, C1C5C9C13's H); δ [CHES], 0.94 (10H, m, C2-C6's H), 2.38-2.47 (H, m, C1's H), 2.95 (2H, m, C8's H), 2.95 (2H, t, C7's H). ¹³C NMR (75.47 MHz, D₂O/TSP); δ [P₄₄₄₄], 15.43 (C4C8C12C16), 20.15 (C3C7C11C15), 20.79 (C2C6C10C14), 25.60 (C1C5C9C13); δ [CHES], 26.08 (C3C5), 26.28 (C4), 39.56 (C2C6), 53.42 (C8), 63.09 (C7), 63.37 (C1); melting point = 55 °C.</p>	 <p style="text-align: center;">[P₄₄₄₄][CHES]</p>

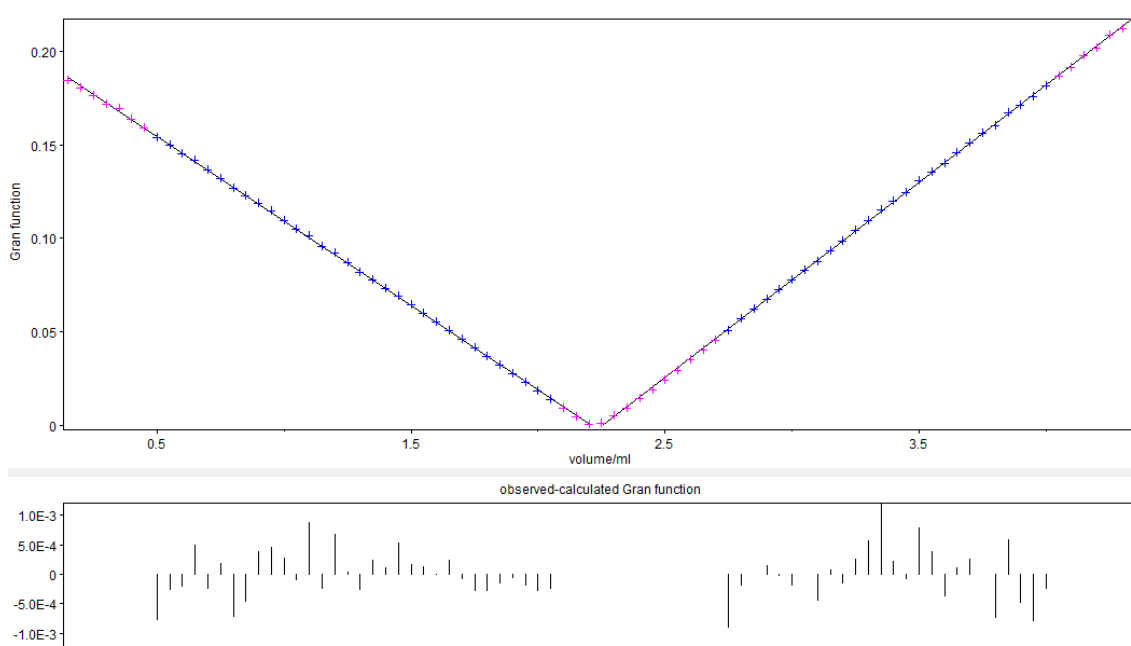


Figure B.1.2 GLEE output showing measured electrode potentials and residuals as a function of the calculated $-\log[\text{H}^+]$.

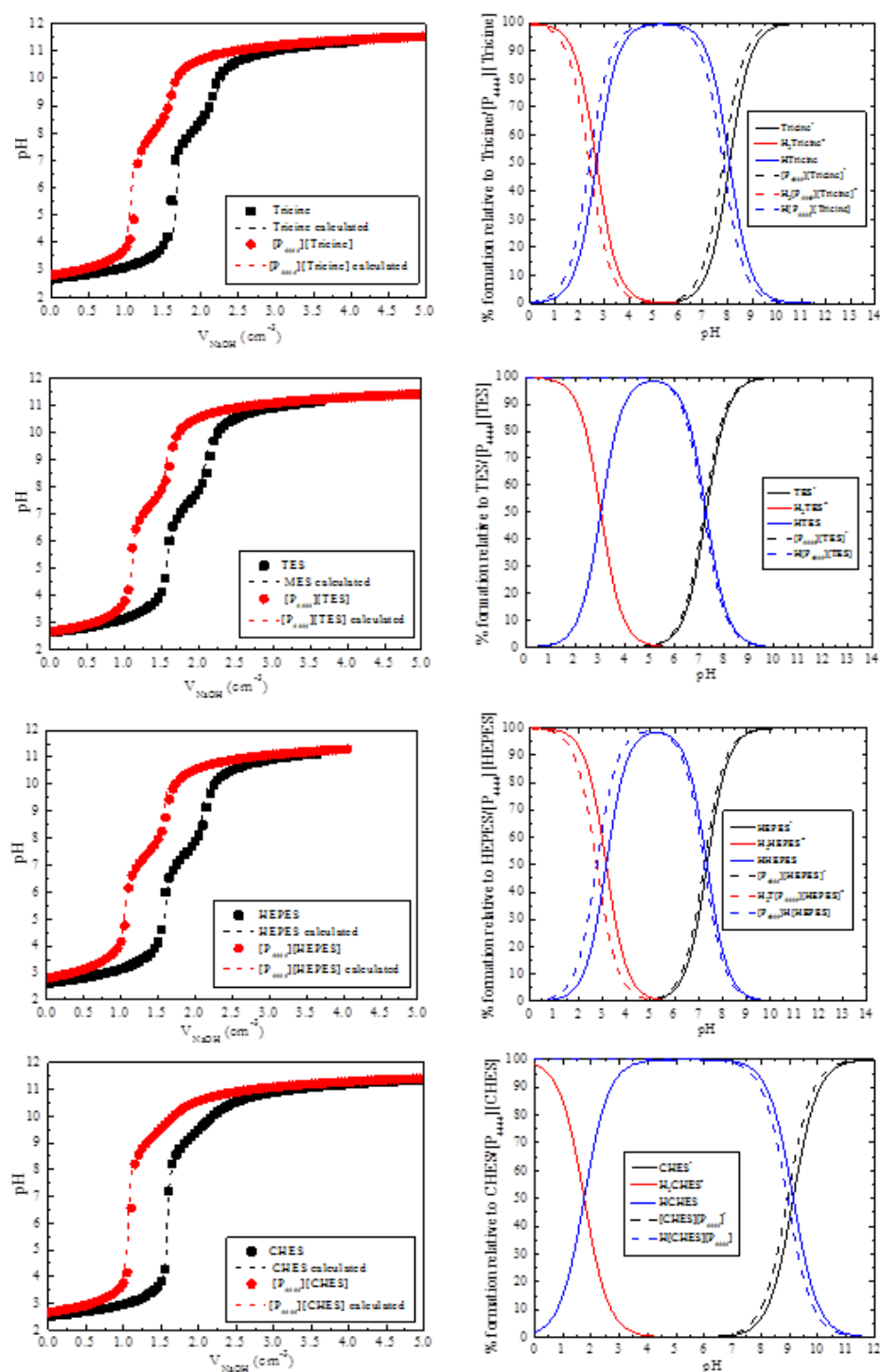


Figure B.1.3 pH titration curves of $1 \cdot 10^{-3} \text{ mol} \cdot \text{dm}^{-3}$ of GB/ P_{444} [GB] at 25°C and $I = 0.1 \text{ mol} \cdot \text{dm}^{-3}$ of NaNO_3 . The dashed lines are the calculated pH from the refinement operations. (b) Species-distribution diagrams of $1 \cdot 10^{-3} \text{ mol} \cdot \text{dm}^{-3}$ of GB/ P_{444} [GB] at 25°C and $I = 0.1 \text{ mol} \cdot \text{dm}^{-3}$ of NaNO_3 .

Table B.1.2 Experimental weight fraction data for the binodal curve of the systems composed of [P₄₄₄₄][GB] (*w*₁) + K₃C₆H₅O₇ (*w*₂) at (25 ± 1) °C.

[P ₄₄₄₄][TES]		[P ₄₄₄₄][MES]				[P ₄₄₄₄][HEPES]	
<i>w</i> ₁	<i>w</i> ₂	<i>w</i> ₁	<i>w</i> ₂	<i>w</i> ₁	<i>w</i> ₂	<i>w</i> ₁	<i>w</i> ₂
61.87	4.37	62.37	1.95	14.47	21.49	60.68	1.78
47.02	8.97	55.07	3.07	14.02	21.86	48.71	4.78
25.52	19.15	46.15	5.21	13.60	22.21	44.95	6.08
23.75	20.22	38.99	7.55	13.35	22.44	39.04	8.30
22.00	21.44	35.53	9.45	13.12	22.55	25.28	15.25
20.31	22.47	32.17	10.43	12.86	22.75	22.19	18.35
19.24	23.17	29.24	12.18	12.62	22.89	19.02	20.85
18.35	23.72	25.01	14.22	12.33	23.10	18.80	21.06
17.37	24.41	24.37	14.94	12.13	23.25	18.23	21.38
16.52	24.96	23.45	15.59	11.94	23.41	17.95	21.63
15.50	25.68	22.73	15.99	11.64	23.79	17.67	21.87
14.54	26.39	22.10	16.27	11.41	23.87	17.20	22.15
13.98	26.79	21.05	17.21	11.19	24.14	16.91	22.26
12.66	28.22	20.19	17.49	10.81	24.41	16.52	22.54
11.98	28.75	19.88	17.71	10.64	24.57		
11.48	29.15	19.30	18.08	10.26	25.32		
11.02	29.45	18.82	18.32	10.05	25.33		
9.73	30.41	18.48	18.78	9.90	25.44		
9.31	30.82	17.96	19.05	9.76	25.58		
9.07	30.88	17.56	19.34	9.49	25.92		
8.73	31.18	17.16	19.51				
8.00	31.88	16.73	19.90				
7.64	32.21	16.30	20.01				
7.15	32.68	15.93	20.21				
6.80	33.07	15.77	20.58				
6.26	33.70	15.05	21.16				
5.85	34.17	14.78	21.34				
5.30	34.72	14.47	21.49				
		14.02	21.86				
		13.60	22.21				
		13.35	22.44				
		13.12	22.55				
		12.86	22.75				
		12.62	22.89				

Table B.1.3 Experimental weight fraction data for the binodal curve of the systems composed of $[P_{4444}][GB] (w_1) + K_3C_6H_5O_7 (w_2)$ at $(25 \pm 1) ^\circ C$.

[P ₄₄₄₄][CHES]				[P ₄₄₄₄][TRICINE]	
w ₁	w ₂	w ₁	w ₂	w ₁	w ₂
56.03	2.15	16.45	13.89	49.06	8.70
49.84	3.00	15.99	14.29	43.97	10.21
44.57	4.00	15.59	14.18	47.70	9.15
32.64	7.78	15.34	14.33	32.05	15.84
31.63	8.05	15.07	14.48	27.35	19.33
27.81	9.15	14.68	14.61	19.56	25.36
26.97	9.60	14.39	14.75	16.67	27.81
26.32	9.76	14.08	14.88	15.34	28.95
25.90	9.93	13.79	15.04	13.32	30.56
25.13	10.40	13.47	15.17	11.27	32.48
24.61	10.45	13.13	15.40	10.38	33.18
23.90	10.97	12.83	15.45	9.04	34.23
23.18	11.16	12.54	15.62	8.45	34.72
22.35	11.41	12.22	15.80	7.75	35.28
21.72	11.67	11.96	15.91	7.30	35.54
21.10	11.98	11.81	16.06	6.93	35.89
20.65	12.16	11.51	16.21	6.54	36.12
20.24	12.27			6.21	36.43
19.61	12.48			5.81	36.36
19.40	12.66			5.54	36.62
19.13	12.77			5.31	36.73
18.83	13.02			5.02	36.86
18.49	13.10				
17.95	13.41				
17.50	13.55				
17.05	13.66				
16.60	13.86				

Table B.1.4 Correlation parameters used to describe the experimental binodal data by Equation proposed by Merchuk et al.¹, and respective standard deviations (σ) and correlation coefficients.

GB-ILs	$A \pm \sigma$	$B \pm \sigma$	$10^5 (C \pm \sigma)$	R^2
[P ₄₄₄₄][TES]	113.0 \pm 1.2	-0.287 \pm 0.003	3.1 \pm 0.0	0.9997
[P ₄₄₄₄][TRICINE]	110.1 \pm 8.5	-0.373 \pm 0.002	2.4 \pm 0.2	0.9963
[P ₄₄₄₄][MES]	98.3 \pm 0.5	-0.328 \pm 0.002	4.0 \pm 0.1	0.9996
[P ₄₄₄₄][HEPES]	89.9 \pm 1.65	-0.280 \pm 0.008	3.05 \pm 0.3	0.9987
[P ₄₄₄₄][CHES]	93.2 \pm 1.0	-0.355 \pm 0.005	15.4 \pm 0.3	0.9991

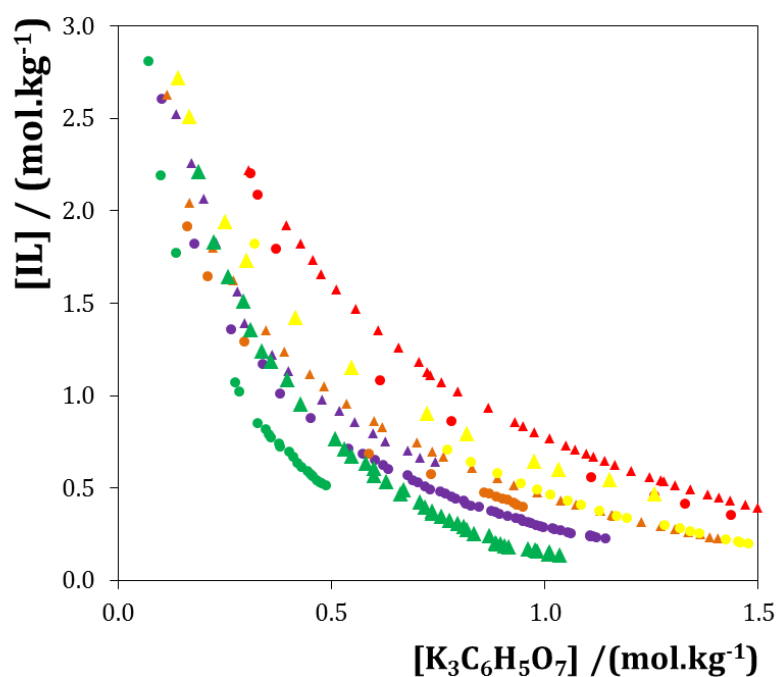


Figure B.1.4 Evaluation of the cation nature in the ternary phase diagrams (in mol.kg⁻¹) composed of GB-IL + K₃C₆H₅O₇ + water at 25 °C and atmospheric pressure: (●) [P₄₄₄₄][TRICINE], (●) [P₄₄₄₄][MES], (●) [P₄₄₄₄][HEPES], (●) [P₄₄₄₄][TES], (●) [P₄₄₄₄][CHES], (▲) [N₄₄₄₄][TRICINE], (▲) [N₄₄₄₄][MES], (▲) [N₄₄₄₄][HEPES], (▲) [N₄₄₄₄][TES], (▲) [N₄₄₄₄][CHES]. The [N₄₄₄₄][GBs] data from were taken from the literature².

Table B.1.5 Data for the tie-lines (TLs) and tie-line lengths (TLLs). Initial mixture compositions are represented as $[\text{Salt}]_{\text{M}}$ and $[\text{IL}]_{\text{M}}$ whereas $[\text{Salt}]_{\text{Salt}}$ and $[\text{IL}]_{\text{Salt}}$ are the composition of IL and salt at the IL-rich phase, respectively, and vice-versa.

IL	Weight fraction composition / wt%						TLL
	$[\text{IL}]_{\text{IL}}$	$[\text{Salt}]_{\text{IL}}$	$[\text{IL}]_{\text{M}}$	$[\text{Salt}]_{\text{M}}$	$[\text{IL}]_{\text{Salt}}$	$[\text{Salt}]_{\text{Salt}}$	
$[\text{P}_{4444}][\text{TES}]$	79.51	1.51	39.46	19.77	5.09	35.43	78.40
	55.66	5.99	39.52	14.42	10.64	29.50	50.80
$[\text{P}_{4444}][\text{TRICINE}]$	81.47	1.26	39.74	18.77	13.20	29.91	89.85
	55.81	6.19	38.91	15.48	14.31	28.98	67.52
$[\text{P}_{4444}][\text{HEPES}]$	79.66	0.187	40.40	18.22	5.02	34.44	82.12
	71.07	0.706	40.59	15.00	8.46	30.08	69.16
$[\text{P}_{4444}][\text{CHES}]$	81.30	0.149	39.87	19.18	0.0003	37.49	89.46
	77.40	0.275	42.94	16.12	0.001	35.85	41.41
$[\text{P}_{4444}][\text{MES}]$	3.60	33.01	40.23	17.77	82.22	0.297	85.15
	30.08	5.55	38.98	16.30	77.21	0.543	77.51
$[\text{P}_{4444}]\text{Cl}$	76.76	2.70	38.31	22.61	2.43	41.19	83.71
	56.50	5.17	38.91	13.99	8.12	29.43	54.13
	57.71	4.97	39.22	14.89	7.32	30.61	56.54

References

1. J. C. Merchuk, B. A. Andrews and J. A. Asenjo, J. Chromatogr. B Biomed. Sci. Appl., 1998, 711, 285-293.
2. T. Mohammed, F. Silva, M.V. Quental, S.P.M. Ventura, M.G. Freire, J.A.P. Coutinho, Green Chem., 2014., 3149–3159.

B2.

Table B.2.1 Summary of the bio-based ILs synthesized.

Cation	Anion	Sources of anion	Observation
Cholinium	Indole-3-acetate	Naturally occurring plant growth hormone found in all type of plants	Liquid at r.t.
	Indole-3-butyrate	Naturally occurring plant growth hormone found in all type of plants	Liquid at r.t.
	Glycolate	Sugarcane, sugar beets, pineapple and unripe grapes	Liquid at r.t.
	Pyruvate	Apple and wine	Liquid at r.t.
	Abeitate	Trees, pine wood & resins	Liquid at r.t.
	L-ascorbate	Orange, green pepper, papaya, kiwi, cauliflower, broccoli, citrus juice	Liquid at r.t.
	Coumarine-3-carboxylate	Tonka beans, vanilla grass, sweet grass and cassia cinnamon, Cherries, Apricot	Highly viscous at r.t.
	Genistate	African tree <i>Alchorneacordifolia</i> and wine	Semi-solid at r.t.
	D-(+)-Galactouronate	Fresh apple and trees	Liquid at r.t.
	D-(–)-Quinate	Cinchona bark & coffee beans	Liquid at r.t.

Note: r.t. = room temperature (25 °C)

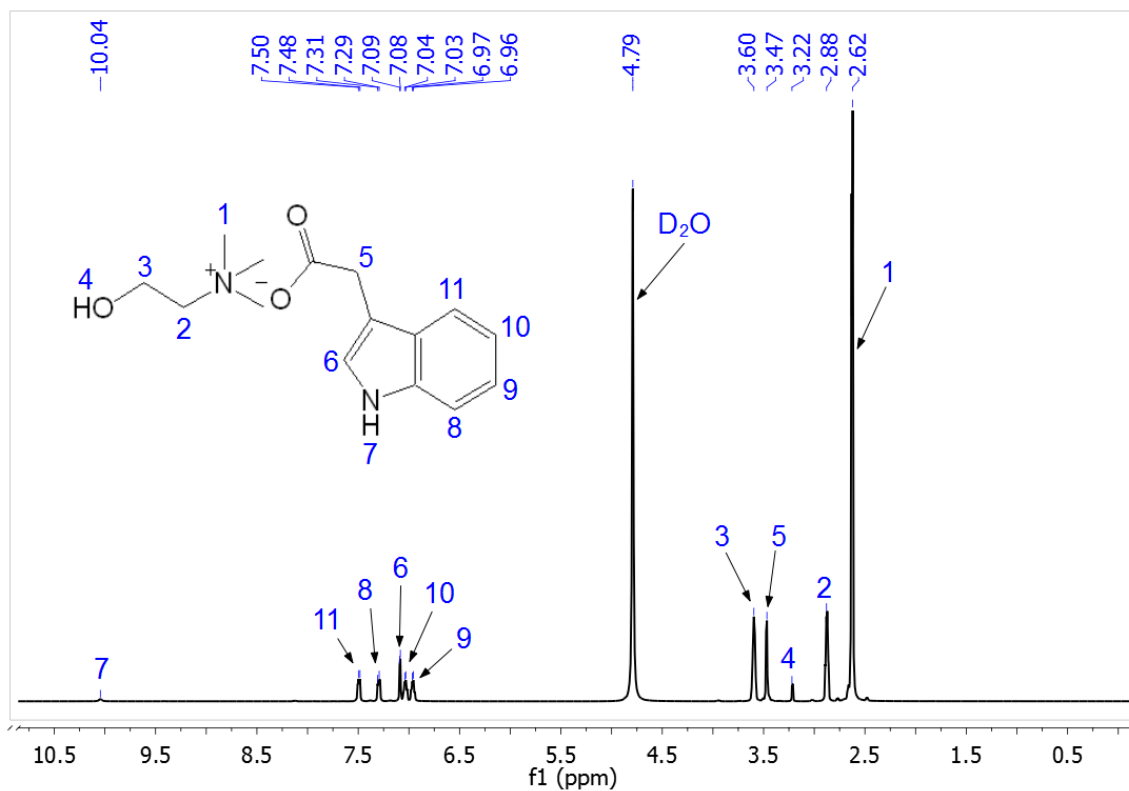


Figure B.2.1 ^1H NMR spectra of [Ch][IA].

^1H NMR (D₂O, 500 MHz, δ /ppm relative to TMS): 2.62 (s, 9H, -CH₃), 2.88 (t, 2H, -CH₂-N-), 3.22 (s, 1H, -OH), 3.47 (s, 2H, -CH₂-CO-), 3.60 (t, 2H, -O-CH₂-), 7.08 (d, 1H, =CH-N-), 6.96-7.51 (m, 4H, aromatic protons), 10.04 (s, 1H, -HN-). ESI-MS: Calculated for C₁₅H₂₂N₂O₃ [M]⁺: m/z = 104.11; Found: 104.17, [M]⁻: m/z = 174.06; Found: 174.29.

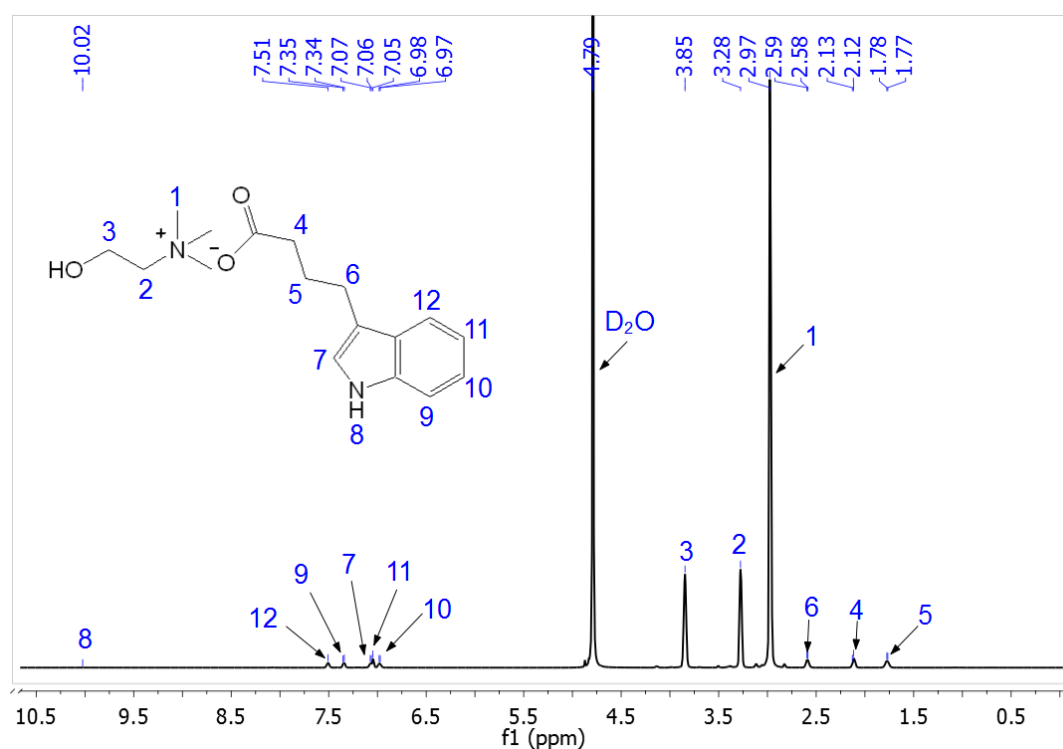


Figure B.2.2 ^1H NMR spectra of [Ch][BI].

^1H NMR (D_2O , 500 MHz, δ/ppm relative to TMS): 1.77 (t, 2H, -CH₂-), 2.12 (t, 2H, -CH₂-CO-), 2.58 (t, 2H, -CH₂-), 2.97 (s, 9H, -CH₃), 3.28 (t, 2H, -CH₂-N-), 3.85 (t, 2H, -O-CH₂-), 7.07 (d, 1H, -CH-N-), 6.97-7.51 (m, 4H, aromatic protons), 10.02 (s, 1H, -NH-). ESI-MS: Calculated for $\text{C}_{17}\text{H}_{26}\text{N}_2\text{O}_3$ $[\text{M}]^+$: m/z = 104.11; Found: 104.13, $[\text{M}]^-$: m/z = 202.09; Found: 202.14.

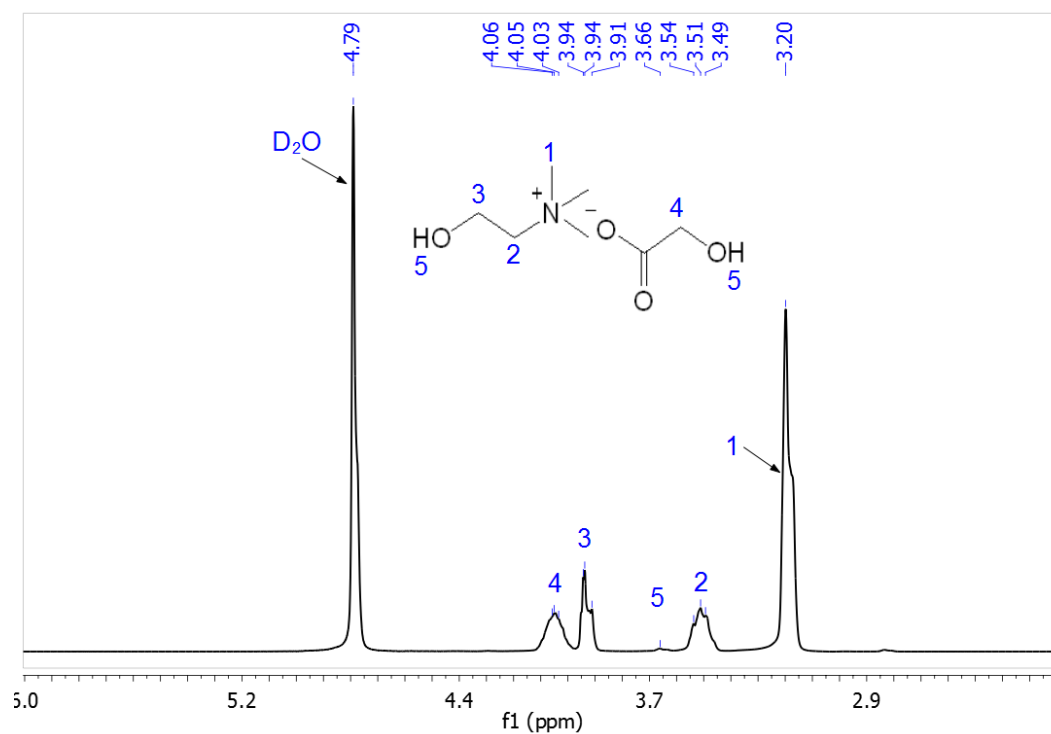


Figure B.2.3 ^1H NMR spectra of [Ch][Gly].

^1H NMR (D_2O , 500 MHz, δ/ppm relative to TMS): 3.20 (s, 9H, -N-CH₃), 3.51 (t, 2H, -CH₂-N-), 3.66 (s, 2H, -OH), 3.94 (t, 2H, -O-CH₂-), 4.05 (t, 1H, -CH₂-O-). ESI-MS: Calculated for $\text{C}_7\text{H}_{17}\text{NO}_4$ $[\text{M}]^+$: $m/z = 104.11$; Found: 103.97, $[\text{M}]^-$: $m/z = 75.01$; Found: 75.05.

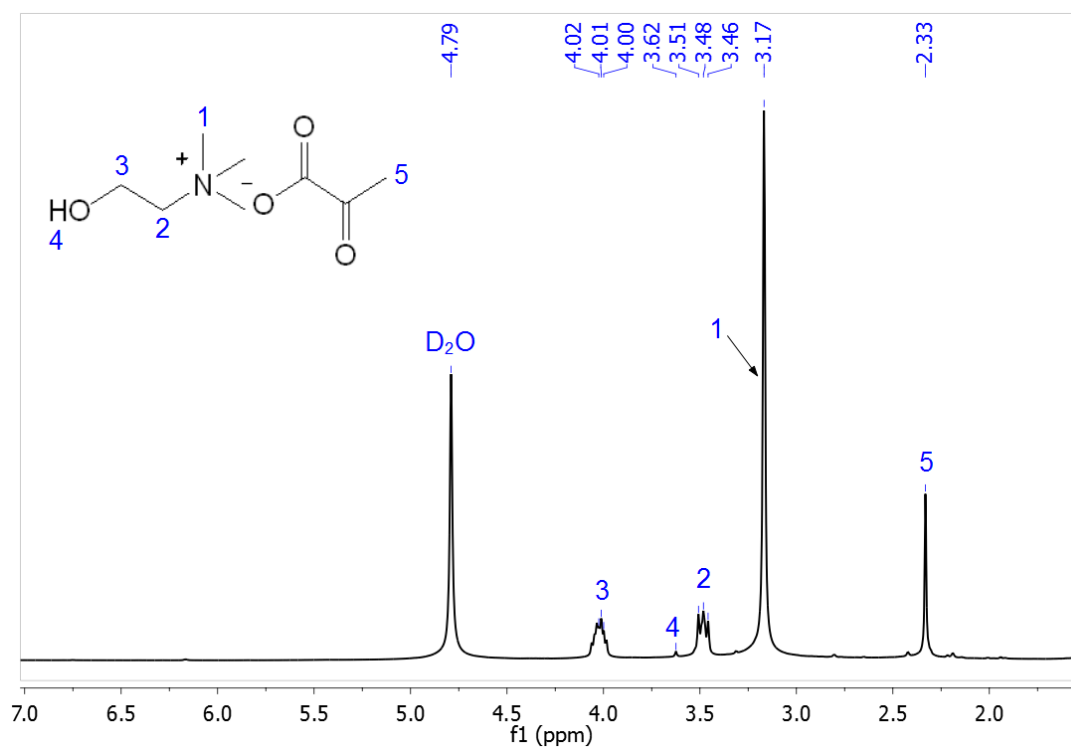


Figure B.2.4 ^1H NMR spectra of [Ch][Pyr].

^1H NMR (D_2O , 500 MHz, δ/ppm relative to TMS): 2.33 (s, 3H, -CH₃), 3.17 (s, 9H, -N-CH₃), 3.48 (t, 2H, -CH₂-N-), 3.62 (s, 1H, -OH), 4.01 (t, 2H, -O-CH₂-). ESI-MS: Calculated for $\text{C}_8\text{H}_{17}\text{NO}_4$ [M]⁺: m/z = 104.11; Found: 104.00, [M]⁻: m/z = 87.01; Found: 87.07.

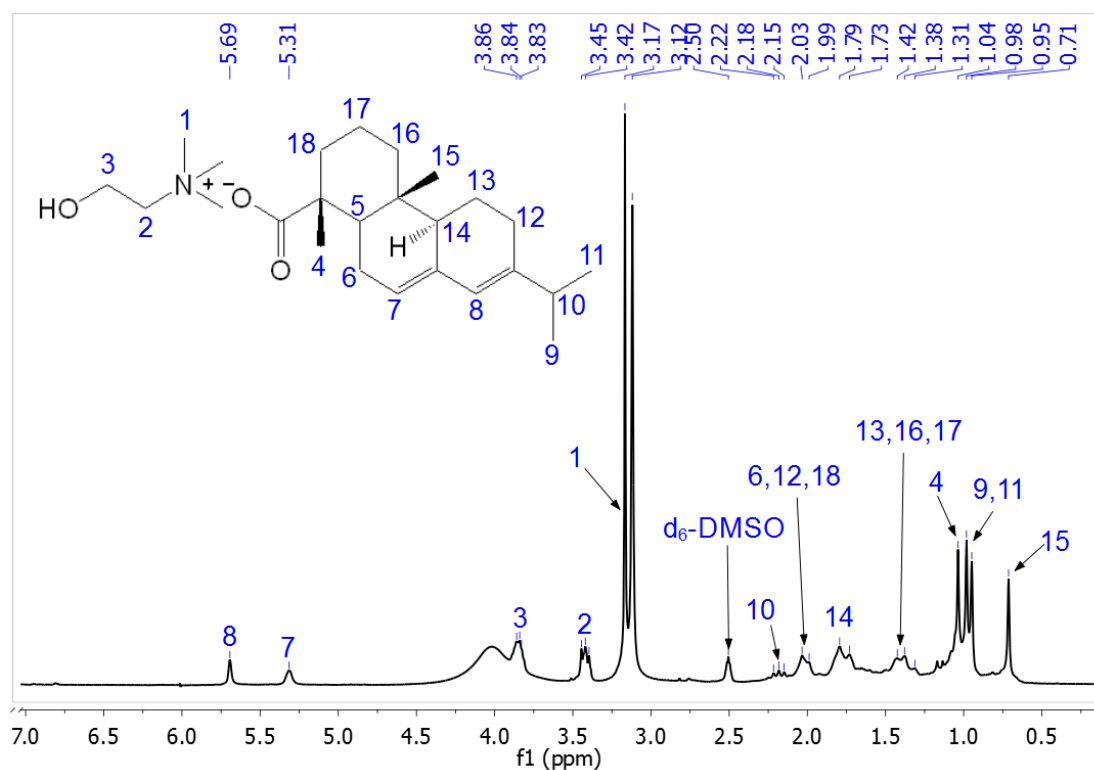


Figure B.2.5 ^1H NMR spectra of [Ch][Abt].

^1H NMR (d_6 -DMSO, 500 MHz, δ /ppm relative to TMS): 0.71 (s, 3H, $-\text{CH}_3$), 0.95 (d, 6H, $-\text{CH}_3$), 1.04 (s, 3H, $-\text{CH}_3$), 1.38 (m, 6H, $-\text{CH}_2-$), 1.73 (m, 1H, $-\text{C}-\text{CH}-\text{C}$), 1.99 (m, 6H, $-\text{CH}_2-$), 2.15 (m, 1H, $-\text{CH}-$), 3.17 (s, 9H, $-\text{N}-\text{CH}_3$), 3.42 (t, 2H, $-\text{CH}_2-\text{N}-$), 3.83 (t, 2H, $-\text{O}-\text{CH}_2-$), 5.31 (s, 1H, $-\text{HC}=\text{C}-$), 5.69 (s, 1H, $-\text{HC}=\text{C}-$). ESI-MS: Calculated for $\text{C}_{25}\text{H}_{43}\text{NO}_3$ $[\text{M}]^+$: $m/z = 104.11$; Found: 104.17, $[\text{M}]^-$: $m/z = 301.22$; Found: 301.28.

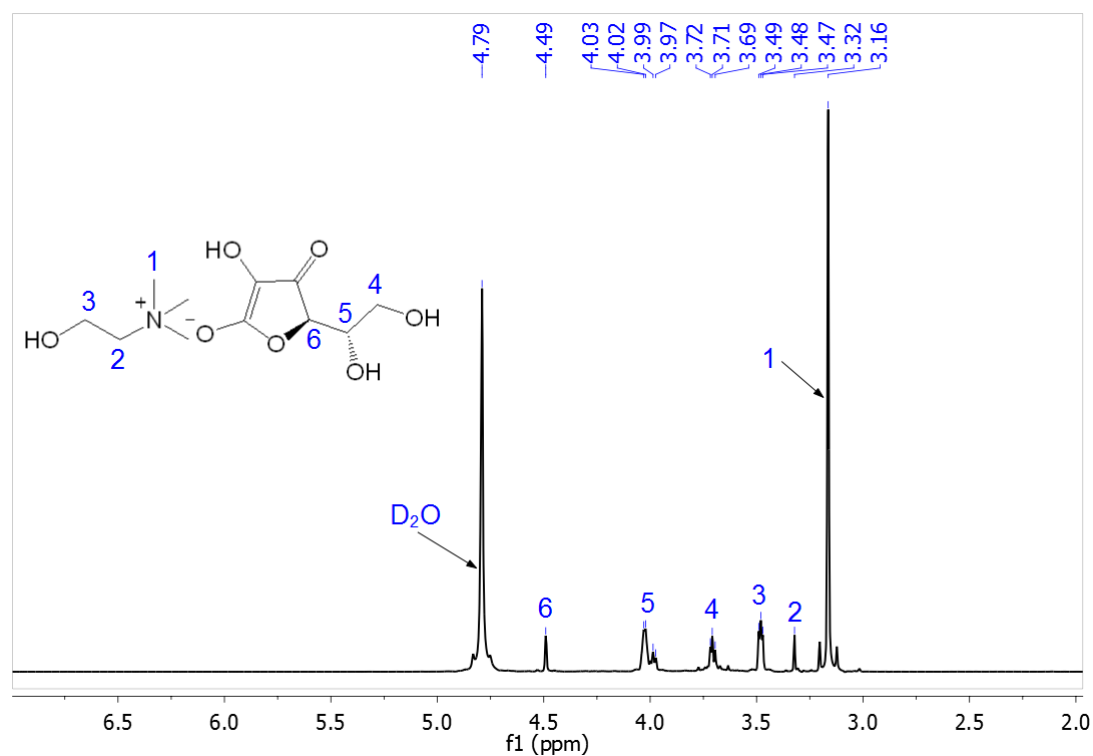


Figure B.2.6 ^1H NMR spectra of [Ch][Asc].

^1H NMR (D_2O , 500 MHz, δ/ppm relative to TMS): 3.16 (s, 9H, -N- CH_3), 3.32 (t, 2H, - CH_2 -N-), 3.48 (t, 2H, -O- CH_2 -), 3.71 (dt, 2H, - CH_2 -O), 4.01 (m, 1H, -HC-OH), 4.49 (s, 1H, -O-CH-). ESI-MS: Calculated for $\text{C}_{11}\text{H}_{21}\text{NO}_7$ $[\text{M}]^+$: $m/z = 104.11$; Found: 104.20, $[\text{M}]^-$: $m/z = 175.02$; Found: 175.13.

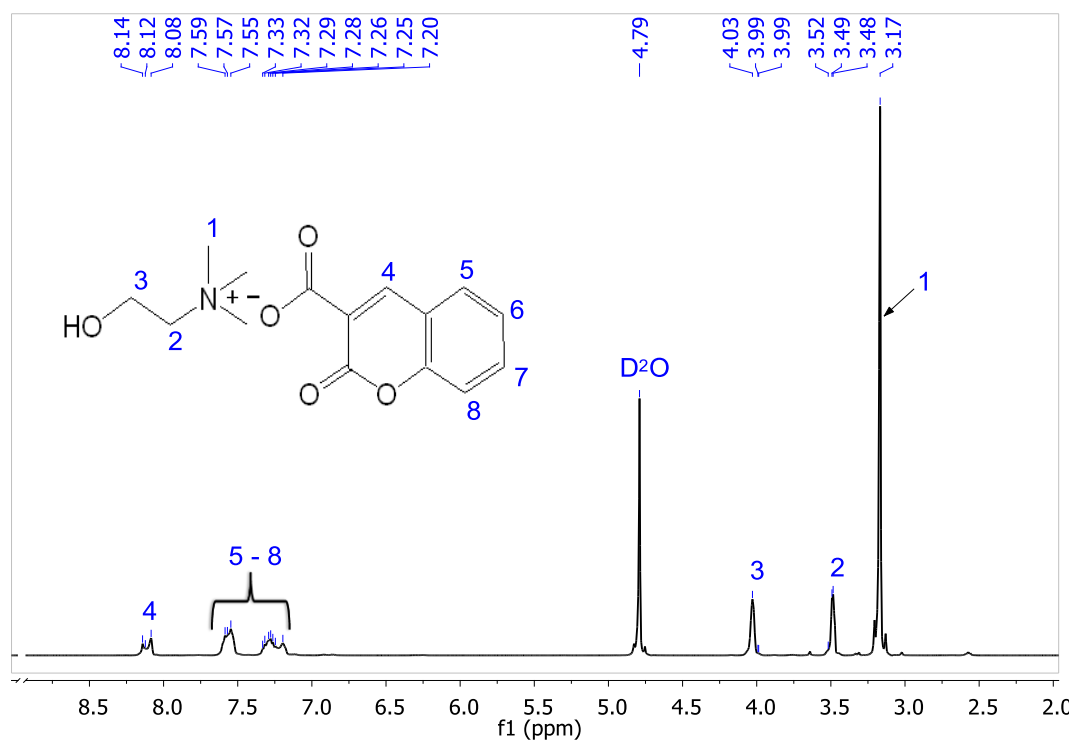


Figure B.2.7 ^1H NMR spectra of [Ch][C3C].

^1H NMR (D_2O , 500 MHz, δ/ppm relative to TMS): 3.17 (s, 9H, -N-CH₃), 3.49 (t, 2H, -CH₂-N-), 3.99 (t, 2H, -CH₂-OH), 7.20-7.59 (m, 4H, aromatic protons), 8.12 (t, 1H, =CH-Ar). ESI-MS: Calculated for $\text{C}_{15}\text{H}_{19}\text{NO}_5$ [M]⁺: m/z = 104.11; Found: 104.18, [M]⁻: m/z = 189.02; Found: 189.15.

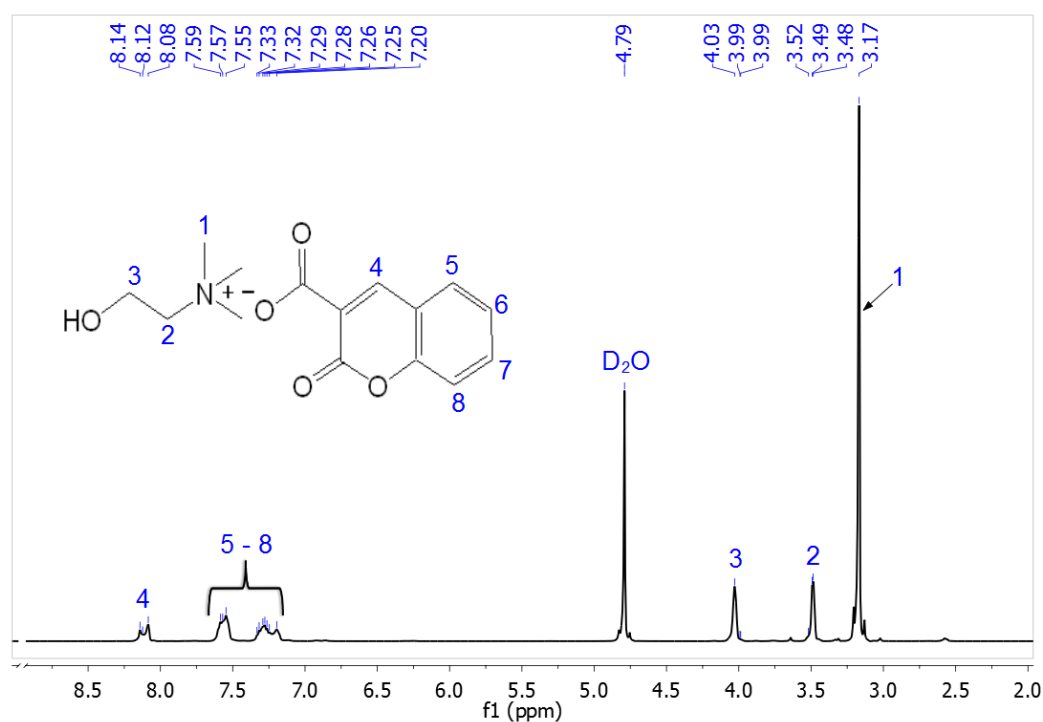


Figure B.2.8 ¹H NMR spectra of [Ch][Gen].

¹H NMR (D₂O, 500 MHz, δ/ppm relative to TMS): 3.00 (s, 9H, -N-CH₃), 3.30 (t, 2H, -CH₂-N-), 3.57 (s, 3H, -OH), 3.89 (t, 2H, -O-CH₂-), 6.67 (d, 1H, =CH- aromatic), 6.84 (dd, 1H, =CH- aromatic), 7.13 (d, 1H, =CH- aromatic). ESI-MS: Calculated for C₁₂H₁₉NO₅ [M]⁺: *m/z* = 104.11; Found: 104.13, [M]⁻: *m/z* = 153.02; Found: 153.06

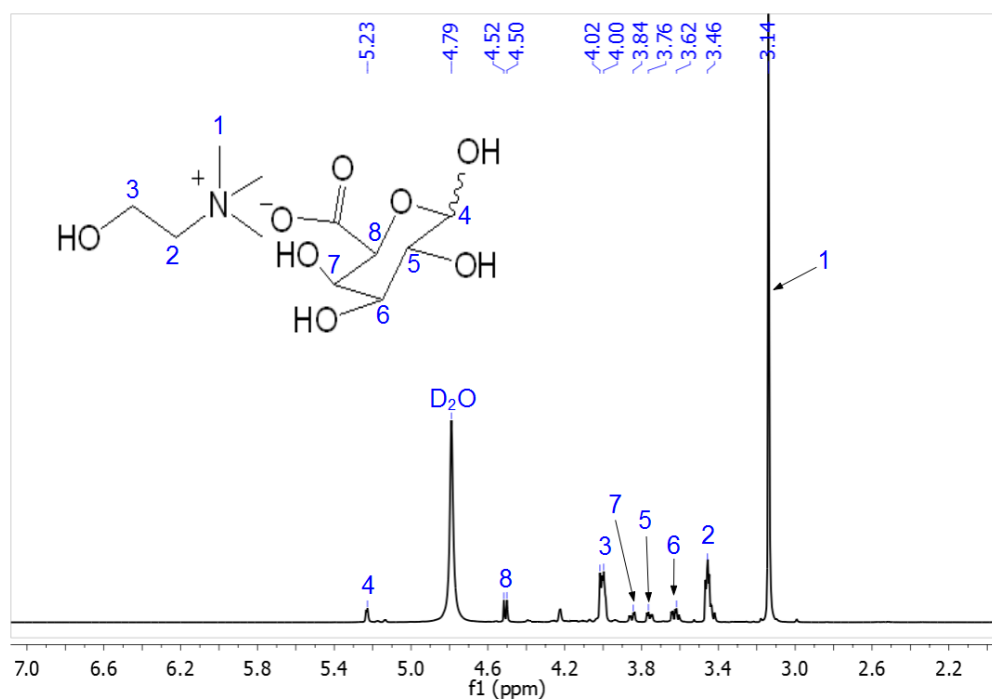


Figure B.2.9 ^1H NMR spectra of [Ch][Gal].

^1H NMR (D_2O , 500 MHz, δ/ppm relative to TMS): 3.14 (s, 9H, -N-CH₃), 3.46 (t, 2H, -CH₂-N-), 3.62 (dd, 1H, -CH-OH), 3.76 (dd, 1H, -CH-OH), 3.84 (dd, 1H, -CH-OH), 4.00 (t, 2H, -O-CH₂-), 4.50 (d, 1H, -CH-COO⁻), 5.23 (d, 1H, -CH-OH). ESI-MS: Calculated for C₁₁H₂₃NO₈ [M]⁺: m/z = 104.11; Found: 104.17, [M]⁻: m/z = 193.03; Found: 193.14.

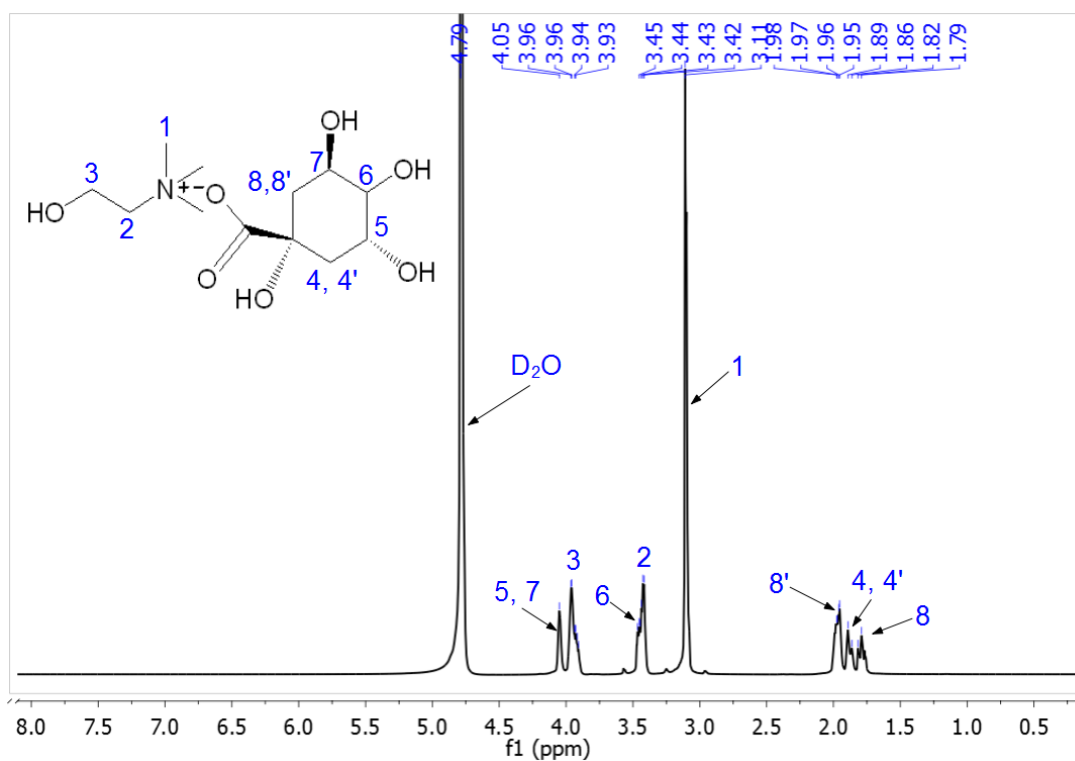


Figure B.2.10 ^1H NMR spectra of [Ch][Qui].

^1H NMR (D_2O , 500 MHz, δ/ppm relative to TMS): 1.79 (m, 1H, $-\text{CH}_2-$), 1.86 (m, 1H, $-\text{CH}_2-$), 1.89 (m, 1H, $-\text{CH}_2-$), 1.96 (m, 1H, $-\text{CH}_2-$), 3.11 (s, 9H, $-\text{N-CH}_3$), 3.43 (t, 2H, $-\text{CH}_2-\text{N-}$), 3.46 (m, 1H, $-\text{HC-OH}$), 3.96 (t, 2H, $-\text{O-CH}_2-$), 4.05 (m, 2H, $-\text{HC-OH}$). ESI-MS: Calculated for $\text{C}_{12}\text{H}_{25}\text{NO}_7$ $[\text{M}]^+$: m/z = 104.11; Found: 104.17, $[\text{M}]^-$: m/z = 191.05; Found: 191.16.

Table B.2.1 Experimental weight fraction data for the systems composed of PPG400 (w_1) + IL (w_2) + H₂O at 25 °C.

[Ch][IA]		[Ch][Gal]		[Ch][Asc]		[Ch][Qui]	
w_1	w_2	w_1	w_2	w_1	w_2	w_1	w_2
82.45	2.66	97.58	1.20	70.85	1.96	9.16	9.16
73.11	6.16	66.24	1.84	64.51	3.05	9.73	9.73
63.41	11.82	58.76	2.80	51.79	5.75	11.40	11.40
56.75	17.19	54.88	3.65	47.27	6.81	12.53	12.53
49.16	24.44	50.90	4.28	41.31	7.92	14.33	14.33
41.20	33.16	47.24	5.04	37.48	8.82	16.84	16.84
33.62	42.57	44.50	5.17	27.88	12.61	23.11	23.11
26.84	51.97	43.25	5.49	24.60	16.04	25.30	25.30
21.62	59.49	42.05	5.72	20.88	19.95	26.50	26.50
17.87	64.97	40.70	6.14	19.50	20.22	27.62	27.62
14.66	69.68	39.54	6.47	18.53	21.12	29.86	29.86
12.66	72.58	37.78	6.88	17.63	21.84	48.71	48.71
10.58	75.60	35.82	7.01	16.69	22.73	51.72	51.72
9.36	77.44	35.00	7.31	22.84	15.24	54.27	54.27
8.49	78.78	34.32	7.90	13.59	26.42	57.42	57.42
7.66	80.12	31.41	8.09	14.39	25.20	60.90	60.90
7.00	81.08	30.03	8.47	14.47	23.99	68.18	68.18
6.38	82.09	28.56	9.12	15.24	22.84		
6.08	82.50	27.00	9.64	4.25	71.12		
5.71	83.10	25.41	10.20	7.31	51.45		
5.29	83.79	24.14	10.66	8.68	33.59		
4.94	84.30	23.14	11.28	10.91	27.61		
4.62	84.87	21.99	11.78	12.18	25.41		
4.35	85.27	20.73	12.55				
4.15	85.57	19.68	13.07				
3.95	85.88	18.45	13.74				
		17.25	14.83				
		16.00	15.41				
		15.16	16.14				
		14.06	17.11				
		13.11	17.80				

Table B.2.2 Experimental weight fraction data for the systems composed of PPG400 (w_1) + IL (w_2) + H₂O at 25 °C.

[Ch][Pyr]				[Ch][Gly]			
w_1	w_2	w_1	w_2	w_1	w_2	w_1	w_2
51.62	5.77	16.58	19.84	29.98	7.25	8.75	20.97
40.83	7.43	16.41	18.23	29.52	7.48	11.35	19.17
35.65	8.20	20.24	15.61	22.85	9.22	12.05	18.14
31.47	9.07	3.85	67.82	21.09	9.70	13.63	16.70
29.06	9.79	5.52	42.80	20.00	10.58	13.83	16.20
27.13	11.15	5.36	36.86	17.68	11.85	14.04	15.16
25.13	11.75	8.00	32.64	15.33	13.66	14.66	14.42
23.68	12.33	10.88	26.67	14.34	14.42	17.84	12.95
20.98	13.95	10.65	23.24	13.57	15.66	23.14	10.66
19.88	14.52	17.69	19.36	12.63	16.73	33.81	6.75
19.23	15.11	18.25	17.03	17.68	11.85		
17.73	18.94	19.75	14.51	4.23	52.05		
13.18	26.09	23.15	12.94	3.90	37.11		
12.61	27.09			5.79	33.99		
12.17	27.38			5.83	29.15		
11.62	28.09			6.45	27.64		
11.10	28.82			7.88	24.58		
12.95	22.33			7.73	21.98		

Table B.2.3 Correlation parameters obtained from the fitting of the experimental binodal data by Equation 1, respective standard deviations (σ) and correlation coefficients (R^2).

IL	$A \pm \sigma$	$B \pm \sigma$	$10^{-5}(C \pm \sigma)$	R^2
[Ch][Gly]	313.3 ± 38.6	-0.88 ± 0.05	-8.9 ± 1.7	0.9872
[Ch][Gal]	131.5 ± 0.7	-0.48 ± 0.00	7.1 ± 0.8	0.9963
[Ch][Qui]	975.0 ± 175.3	-1.15 ± 0.07	-7.8 ± 0.3	0.9862
[Ch][Pyr]	284.3 ± 23.6	-0.72 ± 0.03	-3.0 ± 0.4	0.9620
[Ch][Asc]	217.5 ± 19.7	0.57 ± 0.03	-13.3 ± 0.1	0.9967
[Cho][IA]	162.0 ± 6.1	-0.50 ± 0.02	0.5 ± 0.0	0.9986

Table B.2.4 Tie-lines (TLs) and tie-line lengths (TLLs). Initial mixture compositions are represented as $[IL]_M$ and $[PPG]_M$ whereas $[IL]_{IL}$ and $[PPG]_{IL}$ are the compositions of IL and PPG at the IL-rich phase, respectively, and *vice-versa*.

IL	Weight fraction composition / wt%						TLL
	$[PPG]_{PPG}$	$[IL]_{PPG}$	$[PPG]_M$	$[IL]_M$	$[PPG]_{IL}$	$[IL]_{IL}$	
[Ch][IA]	48.27	1.73	40.16	39.77	1.73	82.53	69.63
[Ch][Gal]	85.66	0.81	29.76	26.20	0.078	39.68	93.99
[Ch][Pyr]	93.02	1.38	29.99	25.01	7.32	33.50	91.52
[Ch][Qui]	-	-	29.99	25.84	-	-	ND*
[Ch][Gly]	-	-	29.99	24.97	-	-	ND
[Ch][Asc]	72.96	3.71	30.20	25.36	6.52	36.85	74.25

*ND: not determined

Table B.2.5 Extraction efficiencies of IgG ($EE_{IgG}\%$), IgG recovery yield ($Y_{IgG}\%$) and IgG percentage purity (%) from rabbit serum in ABS composed of PPG 400 (30 wt%) + bio-based IL (25 wt%) + 45 wt% of rabbit serum (diluted at 1:10 (v/v); pH \approx 7).

Bio-IL	$EE\%_{IgG}$	$Y\%_{IgG}$	% purity
[Ch][Gly]	100	45.1	24.8
[Ch][Pyr]	100	58.9	23.3
[Ch][Asc]	100	85.4	30.4
[Ch][Qui]	100	51.5	27.1

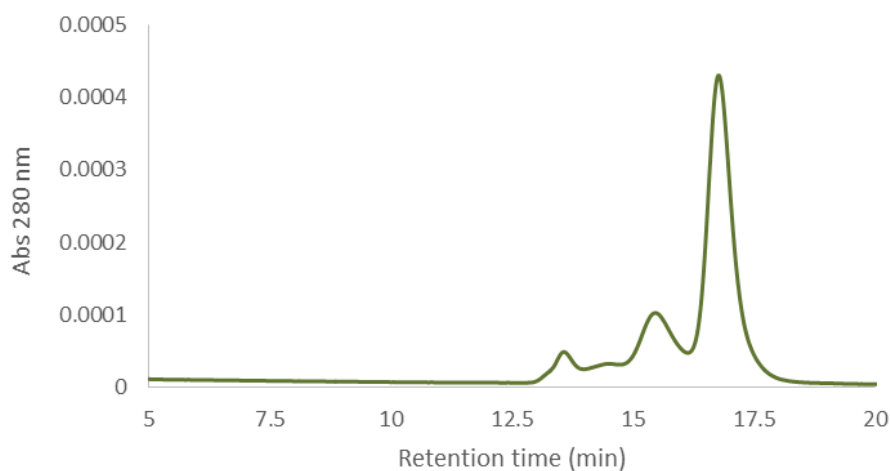


Figure B.2.11 Size-exclusion chromatograms of commercial rabbit serum. IgG peak is characterized by a retention time around 15.6 min.

Appendix C

C1.

Table C.1.1 pH values (25 °C) of aqueous solutions of 20 and 50 wt% of the ionic liquids used in this study.

IL	IL concentration	
	20 wt%	50 wt%
[Ch][HEPES]	9.26 ± 0.09	9.53 ± 0.03
[Ch][MES]	11.29 ± 0.10	12.38 ± 0.03
[Ch][Tricine]	9.76 ± 0.03	10.13 ± 0.03
[Ch][TES]	8.62 ± 0.02	8.92 ± 0.04
Non-Buffered [Ch][DHP]	3.54 ± 0.04	4.17 ± 0.09
Buffered [Ch][DHP]	7.00 ± 0.04	7.10 ± 0.06

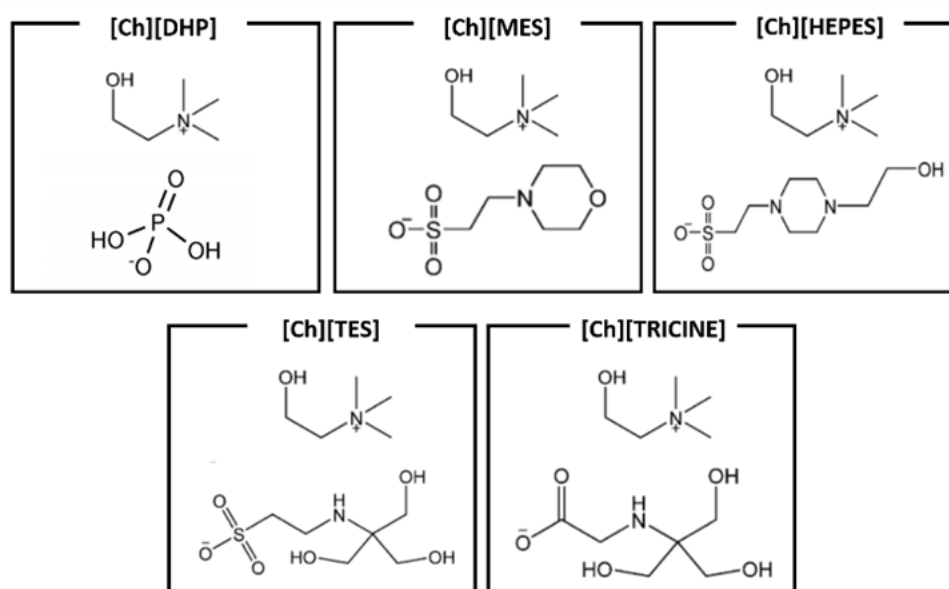


Figure C.1.1. Chemical structure of GB-ILs.

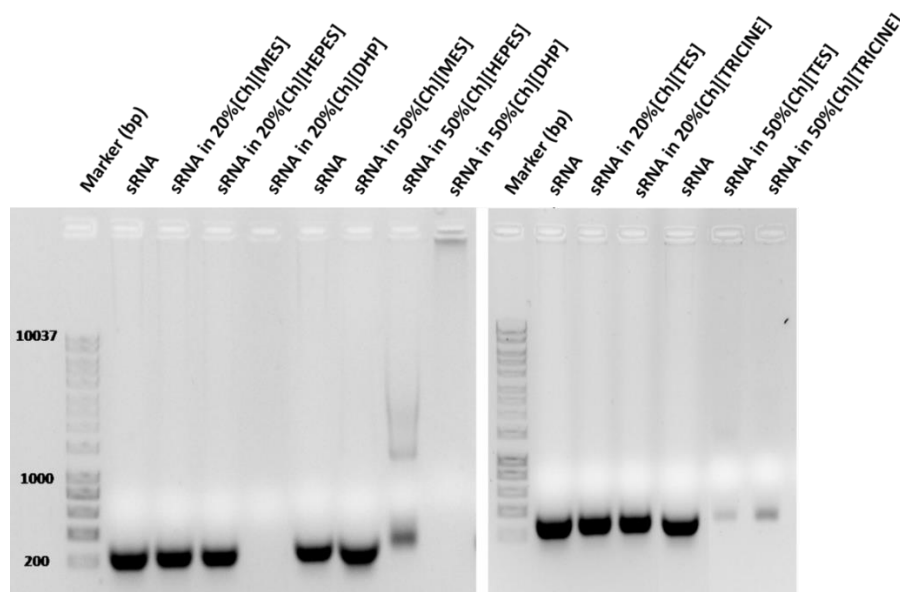


Figure C.1.2 Agarose gel electrophoresis analysis of the structural integrity of a sRNA fraction from *E. coli* DH5 α obtained by the phenol-chloroform method in presence of aqueous solutions of 20 and 50 wt% of the following ILs: [Ch][DHP], [Ch][MES], [Ch][HEPES], [Ch][TES], and [Ch][TRICINE]. RNA control samples without ILs are also included.

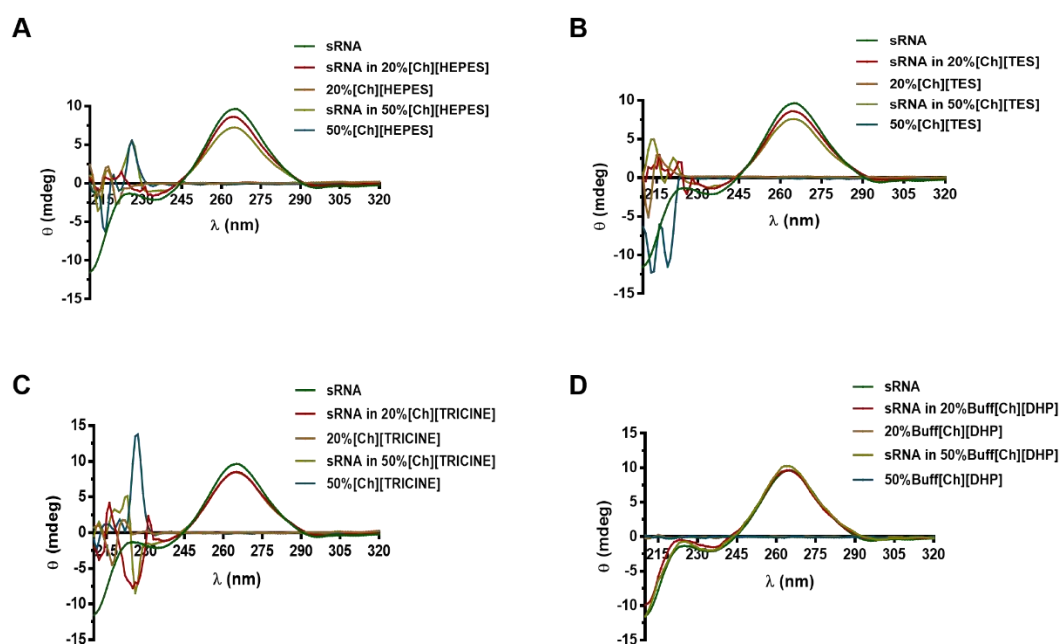


Figure C.1.3 CD spectra (210 – 320 nm) of a sRNA fraction from *E. coli* DH5 α in the absence and presence of ILs: A) 20 and 50 wt% of [Ch][HEPES]; B) 20 and 50 wt% of [Ch][TES]; C) 20 and 50 wt% [Ch][TRICINE]; D) 20 and 50 wt% Buff[Ch][DHP]. For each set, the green line represents RNA, the red line RNA in 20 wt% IL, the brown line 20 wt% IL, the light green line RNA in 50 wt% IL, and the blue line 50 wt% IL. Total RNA concentration was 150 μ g/mL. sRNA was incubated with ILs for 1 h at 4 $^{\circ}$ C.

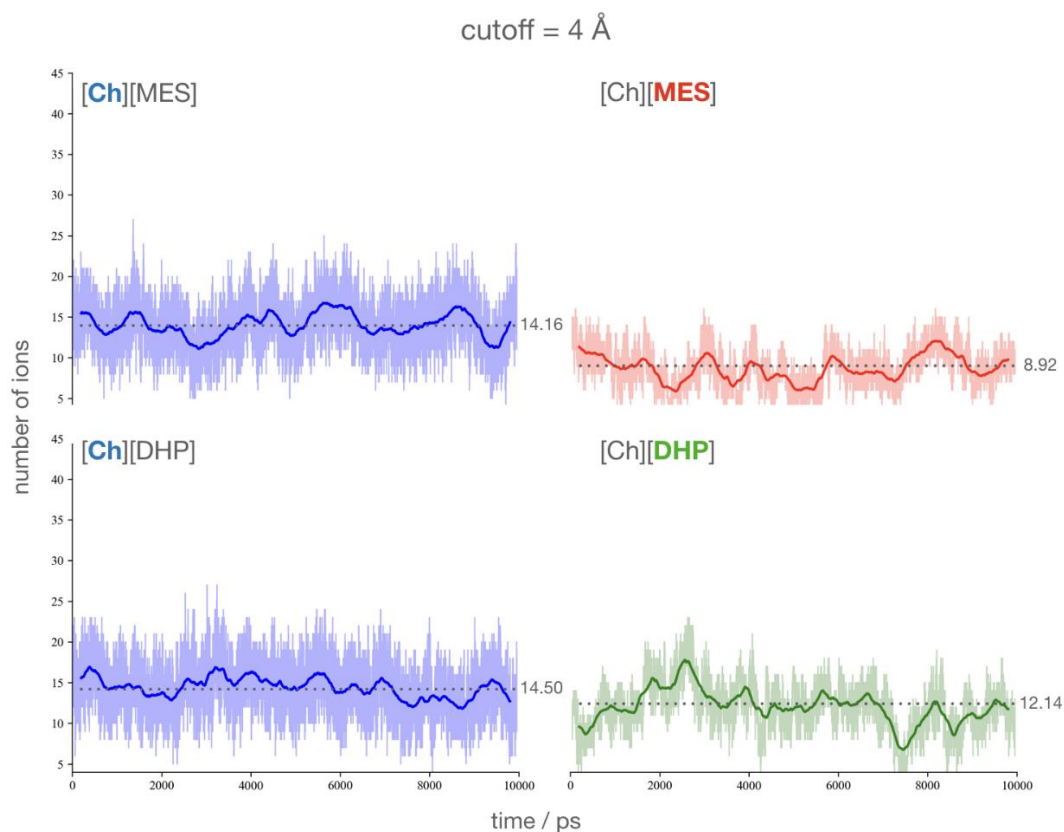


Figure C.1.4 Time evolution of the number of contacts below 4 Å between the representative atom of the IL component (highlighted in bold) and the surface (represented by any atom of the chain) of the sRNA chain, at an IL concentration of 20 wt% in water. The representative atom of each IL was taken as N for [Ch]⁺, S for [MES][−] and P for [DHP][−]. The faded curves correspond to data points collected every 0.1 ps, whereas the bold line corresponds to the associated running average obtained using a sliding window of 0.01 ps; the average contact number is depicted by the horizontal dashed line. The number of [Ch]⁺ cations (approx. 14) surrounding the sRNA chain is similar in both [Ch][MES] and [Ch][DHP]; however, the number of [DHP][−] anions (approx. 12) in direct contact with the RNA chain is *ca.* 33% higher than the number of [MES][−] anions (approx. 9) under similar conditions.

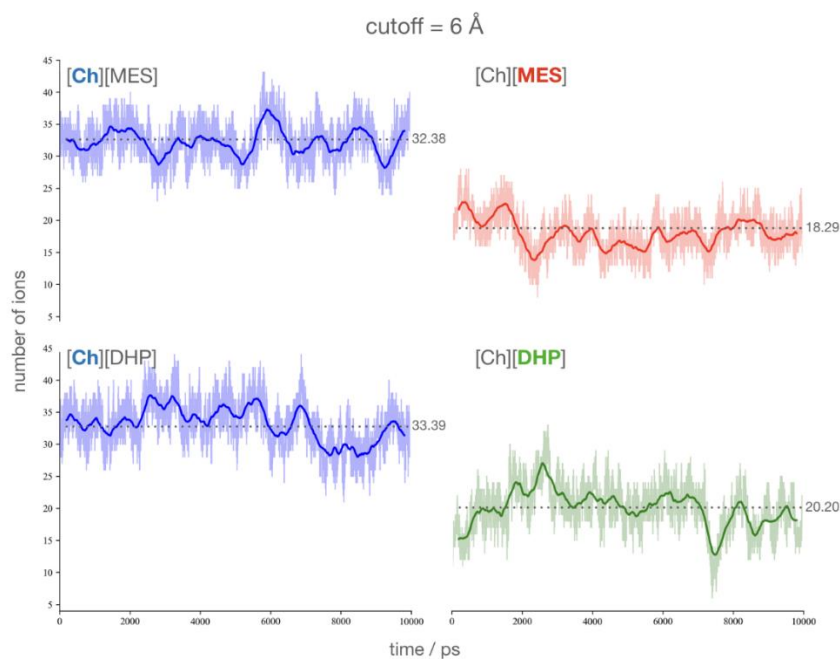


Figure C.1.5 Time evolution of the number of contacts below 6 Å between the representative atom of the IL component (highlighted in bold) and the surface (represented by any atom of the chain) of the sRNA chain, at an IL concentration of 20 wt% in water. Remaining details as in Figure B.1.2.

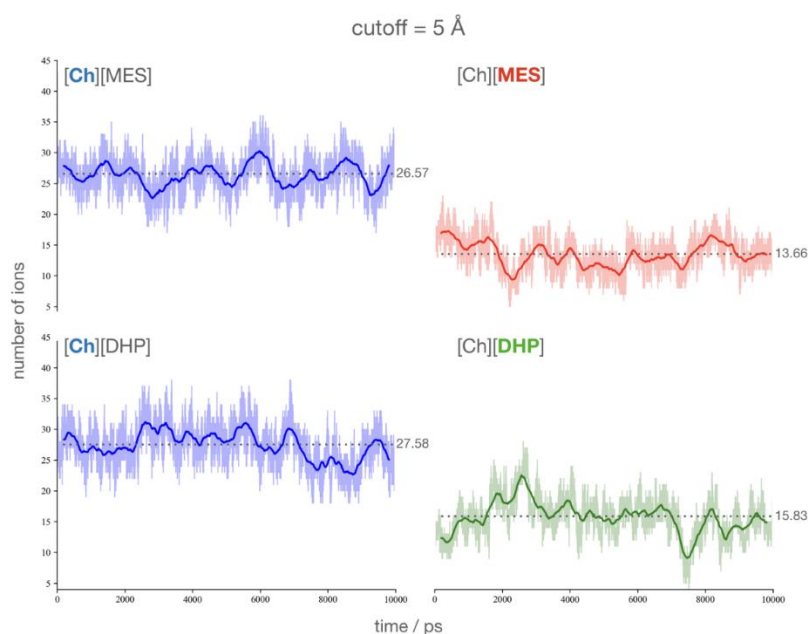


Figure C.1.6 Time evolution of the number of contacts below 5 Å between the representative atom of the IL component (highlighted in bold) and the surface (represented by any atom of the chain) of the sRNA chain, at an IL concentration of 20 wt% in water. Remaining details as in Figure S3. At a cutoff distance of 5 Å, the number of [DHP]⁻ anions (*ca.* 16) surrounding the sRNA chain remains higher than the equivalent number of [MES]⁻ anions (*ca.* 14).

C2.

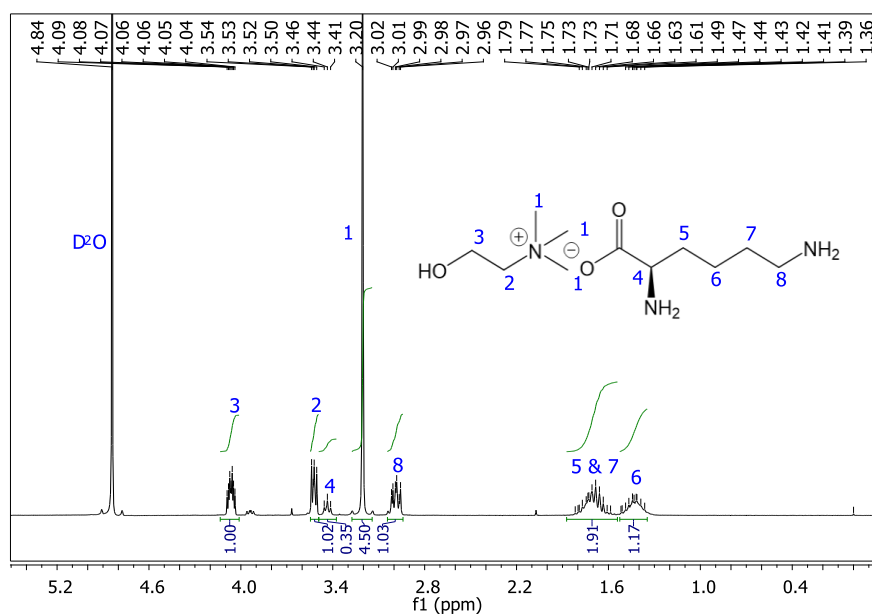


Figure C.2.1 [Ch][Lys] - ^1H NMR (D_2O , 75 MHz, δ/ppm): 1.36 (m, 2H, $-\text{CH}_2-$), 1.61-1.79 (m, 4H, $-\text{CH}_2-$), 2.96 (m, 2H, $-\text{CH}_2\text{-N-}$), 3.20 (s, 9H, $-\text{N-CH}_3$), 3.41 (t, 1H, $-\text{CO-CH-N-}$), 3.50 (m, 2H, $-\text{CH}_2\text{-N-}$), 4.04 (m, 2H, $-\text{CH}_2\text{-OH}$). Elemental analysis: Calculated C 52.99, H 10.91, N 16.85; Found C 50.17, H 10.33, N 13.86.

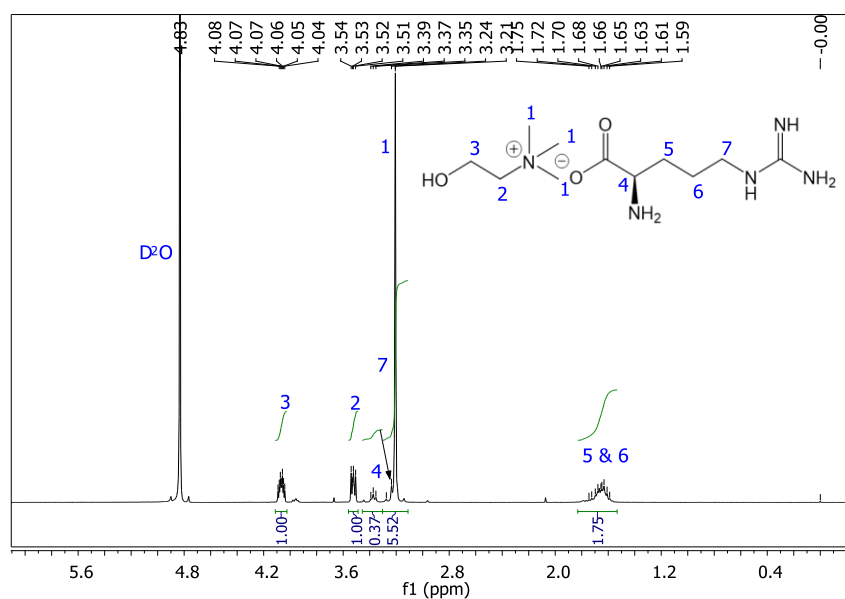


Figure C.2.2 [Ch][Arg] - ^1H NMR (D_2O , 75 MHz, δ/ppm): 1.59-1.75 (m, 4H, $-\text{CH}_2-$), 3.21 (s, 9H, $-\text{CH}_3$), 3.24 (s, 2H, $-\text{CH}_2-\text{N}-$), 3.35 (t, 1H, $-\text{CO}-\text{CH}-\text{N}-$), 3.51 (q, 2H, $-\text{CH}_2-\text{N}-$), 4.04 (m, 2H, $-\text{CH}_2-\text{OH}$). Elemental analysis: Calculated C 47.63, H 9.81, N 25.25; Found C 47.73, H 7.94, N 19.91.

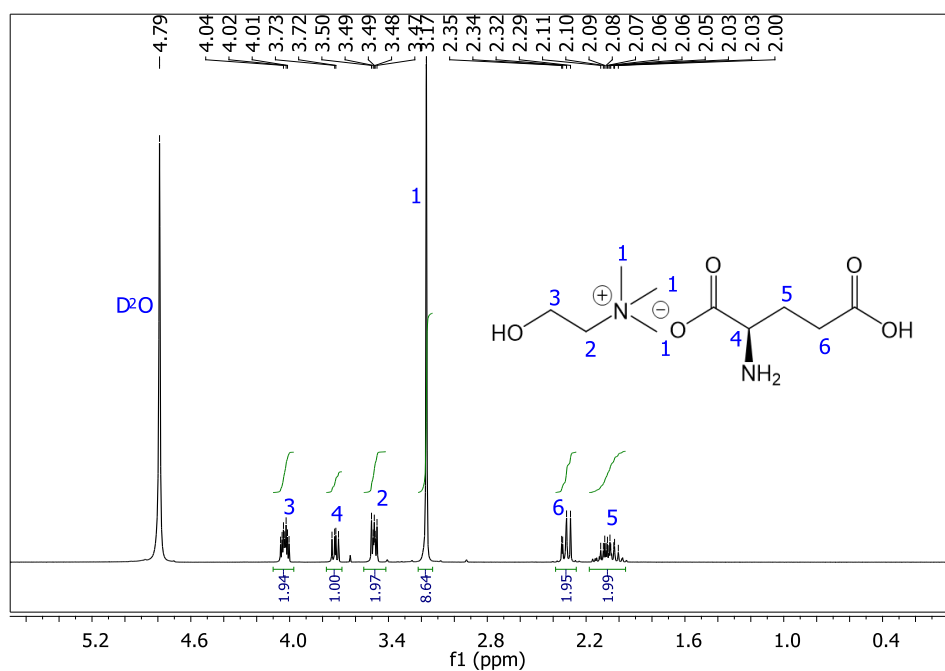


Figure C.2.3 [Ch][Glu] - ^1H NMR (D_2O , 75 MHz, δ/ppm): 2.00 (m, 2H, $-\text{CH}_2-$), 2.29 (dd, 2H, $-\text{CH}_2-$), 3.17 (s, 9H, $-\text{CH}_3$), 3.47 (m, 2H, $-\text{CH}_2-\text{N}-$), 3.72 (q, 1H, $-\text{CH}-\text{NH}_2$), 4.01 (m, 2H, $-\text{CH}_2-\text{OH}$). Elemental analysis: Calculated C 47.99, H 8.86, N 11.19; Found C 47.71, H 8.80, N 10.22.

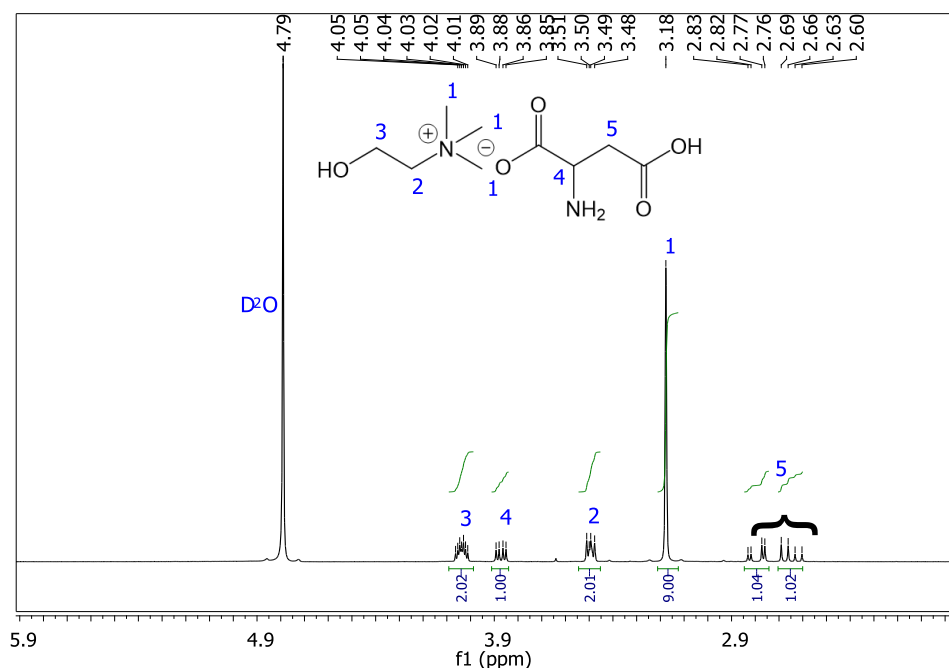


Figure C.2.4 [Ch][Asp] - ^1H NMR (D_2O , 75 MHz, δ/ppm): 2.60 (dd, 1H, $-\text{CH}_2-$), 2.76 (dd, 1H, $-\text{CH}_2-$), 3.18 (s, 9H, $-\text{N}-\text{CH}_3$), 3.48 (m, 2H, $-\text{CH}_2-\text{N}-$), 3.85 (q, 1H, $-\text{CO}-\text{CH}-\text{NH}_2$), 4.01 (m, 2H, $-\text{CH}_2-\text{OH}$). Elemental analysis: Calculated C 45.75, H 8.53, N 11.86; Found C 45.43, H 8.86, N 11.75.

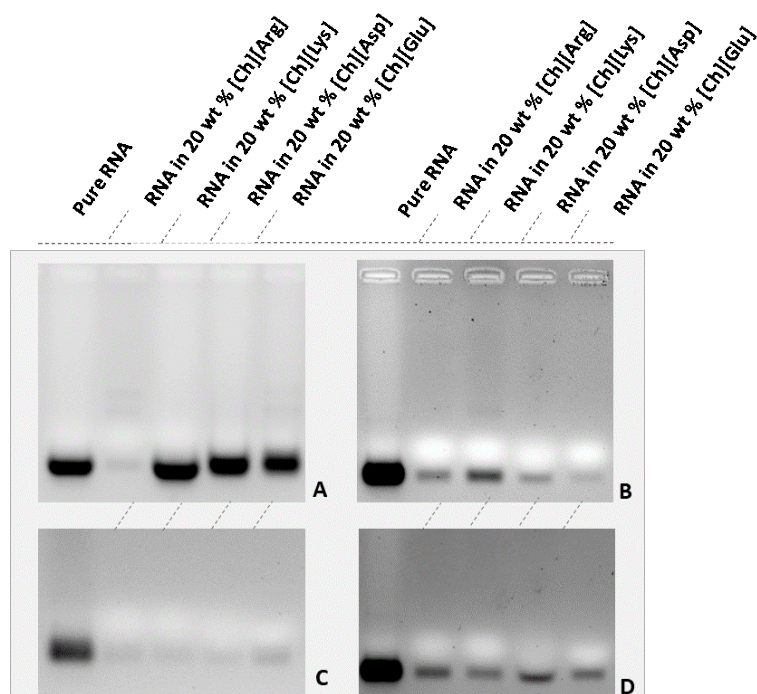


Figure C.2.5 Agarose Gel electrophoresis of RNA recovery tests from the IL rich phase using a protocol based on alcohol addition; **A** – precipitation with ethanol; **B** – precipitation with propan-2-ol; **C** – precipitation with propanol and **D** – precipitation with butanol).

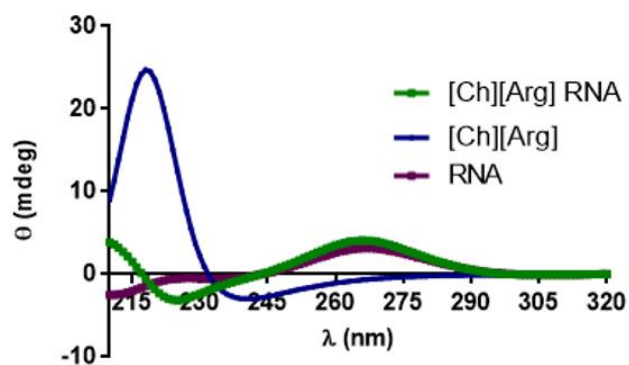


Figure C.2.6 Representative CD spectra of [Ch][Arg] (blue), RNA dissolved in 20 wt% [Ch][Arg] (green) and high-purity water (purple).

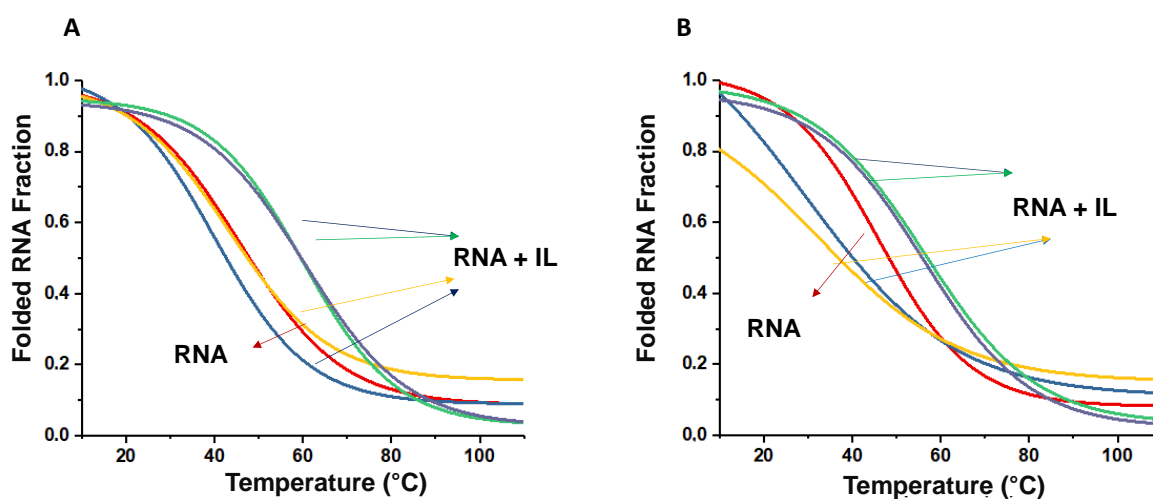


Figure C.2.7 CD melting curves (265 nm) of a RNA after incubated with ILs for 1 hour - A and after 15 days - B. Pure RNA – Red, RNA in the presence of 20 wt% ILs: [Ch][Lys] – yellow; [Ch][Arg] – blue; [Ch][Glu] – green and [Ch][Asp] –purple.

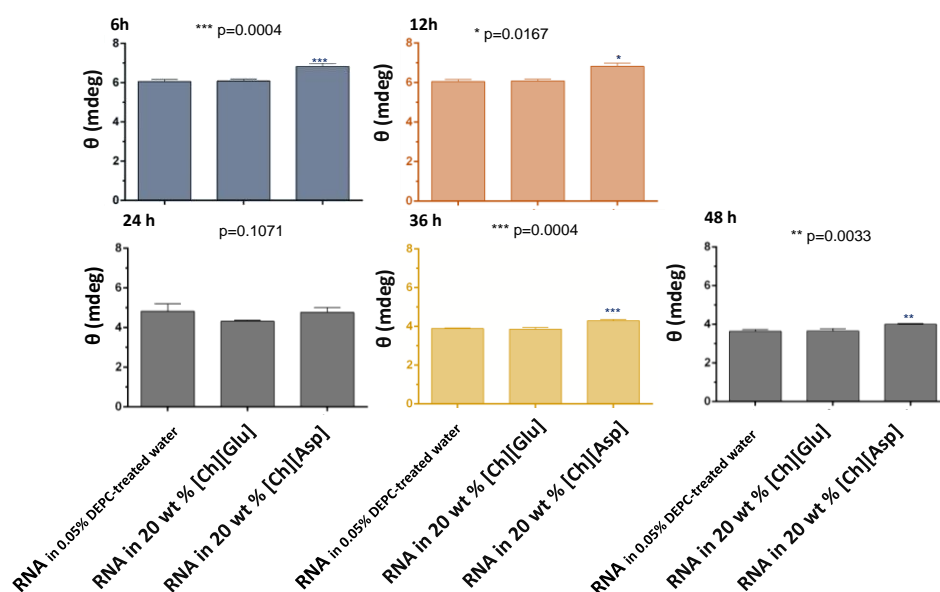


Figure C.2.8 RNA average ellipticity at 265 nm dissolved in 0.05 % DEPC-treated water and in aqueous solutions of 20 wt% of [Ch][Glu] or [Ch][Asp], in presence of 1 % (v/v) FBS. Distinct incubation periods: 6, 12, 24, 36 and 48 h.

Table C.2.1 Experimental binodal curve mass fraction data for the system PPG400 (w_1) + [Ch][AA] (w_2) + H₂O at 25 °C and atmospheric pressure.

[Ch][Lys]		[Ch][Arg]		[Ch][Glu]		[Ch][Asp]	
w_1	w_2	w_1	w_2	w_1	w_2	w_1	w_2
49.84	3.32	73.74	1.76	57.06	21.39	53.12	6.02
43.77	4.11	62.99	3.24	54.36	22.61	50.02	7.45
35.44	5.52	58.85	4.04	42.95	26.65	44.63	7.89
29.60	7.10	44.27	7.26	42.62	27.16	42.45	8.69
24.58	8.67	34.25	9.57	42.62	27.17	39.30	8.89
20.23	10.69	29.40	10.74	36.45	30.92	37.45	9.76
17.48	11.67	26.25	12.34	33.30	34.49	34.95	10.07
14.61	13.36	22.42	14.92	28.92	39.26	32.66	10.74
14.20	13.48	18.90	17.73	25.19	40.48	31.06	11.01
12.88	14.56	16.80	19.12	24.85	40.71	29.13	11.73
11.84	14.93	12.37	22.59			20.07	14.84
10.04	17.36					18.13	16.03
						16.11	17.62
						14.33	19.48
						13.03	20.29
						11.89	21.09

Table C.2.2 *A*, *B* and *C* parameters of the equation proposed by Merchuk et al.¹ and respective correlation coefficients, R^2 , for the ABS formed by PPG 400 + [Ch][AA] + H₂O systems at 25 °C.

[Ch][AA]	$A \pm \sigma$	$B \pm \sigma$	$10^5 (C \pm \sigma)$	R^2
[Ch][Lys]	145.9 ± 20.58	-0.6314 ± 0.06	2.14 ± 1.27	0.998
[Ch][Arg]	122.6 ± 14.68	-0.4037 ± 0.05	4.57 ± 2.32	0.999
[Ch][Glu]	238.7 ± 24.79	-0.6926 ± 0.06	0.09 ± 1.46	0.993
[Ch][Asp]	159.4 ± 24.79	-0.4879 ± 0.06	5.76 ± 1.46	0.992

Table C.2.3 Weight fraction compositions for the PPG 400 + [Ch][AA] + H₂O systems at 25 °C and respective values of tie-line length (TLL). Initial mixture compositions are represented as [PPG]_M and [IL]_M whereas [PPG]_{PPG} and [IL]_{PPG} are the composition of PPG400 and IL at the PPG-rich phase, respectively, and vice-versa.

[Ch][AA]	Weight fraction composition wt%						TLL
	PPG _{PPG}	IL _{PPG}	PPG _M	IL _M	PPG _{IL}	IL _{IL}	
[Ch][Lys]	93.31	0.47	19.88	20.2	4.825	24.19	92.57
[Ch][Arg]	96.40	0.35	20.01	19.96	11.00	22.27	88.17
[Ch][Glu]	90.96	1.94	19.89	20.14	8.46	23.06	85.15
[Ch][Asp]	95.62	1.09	19.99	20.00	7.48	23.13	90.85

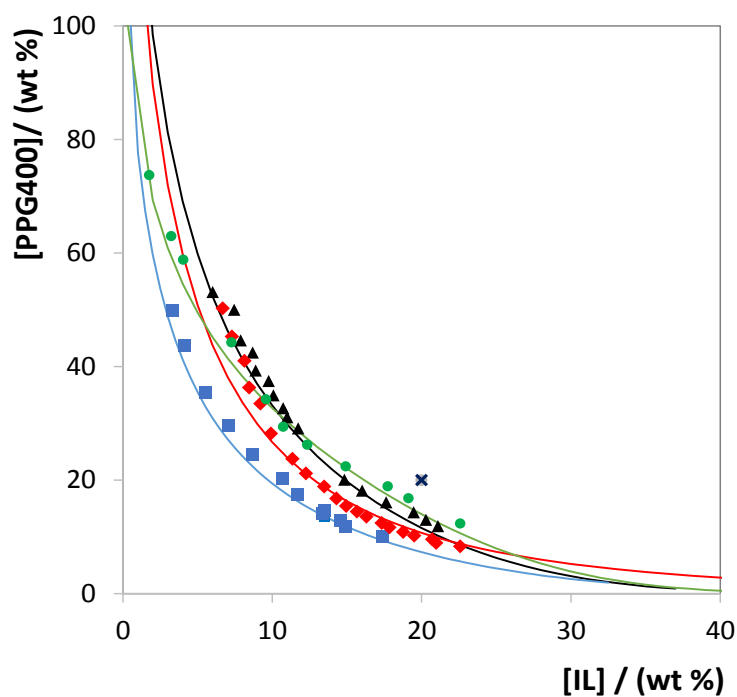


Figure C.2.9 Phase diagrams of ABS composed of PPG 400 + AA-ILs + H₂O and respective fitting (—)⁴ at 25 °C: [Ch][Lys] (■); [Ch][Arg] (●); [Ch][Glu] (◆); [Ch][Asp] (▲). Mixture point for the RNA extraction assays (×).

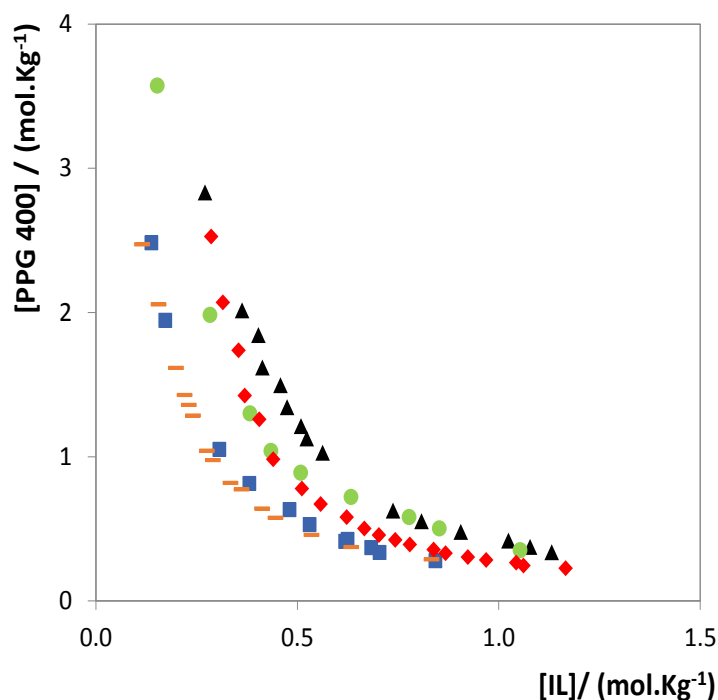


Figure C.2.10 Phase diagrams in molality units of ABS composed of PPG 400 + AA-IL + H₂O at 25 °C: [Ch][Lys] (■); [Ch][Arg] (●); [Ch][Glu] (◆); [Ch][Asp] (▲). Binodal curve for the ABS formed by PPG 400 + [Ch][Lys] + H₂O from the literature (—)¹.

Bacterial lysate preparation from *Escherichia coli* DH5α cultivations - The bacterial lysate sample was obtained from a cell culture of *Escherichia coli* DH5α, and as previously described.¹ Cell growth was carried out in shake flasks at 37 °C and 250 rpm containing 250 mL of Terrific Broth medium (12 g/L tryptone, 24 g/L yeast extract, 4 mL/L glycerol, 0.017 M KH₂PO₄, 0.072 M K₂HPO₄). The bacterial growth was suspended in at the beginning of logarithmic decline phase, approximately after 8 h (OD₆₀₀ ± 5.4). Cells were recovered by centrifugation (4,000 × g, 10 min, 4 °C), and the bacterial pellets were stored at -20 °C. The bacterial pellets were lysed based on the protocol described by Chomczynski and co-workers². Briefly, 50 mL of bacterial pellets were resuspended in 5 mL of denaturing cell lysis solution (4 M guanidine thiocyanate; 25 mM sodium citrate, pH 7.0; 0.5 % (m/v) N-lauroylsarcosine and 0.1 M β-mercaptoethanol) to perform lysis and then incubated on ice for 10 min. After incubation, the suspension was centrifuged at 19,000 × g and 4 °C, for 30 min at 4 °C and the soluble nucleic acids present in the supernatant was concentrated by adding 5 mL of ice-cold isopropanol. The precipitate was recovered by centrifugation at 16,000 × g for 20 min at 4 °C. The supernatant was discarded, and the resulting pellet was washed with 2.5 mL of 75 % ethanol and incubated at room temperature for 10 min.^{2, 3} After the centrifugation at 16,000

× g for 5 min at 4 °C, the air-dried pellet was dissolved in 2 mL of 0.05% DEPC-treated water and incubated for 10 min at 60 °C to ensure complete solubilization.

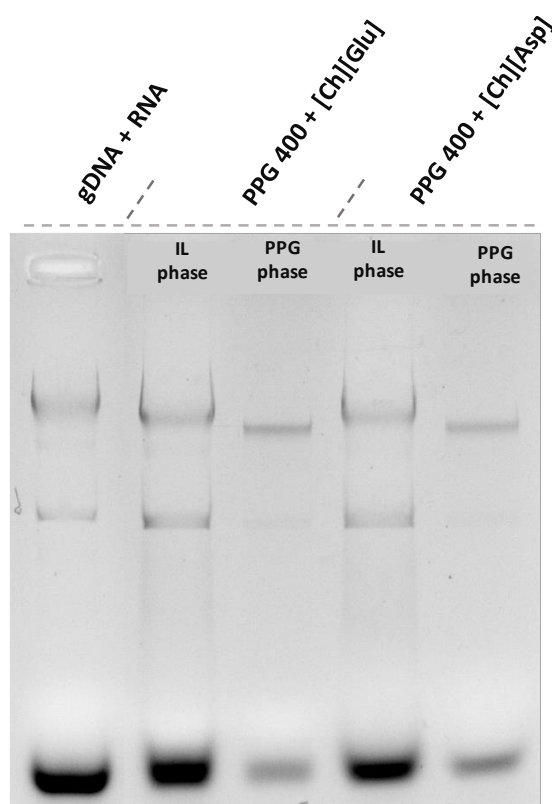


Figure C.2.11 Agarose gel electrophoresis of the ABS coexisting phases with 20 wt% PPG 400 + 20 wt% [Ch][AA] IL + 60 wt% bacterial lysate. The initial lysate sample containing RNA and genomic DNA was also analyzed.

References

1. J. C. Merchuk, B. A. Andrews and J. A. Asenjo, *J. Chromatogr., B: Biomed. Appl.*, 1998, 711, 285–293.
2. P. Chomczynski and N. Sacchi, *Anal. Biochemistry*, 1987, 162, 156–159.